Distribution Agreement

In presenting this thesis or dissertation as a partial fulfillment of the requirements for an advanced degree from Emory University, I hereby grant to Emory University and its agents the non-exclusive license to archive, make accessible, and display my thesis or dissertation in whole or in part in all forms of media, now or hereafter known, including display on the world wide web. I understand that I may select some access restrictions as part of the online submission of this thesis or dissertation. I retain all ownership rights to the copyright of the thesis or dissertation. I also retain the right to use in future works (such as articles or books) all or part of this thesis or dissertation.

Signature:

_____ _____

Amanda K. Engstrom **Date**

AN INVESTIGATION OF THE ROLE OF THE HISTONE DEMETHYLASE LSD1, AND ITS DISORDERED DOMAIN, IN NEURONAL MAINTENANCE AND TAU-MEDIATED NEURODEGENERATION

By

Amanda K. Engstrom
Doctor of Philosophy

Graduate Division of Biological and Biomedical Science
Biochemistry, Cell, and Developmental Biology

David Katz PhD, Advisor

Gary Bassell PhD, Committee Member

Victor Corces PhD, Committee Member

Dorothy Lerit PhD, Committee Member

Allan Levey MD, PhD, Committee Member

Nicholas Seyfried PhD, Committee Member

Accepted:

Lisa A. Tedesco, Ph.D.
Dean of the James T. Laney School of Graduate Studies

April 23, 2020

AN INVESTIGATION OF THE ROLE OF THE HISTONE DEMETHYLASE LSD1, AND ITS DISORDERED DOMAIN, IN NEURONAL MAINTENANCE AND TAU-MEDIATED NEURODEGENERATION

By

Amanda K. Engstrom

B.A., The College of the Holy Cross, 2012

Advisor: David J. Katz, Ph.D.

An abstract of

A dissertation submitted to the Faculty of the

James. T Laney School of Graduate Studies of Emory University

in partial fulfillment of the requirements for the degree of

Doctor of Philosophy

in the Graduate Division of Biological and Biomedical Sciences

Biochemistry, Cell, and Developmental Biology

2020

Abstract

AN INVESTIGATION OF THE ROLE OF THE HISTONE DEMETHYLASE LSD1, AND ITS DISORDERED DOMAIN, IN NEURONAL MAINTENANCE AND TAU-MEDIATED NEURODEGENERATION

By Amanda K. Engstrom

Over a century ago, Alois Alzheimer first investigated the brains of dementia patients. Since then, researchers have been investigating the mechanism of neurodegeneration. Alzheimer's disease (AD) is a tauopathy, due to deposition of tau protein into filamentous and insoluble aggregates. In AD, the amount of pathological tau (pTau) highly correlates with the degree of dementia, implicating pTau in the mechanism. In this dissertation, we provide evidence that pTau causes neurodegeneration by interfering with the lysine specific histone demethylase 1 (LSD1/KDM1A). We show that deletion of *Lsd1* in adult mice results in paralysis, hippocampal and cortical neurodegeneration, and genome-wide transcriptional changes that highly correlate with the those in the degenerating brain of AD cases. We find LSD1 aberrantly co-localized with pTau in the cytoplasm of AD cases. Additionally, in mice, we show that LSD1 is completely depleted from the nucleus of neurons with pTau. These data raise the possibility that tau contributes to neuronal cell death by sequestering LSD1 in the cytoplasm, which interferes with its required nuclear function. If LSD1 is the main target of pTau, then altering LSD1 levels should be sufficient to modulate the tauopathy phenotype. Strikingly, making tauopathy mice heterozygous for *Lsd1* exacerbates the neurodegenerative phenotypes while overexpressing LSD1 in hippocampal neurons with pTau present can block the neurodegeneration. Additionally, *Lsd1* heterozygosity exacerbates the expression changes induced by pTau, but does not induce new pathways. These data argue that pTau is functioning through LSD1 to induce neurodegeneration. This suggests that it may be possible to target the LSD1 pathway for therapeutic intervention. Therefore, we focused on the interaction between pTau and LSD1. Preliminarily, our data suggests that the N-terminal disordered domain of LSD1 is necessary for the interaction with pTau. This makes this domain a potential target for therapeutic intervention. However, utilizing a novel N-terminal deletion of *Lsd1* mouse model, we find that this domain may have a required function. Our results provide direct functional evidence that pTau induces neurodegeneration through the sequestration of LSD1, likely by interacting with the N-terminal disordered domain. This novel mechanism provides a highly promising target for therapeutic intervention in tau-mediated neurodegeneration.

AN INVESTIGATION OF THE ROLE OF THE HISTONE DEMETHYLASE LSD1, AND ITS DISORDERED DOMAIN, IN NEURONAL MAINTENANCE AND TAU-MEDIATED NEURODEGENERATION

By

Amanda K. Engstrom

B.A., The College of the Holy Cross, 2012

Advisor: David J. Katz, Ph.D

A dissertation submitted to the Faculty of the

James. T Laney School of Graduate Studies of Emory University

in partial fulfillment of the requirements for the degree of

Doctor of Philosophy

in the Graduate Division of Biological and Biomedical Sciences

Biochemistry, Cell, and Developmental Biology

2020

ACKNOWLEDGEMENTS

First and foremost I have to thank Dave. His support and guidance during these last few weeks are only a small example of the amount of effort he has put into my training. I chose to join the Katz lab because, at the time, his view towards his role as a mentor followed those of the excellent mentors I've had in the past. As I complete my graduate career, I now know those ideals have not only resulted in the best training for me, but have also shaped the type of mentor I strive to be. So thank you to Dave, for your patience, understanding, and for your never ending support and encouragement. I would not be the scientist I am today without him. I would like to also thank my previous mentors, Michelle Mondoux, Daniel Haber, and Shyamala Maheswaran. They have continued to support and guide me, standing by their commitment that I will "always be their trainee". In addition to Dave's great mentorship, I am so grateful to him for creating the amazing lab environment I get to work in every day (even during our social distancing!). The members of the Katz lab are truly the reason I made it through the long years of graduate school. Thank you to all the members who laughed and cried with me, let me vent to them, and all of those who shared in my most exciting moments both science and none-science related.

I have been fortunate in grad school to not only have support from within in my lab, but throughout the Emory community. Thank you to the Biochemistry, Cell, and Developmental Program. My work within the graduate program, was some of the most challenging but most rewarding experiences. I am so grateful for the friendships that formed so easily after seeing the same people at 8 am every day for a year. Also, to the faculty that are committed to our success in class, but more importantly in our scientific careers. Thank you to my thesis committee. Allan Levey, Gary Bassell, and Victor Corces who helped shape my project from the first qualifying exam meeting. As well as, Nick Seyfried and Dorothy Lerit who generously agreed to join and help guide me along the way. Thank you for your expert advice on experiments, and even more so on career decisions. Also, for all of the letters of recommendation and grant support letters. Thank you to Xiaodong Cheng, my former committee member for writing letters even after leaving Emory in only my second year.

In addition to support from graduate school, I have the greatest support in my friends. Thank you to each and every one of you for listening to me talk about science, and only slightly making fun of me for it. Thank you to my friends in Atlanta, you have made this city feel like home. Thank you to my friends who have supported me long before my days in graduate school. Thank you for always making me laugh. Thank you to my lobsters. They are the greatest ladies I have even known. Thank you for always supporting me and reminding me to never take myself to seriously.

I cannot think of my support system without thinking of how lucky I am to have my husband support me every day. Alexi is not only the smartest and funniest/goofiest person I know, he is my rock. He is the first one to celebrate in all my successes and pick me up from my biggest hardships. I am so grateful for all the amazing adventures we've had together. I couldn't have done grad school without him, and I am lucky to get to do life with him. He is also the reason we have our puppy Cherry. Cherry had to listen to a lot of practice talks, and for that I will always be grateful!

My growing support system started with the amazing support I have receive my whole life from my family. Thank you to my parents and my brother for always being there for me. Thank you mom and dad for always encouraging me to follow my dreams. It is through their example that I have grown into the person I am today. They have given me the independence to move away from home and start my own life, but have always been just a phone call away to help. Thank you for making the long road trips to visit me, care for me when I was sick, and help me fix a leaky pipe via Facetime. Additionally, thank to my all the members of my growing family. Thank you to all my in-laws who have welcomed me into their lives, and accepted the challenge of being related to a graduate student.

The wonderful people in my life are the reason I got through graduate school, and they made the experience worth it. Thank you to everyone who every listened to me talk about science, whether you wanted to or not. I am forever grateful for the memoires I have from the last six years. Thank you for being a part of them.

TABLE OF CONTENTS

LIST OF TABLES

LIST OF FIGURES

CHAPTER 1:

An Introduction to Neurodegeneration and Epigenetic Regulation

1.1 Tau's neuronal function and role in neurodegeneration

Neurodegenerative diseases are progressive brain disorders that result in dementia due to neuronal cell death. Patients are unable to form or recall memories, problem solve, perform basic daily functions, and even have personality changes[1]. A subset of neurodegenerative diseases are classified as tauopathies such as, Pick's disease, cortobasical degeneration, frontotemporal dementia with Parkinsonism linked to chromosome 17(FTDP-17), and Alzheimer's disease (AD)[2,3]. Currently, there are no methods to prevent or cure tauopathies, only temporary treatments for the symptoms[4]. Despite the identification of tau-mediated neurodegeneration as a leading cause of dementia, the molecular mechanism(s) of neuronal cell death is unclear[5]. Therefore there is a pressing need to further understand tau biology and the mechanism of neuronal cell death when tau aggregation has occurred.

1.1.1 Biological function of tau in neurons

The tau protein is highly conserved from flies to humans. Tau is predominately present in the axons of neurons and functions to stabilize microtubules (MTs), although tau is also found in oligodendtrytes and astrocytes[6]. There are six major isoforms of tau expressed in the adult human brain. All are derived from the single *MAPT* gene and generated by alternative splicing. The *MAPT* gene consists of 16 exons and alternative splicing occurs at exons 2,3, and 10[7]. The tau protein is characterized by a MT-binding domain at the carboxy-terminal (C-terminus) followed by a basic proline-rich region and an acidic amino-terminal (N-terminus) referred to as the 'projection domain'. The MT-binding domain is composed of repeats of a highly conserved tubulin-binding motif. This domain is made up of either three or four repeats (depending on the splicing of exon 10), which is the first major difference between the various isoforms[8].

Additionally the isoforms can differ in the presence or absence of either one or two 29 amino-acid-long inserts at the N-terminal domain. Therefore the six isoforms are referred to in two parts, first as either 3or 4R and then as 0 or 1 or 2N signifying the number of MT-binding repeats and the number of acidic N-terminal inserts present in the protein. For example, the 4R2N tau protein contains all four MT-binding repeats and two of the amino-acid inserts in the N-terminal domain[9,10]. All isoforms are broadly functionally similar, but it is likely that they have precise differences in their cellular function[11]. There are also some differences in the expression of the isoforms during development, however in most regions of the adult brain, the 3R and 4R tau isoforms are expressed in a 1:1 ratio[12]. Deviations in this ratio are characteristic of neurodegenerative diseases[7,12]. Additionally, in some disease such as AD, all isoforms are present in tau pathology, however there are tauopathies in which only specific isoforms become pathogenic[9,12].

Functionally, it has been shown that the MT-binding repeats bind to specific pockets of β-tubulin at the inner surface of the MTs. The positively charged proline-rich regions tightly bind to the negatively charge MT-surface.[12] Tau is one of many MAPs (Microtubule Associated Proteins) that are redundant in function in order to stabilize MTs throughout the entire axon[13]. Interestingly, there is evidence that tau may also engage with other structures and enzymes, including RNA and presenilin 1 (PS1)[9]. The biological relevance of these functions are unclear, however this does support the notion that tau is a promiscuous binding protein that is prone to heterogenous interactions.

Another important aspect of tau function is its post-translational regulation primarily through serine/threonine-directed phosphorylation[14]. This phosphorylation is important to modulate the binding affinity of tau for MTs, and it is tightly regulated[15]. Tau phosphorylation is

substantially higher during development of the fetal brain, and considerably lower in the adult brain. Under normal physiological conditions, tau is in a constant dynamic equilibrium on and off MTs, which is controlled primarily by the phosphorylation state of tau[14]. Importantly, aberrant tau phosphorylation is always observed in the course of tau-mediated neurodegeneration.

1.1.2 The pathophysiology of tauopathies

Under pathological conditions, tau is highly phosphorylated, and the negative charge of the phosphate residues neutralize the positive charge of the MT-binding domain[15]. This neutralization induces detachment of tau from tubulin and perturbs the tightly regulated equilibrium of bound versus unbound tau, resulting in an abnormal increase in the level of free tau[16]. It has been suggested that the higher cytosolic concentration of tau increases the chances of the pathogenic conformational changes that in turn lead to the aggregation and fibrillization of tau[9]. Additionally, the altered conformation of tau, due to hyperphosphorylation, could contribute to its higher susceptibility for aggregation[17]. Ultimately, it is this aggregate form of tau that is the hallmark of tauopathies.

All tauopathies have deposition of tau protein into filamentous and insoluble aggregates that become sequestered into neurofibrillary tangles (NFTs) in neurons and into glial tangles in astrocytes and oligodendrocytes. However, each tauopathy varies in manifestation and clinical presentation. Firstly, there are those tauopathies that primarily affect neurons versus those that primarily affect glial cells. Additionally, tauopathies differ in isoform composition, aggregate conformation, and anatomical distribution of cellular tau pathology. The clinical spectrum of

tauopathies includes a range of symptoms from primary motor defects to primary cognitive dysfunction, and combinations of the two[4].

Tauopathies include, but are not limited to, Alzheimer disease (AD) and frontotemporal lobar degeneration with tau (FTLD-Tau). FTLD-Tau subtypes include, progressive supranuclear palsy (PSP), corticobasal degeneration (CBD), Pick disease (PiD), and frontotemporal dementia with parkinsonism-17 (FTDP-17) [2,10,18]. AD is classified as a secondary tauopathy and will be described in further detail below[19]. Presently, FTLD is the preferred term used to describe a spectrum of non-Alzheimer's degenerative conditions associated with focal atrophy of the frontal lobes and/or temporal lobes[20]. However not all FTLD patients have tau aggregates. In addition to tau, FTLD patients can present with inclusions of TDP-43, FUS, or ubiquitin inclusions. In addition to FTLD-Tau, our lab is also interested in FTLD with TDP-43 inclusions (FTLD-TDP)[21-23]. Our efforts to understand FTLD-TDP will be discussed later in the ongoing experiments.

One of the major distinguishing features between tauopathies is the tau isoform involved. In AD, all six isoforms are abnormally hyperphosphorylated. However, in Pick's disease there is a prominence of pathological 3R tau, which forms aggregates (in this case called Pick bodies), while CBD and PSP tau pathology primarily consists of the 4R tau isoforms[21,23]. In addition, the confirmation of the tau pathology varies among tauopathies. Recently, structural analysis has shown that each tauopathy could be characterized by disease-specific misfolded conformation[24]. It has been suggested that cross-talk between different post translational modifications, such as ubiquitination, influence tau filament structure which contributes to the structural diversity of tauopathies[25]. Lastly, the variations of pathological tau give rise to distinct clinical presentation. Patients with CBD and PSP typically present with motor deficits and eventually cognitive

dementia due to nerve cell loss and atrophy in the cerebral cortex, basal ganglia and brain stem[21]. Interestingly, analysis of post mortem brains of both CBD and PSP cases suggests that there is tau pathology present in glial cells as well as neurons[26]. Although rare, there is also a familial form of FTLD-Tau caused by *MAPT* mutations. The *MAPT* gene is located on chromosome 17q21.1, and over 50 different pathogenic mutation have been reported including missense, silent, and splice-site mutations[27].

1.1.3 Tau's role in Alzheimer's disease

The most common form of late onset dementia is Alzheimer's disease (AD)[1]. The etiology of AD is different from the FTLDs in many ways. AD is characterized as a secondary tauopathy due to the accumulation of β-amyloid plaques as well as tau pathology[28]. Genetic forms of AD, known as early onset or familial AD, are the result of mutations in the amyloid precursor protein (APP), as well as presenilin-1 (PS1). APP is a type 1 transmembrane protein, and PS1 is the catalytic subunit of γ-secretase, an intramembranous protease that cleaves a variety of type 1 transmembrane proteins, including APP[29,30]. The identification of these causative mutations in APP and PS1 gave rise to the "amyloid cascade hypothesis." This hypothesis postulates that β-amyloid is the causative agent of AD's pathology and that the NFTs, cell loss, vascular damage, and dementia follow as a direct result of the deposition of β-amyloid[31]. The amyloid cascade hypothesis highlights the importance of both β-amyloid and tau in the pathway of AD. However, thus far trials in AD patients using drugs that target β-amyloid plaques have been shown to reduce β-amyloid plaque burden in the brain, but have had no effect on dementia. Additionally, in AD patients, tau aggregation is more tightly correlated to severity of disease. This has led to the current thinking that β-amyloid may be critical in the initiating process, but may not be the

factor that ultimately results in neuronal cell death. Instead β-amyloid may serve as the catalyst that initiates a series of pathophysiological events, including the formation of NFTs[31-36].

NFTs are primarily composed of aggregated hyperphosphorylated tau, which ultra-structurally appears as paired helical filaments. The hyperphosphorylation releases tau from binding to microtubules, enabling it to aggregate and form NFTs within the neuronal processes and the cell body of neurons[9]. In AD, the paired helical filaments that are associated with neuritic plaques are referred to as neuropil threads. Lastly, tau aggregates can be found intraneuronal as ghost tangles, which are the result of the death of neurons containing NFTs and distinguished by the absence of a nucleus or cytoplasm[37].

Neuropathological studies on the postmortem brains of AD cases provided the first evidence that there is a temporal and special hierarchy to the observed tau pathology. Recent studies have shown that the temporal and spatial accumulation of tau inclusions in specific brain regions may be due to the propagation of aggregated tau between synaptically connected neurons[38,39]. The inter-neuronal propagation of abnormal tau is referred to as "tau spread."[40,41] The progression of this spreading gave rise to what is now referred to as Braak staging. Originally, it was thought that the first appearance of tau pathology was in the transentorhinal cortex (Braak I-II). However recent data has shown that tau pathology can be observed earlier in the locus caeruleus (Braak a-c). From the entorhinal cortex, neurons project into the hippocampus, and tau pathology gradually advances into the CA1 of the hippocampus (Braak II). Tau pathology eventually spreads into the limbic structures and the inferior temporal neocortex (Braak III), then the amygdala and thalamus (Braak IV) and ultimately into the neocortex (Braak V-VI)[42-44].

1.1.4 Modeling tauopathy in animal models

Many animal models and cell culture systems have been used to investigate the effects of pathological forms of tau and how this leads to neurodegeneration. Despite the fact that mouse and human tau share 88% identity, spontaneous developments of tau pathology has not been observed in rodents[45,46]. Thus, it is necessary to utilize animal models that develop artificially driven tau pathology. A wide variety of models have been utilized, including *C. elegans*, *Drosophila*, mice, and cell lines[47]. Additionally, there are various approaches to modeling tau pathology, ranging from altering or deleting endogenous tau to overexpressing wildtype or mutated forms of human tau, and altering proteins that affect tau phosphorylation. Models have also been made to specifically target pathological tau to neurons or glial cells, and even specific neuronal cell types within the brain[45,48]. All of these models have contributed to our knowledge of tau etiology. However, many of these are outside of the scope of this thesis. For this introduction, I have included a description of the tauopathy mouse model that was utilized in this dissertation, and discuss any other models of relevance where necessary later in the dissertation.

My research utilized the PS19 tauopathy mouse generated by Virginia Lee's lab in 2007[49]. The PS19 mouse (referred throughout this dissertation as PS19 Tau) is a transgenic mouse that overexpresses the P301S mutated form of the 4R/1N human tau protein five-fold higher than the endogenous mouse tau protein[49]. The transgene insertion occurred at Chr3:140354280-140603283 (Build GRCm38/mm10) and causes a 249Kb deletion that does not affect any known genes[50]. It is driven by the prion (PrP) promoter and therefore is predominantly expressed in neurons throughout the entire nervous system. The P301S mutation was first identified in a patient with familial early onset frontotemporal dementia with parkinsonism (FTDP-17). The P301S mutation, where a proline at position 301 is replaced with a serine, is due

to a point mutation at chromosome 17:44087754 that converts the genetic code from CCG to TCG[51]. *In vitro*, the P301S mutation in the tau protein results in greatly impaired microtubule binding and an increased tendency to self-assemble into paired helical filaments[49].

PS19 Tau transgenic mice have abundant hyperphosphorylated Tau4R filaments form NFTs throughout the brain and spinal cord. These mice develop neuronal loss and brain atrophy primarily in the hippocampus but also spreading into other brain regions including the neocortex and the entorhinal cortex. Importantly they do not have β-amyloid plaques and all effects are due to the transgenic tau. In contrast, overexpression of wildtype human tau in the same mouse system does not cause tau aggregation or neuronal cell death. PS19 Tau mice have a highly stereotyped onset and progression of disease. Although time of the progression of paralysis (how long it takes to progress from a hindlimb clasp to terminal paralysis) is variable, all mice with the P301S tau transgene develop the tauopathy phenotype. Prior to the appearance of tau by histology, hyperphosphorylated tau can be found in brain homogenates as early as 1.5 months. At three months, mice display a clasp or hind limb retention, along with synapse loss and the first signs of microgliosis. At six months, there is reduced long term potential (LTP) in the CA1 region of the hippocampus and cognitive impairments. Particularly there are severe deficits in spatial learning and memory, as well as deficits in contextual fear conditioning. Histologically, between six to eight months, hyperphosphorylated tau aggregates are present throughout the hippocampus. Over time tau aggregation forms NFTs throughout the neocortex, amygdala, brain stem, and spinal cord. This is coupled with increased gliosis throughout the brain. Ultimately PS19 Tau mice undergo neuronal loss, which results in roughly a 20% reduction in brain volume at one year of age, and terminal paralysis due to motor neuron loss in the spinal cord. Overall, by one year, 80% of PS19 Tau mice are dead, with a median survival of about nine months[49].

Recently, there have been reports that indicate a delay in onset of pathology based on the genetic background. Importantly, we do not observe genotypic background effects because all mice are maintained on the same genetic background.

The PS19 Tau mouse serves as our model for tauopathy and allows us to investigate the mechanism of cell death. To this point, PS19 Tau mice have been well characterized and utilized to investigate the effect of tau aggregation throughout the brain. In this study, we utilize the PS19 Tau mouse to address the novel question - "How does accumulation of pathological forms of tau directly result in neuronal cell death?" In order to address this question, we will combine the fields of tau mediated neurodegeneration, and epigenetic regulation in post-mitotic neurons.

1.2 Epigenetic regulation in the nervous system

Over the past few decades genetic mutations have shed light on many neurological diseases. However in some cases genetic mutations were not sufficient to fully explain the mechanism. Epigenetic regulation offers an additional layer of complexity to neurological diseases. This has given rise to the field of neuroepigenetics. For the scope of this dissertation I will first describe the basic mechanisms of epigenetic regulation, with a focus on their role within the central nervous system (CNS). Then I will describe the role of epigenetic regulatory proteins in CNS aging and degeneration. Lastly, I will describe the function of the histone-modifying enzyme LSD1, and propose a model for how LSD1 is involved in tau mediated neurodegeneration.

1.2.1 DNA methylation

DNA methylation is a well-described epigenetic layer of gene expression classically associated with suppression of gene transcription[52]. This is generally the case for DNA

methylation in regions near the transcription start site (TSS), however recent data suggests that gene body methylation likely increases transcriptional activity[53]. The process of cytosine methylation occurs by the addition of a methyl group to the fifth position of the cytosine base (5mC or 5-methylcytosine). DNA methylation in mammals predominantly occurs within cytosine-guanine (CpG) dinucleotide sequences[54,55]. However, recent data has demonstrated that a small amount of 5mC can occur at non-CpG sites, as well as methylation on other nucleotides. During methylation, the methyl group is donated by S-adenosylmethionine and the reaction is catalyzed by DNA methyltransferase enzymes (DNMTs). Although 5mC is very stable, some DNA demethylation by-products, such as 5-hydroxymethylcytosine (5hmC)[56], have been shown to be biologically functional suggesting DNA methylation and demethylation is a dynamic process. The removal of the methyl group can take place in an active or passive manner, leading to the recovery of nonmethylated cytosine. The passive process occurs during DNA replication. However, since neurons are post-mitotic, they require active demethylation[57]. This active demethylation of 5mC, which results in variations of methylated cytosine, has been shown to play important roles in CNS development, function, and disease[57-59].

DNMT1, the maintenance methyltransferase, recognizes palindromic hemimethylated CpG dinucleotides and adds a methyl group to the unmethylated cytosine on the opposite strand[60]. DNMT1 is the enzyme that allows for the inheritance of methylation marks on DNA through replication and cell divisions[56]. In addition, the methyltransferases DNMT3a and DNMT3b can methylate cytosines *de novo*, without the context of other methylated residues[61]. The removal of methyl marks on DNA involves enzymes that were previously implicated as part of the DNA repair machinery such as ten eleven translocation proteins (TET 1-3), growth arrest and DNA damage-45 (GADD45), and activation-induced cytidine deaminase (AID)[55]. TET1 removes

DNA methylation through a series of oxidation reactions, which leads to variant forms of 5mC, starting with 5hmC mentioned above, then 5-formylcytosine, and 5-carboxylcytosine[62,63].

DNMTs and DNA methylation are dynamically regulated through development and in the adult nervous system[64]. Non-specific inhibition of DNMT activity altered the methylation landscape surrounding plasticity promoting genes such as brain-derived neurotrophic factor (BDNF)[65]. In neuronal stem cells, DNMT3a was associated with methylated non-proximal promoter regions of genes that are transcribed during neurogenesis. Furthermore, when *Dnmt3a* and *Dnmt1* were deleted in excitatory neurons of the postnatal forebrain in mice, mutants displayed impaired long-term spatial and contextual memory. Deletion of *Dnmt3a* and *Dnmt1* in post mitotic neurons also resulted in learning and memory deficits, but not neuronal cell loss, and hippocampi from these mice displayed abnormal long-term potentiation following stimulation, suggesting that learning deficits are due to neuronal plasticity[66]. Interestingly, mice with a single mutation in either *Dnmt3a* or *Dnmt1* in the brain do not display these deficits, suggesting some redundancy in their role in regulating neuronal processes.

Similar to the regulation of DNA methyltransferases, enzymes that remove DNA methylation are highly regulated. TET1 enzymatic function is induced by neuronal activity to catalyze 5mC to 5hmC. As a result, 5hmC is most highly enriched in the brain compared to any other tissue. 5hmC, which occurs exclusively in the CpG context, is acquired in a developmentally dependent manner, and is enriched in the gene bodies of highly expressed genes[65,67,68]. TET1 expression has been shown to positively regulate subsets of genes associated with learning and memory[69], and TET1 null mice have impaired synaptic plasticity and memory extinction[70]. Together this suggests that 5hmC, and the function of TET1 DNA demethylation, is involved in active transcription of activity-related genes within neurons.

1.2.2 Histone modifications

Histones are a highly conserved set of proteins that, along with DNA, make up the nucleosome. Nucleosomes are the basic repeating unit of chromatin fibers which provide structure and support in order to compact the genome in an organized and regulated manor. Histones assemble in an octamer comprised of two copies of each of the four core histones H3, H4, H2A, and H2B[72,73]. Roughly 147 base pairs of DNA is wrapped around a single histone octamer to form a nucleosome. Histone modifications influence local gene expression by altering the charge of nucleosomes, or by recruiting proteins that alter the spacing of nucleosomes[71]. Individual nucleosomes are linked by the histone H1, referred to as a linker histone, which associates with a short linker DNA segment[71,74,75]. This nucleosomal organization provides for higher-order chromatin structure, which facilitates or inhibits access of gene regulatory machinery, thereby adding an additional layer of transcriptional control. The mechanism for this control is through post-translational modifications (PTMs). These PTMS occur predominantly on the N-terminal tails, which are less structured than the core of the octamer. Modifications such as acetylation directly affect the three-dimensional structure of the chromatin, whereas methylation, phosphorylation, and ubiquitination recruit proteins that can either activate or repress gene transcription by using ATP to alter the spacing of nucleosomes[59].

Similar to DNA methylation, histone modifications are reversible and highly dynamic. Enzymes that add PTMs to histones are referred to as ‘writers’ while those that remove PTMs are referred to as ‘erasers.’[74,76,77] Proteins that recognize modifications on chromatin to direct transcriptional outputs are referred to as “readers”. Reader proteins such as chromatin remodelers, recognize specific histone modifications and reposition the histone octamers along the linear DNA in order to regulate the spacing of nucleosomes and DNA accessibility[78,79].

Additionally, histone variants including H2A.Z, H2A.X, and H3.1-3, are all structurally different from the canonical histones. These structural differences affect the stability of nucleosomes within the chromatin fiber. Histone variants are also subject to PTMs and can influence chromatin dynamics in specific tissues or developmental paradigms[75].

Histone acetylation at lysine residues is generally associated with transcriptional activation by promoting euchromatin formation through loosening DNA-histone binding. Acetylation of a lysine residue removes the positive charge of the nucleosome and therefore increases the space between the nucleosome and DNA. This can be functionally seen by the disruption of the proposed higher-order chromatin structure called the 30nm fiber by acetylation of lysine 16 on histone 4 (H4K16)[80]. This state facilitates the binding of transcription factors and other regulatory proteins. Histone acetylation is regulated by two classes of enzymes: histone acetyltransferases (HATs) that add acetylation and histone deacetylases (HDACs) that remove acetylation[57].

Histone methylation can occur at lysine and arginine residues and will alter the three-dimensional structure of chromatin, however the effect on transcription is dependent on the methylation state and the residue being modified[81]. Enzymes that add methyl groups to either lysine or arginine residues are histone methyltransferases (HMTs), such as the SET family of enzymes. Methylation marks are removed by histone demethylases. HMTs can transfer one, two, or three methyl groups to each residue[82,83]. However in the case of histone demethylases there are two major classes. Amine oxidase demethylases, LSD1/KDM1A and LSD2/KDM1B, are only capable of removing mono- and dimethylated residues[84]. Removal of trimethylation marks is accomplished by a set of Jumonji domain (Jmj) containing demethylases[85].

The most well characterized histone methylation mark is methylation of lysine 4 on histone 3 (H3K4). H3K4 can be mon-, di-, or trimethylated by the HMT called mixed lineage leukemia (MLL) in mammals. H3K4 mono- and di- methylation (H3K4me1/me2) are removed by the amino oxidase demethylase, LSD1, while H3K4 trimethylation (H3K4me3) is removed by the Jmj containing demethylases JARID1a/KDM5A and JARID1b/KDM5B. H3K4me3 facilitates transcriptional activation and is primarily found at the promoters of active or poised genes[86,87]. In addition to being found at promoters and the 3' region of active genes, H3K4me1 is also associated with enhancer regions that can be distant from the transcriptional start sites of genes[88].

In contrast to H3K4 methylation, methylation of lysine 9 on histone 3 (H3K9) is associated with gene repression. H3K9 is primarily di-, or trimethylated (H3K9me2/me3) and can be methylated by several methyltransferases, including SUV39H1, G9a, and SETDB1[89,90]. H3K9me is removed by the Jmj containing demethylase JHDM2A/KDM3A. H3K9me2/me3 often correlates with the presence of DNA methylation in the mammalian genome, and it has been suggested that H3K9me can be inherited together with DNA methylation through cell division to maintain repressive chromatin regions. Additional histone methylation marks such as H3K36, H3K27, and H4K20 all play distinct roles in either active (H3K36 and H4K20) or repressive (H3K27) chromatin states[57,91,92]. These and other histone PTMs, and well as DNA methylation, operate in tandem to regulate chromatin structure and in most cases the relationship between them is complex and still unclear[93].

Many histone-modifying proteins play important roles during differentiation and early development. For example, in mammals many histone-modifying enzymes are essential and deletion of them is embryonic lethal. However, histone-modifying enzymes also continue to play

important roles in the adult CNS. Histone-modifying enzymes and their corresponding histone function in synaptic plasticity, learning, and long-term memory formation[58]. Manipulation of HDACs and HATs affect a range of cognitive functions ranging from memory performance, such as in fear conditioning and spatial learning, to long-term potentiation (LTP). But the exact phenotype observed is dependent on which HDAC is manipulated and whether the HDAC is deleted or overexpressed. These findings suggest that different HDACs act as crucial positive and negative regulators of learning and memory[94-97]. Deletion of enzymes that modulate histone methylation, such as LSD1 and some of the JARID proteins, are typically embryonic or neonatal lethal[98]. Nevertheless, manipulation of these enzymes in the CNS typically results in learning and memory defects, reduced spin density, and neurite maturation defects[99].

1.2.3 Noncoding RNAs that regulate chromatin

Noncoding RNAs (ncRNAs) are functional RNA molecules that are transcribed from DNA but not translated into proteins. ncRNAs are divided into classes by their length. The arbitrary cutoff between long and short RNAs (lncRNAs and sncRNAs respectively) was set at 200 bases, regardless of function. Three major classes of sncRNAs are microRNAs (miRNAs), short interfering RNAs (siRNAs), and piwi-interacting RNAs (piRNAs)[100]. All of these groups of ncRNAs have been implicated in establishment and regulation of chromatin states, and have been shown to play a role in heterochromatin formation, histone modification, DNA methylation targeting, and gene silencing[101].

The best-studied example of ncRNAs role in chromatin regulation is the process of X-inactivation by the lncRNA, *X-inactivation specific transcript* (*Xist)*[102]. In placental mammals, female XX cells express the *Xist* transcript in order to repress expression from one of the X

chromosomes, a process called X-chromosome inactivation. *Xist* transcripts bind to and recruit the heterochromatin- forming PRC2 complex that silences the inactive X chromosome[103,104]. Additionally, lncRNAs have been shown to function cooperatively with histone modifying enzymes. For example, the HOX transcript antisense RNA (*HOTAIR*) can function as a scaffold between the H3K27 methyltransferase PRC2 complex and the histone demethylase LSD1-CoREST complex, allowing for the removal of activating H3K4 methylation while simultaneously adding the repressive H3K27 methylation mark to the same residue[105]. Similar to lncRNAs, sncRNAs such as piRNAs, named for their interactions with piwi family of proteins, are involved in chromatin regulation through their ability to target and suppress transposon activity in the germline[106].

Taken together, the regulation of chromatin state in the mammalian system through DNA methylation, histone modification and noncoding RNAs, is a complex and dynamic process[101]. During neuronal development, these mechanisms function cooperatively in the maintenance and function of mature neurons.

1.3 Neuroepigenetic mechanisms of degeneration

Epigenetic regulation plays critical roles in development, maintenance, and neuronal function in the CNS, however these epigenetic mechanisms are altered both in normal aging as well as in degeneration. Since neurodegeneration is a multifactorial disease with low genetic penetrance, it is perhaps not surprising that epigenetic mechanisms are particularly relevant.

1.3.1 Chromatin changes in the aging brain

As with various other cellular processes, epigenetic regulation is affected by aging. Effects of aging have been observed for both DNA methylation and chromatin modifications. Interestingly, most of the changes result in an increase of repressive chromatin. At a functional level, aging results in deficits in learning and memory[107]. One mechanism for this could be the alterations in histone modifications that result in repression (or decreased chromatin accessibility) of memory-related genes. For example, aging leads to a decrease in acetylation of histone 4 lysine 12 (H4K12)[58]. Reduction of H4K12ac in mice disrupts memory-associated activities due to reduction of transcription of several memory-related genes[108]. Administration of HDAC inhibitors, such as hydroxamic acid, in the hippocampus can restore the transcriptional activation of several memory-related genes and improve neurobehavioral outcomes in aged mice[109]. Similar to decreases in acetylation, increases in repressive methylation marks such as H3K9me2/3 and H3K27me3, as well as loss of active methylation marks such as H4K20me and H3K36me3 are observed in aged mouse models[110]. Increases in repressive chromatin occurs in both neurons and oligodendrocytes[111-113]. This results in a decline in signaling in nerve cells as well as defects in axon myelination that have both deleterious effects on neuronal function and memory consolidation.

Changes in dynamic DNA methylation are also associated with the aging process. Age dependent changes in DNA methylation largely consist of global hypomethylation. However region-specific hypermethylation is also observed[114,115]. Because DNA methylation consistently changes with age, it has become a major focus of research to generate an epigenetic predictor of biological age[116]. Over the lifetime of a mammal, global levels of 5mC are highest in embryos and decrease gradually[115]. However, there are also site-specific regions, such as bivalent chromatin domains, that have been shown to become hypermethylated during aging. Current data

suggests that decreases in DNA methylation are due to down-regulation of the expression of DNMTs, along with an insufficient supply of folic acid (which is utilized in the enzymatic reaction of DNA methylation) in elderly patients[64,117,118].

1.3.2 Epigenetic component of Parkinson's disease

Currently, Parkinson's disease (PD) is the second most prevalent neurodegenerative disorder. Patients with PD typically suffer from motor dysfunction such as bradykinesia, muscle rigidity, resting tremor, and postural instability, due to degeneration of dopaminergic neurons of the substantia nigra. PD patients can also suffer from nonmotor symptoms including anxiety, depression, dementia, and sleep disturbances[51,119]. The pathological hallmark of PD cases is the accumulation of intracellular protein inclusions referred to as Lewy bodies, which are mainly composed of the protein alpha-synuclein (αSyn)[120]. Most of the PD cases are sporadic. However, familial cases make up roughly 10% of all PD cases. Amongst the familial cases, there are many genes that have been implicated in onset of PD such as *SNCA, Parkin, PINK1, and LRRK2*[119]. Together these genes are known as the PARK family of genes[119].

In PD, depositions of misfolded αSyn form within neurons, and it has been suggested that their primary toxic effects occur in the nucleus where they can disrupt chromatin conformation[121]. αSyn was shown to associate with histones and inhibit acetylation through its association with the HDAC Sirtuin-2 (Sirt2). In a *Drosophila* model for PD, down-regulation of Sirt2 resulted in reduction of αSyn toxicity[122,123]. Conversely, in isolated dopaminergic neurons from the brain of post-mortem human PD cases, there was increased acetylation levels and reduction of the expression of various HDACs[124]. This and other work has shown that there is a complex relationship between histone acetylation and PD, and that the balance between HAT

and HDAC activities is vital for normal cellular function. Studies have also shown that HDAC inhibitors have therapeutic potential for PD, but adverse side effects have also been observed[125-127]. Similarly, the role of DNA methylation in PD is complex. Analysis of blood and brain tissue from PD cases showed genome-wide DNA methylation changes. This included significant dysregulation of CpG island methylation where many genes, including PD risk genes, were found to be either hypo- or hypermethylated[128]. However, the specific sites and implications of the genes that are hypo- or hypermethylated have been controversial and difficult to reproduce[129]. Lastly, miRNAs have been implicated in PD. Recently tissue samples isolated from PD cases showed an overall downregulation of miRNAs compared to healthy controls. Differences in expression of several miRNAs have also been detected in mouse models of PD[130]. For example, miR-133b, a miRNA that is specifically expressed in midbrain dopaminergic neurons, is deficient in midbrain tissue from post-mortem PD cases[131]. Additionally, alternations of miRNAs were detected in blood samples of PD patients when tested pre- and post-treatment[132,133]. This suggests that there is potential for miRNAs in blood to serve as a screening method for PD.

1.3.3 Epigenetic component of Huntington's disease

Huntington's disease (HD) is a neurodegenerative disorder that typically occurs midlife with symptoms such as chorea, dementia, and changes in personality due to degeneration of cells within the striatum[134]. Unlike most neurodegenerative diseases, HD is exclusively due to a fatal autosomal dominant mutation consisting of a CAG trinucleotide repeat expansion within exon 1 of the HD gene. The extended CAG repeat is translated into a lengthened glutamine tract at the amino terminus of the HD protein. This expansion of the protein disrupts both its function and

structural properties so that the HD protein forms aggregates within the cell[135-137]. Despite knowing the genetic basis for the disease, the mechanism (or mechanisms) of neurodegeneration are still unclear because of the variety of cellular processes that are disrupted. Recently, an altered chromatin state has been observed in HD[138]. In addition, treatment with inhibitors targeting chromatin modifying proteins have been shown to alleviate the neurodegenerative phenotype in mouse models[139]. Together these data suggest that there is a possible epigenetic component to HD.

Increased H3K9 methylation[140], as well as increased expression of the variant histone macro H2A1[141], were observed in blood and brain tissue from HD patients. These changes were shown to lead to the decreased expression of the neurotropic factor BDNF, dopamine receptors and MAP kinase signaling components, all of which have all been observed in the striatum[142,143]. Pharmacological intervention reducing the HMT SETDB1 function resulted in decreased H3K9me3 and ameliorated the behavioral and neuropathological phenotype of HD mice[138,144]. Additionally, inhibition of the H3K4 demethylase, JARID1C, in primary neurons increased the expression of neuronal genes that are downregulated by the HD gene mutation[145,146]. These data from Huntington's disease suggest that epigenetic regulation can play a role in neurodegenerative disease even when there is a specific genetic cause. Thus, manipulation of chromatin modifying enzymes may aid treatment by alleviating some of the downstream transcriptional alterations.

1.3.4 Epigenetics in Alzheimer's disease

AD is characterized by β-amyloid plaques and NFTs of hyperphosphorylated tau present in the post-mortem brain. Despite intensive investigation into the etiology of AD, clinical trials

targeting these pathologies have been unsuccessful, likely because the intervention occurs to late in the process of neurodegeneration[1]. This has led to the search for downstream mechanisms. Recently, AD models have implicated multiple processes in the connection between protein aggregates and neuronal cell death. These include neuroinflammation, cell cycle reactivation, nuclear pore instability, and deficits in mitochondria resulting in reactive oxygen species[147,148]. However, it remains unclear how protein aggregates lead to these downstream defects. One possibility is that protein aggregates lead to these downstream defects by disrupting epigenetic mechanisms.

As detailed above epigenetic regulation is critical to neuronal function, and multiple epigenetic disruptions have been observed in AD patients and models. For example, decreased histone acetylation on both H3 and H4 has been observed in neuronal cultures of the APP overexpression mouse, as well as in two different APP/PS1 mouse models of familial AD[149,150]. Additionally, several studies have suggested that APP can directly modulate lysine acetylation of histones during the progression of AD[150,151]. Furthermore, in an AD mouse model, HDAC2 was found to be highly expressed in the hippocampus and prefrontal cortex. In support of this finding, neuron-specific overexpression of HDAC2 led to a decrease in dendritic spine density, synapse number, synaptic plasticity, and memory formation. Also administration of a class I HDAC inhibitor in the DK-p25 mouse model of AD, rescued memory impairments, though it did not affect neuronal loss[58]. This suggests that, at least for class I HDACs, histone acetylation plays a more signification role in neuronal function rather neuronal cell maintenance. Consistent with the data from mouse, in human postmortem brain samples there was an increase in HDAC2 levels in the hippocampus and entorhinal cortex[152,153]. Another class of histone deacetylates, the sirtuin family, are also reduced in the cortex of AD patients. Interestingly, SIRT1 levels are

negatively correlated with the accumulation of paired helical tau filaments. Tau acetylation can promote pathological tau aggregation, while SIRT1 causes tau deacetylation[153].

Changes in chromatin structure have also been implicated in tau-induced neurodegeneration. For example, it was recently shown that in tau transgenic *Drosophila* and mice, as well as human AD cases, that there is widespread loss of heterochromatin which leads to aberrant gene expression. This was suggested to be due to oxidative stress and subsequent DNA damage caused by tau overexpression. Consistent with a function for heterochromatin in tau-induced neurodegeneration, genetic rescue of tau-induced heterochromatin loss reduced neurodegeneration in *Drosophila*[154]. This raises the possibility that epigenetic regulation could be targeted therapeutically to inhibit tau-mediated neurodegeneration or counteract the downstream effects of aberrant transcription in AD.

1.4 The lysine specific histone demethylase LSD1

The histone demethylase LSD1 is a transcriptional repressor most well studied for its role facilitating cell fate transitions. Histone methylation is a dynamic and highly regulated process, and disruption of this process can have detrimental effects on cellular functions. LSD1 is continuously expressed in cells that are terminally differentiated, but its role in these cells requires further investigation.

1.4.1 LSD1 decommissions enhancers at stem cell genes

LSD1/KDM1A is an amine-oxidase lysine specific histone demethylase. It specifically removes mono- and dimethylation from lysine 4 on histone 3 (H3K4me/me2). LSD1 was first characterized by the Shi lab in 2004, as both a histone demethylase and transcriptional

corepressor[84]. LSD1 consists of an unstructured N-terminal domain, a SWIRM domain, a FAD binding motif, and the amine oxidase domain, which contains a helical insertion domain within it. In its three-dimensional structure the helical insertion, referred to as the tower domain, forms the primary domain for LSD1's interaction with its binding partners[84]. LSD1 operates in a variety of cell types, and its functional specificity is due to the cell-type dependent interactions with its binding partners. It is most well-known for its role within the CoREST complex. LSD1 requires the corepressor CoREST in order to demethylate H3K4 in the context of nucleosomes[155]. Other binding partners of LSD1 include, but are not limited to, Snail1, HDAC1/2, BRAF35, PRKCB, NuRD, AXL1, BHC80, and ZFP516[156]. Although LSD1 is thought to primarily function as an H3K4 demethylase, the specificity of LSD1's target histone modification can be modulated depending on the binding partner. For example, when bound to the androgen receptor, LSD1 has been shown to act as a transcriptional activator by demethylating H3K9me2[157]. Additionally, LSD1 has non-histone targets such as p53 and DNMT1[158].

LSD1 is evolutionarily conserved from *S. pombe* to mammals. Predominantly, LSD1 has been shown to play a critical role in cell fate transitions in multiple model systems. In *C. elegans,* mutation of the LSD1 ortholog *spr-5* results in transgenerational progressive sterility. The sterility in *spr-5* mutants is thought to be due to the observed accumulation of H3K4me2 in spermatogenesis genes[159]. *Drosophila* mutants of *Lsd1* have an even more severe phenotype, with sterility occurring in the first generation[160,161]. In mouse models, deletion of *Lsd1* is lethal by embryonic day 7.5[98,162]. In addition, deletion of LSD1 in the female oocyte alone results in embryonic lethality at the one-two cell stage, with embryos failing to properly undergo the maternal-to-zygotic transition[163,164]. Taken together, these data support the hypothesis that

LSD1's evolutionarily conserved role is to prevent the passage of cell fate information between generations, likely by removing the epigenetic memory associated with H3K4 methylation.

In addition to LSD1's evolutionarily conserved role, in mammals, LSD1 functions in other cell fate transitions. For example, LSD1's most well studied role is in transition from the embryonic stem cell (ESC) fate to the differentiated cell fate. LSD1 is not required for the maintenance of stem cells, however without LSD1 ESCs cannot differentiate. In mouse embryonic stem cells (mESCs), it was shown that LSD1 binds to the promoters and enhancers of critical stem cell genes. However, LSD1 does not actively remove the H3K4 methylation mark until the mESCs undergo differentiation. In this context, LSD1 erases the H3K4methylation in coordination with the NuRD (nucleosome remodeling and deacetylase) complex. When LSD1 function is inhibited during mESC differentiation, critical stem cell genes continue to be expressed, and there is aberrant H3K4 methylation both at enhancers and promoters of these loci. A similar mechanism has been shown during murine hematopoietic stem cells, and almost all other mammalian stem cell population[165]. In this context, H3K4 methylation at enhancers appears to act as an epigenetic memory, allowing cells to maintain their stem fate and removal of this memory by LSD1 is required to allow a transition in cell fate.

1.4.2 LSD1 in neurons

In addition to the critical role during stem cell differentiation, loss of LSD1 in specific cell types causes a wide range of phenotypes. For example, LSD1 depletion in the developing telencephalon causes defects in olfactory receptor choice.[166] Conversely, transgenic mice that overexpress of *Lsd1* have increased oxidative phosphorylation and fat retention[167]. Recently, there has also been increasing evidence that LSD1 plays an important role in neuronal

differentiation. When in the CoREST complex, LSD1 has been shown to orchestrate radial migration during pyramidal neuron development. Additionally, inhibition of the LSD1/CoREST complex during development results in a dramatic reduction of neural migration where neurons pause in both the ventricular zone and subventricular zone and ultimately retain a multipolar shape characteristic of intermediate progenitor cells[168].

In mammals, LSD1 can also be alternatively spliced into a neuronal- specific isoform, LSD1n. LSd1n contains the additional exon 8a. Exon 8a is only 12 bp long, translated into 4 amino acids, and immediately precedes the CoREST-binding tower domain[169]. This isoform has been reported to demethylate H3K9me1/2 when complexed with supervillain (SVIL)[170] and H4K20me1/2 when complexed with CoREST[171]. *In vitro* knockdown of LSD1n in cortical neurons resulted in inhibition of neurite maturation and outgrowth and overexpression enhances it[170]. Consistent with the *in vitro* results, *Lsd1n* mutation in mice results in deficits in spatial learning and long-term memory formation[169]. In cell lines, LSD1n was shown to be required for transcription initiation and elongation in response to neuronal activity[171].

Until investigated by our lab, there had been no direct indication that LSD1 is involved in neurodegenerative disease. However there were data that suggested a possible connection. LSD1 has been shown to have a functional role in differentiated neurons, as it is neuroprotective against oxygen glucose deprivation in rat cortical neurons[172]. Additionally, the observation of loss of heterochromatin in human AD could suggest a defect in histone modifying proteins that regulate chromatin confirmation. As is the case with most neurodegenerative diseases, the balance of epigenetic regulation, and therefore transcriptional regulation, may be critical to the etiology or treatment of AD.

1.5 Outstanding questions and objectives

In recent years, researchers have come to appreciate the extensive role that epigenetic regulation plays in the central nervous system. Given these data it has become increasingly clear that transcriptional regulation and neuronal function through epigenetics is a critical component in neurodegenerative disease. At the start of my work, the investigation into the role of LSD1 in neurons and the relationship to AD was ongoing. Our lab had observed that deletion of *Lsd1* in the adult mouse is sufficient to cause neurodegeneration. *Lsd1* deletion mice recapitulate many aspects of human degeneration. In addition to neuronal cell loss, *Lsd1* deletion mice have learning and memory defects, increased gliosis in the brain, and genome-wide transcriptional changes in the hippocampus that highly correlate with AD and FTD patients specifically[173]. Additionally, I showed that the loss of LSD1 was specific to neurons in this system, and showed that LSD1 is not expressed in microglia. Finally, it was shown that LSD1 mislocalizes to NFTs of pathological tau protein in human AD, and TDP-43 inclusions in human FTD-TDP43 cases. These data suggested that mislocalization of LSD1 with these pathologies in the cytoplasm may contribute to neurodegeneration by sequestering LSD1 outside of the nucleus. This would deplete the nuclear pool of LSD1 protein, leading to aberrant transcription and neuronal cell death. For my dissertation, I interrogated this model by focusing on the interaction of LSD1 and tau pathology. Thus the main objectives of this dissertation were to (1) investigate the *in vivo* functional interaction between LSD1 and pathological tau, (2) demonstrate that AD can be targeted therapeutically by manipulating LSD1, and (3) investigate the mechanism of the interaction between LSD1 and pathological tau.

CHAPTER 2:

Materials and Methods

2.1 Solutions and buffers

0.1 M Phosphate buffer

0.2 M Solution A: NaH2PO4 24.0 g/L

0.2 M Solution B: Na2HPO4 28.4 g/L

To 1,000 mL Solution B, add Solution A slowly to bring pH to 7.3 (about 220 mL Solution A).

Dilute 1/2 with diH2O when needed to make 0.1 M

Tail prep buffer

10 mL 1 M Tris-Cl

2 0mL 5 M NaCl

20 mL 0.5 M EDTA

50 mL 10% SDS

900 mL diH2O

1X TBS

7.88 g Tris-Cl

9.0 g NaCl

1,000 mL diH2O

10X Citrate Buffer

2.0 g Citrate Monohydrate

1000 mL diH2O

pH to 6.0 with NaOH

dilute 1:10 for working 1X solution

H20 Brij

1,000 mL of diH2O

2.5 mL of 30% Brij 35 solution (Sigma)

Tris Brij

100 mL 1 M Tris-Cl pH 7.5

100 mL 1 M NaCl

5 mL 1 M MgCl2

2.5 mL 30% Brij 35

797.5 mL diH2O

Tau secret formula

10 mL 1 M Tris-Cl pH 7.5

1.5 mL 1 M NaCl

0.5 mL 1 M MgCl2

88 mL diH2O

2.2 Mouse work

All mouse work was approved by and conducted in accordance with the Emory University Institutional Animal Care and Use Committee

2.2.1 Mouse lines

Lsd1$^{fl/fl}$ mice[98] were crossed to *CAGG-CreERTM*[174], a tamoxifen inducible Cre, to generate *CAGG-CreER*^{TM}*, Lsd1*$^{fl/+}$ mice, which were then intercrossed to produce *CAGG-CreER*^{TM}*, Lsd1*$^{fl/fl}$ mice. This cross also produced *CAGG-CreER*^{TM} negative animals with *Lsd1*$^{fl/fl}$,

which were used as littermate controls in all experiments. The line was maintained by crossing *CAGG-CreER*^{TM} negative, *Lsd1*$^{fl/fl}$ mice with *CAGG-CreER*^{TM}, *Lsd1*$^{fl/fl}$ mice.

Using the same *Lsd1*$^{fl/fl}$ mice we generated *Lsd1*$^{\Delta/+}$ mice that were maintained as heterozygotes. *Lsd1*$^{\Delta/+}$ mice were crossed with PS19 Tau mice[49]. PS19 Tau mice are hemizygous for the P301S mutated form of the human tau protein identified from a human patient. PS19 Tau mice were maintained as hemizygotes. These crosses generated four experimental genotypes: wildtype, *Lsd1*$^{\Delta/+}$, PS19 Tau, and PS19;*Lsd1*$^{\Delta/+}$ mice. Additionally, we maintain a colony of mice that harbor the TDP-43 transgene[175].

We additionally generated a novel mouse line heterozygous for an exon 1 deletion of *Lsd1* (hereafter referred to as *Lsd1*$^{\Delta N/+}$). *Lsd1*$^{\Delta N/+}$ mice were crossed with PS19 Tau mice, generating four experimental genotypes: wildtype, *Lsd1*$^{\Delta N/+}$, PS19 Tau, and PS19;*Lsd1*$^{\Delta N/+}$. PS19;*Lsd1*$^{\Delta N/+}$ mice were crossed with *Lsd1*$^{\Delta N/+}$ mice to generate mice homozygous for the exon 1 deletion of *Lsd1* (hereafter referred to as *Lsd1*$^{\Delta N/\Delta N}$) in the Tau background. These crosses generated five experimental genotypes: wildtype, PS19 Tau, *Lsd1*$^{\Delta N/+}$, PS19;*Lsd1*$^{\Delta N/+}$, and PS19;*Lsd1*$^{\Delta N/\Delta N}$.

2.2.2 Mouse genotyping by PCR

At weaning, a 5 mm piece of mouse tail was removed with a razor blade and digested overnight in a 50 °C water bath with 500 µL tail prep buffer and 5 µL of 20 mg/mL protease K (Ambion). This digest was then phenol/chloroform extracted by adding 500 µL phenol/chloroform and vigorously vortexing followed by separation of the aqueous and organic layers by centrifugation (5 minutes). The 250 µL of the aqueous (top) layer was extracted, brought back up to 500 µL with water, and then re-extracted with 500 µL phenol/chloroform.

The aqueous layer of the second extraction was recovered (400 µL) and DNA was precipitated with ethanol by adding 40 µL of 3 M sodium acetate and 800 µL of ice cold 100% ethanol, followed by inversion. The mixture was then centrifuged at 4 °C for 10 minutes to produce a pellet and the supernatant was discarded. The pellet was washed with 150 µL of 70% ethanol (room temperature) and centrifuged again for 5 minutes, followed by careful removal of the ethanol and allowed to dry at room temperature for 5 minutes and finally reconstituted with water. This DNA served as the template for genotyping PCR reactions.

For genotyping, each PCR reaction contained 3 µL of template DNA diluted either 1/100 (Cre, Tau) or 1/1000 (Lsd1) and 22 µL of PCR reaction mix. Each PCR reaction mix contained 2.5 µL 10X AmpliTaq Gold 360 buffer, 0.5 µL 10mM dNTPs, 1.0 µL each primer (50 µM stock, Table 2-1), 35.0 µL 25mM MgCl2, 0.2 µL AmpliTaq Gold 360 Polymerase and water. The Lsd1genotyping reaction yields two possible products: 483bp for wildtype and289bp for deleted. The Cre genotyping reaction yields a positive control product (250bp) and 320bp product when the Cre transgene is present. The Tau genotyping reaction yields a positive control product (250bp) and 350bp product when the Tau transgene is present. Each genotyping reaction is optimized for the specific primer set. Detailed protocol (reagent concentrations can vary) for each genotyping PCR reaction are in the protocols binder for all mouse work.

2.2.3 Euthanasia and tissue fixation

Mice were given a lethal dose of isoflurane via inhalation, then transcardially perfused with ice cold 4.0% paraformaldehyde in 0.1M phosphate buffer. Brain and spinal cord were dissected and post fixed in cold paraformaldehyde solution for 2 hours. Brain weights and sizes were taken from mice that were euthanized by cervical dislocation. Brain was dissected,

immediately weighed, imaged, and fixed in cold 4.0% paraformaldehyde in 0.1M phosphate buffer overnight. In all cases, tissues were transferred to cold PBS, then serially dehydrated and embedded in paraffin and serially sectioned into 8µm coronal sections.

2.2.4 Quantitative Analysis of Paralysis: Rotarod and Grid Performance

We performed experiments on PS19 Tau, *Lsd1*$^{\Delta/+}$, PS19;*Lsd1*$^{\Delta/+}$ mice at 6, 8, and 10 months. For the rotarod experiments, mice were given two practice trials and then placed on the rotating cylinder at 4 rpm. Rotational speed then gradually increased over a 5-minute test session up to a maximum rotational speed of 40 rpm. Latency to fall off of the accelerating rotarod was used as the dependent variable. We calculated the latency to fall, maximum speed in rotations per minute, and distance traveled. For grid performance, mice were placed on a horizontal grid that was then inverted so mice are hanging upside down by their paws. Mice were videotaped for 10 s, and then scored for forepaw and back paw distance traveled. Mice that could not hold onto grid for 10 s were censored. Investigators were blinded to the genotypes for both experiments.

2.2.5 Mouse magnetic resonance imagining (MRI)

MRI studies were conducted on PS19 Tau, *Lsd1*$^{\Delta/+}$, PS19;*Lsd1*$^{\Delta/+}$ mice at 6 months and 10 months (n=3/genotype). Mice were anesthetized with isoflurane, and monitored for heart rate and temperature changes while anesthetized. MRI measurements were performed using a 9.4 T/20 cm horizontal bore Bruker magnet, interfaced to an AVANCE console (Bruker, Billerica, MA, USA). A two-coil actively decoupled imaging set-up was used (a 2 cm diameter surface coil for reception and a 7.2 cm diameter volume coil for transmission). Axial T2-weighted images were acquired with a RARE (Rapid Acquisition with Refocused Echos) sequence. Its

imaging parameters were as follows: TR = 3000 ms, Eff.TE = 64 ms, RARE factor = 4, field of view (FOV) = 23.04 × 23.04 mm2, matrix = 192 × 192, Avg = 4, slice thickness (thk) = 0.6 mm, number of slice(NSL)=20. Specific emphasis was placed on the neocortex and hippocampus in the coronal images (1.0 – 4.0 mm posterior to the bregma).

2.2.6 Stereotaxic surgery and viral infusion

All surgical procedures were approved by and conducted in accordance with the Emory University Institutional Animal Care and Use Committee. Mice were anesthetized with isoflurane (3% induction, 1-2% maintenance) and administered the analgesic meloxicam (5 mg/kg). Using a Stoeling Quintessential Stereotaxic Injector pump and Hamilton syringe, mice were injected with either the AAV-DJ-LSD1- HA virus, the N-terminally truncated LSD1 construct (AAV-DJ- LSD1ΔN) or the control AAV-DJ- HA virus into both hippocampi. Each virus was injected into the rostral (AP: -2.5, ML:± 2.2, DV: -1.6, relative to bregma) and caudal (AP: -3.1, ML:± 3.0, DV: -3.5) hippocampus of both hemispheres (four injection sites total). Infusion volumes were 0.5 µL per injection site, administered at a rate of 0.15 µL/min. Following surgery, mice were monitored daily for the duration of the experiment. Brains were extracted 3 months post-surgery which allows sufficient time for viral expression. Injection accuracy was confirmed by HA positive staining, and those mice where staining was outside the hippocampus or that did not fully reach hippocampus were censored.

2.2.7 Tamoxifen injections and quantification of *Lsd1* deletion

Each mouse was weighed to determine appropriate dosage for 75.0 mg tamoxifen per kilogram of body mass. Tamoxifen for injections was prepared from a 10 mg/mL in 100%

ethanol stock by vigorously vortexing with 300 µL corn oil for 30 s followed by 1 minute of centrifugation to separate corn oil and ethanol. The ethanol was evaporated off by vacuum centrifugation at 26 room temperature for 15 minutes (Pallas lab vacuum centrifuge). Mice were intraperitoneally injected once a day on days 1, 2, 4, 5, and 7 of a seven day period using a one milliliter syringe with a 25 gauge needle.

Hippocampus, cortex and cerebellum tissues from tamoxifen injected $Lsd1^{CAGG}$ mice were collected at 24 hours after the last injection (hippocampus) and the terminal neurodegeneration phenotype (cortex and cerebellum) and genomic DNA was extracted as described in 2.2.2. Intact *Lsd1* alleles were quantified with qPCR on the Bio-Rad CFX96 Real-Time System using the following primers: *Lsd1* forward: 5' CCAACACTAAAGAGTATCCCAAGAATA-3'; *Lsd1* reverse: 5'-GGTGATTATTATAGGTTCAGGTGTTTC-3'; *Actb* forward: 5'-AGCCAACTTTACGCCTAGCGT-3'; *Actb* reverse: 5'-TCTCAAGATGGACCTAATACGGC-3'. The *Lsd1* reverse primer anneals to exon 6 of Lsd1, which is deleted in $Lsd1^{CAGG}$. Each reaction contained 7.5 µL Bio-Rad iQ Sybr Green Supermix, 1.5 µL of 1/100 diluted forward primer, 1.5 µL of 1/100 diluted reverse primer, 1 µL of 1/20 diluted sample, and water. Starting quantities of intact *Lsd1*alleles were normalized to the amount of *ActB* for each sample to determine the amount of deletion.

2.2.8 Learning and memory testing: Morris water maze and fear conditioning

A cohort of 15 control and 23 Lsd1CAGG mice were tamoxifen injected, and then trained on the Morris water maze 28 days later. Training was carried out in a round, water-filled tub (52 inch diameter). Mice were trained with 4 trials per day for 5 days with a maximum trial length of

60 s and a 15 minute intertrial interval. Subjects that did not reach the platform in the allotted time were manually guided to it. Mice were allowed 5 seconds on the platform to survey spatial cues. Following the 5 day training period, probe trials were performed by removing the escape platform and measuring the amount of time spent in the quadrant that originally contained the escape platform over a 60 s trial. All trials were recorded and performance analyzed by determining the mean values of latency to mount the platform and tracking mice with MazeScan (Clever Sys, Inc.).

Three days after completion of the Morris water maze, the same cohort was subjected to fear conditioning. On Day 1, mice were placed in a fear conditioning apparatus (Colbourn) and allowed to explore for 3 minutes. Following this habituation period, three conditioned stimulus-unconditioned stimulus pairings were presented with a 1 minute intertrial interval. The conditioned stimulus consisted of a 20 s 85db tone and the unconditioned stimulus consisted of a 2 s foot shock that co-terminated with each conditioned stimulus. On Day 2, mice were presented with a context test by placement in Day 1 conditioning apparatus and amount of freezing behavior was recorded by camera and quantified by Colbourn software. On Day 3, subjects were presented with a tone test by exposure to conditioned stimulus in a novel context. Mice were allowed to explore novel context for 2 minutes then presented with the 85db tone for 6 minutes with freezing behavior recorded.

2.3 Staining

2.3.1 Mouse histology and histological quantification

Hematoxylin and eosin staining was performed according to standard procedures. Briefly, sections were dewaxed with xylenes and serial ethanol dilutions then stained with Eosin using

the Richard-Allan Scientific Signature Series Eosin-Y package (ThermoScientific). To derive unbiased estimates of neuronal loss in the hippocampus, the number of primordial neurons in CA1 and CA3 (corresponding approximately to bregma coordinates -2.0 mm and -3.0 mm) were counted from 2 randomly selected regions in the field of a Zeiss Axiophot ocular graticule grid and measured manually using digital micrographs of H&E-stained preparations. Investigators were blinded to the genotype or treatment.

2.3.2 Immunofluorescence and Immunohistochemistry- Mouse

Sections were dewaxed with xylenes and serial ethanol dilutions, then treated with 3% hydrogen peroxide at 40 °C for 5 minutes to quench endogenous peroxidase activity, blocked in 2% serum at 40 °C for 15 minutes, and incubated with primary Ab (Table S1) overnight at 4 °C. Slides were washed, then incubated with biotinylated secondary Ab (Biotinylated Goat α Rabbit, 1:200, Vector Labs BA-1000 or Biotinylated Goat α Mouse, 1:200, Vector Labs BA-9200) at 37 °C for 30 minutes. Signal amplification was then carried out by incubating at 37 °C for 1 hour with Vector Labs Elite ABC reagent (PK-6200). Slides were developed with DAB for 1-5 minutes, counterstained with hematoxylin for 1 minutes, and coverslipped.

For immunofluorescence, dewaxed sections were first rinsed with TBS. Antigen retrieval was performed by microwaving at 10% power 2X for 5 minutes in 0.01 M sodium citrate. Slides were then cooled, washed with TBS, permeabilized in 0.5% Triton X-100 for 20 minutes, followed by blocking in 10% goat serum 20 minutes. Primary Abs (Table S1) were incubated overnight at 4 °C. Slides were then washed and incubated in secondary Abs (Invitrogen A1 1001 and Invitrogen A11012) for 1 hour at room temperature, followed by TBS washes, counterstained with DAPI, and then coverslipped.

2.3.3 Quantification of tau accumulation

For the assessment of tau accumulation, six random sections (sampling from CA1, CA3, and cerebral cortex) per sample were manually counted using digital micrographs of AT8 stained preparations in the field of a Zeiss Axiophot ocular graticule grid. Investigators were blinded to the genotype or treatment. Imagining for immunofluorescence of LSD1 staining was performed on a Yokagawa spinning-disk confocal Nikon-TiE controlled with the software NIS Elements (Nikon). Imaging for all other immunofluorescence staining was performed on an Eclipse Ti2 inverted microscope (Nikon, Toyko, Japan) controlled with the software NIS Elements (Nikon). Image J software ((NIH, http://imagej.nih.gov/ij/) was used for viewing all images.

2.3.4 Immunofluorescence and Immunohistochemistry- Human

All washes and incubations were done on an orbital rotator in mesh tissue culture cups unless noted otherwise. Frozen free floating sections of 40 μm thickness, cut by the Emory Neuropathology and Histopathology core facility, were washed five times for 3 minutes with 0.1 M phosphate buffer to remove cryprotectant. Then, sections were treated with 3.0% H2O2 for 15 minutes to quench endogenous peroxidase activity, and then washed five times for 3 minutes with 0.1 M phosphate buffer, then once with 1X TBS for 3 minutes. Sections were then permeabilized and blocked by incubating in 10μg/mL avidin, 0.1% Triton X-100, and 8% goat serum in 1X TBS for 45 minutes at 4 °C, then washed with 1X TBS three times for 3 minutes. Primary antibodies (Table 2-2) were diluted in 50 μg/mL, 2% goat serum in 1X TBS and incubated with tissues overnight at 4 °C followed by four washes with 1X TBS for 3 minutes. Sections were then incubated with biotinylated goat secondary antibody (Vector Labs BA-1000 and BA-9200) in 2% goat serum in 1X TBS for one hour at 4 °C followed by four 1X TBS

washes for 3 minutes. Signal amplification was performed with Vector Labs Elite ABC reagent, which was prepared by mixing two drops of reagent A and two drops of reagent B with 2.5 mL 1X TBS then incubated on ice for 30 minutes, then brought up to 5.0 mL with 1X TBS prior to treatment of tissue. Sections were incubated with fully prepared ABC reagent for 1 hour at 4 °C, then washed four times with 1X TBS. To detect immunoreactivity, sections were then treated with DAB (Sigma prepared by manufacturer's instructions) for 3-4.5 minutes (until medium brown in color) then moved to four 3 minute 1X TBS washes to stop the reaction. Sections were then mounted on slides by floating them in 0.1 M sodium nitrate then placing them on slides. Slides were then dried overnight and serially dehydrated by incubating (not rotating) in H2O for 3 minutes, 70% ethanol for 3 minutes, twice in 95% ethanol for 3 minutes, twice in 100% ethanol for 3 minutes, then three times in xylenes for 3 minutes, and coverslipped with Permount.

For the peptide block control experiment, the LSD1 primary antibody (Table 2-2) was preincubated for 24 hours at 4°C with 74 fold molar excess of target peptide (Abcam 17763).

For immunofluorescence, sections were prepared as with IHC, except that tissue was incubated with two primary antibodies (Table 2-2), and with two secondary antibodies, fluorescent goat anti-mouse (Invitrogen A11001) and biotinylated goat anti-rabbit (Vector Labs BA-1000). Fluorescent signal amplification of the biotinylated secondary was carried out with Vector Labs Elite ABC reagent as with immunohistochemistry, but developed by incubating with PerkinElmer TSA Plus Cyanine 3 System diluted 1:100 in 0.0015% H2O2, 1X TBS for 10 minutes at room temperature, then washed twice for 3 minutes in 1X TBS. Sections were then mounted as with immunohistochemistry, then air dried for one hour. Slides were incubated with 1X TBS and 20 μL DAPI for 5 minutes, and then rinsed twice with 1X TBS for 5 minutes, then

once with 70% ethanol for 5 minutes. Finally, sections were treated with autofluorescence inhibitor (Millipore 2160) for 5 minutes, then rinsed three times with 70% ethanol for 1 minute and once with 1X TBS for 3 minutes, dabbed on a paper towel to dry, then coverslipped with Prolong.

2.3.5 Quantification of LSD1 colocalization with aggregates

Three random fields per section that contained NFTs marked by pTau at 20X and pTDP-43 inclusions at 40X were manually examined. Beginning with the pTau/pTDP-43 fluorescence channel, each aggregate structure was visually inspected, and then the microscope was switched to the LSD1 fluorescence channel and inspected for LSD1 signal. Structures were scored as positive for LSD1 colocalization if the LSD1 staining pattern was localized to a majority of the aggregate structure. 535 NFTs and 103 pTDP inclusions were scored.

2.3.6 Protein quantification

Protein levels were determined by homogenizing brains in 1 ml/g of tissue in ice-cold lysis buffer (150m M NaCl, 1% Triton X-100, 0.5% Na-deoxycholate, 1% SDS, 50 mM Tris, pH8.0) in a dounce homogenizer, followed by end-over-end spin at 4 °C for 2 hours, and centrifugation at 20,000 x g for 20 minutes at 4 °C. Protein concentrations were determined following standard BCA protocol (Pierce BCA Protein Assay Kit). Equal amounts of protein for each sample were loaded and run on a 12% SDS-PAGE gel, transferred (Semi-dry transfer using BIO RAD Trans-Blot Turbo Transfer System), blocked in 5% BSA, and probed with primary Ab (Table S1) over night at 4 °C. Blots were rinsed and stained with HRP-conjugated secondary Ab,

and detected by chemiluminescence using ChemiDoc MP Imaging System (BIO RAD). Protein levels were normalized using total protein calculated using BIO RAD ImageLab software.

2.3.7 TUNEL assay

Frozen embedded brain tissue was sectioned at 12μm thickness on a cryostat, and then washed for 30 minutes in PBS. Slides were permeabilized in 0.1% Triton X-100, 0.1% sodium citrate for 2 minutes followed by two 2 minute washes in PBS. For antigen retrieval, slides were microwaved in a coplin jar for 1 minute at 10% power in preboiled 0.1M sodium citrate then rapidly cooled by adding deionized water then pouring off the buffer, repeating this twice. Slides were then washed in PBS for 2 minutes and blocked for 30 minutes at room temperature in 0.1M Tris, 3.0% BSA, 10% goat serum. Slides were washed twice with PBS for 2 minutes then incubated with 50μL (5μL enzyme and 45μL labeling reagent) of TUNEL labelling solution (Roche In situ Cell Death Detection Kit, Fluorescein) for 1 hour at 37°C in a humidity chamber. Slides were then washed three times with PBS, the second containing 20 μL DAPI, then dabbed dry with a paper towel and coverslipped.

2.4 RNA sequencing

2.4.1 RNA isolation

Mice were euthanized by cervical dislocation, hippocampi were dissected and snap frozen with liquid nitrogen in 1mL Trizol, and stored at -80°C. For RNA isolation, samples were thawed at 4°C then kept on ice prior to homogenization with Polytron homogenizer with a 5 second pulse. After a 5 minute incubation at room temperature, one tenth the sample volume of 1-bromo-3chloropropane was added, mixed by inversion and incubated for 3 minutes at room

temperature. Samples were then centrifuged at 13,000 X g for 15 minutes at 4°C to separate the aqueous and organic layers. As much of the aqueous layer was recovered as possible, then RNA was precipitated with isoproponal. Pellets were then washed with 75% ethanol and resuspended in 50µL of dionized water.

RNA library preparation and sequencing were performed by HudsonAlpha Genomic Services Lab. RNA was Poly(A) selected and 300bp size selected. Libraries were sequenced for 25 million 50bp paired end reads. All RNA-seq FASTQ files will be uploaded to Gene Expression Omnibus (GEO).

2.4.2 RNA sequencing analysis

The RNA sequencing data described in Chapter 3 were analyzed as follows: Short read FASTQ files were quality trimmed using FASTX toolkit (v. 0.0.14) to trim three bases from the 5' end of the reads. Paired-end reads were then mapped to the mm9 genome using tophat2[175,176] and the UCSC knownGene gtf file. The following parameters were used in the tophat2 call "-N 1 –g 1 –read-gap-length 1 –mate-inner-dis 170". Reads that had the same starting location and strand with mate-pairs that also had the same location and strand were considered to be PCR duplicates and removed from subsequent analyses using Picard tools (v.1.103). Differentially expressed transcripts were determined using Cufflinks and Cuffdiff (v2.1.1)[177]. Downstream analyses were performed in R/Bioconductor[178] and used gene summarized expression levels normalized using Fragments Per Kilobase per Million (FPKM) from Cufflinks. Hierarchical clustering was performed using the pvclust R package were significance was determined using bootstrapping[179]. Principle Components Analysis (PCA) was conducted using the "prcomp" function of the stats package in R/ Bioconductor. Enriched gene ontologies were determined

using the package "GOstats" (v. 3.1.1)[180]. Gene Set Enrichment Analysis (GSEA) was performed using a pre-ranked gene list determined by cuffdiff test statistic and GSEA (v. 2.1.0)[181]. Hierarchical clustering of gene expression data was performed using average clustering in the heatmap.2 package. UCSC-style display of gene expression data were plotted using the "rtracklayer" package[182] and custom R scripts as previously described[183].

The RNA sequencing data described in Chapter 4 were analyzed as follows: The sequencing data were uploaded to the Galaxy web platform, *and* we used the public server at *usegalaxy.org* to analyze the data [184,185]. FASTQ files were quality assessed using FASTQC (v.0.11.7), trimmed using Trimmomatic (v.0.36.5) and minimum QC score of 20 and minimum read length of 36bp. Paired-end reads were subsequently mapped to the GRCm38 genome using HISAT2 (v.2.1.0). Unmapped, unpaired and multiply mapped reads were removed using Filter SAM or BAM (v.1.1.2). Assignment of transcripts to GRCm38 genomic features was performed using Featurecounts (v.1.6.0.6) and the Ensembl GRCm38.93 gtf file. Differentially expressed transcripts were determined using DESEQ2 (v.2.11.40.2) [185]. For all datasets, a cutoff of adjusted p-value < 0.3 and abs ($\log_2$ fold change) > 0.58 was applied. TPM values were calculated from raw data obtained from Featurecounts output. Subsequent downstream analysis was performed using R and normalized counts and adjusted P-values from DESEQ2 (v.2.11.40.2). Heatmaps were produced and hierarchical clustering was done using the gplots package (v. 3.0.1) and normalized counts [186]. Volcano plots were produced using the enhanced volcano package (v.0.99.16) and adjusted p-values [187]. Additionally, Gene Set Enrichment Analysis (Pre-ranked list) was performed using the online platform WebGestalt [188-191]. Custom R-scripts available upon request.

2.4.3 Comparison to human gene expression data

Normalized gene expression data from late onset Alzheimer's disease (LOAD)[192], frontal temporal dementia (FTD)[193] and Parkinson's disease (PD)[194] patients were downloaded from Gene Expression Omnibus gene sets GSE44772, GSE13162 and GSE20295, respectively. Comparison to *Lsd1*^{CAGG} gene expression data was performed by mapping mouse and human genes using the NCBI homologene database (Wheeler et al., 2001). Correlation of *Lsd1*^{CAGG} gene expression changes and those found in LOAD, FTD and PD patients were assessed using Spearman's rank correlation (ρ). P-values were determined by analysis of variance (ANOVA).

Lsd1	Forward	5'-GCACCAACACTAAAGAGTATCC-3'
	Reverse	5'-CCACAGAACTTCAAATTACTAAT-3'
Cre transgene	Forward	5'-GAACCTGATGGACATGTTCAGG-3'
	Reverse	5'-AGTGCGTTCGAACGCTAGAGCCTGT-3'
Tau transgene	Forward	5'-GGGGACACGTCTCCACGGCATCTCAGCAATGTCTCC-3'
	Reverse	5'-TCCCCCAGCCTAGACCACGAGAAT-3'
Cre and Tau control	Forward	5'-TTACGTCCATCGTGGACAGC-3'
	Reverse	TGGGCTGGGTGTTAGCCTTA-3'
Lsd1ΔN deletion	Forward	5'-GATATGCTGGGTCGCACTCC-3'
	Reverse	5'-GTAGACAAACGCGTCGGGAA-3'
Lsd1ΔN control	Forward	5'-GCCCATGGAGACCGGAATA-3'
	Reverse	5'-CACACAGGTAGACAAACGCG-3'
TDP-43	Forward	5'- GGATGAGCTGCGGGAGTTCT-3'
	Reverse	5'- TGCCCATCATACCCCAACTG-3'
TDP-43 control	Forward	5'-CAAATGTTGCTTGTCTGGTG-3'
	Reverse	5'- GTCAGTCGAGTGCACAGTTT-3'

Table 2-1 Genotyping Primers

Mouse genotyping for the Cre transgene and floxed or deleted allele, and the tau transgene of Lsd1 were performed with the listed primers. Lyopholized stocks were reconstituted to 50μM. Forward and Reverse primers are mixed together in equal parts. The Cre Forward, Cre Reverse, Cre Control Forward and Cre Control Reverse were mixed together in equal parts prior to use in the PCR reaction.

Target	Manufacturer	Clone	Lot number	Experiment	Dilution
NeuN	Millipore MAB377	A60	2392283	Mouse IF	1:500
LSD1	Abcam 17721		GR3193508-2	Mouse IF	1:100
				Mouse IHC	1:500
				Human IF	1:500
				Human IHC	1:500
PHF-Tau	ThermoFisher MN 1020	AT8	TI2611431	Mouse IHC	1:1,000
		AT8	TI2611431	Mouse IF	1:200
HA	Abcam ab130275	16B12	GR3190856-12	Mouse IHC	1:500
		16B12	GR3190856-12	Mouse IF	1:100
HA	Abcam ab9110		GF3224022-1	Mouse IF	1:500
GFAP	Dako	Z0334	20047046	Mouse IHC	1:100
IBA1	Synaptic System 234004		2-16	Mouse IF	1:100
Neurofilament (phospho)	Millipore NE1022	SMI-31R		Mouse IHC	1:500
PHF-1	Peter Davies (Albert Einstein College of Medicine, NY)			Mouse IHC	1:1,000
LSD1	Cell Signaling 2139		5	Immunoblot	1:1,000
TLR2	Abcam ab9100	TL2.1	GR3189369-7	Mouse IF	1:100
pTDP-43	Cosmo Bio TIP-PTD-P02			Human IHC	1:1,000
				Mouse IHC	1:4,000
PTDP-43	Cosmo Bio TIP-PTD-P02			Human IF	1:1,000
α- synuclein	J. Trojanowski and V. Lee (University of Pennsylvania, PA)			Human IHC	1:10,000
MAP2	Chemicon	AB5622		Mouse IHC	1:500
Tau	Accurate	BYA10741		Mouse IHC	1:200
SV2	DSHB2	SV2		Mouse IHC	1:500
Aβ	Signet	9220-02		Mouse IHC	1:1,000
KLF4	R&D Systems	AF3158		Mouse IHC	1:100
c-MYC	Santa Cruz	SC-40		Mouse IHC	1:100
OCT-4	BD Transduction Labs	611202		Mouse IHC	1:300
FOXO-1	Santa Cruz	SC-11350		Mouse IHC	1:100
PCNA	Santa Cruz	SC-56		Mouse IHC	1:250
HS310P	Active Motif	39254		Mouse IHC	1:1,000
NESTIN	Abcam	Ab11306		Mouse IHC	1:1,000
VIMENTIN	Dako	M072529-2		Mouse IHC	1:50
MBP	Millipore	MAB386		Mouse IHC	1:100

Table 2-2 Primary Antibodies

Primary antibodies for immunohistochemistry and immunofluorescence staining experiments are given. Also listed are the manufacturer and catalog number, experiment and dilution used.

CHAPTER 3:

LSD1 Protects Against Hippocampal and Cortical Neurodegeneration

Michael A. Christopher, Dexter A. Myrick, Benjamin G. Barwick, Amanda K. Engstrom, Kirsten A. Porter-Stransky, Jeremy M. Boss, David Weinshenker, Allan I. Levey and David J. Katz

This Chapter was published in Nature Communications in October 2018.

Citation: Nature Communications 2017;8(1):805

DOI: 10.1038/s41467-017-00922-9

As an author on this publication I was involved in the overall conceptual design of the project and completion of the manuscript resulting in its publication. Some specific experiments include characterization of LSD1 in glial cells and cell autonomy experiments.

3.1 Abstract

To investigate the mechanisms that maintain differentiated cells, we inducibly deleted the histone demethylase LSD1/KDM1A in adult mice. Loss of LSD1 leads to paralysis, along with widespread hippocampus and cortex neurodegeneration, and learning and memory defects. Here, we focus on the hippocampus neuronal cell death, as well as the potential link between LSD1 and human neurodegenerative disease. We find that loss of LSD1 induces transcription changes in common neurodegeneration pathways, along with the reactivation of stem cell genes, in the degenerating hippocampus. These data implicate LSD1 in the prevention of neurodegeneration via the inhibition of inappropriate transcription. Surprisingly, we also find that transcriptional changes in the hippocampus are similar to Alzheimer's Disease (AD) and Frontotemporal Dementia (FTD) cases, and LSD1 is specifically mislocalized to pathological protein aggregates in these cases. These data raise the possibility that pathological aggregation could compromise the function of LSD1 in AD and FTD.

3.2 Introduction

LSD1/KDM1a (hereafter referred to as LSD1) is an amine oxidase histone demethylase. In conjunction with the CoREST complex, it specifically demethylates mono- and di-methylation of lysine 4 on histone H3 (H3K4me1/2), but not H3K4me3[84,155]. Alternatively, when associated with the Androgen Receptor complex, LSD1 has been shown to demethylate H3K9me2[157]. LSD1 homozygous mutant mice arrest at embryonic day 5.5 and fail to properly elongate the egg cylinder, before being resorbed by embryonic day 7.5[98,162]. In addition, loss of LSD1 results in olfactory receptor choice[166] and circadian rhythm defects[195] when conditionally deleted in mice, along with defects in plasma cell[196] and hematopoietic differentiation[197] *in vitro,* and pituitary[98],

hematopoietic stem cell[198] and trophoblast stem cell[199] differentiation defects *in vivo.* These defects, along with developmental phenotypes in yeast[196], *Arabidopsis*[200], *Drosophila*[160,201] and *C. elegans*[159], indicate that LSD1 may function during changes in cell fate. For example, in mouse embryonic stem cells (ES cells), LSD1 binds to the promoter and enhancers of the critical stem cell genes, *Oct4, Sox2, Klf4* and *Myc*[165]. Upon differentiation, LSD1 is required to remove H3K4me1 to repress the transcription of these stem cell genes and enable proper ES cell differentiation[165]. Similarly, LSD1 has also been implicated in regulating stem cell gene transcription during the differentiation of hematopoietic stem cells[198].

Although LSD1 has many roles throughout development, little is known about its function in differentiated cells. However, one hint comes from studies of the LSD1-containing CoREST complex, which has been implicated in the maintenance of cell fate by repressing the transcription of neuronal genes in non-neuronal cell types[202,203]. Based on this finding, we hypothesized that LSD1 may function similarly in the maintenance of other differentiated cell types. To address this possibility, we inducibly deleted *Lsd1* in adult mice. Loss of LSD1 leads to paralysis, along with widespread neuronal cell death in the hippocampus and cortex, and associated learning and memory deficits. Here we have chosen to focus on the function of LSD1 in preventing hippocampus neurodegeneration, and the potential link to human neurodegenerative disease. In the degenerating hippocampus, we detect transcriptional changes in pathways implicated in human neurodegeneration. This suggests that LSD1 may prevent neuronal cell death by repressing common neurodegenerative pathways. In the degenerating neurons, we also detect the inappropriate expression of stem cell genes. This indicates that LSD1 may be part of an epigenetic maintenance program that continuously prevents inappropriate transcription. Surprisingly, we also find that LSD1 mislocalizes with pathological aggregates

specifically in Alzheimer's Disease (AD) and Frontotemporal dementia (FTD) cases, and the genome-wide transcriptional changes in the degenerating *Lsd1* hippocampus specifically correlate with those found in AD and FTD cases. These data raise the possibility that LSD1 function could be affected in these dementias.

3.3 Results

3.3.1 LSD1 is continuously required to prevent neurodegeneration

To determine if LSD1 is required in terminally differentiated cells within the brain, we inducibly deleted *Lsd1* in adult mice by crossing floxed *Lsd1* mice[98,163,166,204,205] to the *Cagg-Cre* tamoxifen inducible *Cre* transgene[174,206-209] (hereafter referred to as $Lsd1^{CAGG}$). LSD1 is expressed widely in the mouse brain. Specifically, immunofluorescence detected LSD1 protein in the nuclei of NeuN positive neurons throughout the brain, including the hippocampus and cerebral cortex (Figure 3-1a-l). LSD1 protein is also present in astrocytes (Figure 3-2a-d, i-l) and oligodendrocytes (Figure 3-3a-d, i-l, q-t), but not microglia (Figure 3-4a-h). Tamoxifen injection in $Lsd1^{CAGG}$ animals resulted in the widespread loss of LSD1 protein in hippocampal and cerebral cortex neurons between 4 and 9 weeks after the final injection (Figure3-5a-d). However, surprisingly, at this time point LSD1 protein remained unchanged in astrocytes (Figure 3-2e-h, m-p) and oligodendrocytes (Figure 3-3e-h, m-p, u-x) throughout the brain. Thus, within the brain, LSD1 loss is confined to neurons. As a result, $Lsd1^{CAGG}$ animals enable us to interrogate the result of losing LSD1 specifically in these neurons.

We do not observe any defects in non-tamoxifen-injected *Cre* positive $Lsd1^{CAGG}$ mice, nor in tamoxifen-injected *Cre* minus $Lsd1^{CAGG}$ littermate controls (hereafter used as controls in all subsequent experiments). However, all (n = 45) tamoxifen-injected $Lsd1^{CAGG}$ mice developed

a severe motor deficit between 4 and 9 weeks after deletion, characterized initially by weakness in the hindlimbs followed by weakness in the forelimbs. These deficits are associated with hindlimb clasping, failure to maintain body posture, docile behavior, an inability to keep eyes open and ultimately, death (Figure 3-5e-g showing the terminal phenotype used in subsequent assays). Development of this motor defect occurred rapidly, with generally one week elapsing between initial onset and full defect. Importantly, the full motor defect occurred within 4 to 9 weeks after tamoxifen injection regardless of age at *Lsd1* deletion (Figure 3-5g). This suggests that LSD1 is required throughout adulthood to protect against the development of these deficits. Though both males and females ultimately exhibit the motor defect, the number of days after tamoxifen injection to reach the terminal motor phenotype was longer in males compared to females (Figure 3-5g inset). It is unclear at the moment why there is a small sex specific difference in the timing of this defect.

To investigate this phenotype further, we examined the spinal cords, neuromuscular junctions, muscles, and brains of $Lsd1^{CAGG}$ mice. Mutant spinal cords appeared morphologically normal and the number of motor neurons in the spinal cord did not significantly differ from control littermates (Figure 3-6a,b). We also did not detect any defects in the morphology of neuromuscular junctions, or in myelination of the spinal cord (Figure 3-6c-f). Upon examination of limb muscles, we observed severe atrophy in the soleus muscle, as indicated by the much smaller diameter of the muscle cells, and moderate atrophy of the tibialis anterior muscle (Figure 3-6g-j). However, we did not find any evidence of muscle degeneration, suggesting the motor defect is not due to complications in muscles.

Although we do not detect degeneration in the spinal cord or hind limb muscle, we find widespread severe neurodegeneration in the hippocampus and cerebral cortex of $Lsd1^{CAGG}$ mice

(Figure 3-5h,i). As a result, we have initially focused here on the function of LSD1 in preventing this neurodegeneration. Within the hippocampus, many neuronal nuclei of the CA1, CA3, dentate gyrus, and cerebral cortex were pyknotic, and displayed a corresponding loss of the dendrite marker MAP2, as well as the axon marker Tau (Figure 3-5j-s). Of these hippocampal regions, the CA1 was the most affected with 77.3±5.2% pyknotic nuclei (average with s.e.m.), while the CA2 and CA3 were moderately affected (Figure 3-7a,b). Within individuals, the percent of condensed nuclei in all regions of the hippocampus was higher in the posterior of the brain and less affected anteriorly (Figure 3-7c-f). Between individuals, the dentate gyrus was more variably affected, with the nuclei sometimes being completely pyknotic, completely unaffected, or intermediately affected (Figure 3-5n,o and Figure 3-7g-j). In addition, we consistently observed pyknotic neuronal nuclei in the cerebral cortex, amygdala, thalamus and motor cortex, though the effect in the amygdala and thalamus was less severe than the hippocampus or cortex. (Figure 3-5h,i,p,q and Figure 3-7k-r). Within the cerebral cortex, most of the pyknotic nuclei were typically found in layers II/III, IV and VI (Figure 3-7k,l). It is possible that the neurodegeneration in the motor cortex contributes to the observed paralysis phenotype. However, at the moment it is not possible to determine definitively if this is the case. Finally, in the cerebral cortex of *Lsd1*^{CAGG} mice, and to a lesser extent in the hippocampus, we observed a strong reactive gliosis response (Figure 3-5t-w), an effect previously associated with neuronal distress[69].

To confirm that the pyknotic nuclei in the hippocampus and cortex of *Lsd1*^{CAGG} mice have undergone cell death, we performed TUNEL. Nearly every pyknotic nucleus exhibited positive TUNEL staining, indicating that they were undergoing or had undergone cell death (Figure 3-5x-aa). Also, the neuronal cell death was observed at the terminal phenotype regardless

of the age of the mice when *Lsd1* was inducibly deleted. These data indicate that LSD1 is continuously required for the survival of hippocampal and cortex neurons.

Immunohistochemistry verified that LSD1 protein is lost in the degenerating neurons of $Lsd1^{CAGG}$ mice. Specifically, LSD1 was undetectable in most cortical nuclei and nearly all hippocampal nuclei, including all of the pyknotic nuclei in both regions (Figure 3-5a-d). In contrast, LSD1 persisted in the remaining normal uncondensed nuclei within these brain regions (Figure 3-5b,d and Figure 3-8a-d). The reciprocal relationship between LSD1 protein and pyknotic nuclei indicates that the neuronal cell death is likely due to the cell autonomous loss of LSD1. To confirm that hippocampal neurodegeneration is cell autonomous, we also induced deletion of *Lsd1* in $Lsd1^{CAGG}$ mice using a single low dose tamoxifen injection. In contrast to the widespread LSD1 protein loss that we observe in the hippocampus with multiple higher dose tamoxifen injections (Figure 3-8a-d), 10 weeks after tamoxifen injection the low dose injection resulted in the loss of LSD1 protein in only a small number of neurons within the hippocampus (Figure 3-8e-f). Nevertheless, the few neuronal nuclei that lack LSD1 still become pyknotic, indicating that they have undergone neurodegeneration (Figure 3-8e-f). These results suggest that within the hippocampus, the neuronal cell death is cell autonomous.

Despite the severe neurodegeneration of the hippocampus and cortex in $Lsd1^{CAGG}$ mice, the cerebellum appeared normal. This can be seen, for example, by the absence of pyknotic nuclei and the normal distribution of the dendrite marker MAP2 (Figure 3-9a-d). To determine whether the lack of neuronal cell death in this region could be due to the failure of *Lsd1* deletion there, we performed quantitative PCR to assess the extent of remaining undeleted *Lsd1* in different brain regions. This analysis demonstrated high levels of deletion in the hippocampus and to a lesser extent in the cerebral cortex. However, there was very little *Lsd1* deletion in the

cerebellum (Figure 3-9g). Overall, the extent of deletion matches the level of remaining LSD1 protein in each brain region at the terminal stage, with very little LSD1 in the hippocampus, low levels of LSD1 in the cortex, and higher levels of LSD1 in the cerebellum (Figure 3-5a-d and Figure 3-9e,f). This distribution suggests that the brain region specificity of the neurodegeneration in *Lsd1*^{CAGG} mice may be due to the specificity of *Lsd1* deletion. Notably, though *Lsd1* deletion in the hippocampus occurred within the first 24 hours after tamoxifen injection (Figure 3-9g), the loss of LSD1 protein in the hippocampus occurred much later. For example, in the hippocampi of mice just beginning to display hindlimb weakness (approximately one week before the terminal phenotype) we observed some remaining LSD1 immunoreactivity and far fewer pyknotic nuclei (Figure 3-9h,i). This indicates that there is slow RNA or protein turnover in hippocampal neurons, a finding that is consistent with the continuous requirement for LSD1 in these cells.

Many previous mouse models of neurodegeneration display moderate levels of neuronal loss over an extended period of time (many months)[49,210], so the extent of neuronal cell death that we observed in *Lsd1*^{CAGG} mice within nine weeks was striking. Therefore, we considered the possibility that LSD1 is generally required for cell viability. If this were the case, deletion of *Lsd1* throughout the mouse would be expected to result in a similar disruption in other organs and cell types. To address this possibility, we examined the liver and kidneys of terminal *Lsd1*^{CAGG} mice using dual IF. Hepatocytes and nephron epithelial cells lacking LSD1 appeared morphologically normal (Figure 3-10a-l). Additionally, Purkinje neurons lacking LSD1 in the cerebellum did not display any morphological signs of cell death despite the absence of LSD1 (Figure 3-9e,f). Taken together, these data suggest that LSD1 is not required for general cell viability. This conclusion is consistent with what has been reported in the literature

elsewhere[98,165-167,197-199]. Thus, the continuous requirement for LSD1 to prevent neuronal cell death in the hippocampus and cortex appears to be specific to these neurons.

3.3.2 Loss of LSD1 results in learning and memory defects

To determine, whether LSD1-dependent neurodegeneration leads to learning and memory deficits, we assessed female *Lsd1*^{CAGG} mice in the Morris water maze and fear conditioning assays, 28 days after tamoxifen injection (prior to the onset of motor defects). Compared to littermate controls, *Lsd1*^{CAGG} mice had significant defects in the latency to mount the platform in the water maze assay on Day 5 (Figure 3-11a). This is despite the fact that *Lsd1*^{CAGG} mice swam at speeds not significantly different than their littermate controls (Figure 3-12a). Also, on Day 5, there is an increase in overall distance traveled as *Lsd1*^{CAGG} mice swim randomly rather than locating the platform (Figure 3-12b). Together these results suggest that the impaired performance of *Lsd1*^{CAGG} mice in the water maze is not due to motor deficits. On Day 6, when the platform was removed, controls spent nearly half of their time swimming in the platform quadrant, while *Lsd1*^{CAGG} mice spent approximately equal time swimming in each of the four quadrants (Figure 3-11b). These data suggest that *Lsd1*^{CAGG} mice have reduced spatial learning and reference memory capacity. *Lsd1*^{CAGG} mice were also impaired in contextual fear conditioning, spending less time freezing (30.0±8.3% average with s.e.m.) compared to controls (47.9±4.5% average with s.e.m.) (Figure 3-11c). The contextual fear conditioning was reduced in *Lsd1*^{CAGG} mice at all points, and this reduction was statistically significant at 120,180 and 360 seconds (Figure 3-11c). However, *Lsd1*^{CAGG} mice froze normally in response to a conditioned tone during cued fear conditioning (Figure 3-11d). These data suggest that *Lsd1*^{CAGG} mice have defects in contextual, but not cued, learning and memory. This specificity is consistent with the

observed pattern of neuronal cell death in the brains of these mice. Notably, though we do not detect any evidence of visual impairment, it is possible that a slight defect in visual impairment also contributes to the deficit observed in the water maze and contextual fear conditioning assays.

3.3.3 LSD1 inhibits reactivation of stem cell transcription

Previous work has implicated the LSD1 containing CoREST complex in repressing neuronal genes in non-neuronal cell types[202,203]. This raised the possibility that LSD1 may be functioning similarly in terminally differentiated hippocampal neurons to block the expression of genes associated with alternative cell fates. To test this possibility, we examined hippocampal gene expression changes in terminal *Lsd1*^{CAGG} mice by RNA-seq. At this terminal stage, there was no difference in the number of pyknotic nuclei in *Lsd1*^{CAGG} mutants versus the number of normal nuclei in unaffected controls, indicating that neurons in *Lsd1*^{CAGG} were actively undergoing neuronal cell death, but not yet cleared (Figure 3-13a). Comparison of global gene expression by unsupervised hierarchical clustering and principle components analysis in two *Lsd1*^{CAGG} mutants and two tamoxifen-injected *Cre* minus littermate controls, showed that the expression states were similar between biological replicates, but different between *Lsd1*^{CAGG} mutants and controls (Figure 3-13b,c). Also, analysis of differentially expressed genes between *Lsd1*^{CAGG} mutant and control hippocampi revealed more significantly upregulated (281) than significantly downregulated (124) genes (Figure 3-13d,e, FDR < 0.05).

LSD1 has previously been shown to repress the expression of several critical stem cell genes during differentiation in multiple stem cell populations[165,197,199]. Therefore, we hypothesized that LSD1 may also be continuously required in terminally differentiated neurons

to repress the transcription of stem cell genes to block the re-initiation of a stem cell fate. To address this possibility, we examined the expression of stem cell genes in our *Lsd1*^{CAGG} hippocampus RNA-seq dataset. Remarkably, three pluripotency genes (*Klf4, Myc,* and *Foxo1*), two of which are induced pluripotent stem cell (iPSC) factors[211], were amongst the most significantly upregulated genes in *Lsd1*^{CAGG} mice (Figure 3-14a-c). Immunohistochemistry (IHC) analysis confirmed that KLF4 and FOXO1 proteins were reactivated widely in the degenerating pyknotic neurons, as well as in some of the remaining non-condensed nuclei, but not in controls (Figure 3-14e,f,i,j). In contrast, c-MYC was reactivated only in a few nuclei (Figure 3-14g,h). Therefore, to confirm that these c-MYC positive cells are neurons, we performed dual IF with the neuronal marker NeuN. This analysis confirmed that c-MYC is reactivated in neuronal nuclei (Figure 3-15a-h). Interestingly, although we did not observe increased *Oct4* expression in our RNA-seq dataset (Figure 3-14d), one out of four mice analyzed displayed reactivation of OCT4 protein throughout the pyknotic hippocampal nuclei (Figure 3-14k,l). This expression pattern appeared to be specific, as it was not observed in any of the controls or in other brain regions of the affected animal. These results suggest that LSD1 is continuously required to repress the inappropriate expression of stem cell genes in hippocampal neurons.

Amongst the most highly activated genes in our RNA-seq dataset we also noticed the up regulation of the neuronal stem cell genes *Vimentin* and *Nestin* (Figure 3-15i,j). To determine whether VIMENTIN and NESTIN may also be reactivated in the dying neurons of *Lsd1*^{CAGG} mice, we performed IHC to detect the expression of these proteins. IHC detected VIMENTIN protein in a subset of hippocampal neurons, though at a higher frequency in *Lsd1*^{CAGG} mice than controls, while NESTIN protein is found in the reactive glia of the *Lsd1*^{CAGG} hippocampus and cortex (Figure 3-15k-p).

3.3.4 Loss of LSD1 induces common neurodegenerative pathways

To identify additional pathways associated with the hippocampal neuronal cell death, we also performed gene ontology (GO) and Gene Set Enrichment Analysis (GSEA) on our RNA-seq datasets. Amongst the pathways that are affected by the loss of LSD1, we observed the upregulation of inflammatory response genes and complement cascade genes, along with the downregulation of oxidative phosphorylation genes and genes involved in neurotransmission (ion transport) (Figure 3-13f,g). All four of these pathways have been previously linked to neurodegeneration. For example, several studies have implicated the inflammatory response pathway in neurodegeneration. Activation of the inflammatory response pathway could contribute to neurodegeneration via macrophage mediated phagocytosis[212]. There is also evidence linking the complement cascade pathway to neurodegeneration. Activation of the complement cascade pathway could lead to neuronal cell death through axonal pruning[213]. In addition, impaired neurotransmission could contribute to neuronal cell death through the loss of electrical potential[214]. Finally, a defect in oxidative phosphorylation, with the accompanying mitochondrial dysfunction, could lead to neurodegeneration via the generation of reactive oxygen species[215]. To determine the extent that these four neurodegeneration-associated pathways are misregulated in our *Lsd1*^{CAGG} hippocampus RNA-seq, we plotted the enrichment of these gene sets in our dataset for each of these four pathways. This analysis demonstrated that all four of these common neurodegeneration pathways are highly affected (Figure 3-16a-d). Importantly, while each of these pathways has been implicated in neurodegeneration, it is difficult to determine whether these pathways contribute to neuronal cell death, or whether they may simply be a consequence of the neurodegeneration.

3.3.5 *Lsd1*^{CAGG} gene expression changes overlap with AD and FTD cases

The common neurodegeneration pathways affected by loss of LSD1 are also affected in human neurodegeneration patients. For example, systems biology approaches in human late onset Alzheimer's Disease (LOAD) brains have identified a critical microglia and immune transcription network upregulated in AD cases[192]. Interestingly, we noticed that many genes in the LOAD microglia and immune gene signature, including the critical receptor *Tyrobp*, are highly enriched in the *Lsd1*^{CAGG} hippocampus. Also, many of these microglia and immune genes are amongst the 281 most significantly upregulated genes in our RNA-seq dataset. Therefore, to determine if the LOAD microglia and immune response module is similarly misregulated in our mice, we compared the expression changes in the *Lsd1*^{CAGG} hippocampus to previously published expression changes at orthologous loci in LOAD cases[192]. This analysis demonstrated that loss of LSD1 in the mouse hippocampus leads to microglia and immune response gene expression changes that are highly similar to those that occur in the prefrontal cortex of LOAD cases. The microglia and immune expression changes in the *Lsd1*^{CAGG} hippocampus also highly overlap with those that occur in the frontal cortex of FTD cases with progranulin mutations (FTD-progranulin)[193] (Figure 3-16e,f).

Surprisingly, a similar correlation with AD and FTD cases is also found with the other neurodegeneration pathways that are misregulated in our RNA-seq dataset. For example, in the Kyoto Encyclopedia of Genes and Genomes (KEGG) complement cascade genes, expression changes in the *Lsd1*^{CAGG} hippocampus highly overlap with the upregulation that occurs in the prefrontal cortex of AD and FTD cases (Figure 3-16g,h). A correlation is observed in pathways that are downregulated in the *Lsd1*^{CAGG} hippocampus as well. For example, we find a large overlap with expression changes in the neurotransmission genes (Synaptic Transmission

Module) that were also identified using systems biology approaches in LOAD cases (Figure 3-16k,l)[192]. Similarly, we observe a high correlation with the transcriptional changes in oxidative phosphorylation genes (Figure 3-16,j).

Finally, amongst the top upregulated genes in the *Lsd1*^{CAGG} hippocampus we noticed the cell cycle gene *PCNA* (Figure 3-16m). Evidence for the potential re-initiation of the cell cycle has been found in AD cases[216]. Therefore, to determine if PCNA, and other cell cycle markers, are being reactivated in degenerating *Lsd1*^{CAGG} neurons, we performed IHC analysis. This analysis confirmed the reactivation of PCNA protein, along with that of another cell cycle marker, H3S10p, specifically in the remaining non-pyknotic hippocampal nuclei (Figure 3-16n-q). Intriguingly, the observation that c-MYC, PCNA and H3S10p were reactivated predominantly in the remaining uncondensed nuclei of the *Lsd1*^{CAGG} hippocampus raises the possibility that these neurons may be attempting to re-initiate the cell cycle prior to neuronal cell death.

The high degree of overlap within multiple neurodegeneration pathways between *Lsd1*^{CAGG} mice and human dementia cases was unexpected. Thus, we considered the possibility that the expression changes in our mice might overlap more broadly with AD and FTD cases. To address this possibility, we next compared the expression changes in the *Lsd1*^{CAGG} hippocampus with the expression changes in AD and FTD cases genome-wide. Remarkably, we found that the genome-wide expression changes in the prefrontal cortex of LOAD cases highly correlate with the expression changes in the hippocampus of *Lsd1*^{CAGG} mice (Figure 3-17a). Likewise, the correlation was highly significant when compared to the frontal cortex of FTD-progranulin (Figure 3-17b).

The genome-wide correlation in expression changes with AD and FTD cases could indicate the possible involvement of LSD1 in these diseases. However, it is also possible that the overlap is being primarily driven by the consequences of neuronal cell death. To address this second possibility we compared the expression changes in the *Lsd1*^{CAGG} hippocampus with other neurodegenerative diseases that have similar levels of neuronal cell death. If the genome-wide correlation is being driven by a common underlying mechanism, rather than neuronal cell death, we would expect the correlation to be less significant in these comparisons. Importantly, we observe relatively little overlap with the expression changes in the substantia nigra of Parkinson's disease (PD), a region with extensive neuronal cell death (Figure 3-17c)[194]. We also see relatively little overlap with the expression changes that occur in the motor neurons of Amyotrophic Lateral Sclerosis (ALS) cases (Figure 3-17d)[217]. Furthermore, compared to the high degree of correlation that we observe in FTD-progranulin cases, we find a dramatic reduction in the correlation when compared to sporadic FTD cases, despite the fact that these sporadic FTD cases have levels of neuronal cell death that are the same as FTD-progranulin cases (Figure 3-17g). The large decrease in gene expression overlap, that we observe in PD, ALS and sporadic FTD cases, suggests that the genome-wide overlap in expression with AD and FTD cases, is not simply due to neuronal cell death. Finally, we also compared *Lsd1*^{CAGG} hippocampus expression changes to changes in the cerebellum of AD and FTD cases. Compared to the prefrontal cortex, the cerebellum is relatively unaffected in AD and FTD cases. In both AD and FTD, we find that expression changes in the cerebellum overlap much less than the prefrontal cortex (Figure 3-17e,f). This discrepancy indicates that within AD and FTD cases, the overlap in expression may be driven by the neurodegeneration, rather than brain region.

3.3.6 LSD1 is mislocalized in human dementias

The RNA-seq data suggest that deletion of *Lsd1* alone is sufficient to recapitulate transcriptional changes observed in the affected brain regions of AD and FTD-progranulin cases, including many of the individual gene categories that have previously been implicated in the etiology of these dementias. These data potentially implicate the loss of LSD1 function in these human dementias. As a result, we wondered whether LSD1 might be affected in AD and FTD patients. AD is characterized by protein aggregates of amyloid β (Aβ) and Tau, while FTD is associated with aggregates of either Tau or Tar DNA binding protein 43 (TDP-43)[218-220]. These pathological aggregates are thought to lead to downstream pathways of neurodegeneration, but it remains unclear mechanistically how these aggregates are linked to neuronal cell death.

To determine if LSD1 may be affected in AD and FTD patients, we examined the localization of LSD1 in post-mortem AD, FTD with TDP-43 inclusions (FTD-TDP43), and age-matched control cases. We also examined the localization of LSD1 in Parkinson's disease (PD) cases, as a disease control with pathological protein aggregates. Similar to the expression in mice, LSD1 immunoreactivity was found in neuronal nuclei throughout the frontal cortex and hippocampus of age-matched control cases (Figure 3-18a,b). In contrast, in all 14 AD cases analyzed, LSD1 was found both in neuronal nuclei as well as inappropriately associated with cytoplasmic tangle-like aggregates and neurites, (Figure 3-18c,d). This pattern is highly reminiscent of the neurofibrillary tangles and neuropil threads marked by pTau in the same AD cases (Figure 3-18c-f). In addition, in all 14 FTD-TDP43 cases analyzed, LSD1 was abnormally associated with neurites in the frontal cortex, and cytoplasmic inclusions in the hippocampus (Figure 3-18j,k). This pattern is highly similar to the pTDP-43 aggregation observed in FTD-TDP43 cases (Figure 3-18j-m). To confirm the co-localization of LSD1 with pTau and pTDP-43

we performed dual IF. This analysis demonstrated that LSD1 co-localizes with pTau in 56.3% of neurofibrillary tangles in AD (n = 14 patients), and with pTDP-43 in 52.4% of neurites in FTD-TDP43 (n = 5 patients) (Figure 3-18g-i,n-q). Within AD cases the extent of co-localization ranges from 19%-76%, while in FTD-TDP43 cases, the co-localization ranges from 43%-71%. The finding that LSD1 is localized to pathological aggregates raises the possibility that it could be increasingly sequestered in the cytoplasm. This could result in less LSD1 being available to function in the nucleus of affected neurons in AD and FTD cases.

To confirm the specificity of the LSD1 localization, we performed several controls. Preincubation of the LSD1 Antibody (Ab) with its target LSD1 peptide completely abrogated the immunoreactivity (Figure 3-19a,b). We also did not observe the localization of LSD1 to the amyloid β core of senile plaques in the same AD cases where we observed co-localization with pTau (Figure 3-19c,d). Nor do we observe LSD1 localized to any Lewy body-like structures (aggregates of α-synuclein), or any other abnormal localization of LSD1, in the substantia nigra of PD cases (Figure 3-19e-h). These results suggest the mislocalization of LSD1 to neurofibrillary tangles in AD, and pTDP-43 inclusions in FTD cases, is specific. Notably, the co-localization of proteins with these pathological aggregates is exceedingly rare. For example, though many proteins have been recently described as enriched in the insoluble fraction of AD brains, only one was confirmed to be co-localized with neurofibrillary tangles[221].

3.3.7 *Lsd1^{CAGG}* mice do not have protein aggregates

Since LSD1 associates with pathological aggregates in AD and FTD-TDP43 cases, we considered the possibility that the neuronal cell death that we observe in the *Lsd1^{CAGG}* mice could be due to the induction of pathological aggregates in the mice. To test this possibility, we

performed IHC on the brains of terminal *Lsd1*^{CAGG} mice using antibodies to Aβ, pTau, and pTDP-43, along with Gallyas (silver, nonspecific aggregates) staining (Figure 3-20a-h). We find no evidence of any pathological protein aggregates or tangles associated with the degenerating neurons or otherwise. This suggests that if loss of LSD1 is involved in AD and/or FTD, it is likely downstream of pathological aggregation. This finding is consistent with the mislocalization of LSD1 to pathological aggregates in the human cases (Figure 3-18).

3.3.8 Increased stem cell gene expression in AD and FTD patients

The loss of LSD1 in mice is associated with the surprising reactivation of stem cell transcription in hippocampal neurons. If LSD1 is affected in AD and/or FTD, these diseases could be associated with a similar increase in stem cell gene expression. To test this possibility, we re-examined the expression of stem cell genes in previously published microarray experiments from LOAD and FTD-progranulin post-mortem cases[192,193]. This analysis revealed a significant increase in the expression of *Klf4*, *Myc, Oct4, Foxo1*, and *Vimentin* in LOAD cases compared to controls (Figure 3-21a,c,e,g,k,), while *PCNA* expression was unchanged (Figure 3-21i). In FTD-progranulin cases there was also a significant increase in the expression of *Klf4* and *Foxo1*, as well as a trend toward the increased expression of *Myc, Oct4, PCNA* and *Vimentin* (Figure 3-21b,d,f,h,j,l,). These data are consistent with the possibility that LSD1 function could be compromised in AD and FTD patients.

3.4 Discussion

Despite its well-known role throughout development, LSD1 protein can also be found in terminally differentiated cells throughout the brain. To determine if there is an ongoing role for

LSD1 in these terminally differentiated cells, we conditionally deleted *Lsd1* in adult mice. Surprisingly, within the brain at the terminal time point, the inducible loss of LSD1 in $Lsd1^{CAGG}$ mice results in loss of LSD1 protein only in neurons. This indicates that neurons may be more vulnerable to LSD1 protein or RNA turnover, a specificity that mirrors what occurs in AD and FTD cases.

Within the brain, the selective vulnerability of neurons in $Lsd1^{CAGG}$ mice enables us to specifically interrogate the function of LSD1 in these cells. Loss of LSD1 in $Lsd1^{CAGG}$ mice results in widespread hippocampus and cortex neuronal cell death. This demonstrates that loss of LSD1 in hippocampus and cortex neurons is sufficient to induce neuronal cell death. This conclusion is consistent with our high/low tamoxifen mosaic experiments which indicate that LSD1 acts cell autonomously in hippocampal neurons. Thus, we propose that LSD1 functions continuously in hippocampal and cortex neurons to prevent neurodegeneration.

To further investigate the neuronal cell death in the hippocampus, we examined gene expression changes genome-wide. Previous analyses of human neurodegeneration cases and experimental models have implicated common pathways leading to neuronal cell death. These include; activation of genes in the microglia and immune pathways, a defect in oxidative phosphorylation, loss of synaptic transmission, and failure to maintain cell cycle arrest. Remarkably, the loss of LSD1 affects all of these common neurodegenerative pathways. Therefore, it is possible that the loss of LSD1 creates a perfect storm where multiple neurodegenerative pathways are affected simultaneously, with one or more of these pathways leading to the observed neuronal cell death.

The prevailing view in developmental biology is that cells are irreversibly committed to their differentiated cell fate. Indeed, the very word “fate” promotes the idea that a differentiated

cell has reached its final destiny. However, there may be a requirement for differentiated cells to actively maintain their differentiated status. The LSD1-containing CoREST complex has been previously implicated in repressing neuronal genes in non-neuronal cells[202,203]. Based on this, we considered the possibility that LSD1 could be similarly required to maintain terminally differentiated hippocampus and cortex neurons by repressing gene transcription associated with alternative cell fates. In the degenerating neurons of *Lsd1*^{CAGG} mice, we detect the re-activation of stem cell transcription factors, such as KLF4, OCT4, c-MYC and FOXO1. This demonstrates that LSD1 is continuously required in terminally differentiated neurons to block the re-activation of these factors. Also, we detect a widespread decrease in the expression of neuronal pathways. This suggests that LSD1 is also required, directly or indirectly, to maintain the expression of these genes. Therefore, we propose that LSD1 is a key component of an epigenetic maintenance program that reinforces the differentiated state of hippocampal neurons by continuously restraining the re-activation of factors associated with alternative cell fates.

At this moment, we cannot definitively determine why the loss of LSD1 results in a severe motor defect. Nevertheless, *Lsd1*^{CAGG} mice develop a motor defect that is similar to a tauopathy mouse model[49]. For example the P301S mice, which overexpress an aggregation prone form of human Tau, have a motor defect that is reminiscent of *Lsd1*^{CAGG} mice[49]. The concordance of phenotypes between P301S mice and *Lsd1*^{CAGG} mice is consistent with Tau and LSD1 acting in a common pathway. Also consistent with this possibility, we find that that LSD1 inappropriately mislocalizes to cytoplasmic aggregates of pTau in AD, and global gene expression changes in the degenerating *Lsd1*^{CAGG} hippocampus correlate with changes in AD and FTD-progranulin cases. Finally, the re-examination of stem cell genes that are specifically affected by the loss of LSD1 in the mouse hippocampus demonstrates that these genes are also

increased in AD and FTD cases. Together these data indicate a potential link between the loss of LSD1 and these human dementia cases. This could occur through the following potential model: as neurons age, the accumulation of protein aggregates sequesters LSD1 in the cytoplasm, and interferes with the continuous requirement for LSD1. Normally, LSD1 maintains terminally differentiated neurons, and prevents the activation of common neurodegenerative pathways, by continuously repressing the transcription of inappropriate genes. As a result, the inhibition of LSD1 by the pathological aggregates in the aging neurons of AD and FTD brains creates a situation where neurons are subject to an onslaught of detrimental processes. This results in neuronal cell death and dementia.

3.5 Figures

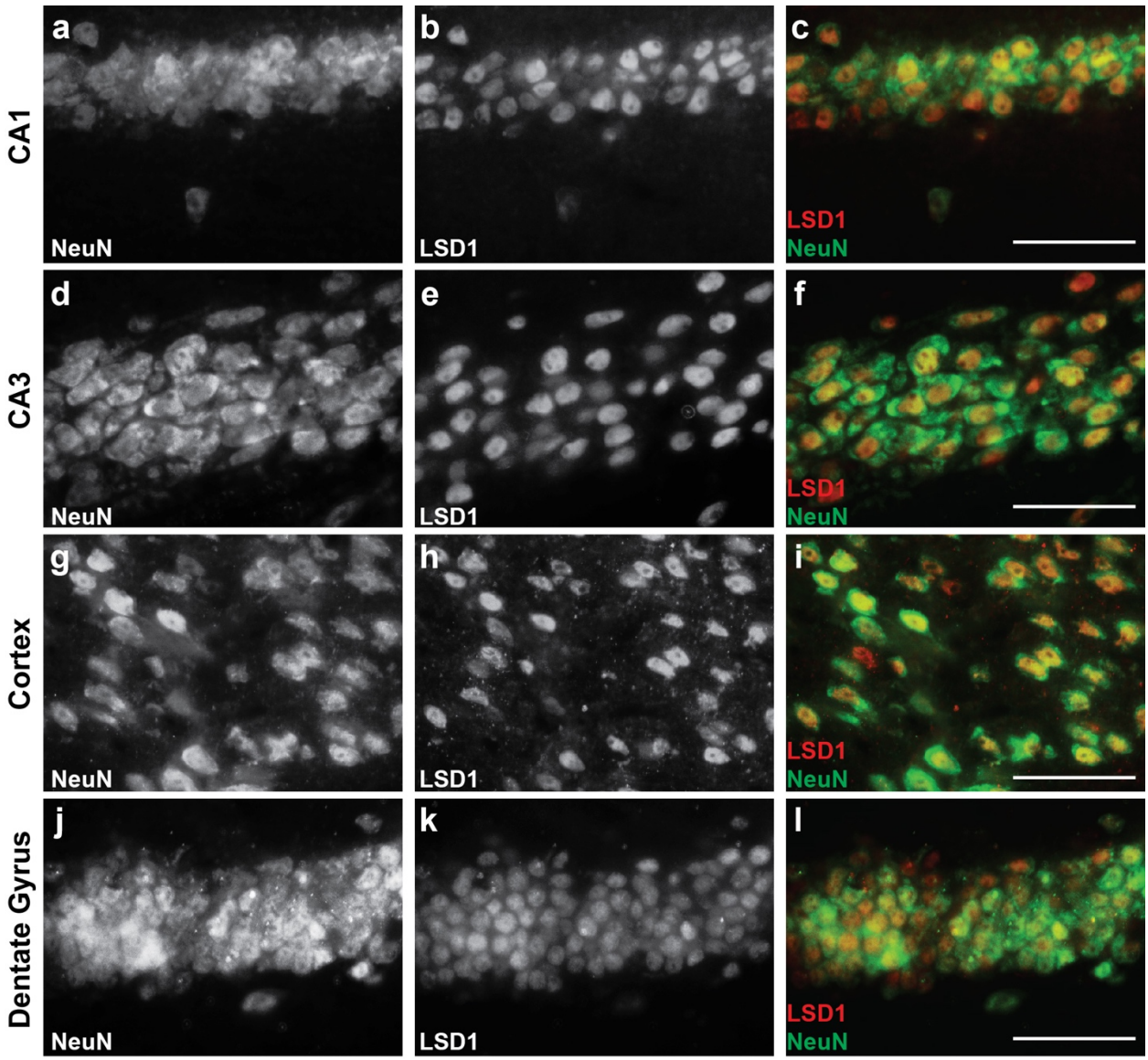

Figure 3-1 LSD1 expression in adult murine hippocampal and cortical neurons.

(**a-l**) Immunofluorescence labelling with the neuronal nucleus marker NeuN (**a,d,g,j**,), LSD1 (**b,e,h,k**,) and merged (**c,f,i,l**) showing LSD1 protein in neurons of the CA1 (**a-c**) and CA3 (**d-f**) of the hippocampus, cortex (**g-i**) and dentate gyrus (**j-l**) of wild-type mice. Scale bars= 50µm.

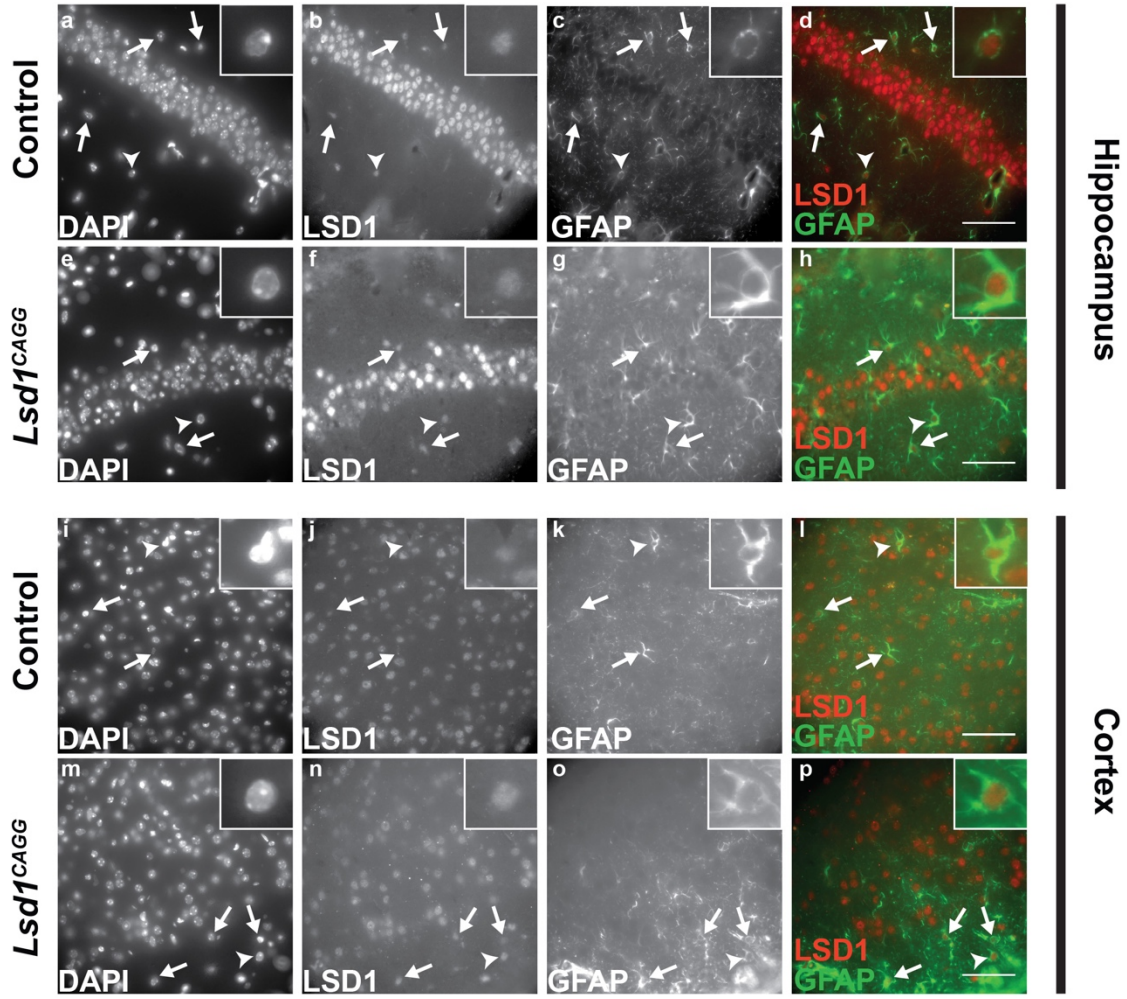

Figure 3-2 LSD1 expression in adult murine hippocampal and cortical astrocytes.

(a-p) Immunofluorescence labeling of DAPI (**a,e,i,m**), LSD1 (**b,f,j,n**), GFAP (**c,g,k,o**) and LSD1/GFAP merge (**d,h,l,p**) showing LSD1 is present in GFAP positive astrocytes both in control hippocampus **(a-d)** and cortex **(i-l),** as well as *Lsd1*^{CAGG} hippocampus (**e-h**) and cortex **(m-p)**, indicating LSD1 expression is not affected in astrocytes. Arrows denote representative nuclei. Arrowheads indicate nuclei magnified in inset. Scale bars= 50µm.

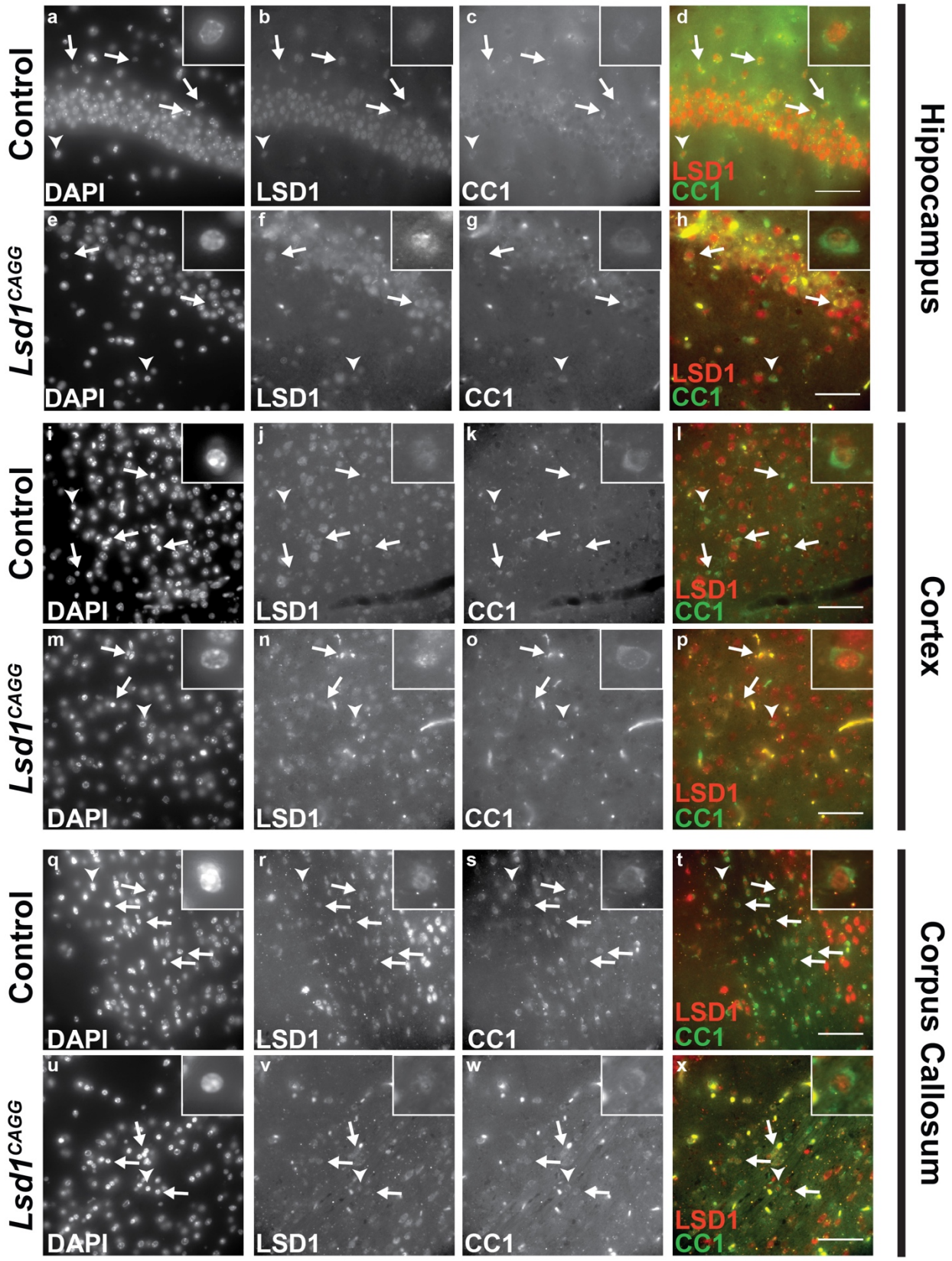
Control
Lsd1CAGG
Hippocampus
Cortex
Corpus Callosum
DAPI
LSD1
CC1
LSD1
CC1

Figure 3-3 LSD1 expression in adult hippocampal and cortical oligodendrocytes.

(a-x) Immunofluorescence labeling of DAPI (**a,e,i,m,q,u**), LSD1 (**b,f,j,n,r,v**), CC1 (**c,g,k,o,s,w**) and LSD1/CC1 merge (**d,h,l,p,t,x**) showing LSD1 is present in CC1 positive oligodendrocytes in the control hippocampus **(a-d)**, cortex **(i-l)**, and corpus callosum **(q-t)**, as well as $Lsd1^{CAGG}$ hippocampus (**e-h**), cortex **(m-p)**, and corpus callosum **(u-x)**, indicating LSD1 expression is not affected in oligodendrocytes. Arrows denote representative nuclei. Arrowheads indicate nuclei magnified in inset. Scale bars= 50μm.

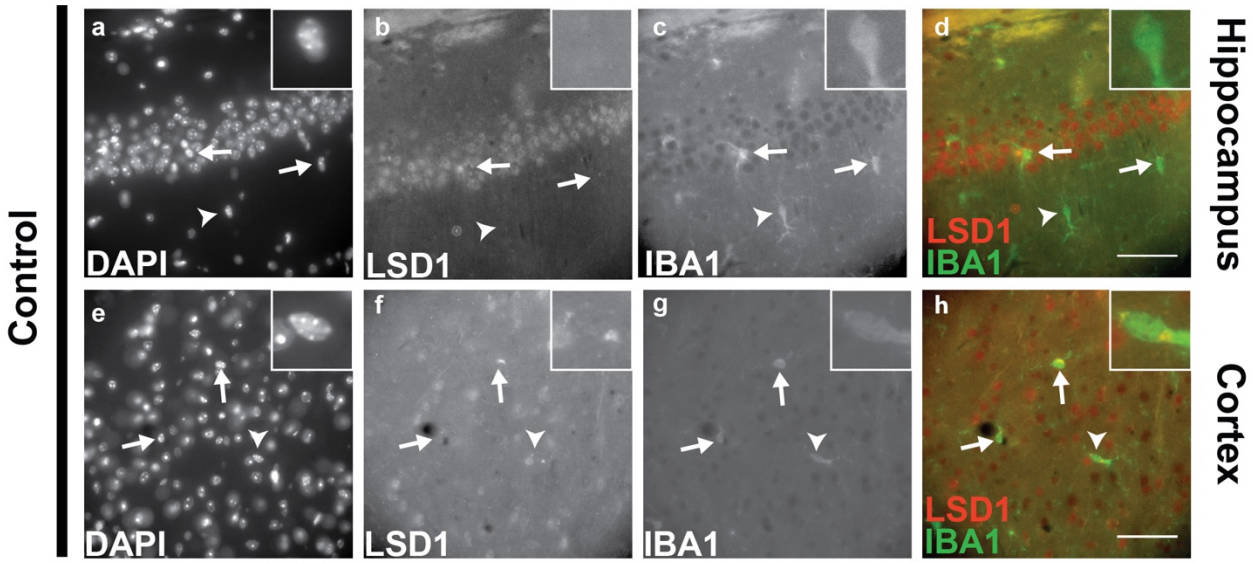

Figure 3-4 LSD1 is not expressed in adult hippocampal and cortical microglia.

(a-h) Immunofluorescence labeling of DAPI (**a,e,i,m**), LSD1 (**b,f,j,n**), IBA1 (**c,g,k,o**) and LSD1/IBA1 merge (**d,h,l,p**) showing LSD1 is absent in IBA1 positive microglia in the hippocampus **(a-d)** and cortex **(e-h)** of control mice. Arrows denote representative nuclei. Arrowheads indicate nuclei magnified in inset. Scale bars= 50µm.

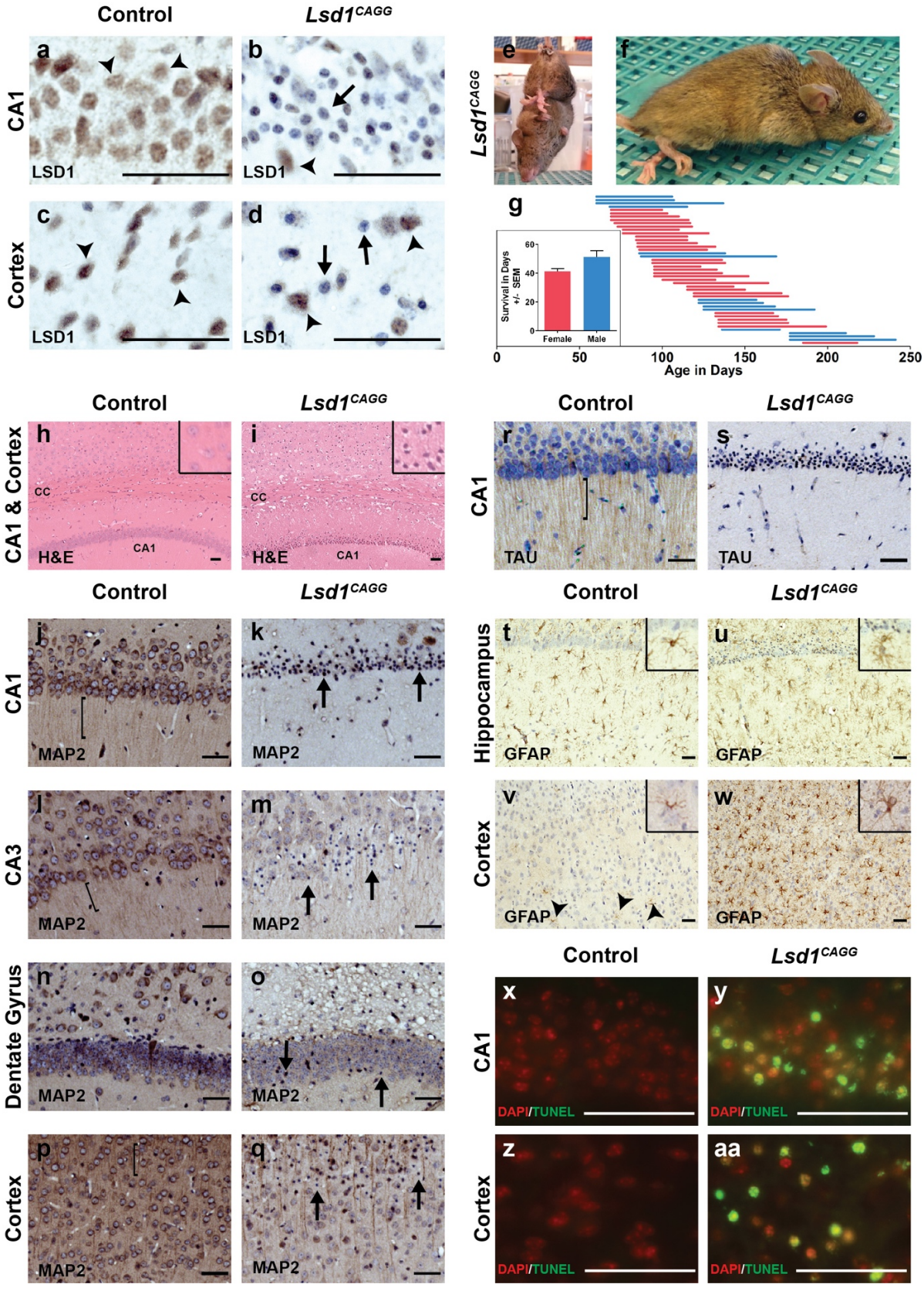
Control
Lsd1CAGG
CA1
Cortex
LSD1
Survival in Days +/- SEM
Female
Male
Age in Days
CA1 & Cortex
CC
H&E
CA1
TAU
Hippocampus
GFAP
MAP2
CA3
Dentate Gyrus
DAPI/TUNEL

Figure 3-5 Neurodegeneration in *Lsd1*^{CAGG} mice.

(**a-d**) LSD1 immunohistochemistry (IHC) of control (**a,c**) and *Lsd1*^{CAGG} (**b,d**) CA1 (**a,b**) and cortex (**c,d**). Arrowheads highlight non-pyknotic LSD1 immunoreactive nuclei. Arrows highlight pyknotic LSD1 negative nuclei. (**e,f**) Representative images of *Lsd1*^{CAGG} mice with the terminal motor defect including hindlimb clasping (**e**) and failure to maintain posture (**f**). (**g**) The age of each individual male (blue) or female (red) mouse at the final tamoxifen injection (start of each line) to inducibly delete *Lsd1*, and the number of days (length of the line) until the terminal motor defect is reached. Inset shows survival in days for each sex. Data are shown as mean survival in days ± s.e.m. (**h,i**) H&E staining of tamoxifen injected *Cre* minus control (control) (**h**) and *Lsd1*^{CAGG} (**i**) CA1 and cortex. Insets are magnified views of non-pyknotic (**h**) and pyknotic (**i**) nuclei. CC denotes corpus callosum. (**j-q**) MAP2 IHC of control (**j, l, n, p**) and *Lsd1*^{CAGG} (**k, m, o, q**) CA1 (**j,k**), CA3 (**l,m**), dentate gyrus (**n,o**) and cortex (**p,q**). Brackets highlight dendrites and arrows highlight pyknotic nuclei. (**r,s**) Tau IHC of control (**r**) and *Lsd1*^{CAGG} (**s**) CA1. Bracket highlights axons. (**t-w**) GFAP IHC of control (**t,v**) and *Lsd1*^{CAGG} (**u,w**) hippocampus (**t,u**) and cortex (**v,w**). Arrowheads highlight sparse astrocytes in control cortex. Insets show magnified view of representative astrocytes. (**x-aa**) Merge of DAPI (red) and TUNEL (green) in control (**x,z**) and *Lsd1*^{CAGG} (**y,aa**) CA1 (**x,y**) and cortex (**z,aa**). All IHC (**j-w**) is counterstained with hematoxylin. All *Lsd1*^{CAGG} images are taken at the terminal phenotype. Scale bars= 50μm.

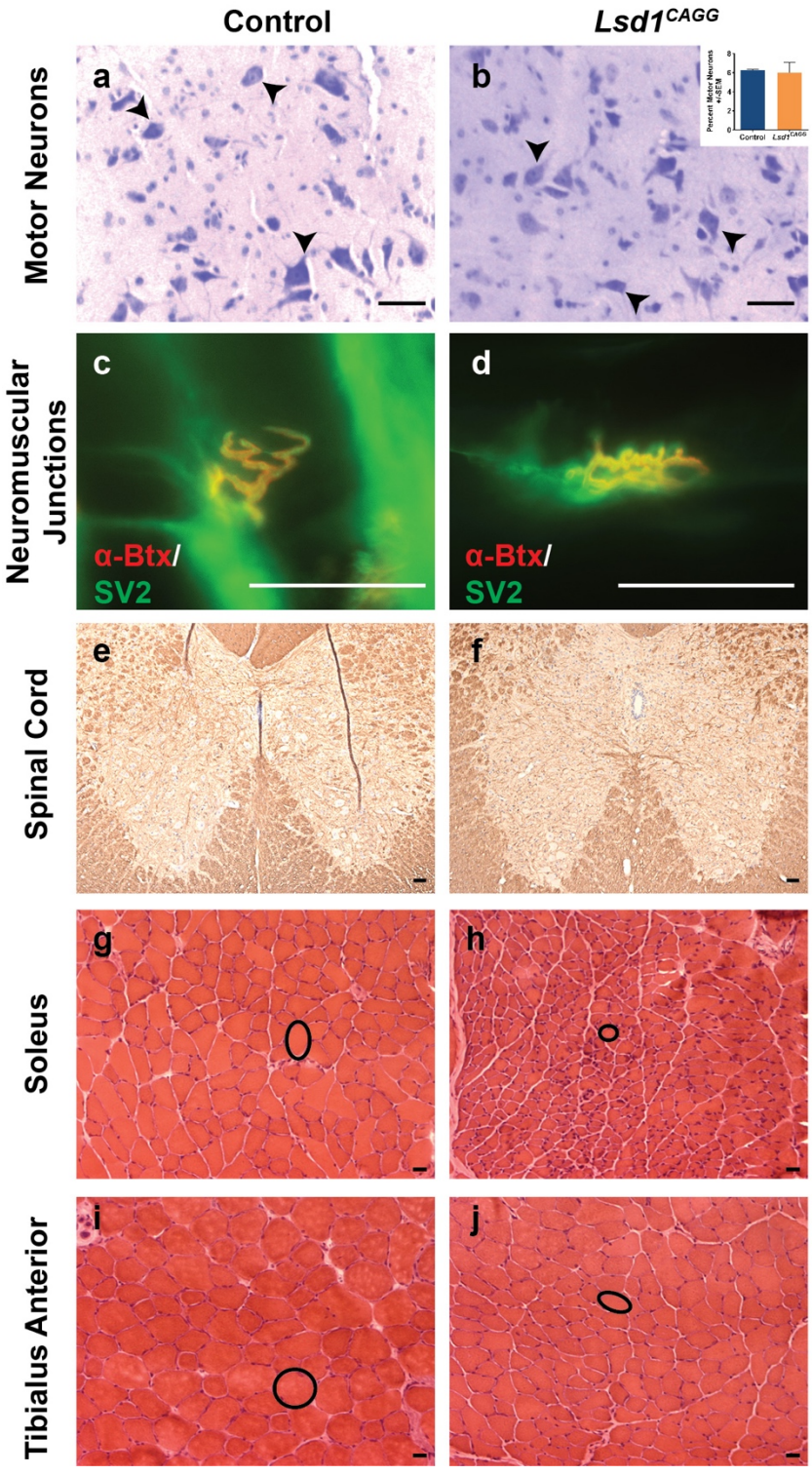
Control
Lsd1CAGG
Motor Neurons
Neuromuscular Junctions
Spinal Cord
Soleus
Tibialus Anterior
a
b
c
d
e
f
g
h
i
j
α-Btx/
SV2
α-Btx/
SV2
Percent Motor Neurons +/-SEM
Control
Lsd1CAGG

Figure 3-6 Absence of spinal cord motor neuron and muscle defects in *Lsd1*^{CAGG} mice.

(**a,b**) Thionin staining of control (**a**) and *Lsd1*^{CAGG} (**b**) ventral horn spinal cord motor neurons (arrowheads). Inset shows histogram of percentage motor neurons (per total ventral horn nuclei) for control (n = 3) and *Lsd1*^{CAGG} (n = 4). Values represent mean ± s.e.m. No significant difference between genotypes (p = 0.838, unpaired t test) (**c,d**) Immunofluorescence of neuromuscular junctions showing SV2 (presynaptic motor neurons, green) and fluorescent α-bungarotoxin (muscle acetylcholine receptors, red) in control (**c**) and *Lsd1*^{CAGG} (**d**). Co-localization SV2 and α-btx demonstrate an intact junction. **(e,f**) Immunohistochemistry (IHC) of myelin basic protein (MBP) in lower cervical spinal cord showing no difference in myelin amount or distribution between control **(e)** and *Lsd1*^{CAGG} **(f)**. IHC is counterstained with hematoxylin. (**g-j**) H&E staining of soleus (**g,h**) and tibialus anterior muscles (**i,j**) showing muscle fiber size (circles) in controls (**g,i**) compared to reduced cell size in *Lsd1*^{CAGG} (**h,j**). Absence of gaps in the tissue and absence of centrally located nuclei indicate a lack of muscle degeneration. Scale bars= 50μm.

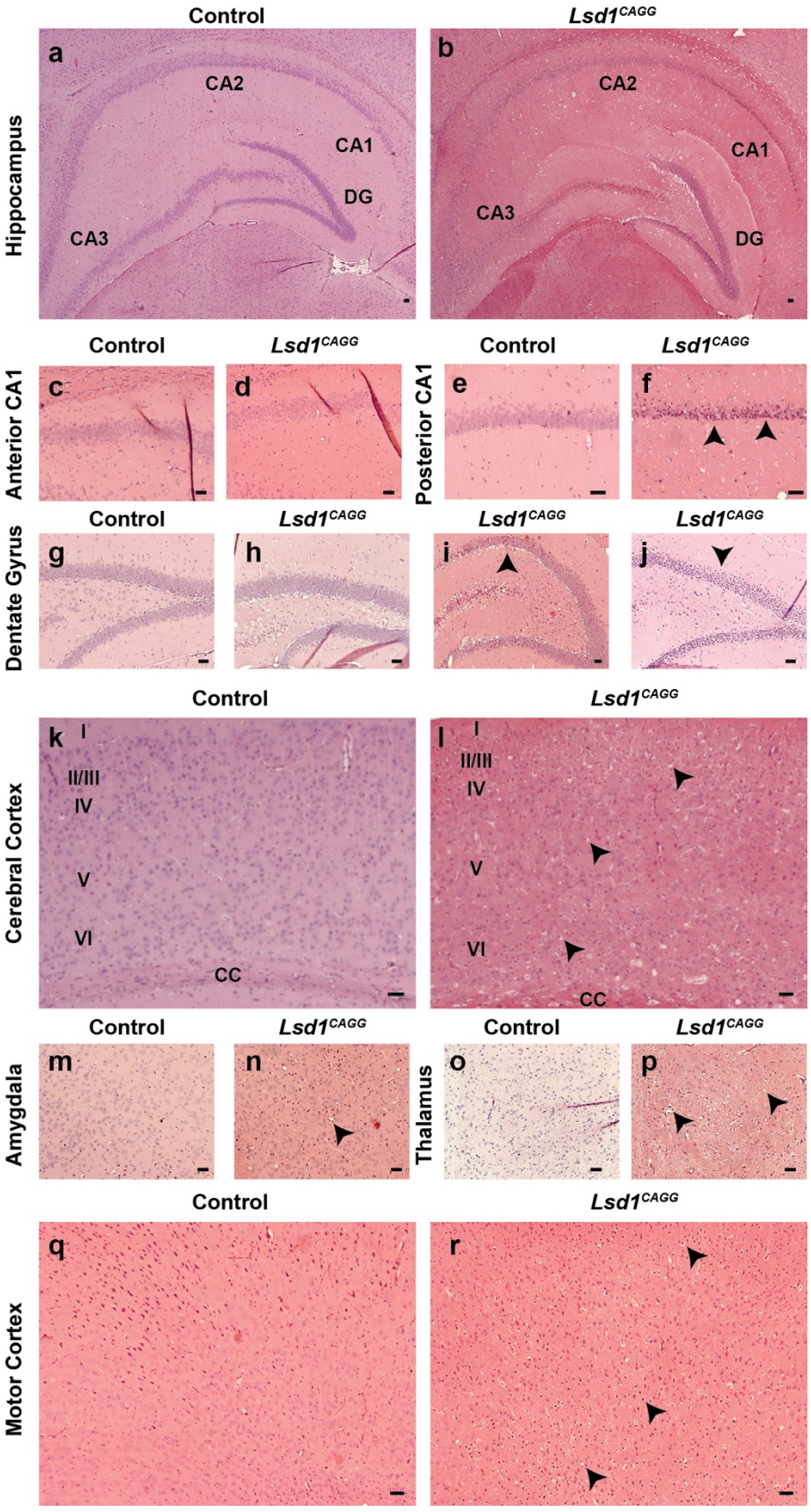
Control
Lsd1CAGG
Hippocampus
a
CA2
CA1
DG
CA3
b
CA2
CA1
CA3
DG
Anterior CA1
Posterior CA1
c
d
e
f
Dentate Gyrus
g
h
i
j
Cerebral Cortex
k
I
II/III
IV
V
VI
CC
l
Amygdala
Thalamus
m
n
o
p
Motor Cortex
q
r

Figure 3-7 Neurodegeneration in *Lsd1*^{CAGG} mice.

(**a-r**) H&E staining of control and *Lsd1*^{CAGG} hippocampus (**a,b**), anterior and posterior CA1 (**c-f**), dentate gyrus (**g-j**), cerebral cortex (**k,l**), amygdala (**m,n**), thalamus (**o,p**), and motor cortex (**q,r**). (**a,b**) Distribution of pyknosis in *Lsd1*^{CAGG} hippocampus with CA1 being most affected, and CA2 and CA3 moderately affected (**b**), compared to control with no pyknosis (**a**). (**c-f**) Increasing severity of pyknosis from anterior (**d**) to posterior (**f**) from the same *Lsd1*^{CAGG} hippocampus compared to control with no pyknosis (**c,e**). (**g-j**) Varying severity of pyknosis from three *Lsd1*^{CAGG} dentate gyruses; unaffected (**h**), moderately affected (**i**) completely affected (**j**) compared to control with no pyknosis (**g**). (**k,l**) Distribution of pyknosis in cerebral cortex of *Lsd1*^{CAGG} (**l**) in layers II/III, IV and VI, compared to control with no pyknosis (**k**), CC designates corpus callosum. (**m-r**) Distribution of pyknosis in the amygdala (**n**), thalamus (**p**) and motor cortex (**r**) of *Lsd1*^{CAGG} compared to control of same brain regions with no pyknosis (**m,o,q**). Arrowheads denote pyknotic nuclei. Scale bars= 50μm.

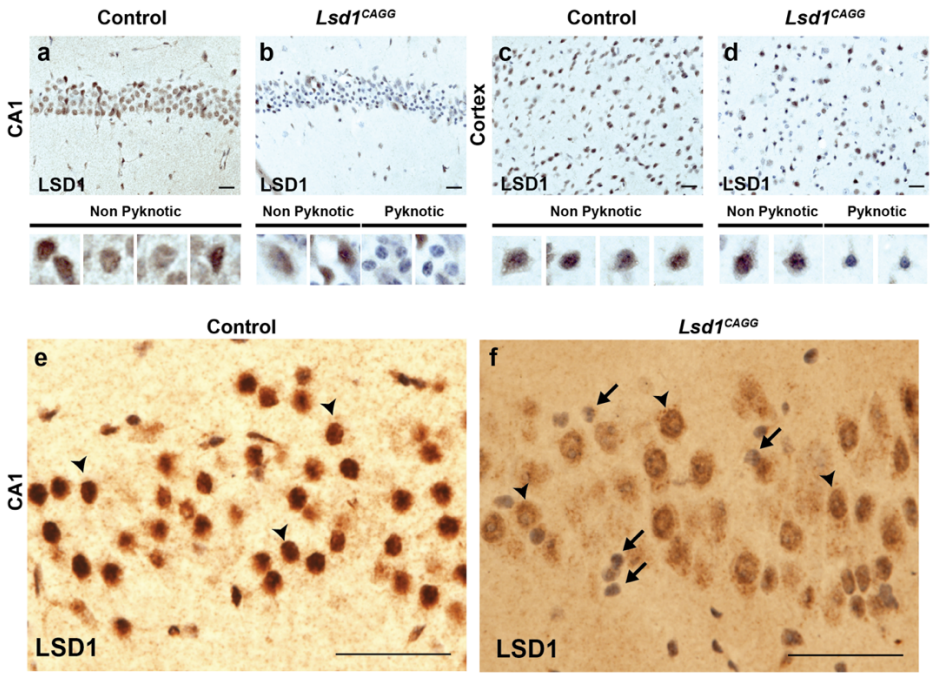

Figure 3-8 LSD1 in different cell types

(**a-d**) LSD immunohistochemistry (IHC) in control (**a,c**) and *Lsd1*^{CAGG} (**b,d**) CA1 (**a,b**) and cerebral cortex (**c,d**) showing the breadth of pyknosis associated with absence of LSD1 immunoreactivity in *Lsd1*^{CAGG} (**b,d**) compared to control (**a,c**) where LSD1 immunoreactivity is ubiquitous and pyknosis is absent. Images are the source images from Figure 1a-d. Insets below highlight immunoreactive non-pyknotic neuronal nuclei and non-immunoreactive pyknotic neuronal nuclei. (**e,f**) LSD1 immunohistochemistry in control (**e**) and *Lsd1*^{CAGG} (**f**) CA1 ten weeks after a single, reduced dose of tamoxifen (1 mg/ 40g of body mass). Every neuronal nucleus in control and most neuronal nuclei in *Lsd1*^{CAGG} mice display normal LSD1 immunoreactivity and are not pyknotic (arrowheads). However, a small number of nuclei are non-immunoreactive for LSD1 and are also pyknotic (arrows), which is consistent with a cell autonomous effect on neuronal cell death.) All IHC **(a-f)** is counter stained with hematoxylin. Scale bars= 50µm.

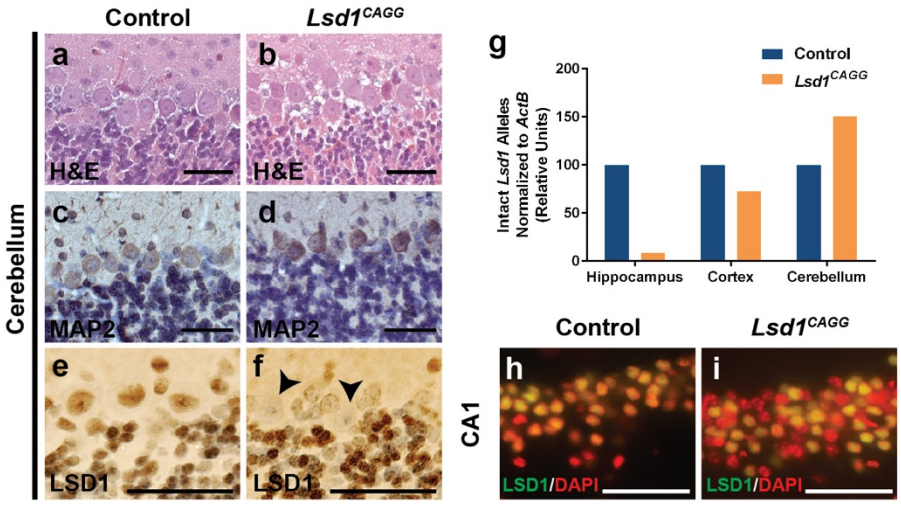

Figure 3-9 Absence of neurodegeneration in the *Lsd1*^{CAGG} cerebellum.

(**a,b**) H&E staining of control (**a**) and *Lsd1*^{CAGG} (**b**) cerebellum showing similar cellular morphology and lack of pyknotic nuclei in *Lsd1*^{CAGG}. (**c,d**) MAP2 immunohistochemistry (IHC) in control (**c**) and *Lsd1*^{CAGG} (**d**) showing similar distribution in cerebellar neurons. (**e,f**) LSD1 IHC in control (**e**) and *Lsd1*^{CAGG} (**f**) cerebellum showing lack of LSD1 in some (arrowheads), but not all *Lsd1*^{CAGG} purkinje neurons. (**g**) Quantification of intact *Lsd1* alleles (revealing the extent of *Lsd1* deletion) in control (blue) and *Lsd1*^{CAGG} (orange) hippocampus 24 hours after tamoxifen injection, and in cortex and cerebellum at terminal phenotype. Data are shown as relative units normalized to *ActB*, where the control value is set to 100. (**h,i**) Merge of LSD1 (green) immunofluorescence and DAPI (red) in control (**h**) and *Lsd1*^{CAGG} (**i**) CA1 nuclei showing LSD1 protein remaining in non-pyknotic nuclei approximately one week before the *Lsd1*^{CAGG} terminal motor phenotype. All IHC (**c-f**) is counterstained with hematoxylin. Scale bars= 50μm.

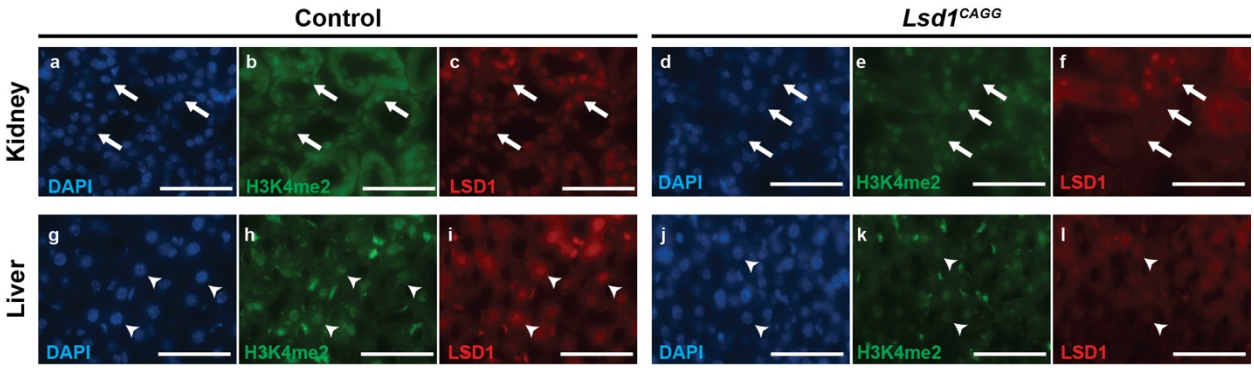

Figure 3-10 LSD1 is not required for kidney and liver cell viability.

(**a-l**) Representative immunofluorescence images showing LSD1 (red), staining control H3K4me2 (green) and DAPI (blue) in mouse epithelial cells of the kidney nephron (**a-f**, arrows) and hepatocytes of the liver (**g-l**, arrowheads). LSD1 is normally ubiquitously expressed in controls (**c,i**). In *Lsd1*^{CAGG} mice, LSD1 is absent (**f,l**), but kidney and liver morphology remains normal compared to controls (**a,d,g,j**). Absence of LSD1 immunoreactivity is not due to lack of antibody penetrance (**b,e,h,k**). Scale bars= 50µm.

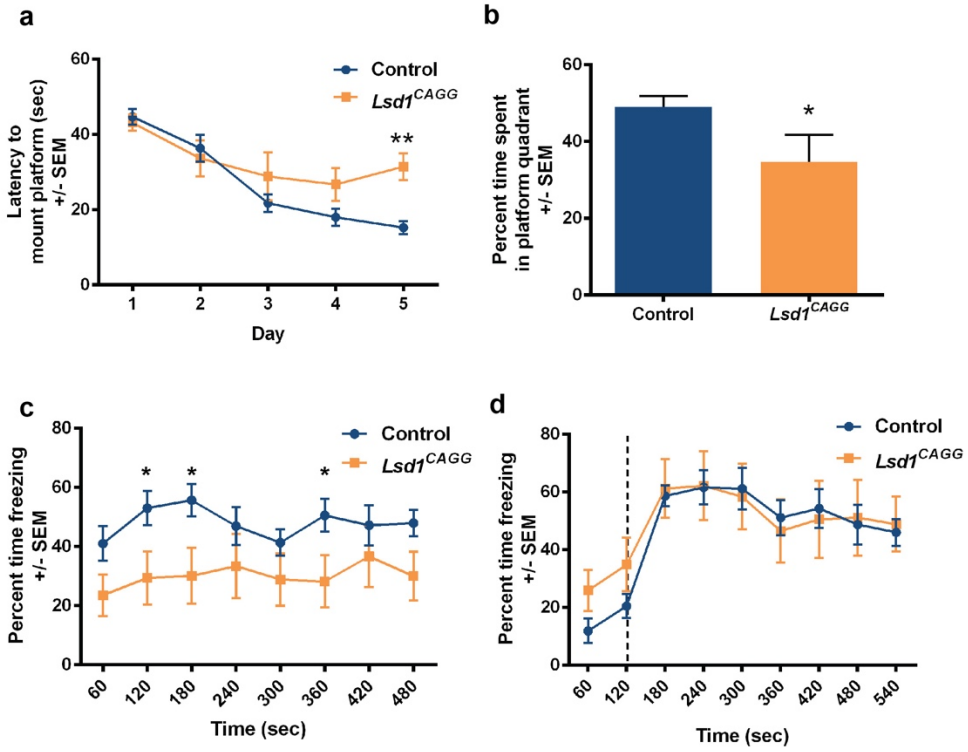

Figure 3-11 Loss of LSD1 results in learning and memory deficits.

(a) Latency to mount platform (in seconds) in the Morris water maze across the 5 day training period of control (blue, $n = 15$) and $Lsd1^{CAGG}$ (orange, $n = 12$) mice. Data are shown as mean ± s.e.m. $^{**}P < 0.01$ on Day 5 compared by repeated measures two-way ANOVA with *post hoc* Sidak's multiple comparisons test. (**b**) Percent time spent swimming in platform quadrant during probe (day 6) after 5 days of water maze training for control (blue $n = 15$) and $Lsd1^{CAGG}$ mice (orange, $n = 11$) mice. Data are shown as mean ± s.e.m. $^{*}P < 0.05$ by unpaired t-test. (**c**) Percent time spent freezing during contextual fear response after fear conditioning of control (blue, $n = 12$) and $Lsd1^{CAGG}$ (orange, $n = 8$) mice. Data are shown as mean ± s.e.m. $^{*}P < 0.05$ by unpaired t-test at individual timepoints. $P = 0.052$ for difference between genotypes by repeated measures two-way ANOVA. (**d**) Percent time spent freezing during cued fear response after fear conditioning of control (blue, $n = 12$) and $Lsd1^{CAGG}$ (orange, $n = 8$) mice. Data are shown as mean ± s.e.m. Dashed line represents sound of tone.

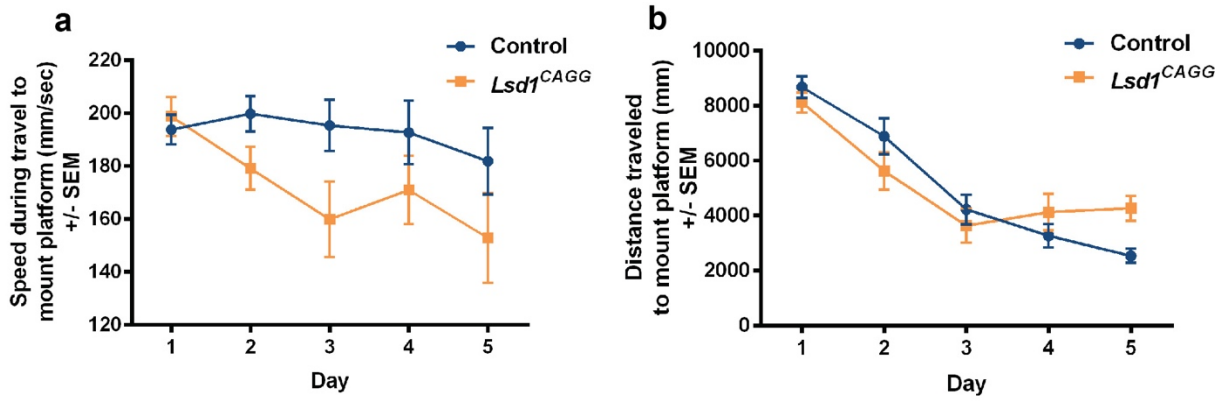

Figure 3-12 *Lsd1*^{CAGG} mice have learning and memory deficits.

(**a**) Speed during travel to mount platform in Morris water maze across 5 day training period of control (blue, n = 15) and *Lsd1*^{CAGG} (orange, n = 12) mice. Data are shown as mean ± s.e.m. No significant difference between genotypes by repeated measures two-way ANOVA. (**b**) Distance traveled to mount platform in Morris water maze across 5 day training period of control (blue, n = 15) and *Lsd1*^{CAGG} (orange, n = 12) mice. Consistent with the increased latency to mount platform (Fig. 2a), *Lsd1*^{CAGG} mice travel longer distance on Day 5. Data are shown as mean ± s.e.m.

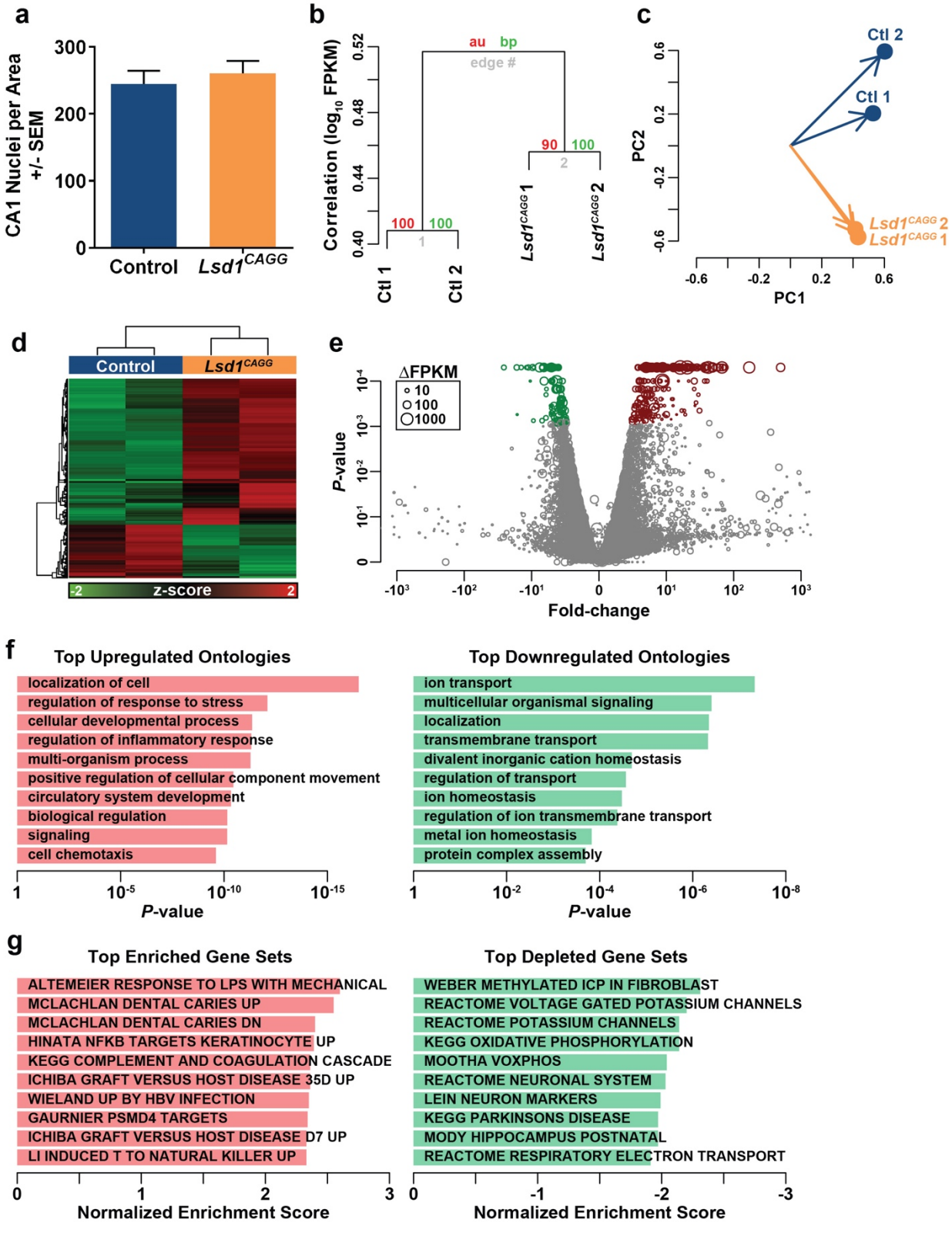
a
CA1 Nuclei per Area +/- SEM
300
200
100
0
Control
Lsd1CAGG
b
Correlation (log10 FPKM)
0.52
0.48
0.44
0.40
au bp
edge #
100 100
1
90 100
2
Ctl 1
Ctl 2
Lsd1CAGG 1
Lsd1CAGG 2
c
PC2
0.6
0.2
-0.2
-0.6
Ctl 2
Ctl 1
Lsd1CAGG 2
Lsd1CAGG 1
-0.6 -0.2 0.2 0.6
PC1
d
Control
Lsd1CAGG
-2
z-score
2
e
ΔFPKM
10
100
1000
P-value
10-4
10-3
10-2
10-1
0
-10³ -10² -10¹ 0 10¹ 10² 10³
Fold-change
f
Top Upregulated Ontologies
localization of cell
regulation of response to stress
cellular developmental process
regulation of inflammatory response
multi-organism process
positive regulation of cellular component movement
circulatory system development
biological regulation
signaling
cell chemotaxis
1 10-5 10-10 10-15
P-value
Top Downregulated Ontologies
ion transport
multicellular organismal signaling
localization
transmembrane transport
divalent inorganic cation homeostasis
regulation of transport
ion homeostasis
regulation of ion transmembrane transport
metal ion homeostasis
protein complex assembly
1 10-2 10-4 10-6 10-8
P-value
g
Top Enriched Gene Sets
ALTEMEIER RESPONSE TO LPS WITH MECHANICAL
MCLACHLAN DENTAL CARIES UP
MCLACHLAN DENTAL CARIES DN
HINATA NFKB TARGETS KERATINOCYTE UP
KEGG COMPLEMENT AND COAGULATION CASCADE
ICHIBA GRAFT VERSUS HOST DISEASE 35D UP
WIELAND UP BY HBV INFECTION
GAURNIER PSMD4 TARGETS
ICHIBA GRAFT VERSUS HOST DISEASE D7 UP
LI INDUCED T TO NATURAL KILLER UP
0 1 2 3
Normalized Enrichment Score
Top Depleted Gene Sets
WEBER METHYLATED ICP IN FIBROBLAST
REACTOME VOLTAGE GATED POTASSIUM CHANNELS
REACTOME POTASSIUM CHANNELS
KEGG OXIDATIVE PHOSPHORYLATION
MOOTHA VOXPHOS
REACTOME NEURONAL SYSTEM
LEIN NEURON MARKERS
KEGG PARKINSONS DISEASE
MODY HIPPOCAMPUS POSTNATAL
REACTOME RESPIRATORY ELECTRON TRANSPORT
0 -1 -2 -3
Normalized Enrichment Score

Figure 3-13 Differential expression of genes in *Lsd1*^{CAGG} hippocampus.

(**a**) Total number of nuclei per area counted in control (n = 4) and terminal *Lsd1*^{CAGG} (n = 10) CA1. Data are shown as mean ± s.e.m. (**b**) Hierarchical clustering of gene expression across 24,412 transcripts (FPKM > 0.5) shows that control and *Lsd1*^{CAGG} replicates significantly segregate by gene expression. The y-axis represents the $\log_{10}$ FPKM correlation. Approximate Unbiased *P*-values (AU, red) and Bootstrap Probabilities (BP, green) for each cluster are shown. (**c**) Principle component analysis (PCA) of 24,412 transcripts (FPKM > 0.5) shows consistent separation of control and *Lsd1*^{CAGG} samples in the first two principle components. (**d**) Heatmap of most significantly differentially expressed (281 upregulated, 124 downregulated) RNA-seq transcripts between *Lsd1*^{CAGG} and control hippocampi. Samples are hierarchically clustered by relative expression of differentially expressed transcripts. Relative higher (red) or lower (green) expression is indicated. (**e**) Volcano plot of fold-changes in gene expression (x-axis) by statistical significance (*P*-value; y-axis). Each circle represents a transcript and the normalized change in expression is represented by the size of the circle (legend). Those transcripts that are significantly (FDR < 0.05) differentially expressed are represented in red (281 upregulated) and green (124 downregulated). (**f**) Histogram of Gene Ontology analysis shows ontologies that are associated with those genes that are upregulated (red) and those genes that are downregulated (green) in the *Lsd1*^{CAGG} RNA-seq dataset. The top 10 ontologies are shown with P-values. (**g**) Histogram of Gene Set Enrichment Analysis shows the most enriched (red) and depleted (green) gene sets in the *Lsd1*^{CAGG} RNA-seq dataset. The top 10 gene sets are shown with normalized enrichment scores.

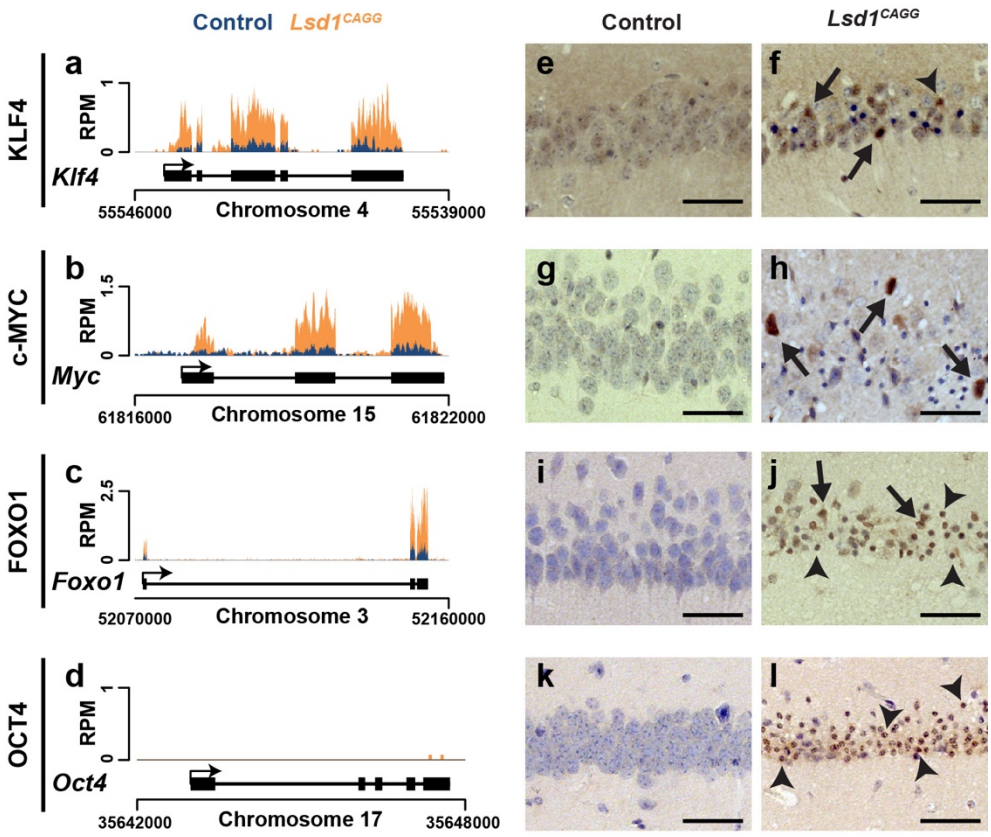

Figure 3-14 Ectopic activation of stem cell genes in *Lsd1*^{CAGG} mice.

(**a-d**) Genome browser style plot of RNA-seq reads per million (RPM) from control (blue) and overlaid *Lsd1*^{CAGG} (orange) hippocampi showing expression of the genes *Klf4* (**a**), *Myc* (**b**), *Foxo1*(**c**), *Oct4* (**d**). (**e-l**) Immunohistochemistry (IHC) with antibodies to KLF4 (**e,f**), c-MYC (**g,h**), FOXO1 (**i,j**), and OCT4 (**k,l**) in control (**e,g,i,k**) and *Lsd1*^{CAGG} (**f,h,j,l**) CA1 neuronal nuclei. Arrows denote non-pyknotic nuclei and arrowheads denote pyknotic nuclei. All IHC is counterstained with hematoxylin. All *Lsd1*^{CAGG} images are taken at the terminal phenotype. Scale bars= 50µm.

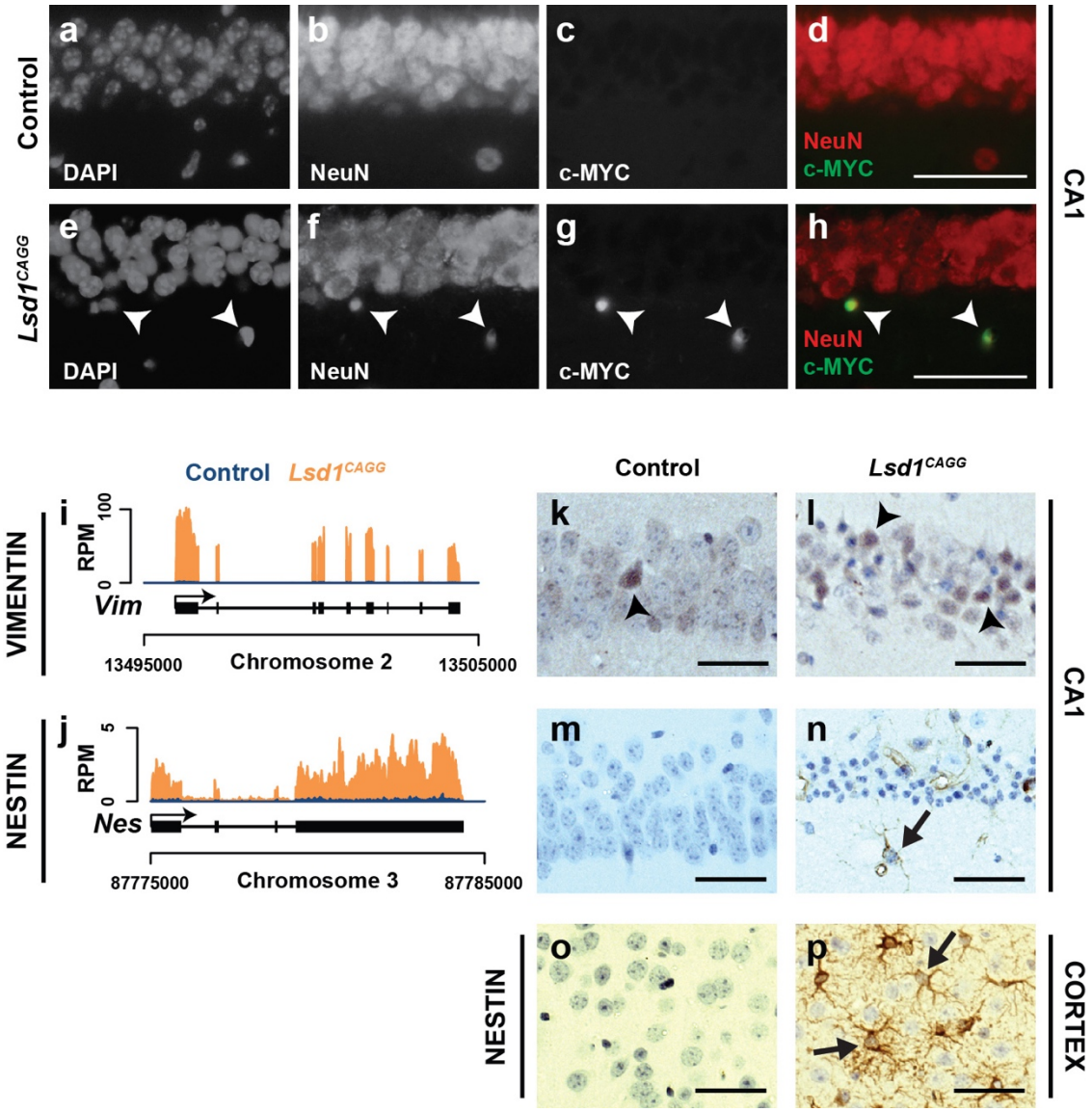

Figure 3-15 Neural stem cell gene expression in *Lsd1*^{CAGG} mice.

(**a-h**) Immunofluorescence labelling of DAPI (**a,e**), NeuN (**b,f**), c-MYC (**c,g**) and NeuN/c-MYC merge (**d,h**) in control (**a-d**) and *Lsd1*^{CAGG} (**e-h**) CA1. c-MYC protein is present in the nuclei of neurons in *Lsd1*^{CAGG} mice (**e-h,** arrowheads), but absent from neurons in control mince. (**i,j**) Genome browser style plot of RNA-seq reads per million (RPM) from control (blue) and overlaid *Lsd1*^{CAGG} (orange) hippocampus showing expression of the genes *Vimentin* (**i**) and *Nestin* (**j**). (**k-p**) Immunohistochemistry (IHC) with antibodies to VIMENTIN (**k,l**) and NESTIN

(**m-p**) in control CA1 (**k,m**) and cortex (**o**), and *Lsd1*^{CAGG} CA1 (**l,n**) and cortex (**p**). VIMENTIN immunoreactivity was present in CA1 neurons in both control (**k**, arrowheads) and *Lsd1*^{CAGG} (**l**, arrowheads), with more immunoreactive neurons in *Lsd1*^{CAGG}. NESTIN immunoreactivity was found in glial-shaped cells in *Lsd1*^{CAGG} hippocampus (**n**) and cortex (**p**, arrows) and absent in control (**m,o**). All IHC is counterstained with hematoxylin. All *Lsd1*^{CAGG} images were taken at the terminal phenotype. Scale bars= 50μm.

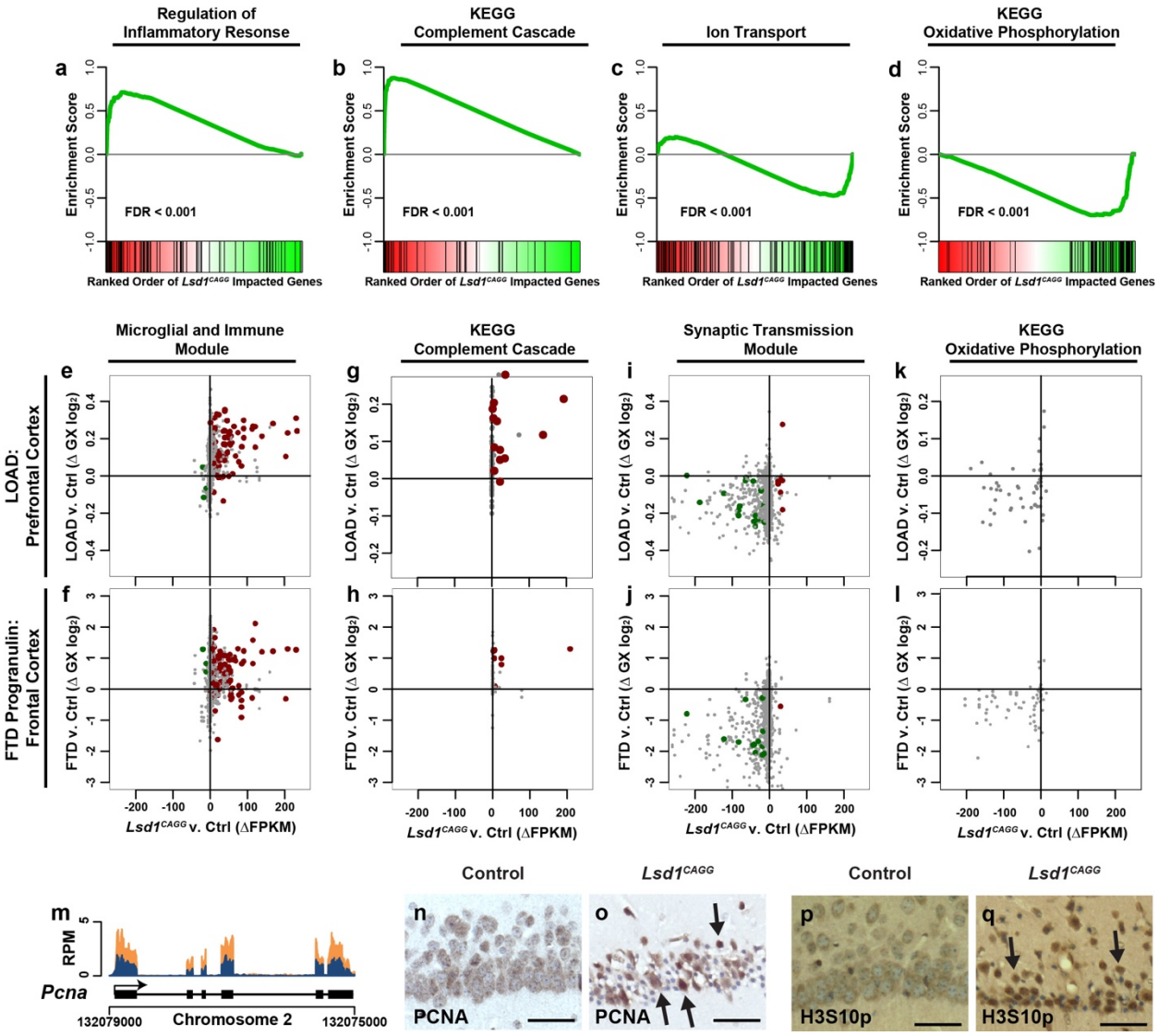

Figure 3-16 Loss of LSD1 induces common neurodegeneration pathways.

(**a-d**) Gene set enrichment plots of neurodegeneration pathways where *Lsd1*^{CAGG} impacted transcripts (x-axis) are sorted by magnitude of upregulation (red) to downregulation (green). The position of each gene from the gene set is represented as a black tick mark (x-axis). Enrichment score (y-axis) shows where enrichment of genes from the set occurs in the *Lsd1*^{CAGG} transcriptome. Gene sets shown are regulation of inflammatory response (**a**), Kyoto Encyclopedia of Genes and Genomes (KEGG) complement cascade (**b**), ion transport (**c**), and KEGG oxidative phosphorylation (**d**). FDR is shown for each plot. (**e-l**) Scatter plots showing

correlated changes in gene expression of genes from the Microglial and Immune Module[192] (**e,f**), KEGG complement cascade (**g,h**), Synaptic Transmission Module[192] (**i,j**) and KEGG oxidative phosphorylation (**k,l**) gene sets between the *Lsd1*^{CAGG} and control hippocampus (FPKM, x-axes) compared to changes in $\log_2$ gene expression between late onset AD (LOAD) and control prefrontal cortex[192] (**e,g,i,k**; y-axis), or compared to changes between FTD-progranulin and control frontal cortex[193] (**f,h,j,l**; y-axis). The most significantly changed genes in the *Lsd1*^{CAGG} hippocampus (Supplementary Fig. 11d,e) are shown in red (upregulated) and green (downregulated). All other genes with a direct mouse/human orthologue are shown in grey. Genes with correlated expression changes are found in the top right and bottom left quadrants, while genes that do not correlate are found in the other quadrants. (**m**) Genome browser style plot (as described in Fig. 3a-d) showing *Pcna* expression in *Lsd1*^{CAGG} hippocampus (orange) compared to control (blue). (**n-q**) Immunohistochemistry with antibodies to PCNA (**n,o**), and H3S10p (**p,q**) in control (**n,p**) and *Lsd1*^{CAGG} (**o,q**) CA1 neuronal nuclei. Arrows denote non-pyknotic nuclei. All IHC is counterstained with hematoxylin. All *Lsd1*^{CAGG} images are taken at the terminal phenotype. Scale bars= 50μm.

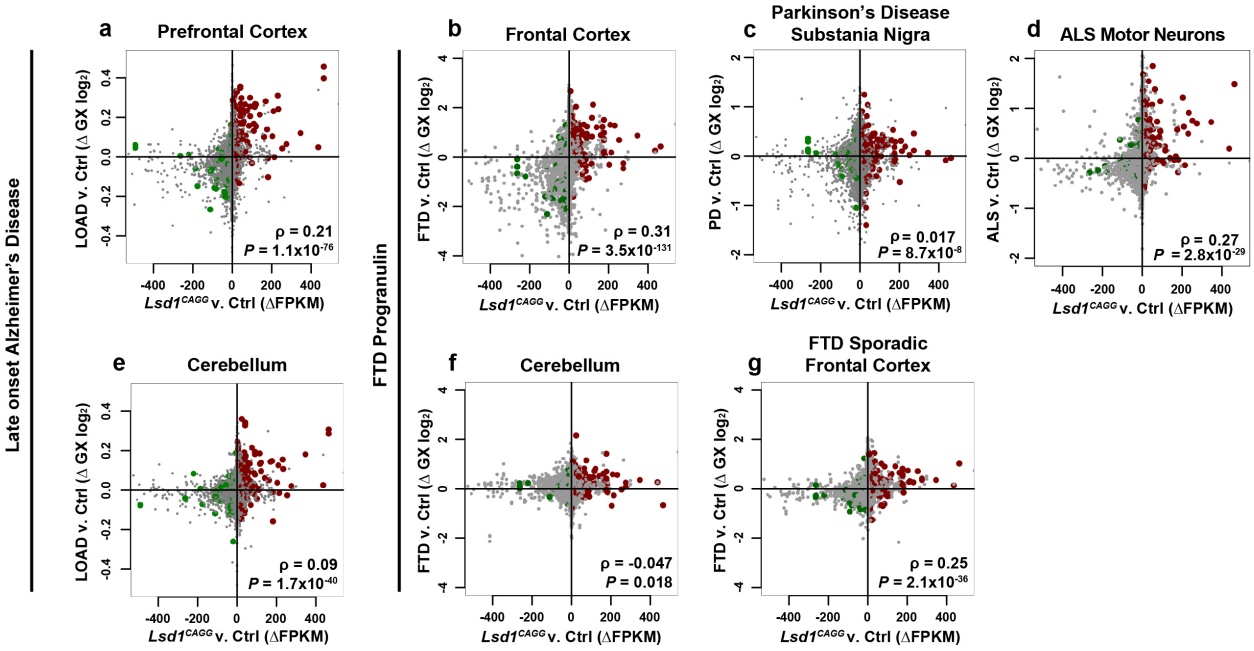

Figure 3-17 Expression changes in *Lsd1*^{CAGG} mice correlate in AD and FTD.

(**a-f**) Scatter plots (as described in Fig. 4**e-l**) showing genome-wide correlated changes in gene expression between the *Lsd1*^{CAGG} and control hippocampus (FPKM, x-axes) compared to $\log_2$ gene expression changes in late onset AD (LOAD) prefrontal cortex[192] (**a**; y-axis), FTD-progranulin frontal cortex[193] (**b**; y-axis), PD substantia nigra[194] (**c**; y-axis), ALS motor neurons[217] (d; y-axis), LOAD cerebellum[192] (**e**; y-axis), FTD-progranulin cerebellum[193] (**f**; y-axis), and sporadic FTD frontal cortex[193] (**g**; y-axis). *P*-values and ρ Pearson correlation coefficient are given.

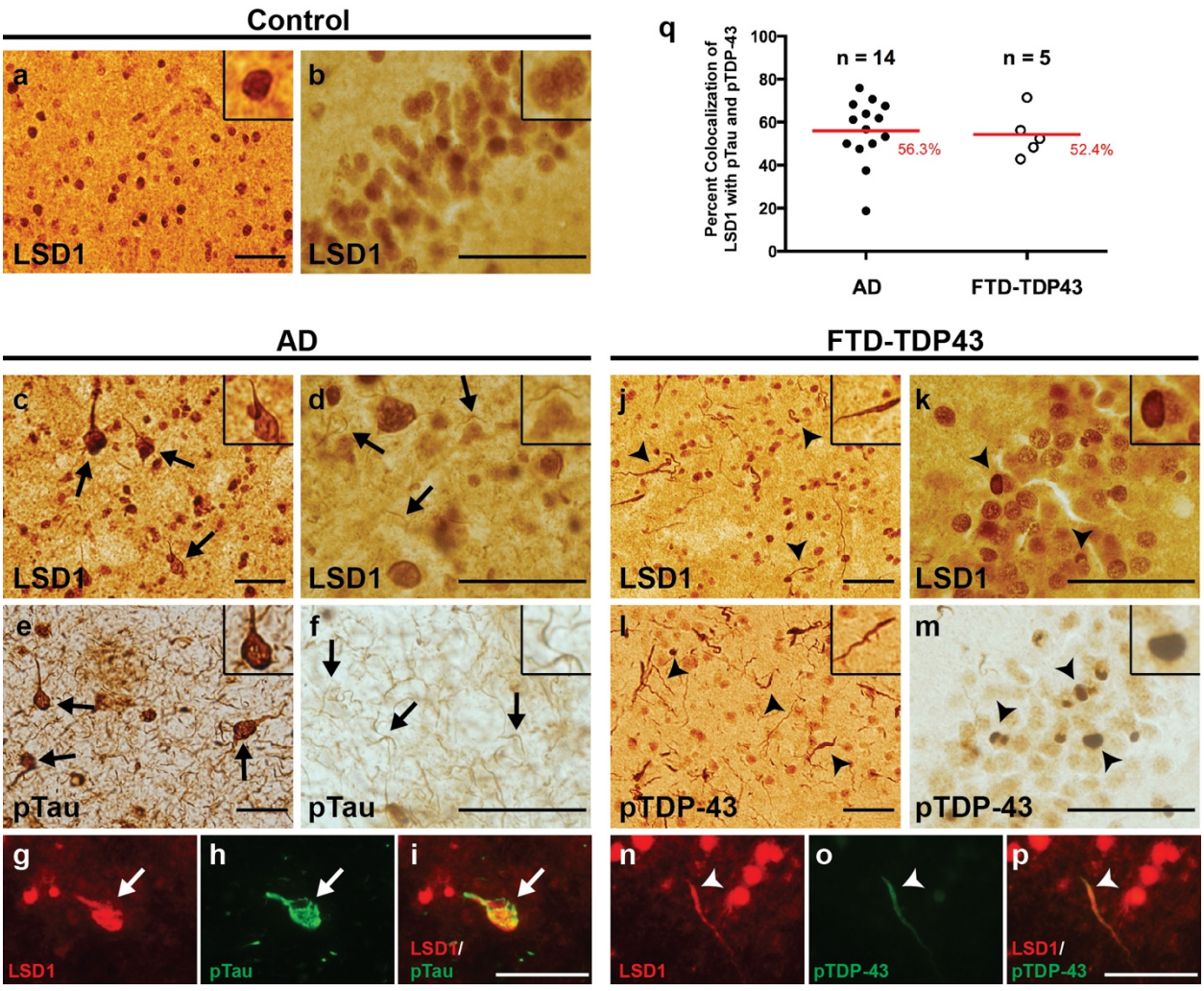

Figure 3-18 LSD1 co-localization with pTau and pTDP-43 aggregates.

(**a,b**) LSD1 immunohistochemistry (IHC) showing expression of LSD1 in age-matched control frontal cortex (**a**) and hippocampus (**b**). (**c,d**) Representative IHC images showing LSD1 immunoreactivity localized to cytoplasmic tangle-like aggregates (**c**, arrows) and neurites (**d**, arrows) in AD frontal cortex. (**e,f**) IHC images showing pTau (AT8 epitope) neurofibrillary tangles (**e**, arrows) and neuropil threads (**f**, arrows) from the same AD frontal cortex as (**c,d**). (**g-i**) Representative image of LSD1 (**g**, red), pTau (**h**, green), and merged (**i**) immunofluorescence (IF) showing co-localization of LSD1 with a pTau neurofibrillary tangle in AD (arrow). (**j,k**) Representative IHC image showing LSD1 immunoreactivity localized to abnormal deposits in

neurites (**j**, arrowheads) and cytoplasmic inclusions (**k**, arrowheads) in FTD-TDP43 frontal cortex (**j**) and hippocampus (**k**). (**l,m**) IHC images showing pTDP-43 in neurites and cytoplasmic inclusions (**l,m**, arrowheads) from the same FTD-TDP43 frontal cortex (**l**) and hippocampus (**m**) as (**j**) and (**k**), respectively. (**n-p**) Representative image of LSD1 (**n**, red), pTDP-43 (**o**, green) and merged (**p**) IF showing co-localization of LSD1 with pTDP-43 in a neurite in FTD-TDP43 (arrowhead). Insets are magnified views of LSD1 nuclear localization (**a,b**) and representative pathologies (**c-f**, **j-m**). Scale bars= 50μm. (**q**) The percentage of neurofibrillary tangles (pTau) with LSD1 colocalization in AD (*n* = 14 cases assayed, closed circles), and neurites (pTDP-43) with LSD1 colocalization in FTD-TDP43 (*n* = 5 cases assayed, open circles), with the average percentage shown (red bar).

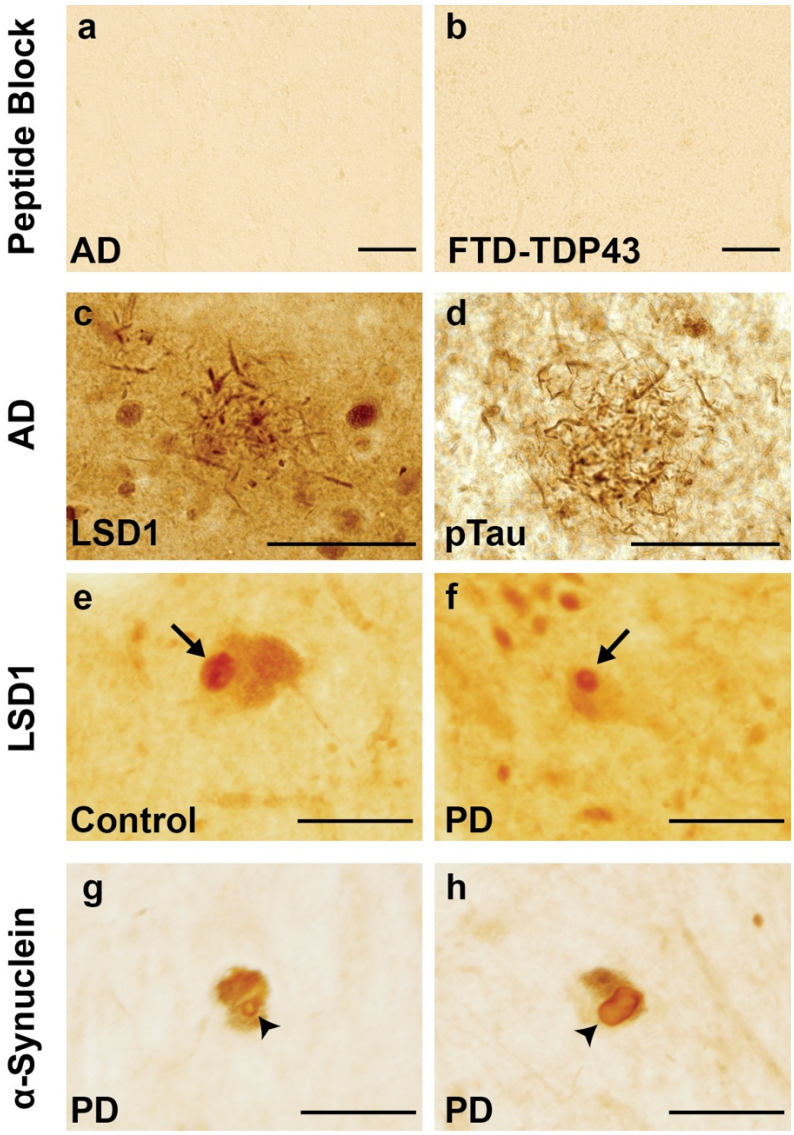

Figure 3-19 LSD1 mislocalization is specific to AD and FTD.

(**a,b**) LSD1 IHC with primary antibody preincubated with the target peptide shows an absence of signal in AD (**a**) and FTD-TDP43 (**b**). (**c,d**) LSD1 (**c**) and pTau (AT8 epitope) (**d**) immunohistochemistry (IHC) showing immunoreactivity localized to neurites (**c**) and neuropil threads (**d**) around a senile plaque, but not to the amyloid core of the plaque. (**e,f**) LSD1 IHC in control (**e**) and PD (**f**) dopaminergic neurons of the substantia nigra shows LSD1 localized to the nucleus (arrows) and not Lewy bodies. (**g,h**) α-Synuclein IHC in PD shows formation of Lewy bodies in dopaminergic neurons of the substantia nigra (arrowheads). Scale bars= 50μm.

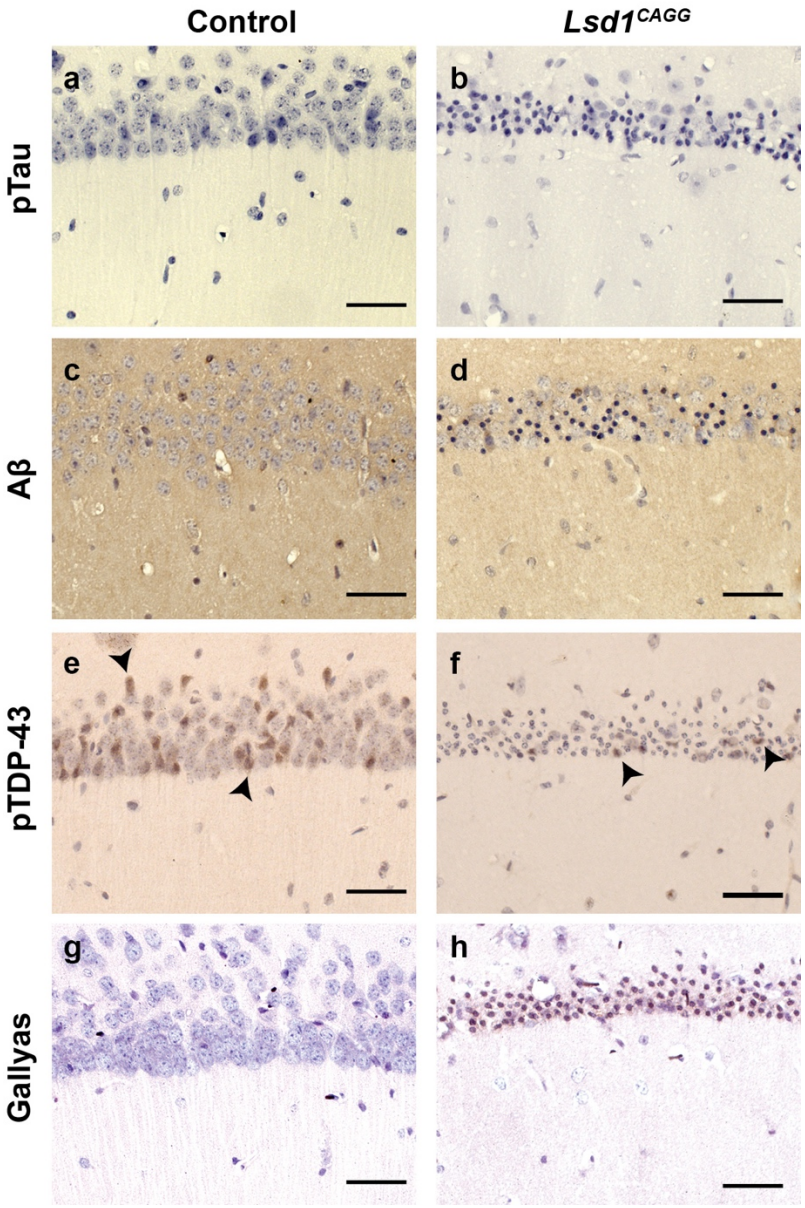

Figure 3-20 Absence of pathological protein aggregates in *Lsd1*^{CAGG} mice.

(**a-f**) pTau (AT8 epitope) (**a,b**), Aβ (**c,d**), and pTDP-43 (**e,f**) immunohistochemistry in control (**a,c,e**) and *Lsd1*^{CAGG} (**b,d,f**) CA1 neurons showing absence of aggregate forms of the proteins. pTDP-43 is found sporadically in control nuclei (**e**, arrowheads) and shows a similar staining pattern in *Lsd1*^{CAGG} non-pyknotic nuclei (**f**, arrowheads), but there is no evidence of pTDP-43 aggregation. (**g,h**) Gallyas silver staining in control (**g**) and *Lsd1*^{CAGG} (**h**) CA1 neurons showing lack of any protein aggregation (positive stain is black). Scale bars= 50μm.

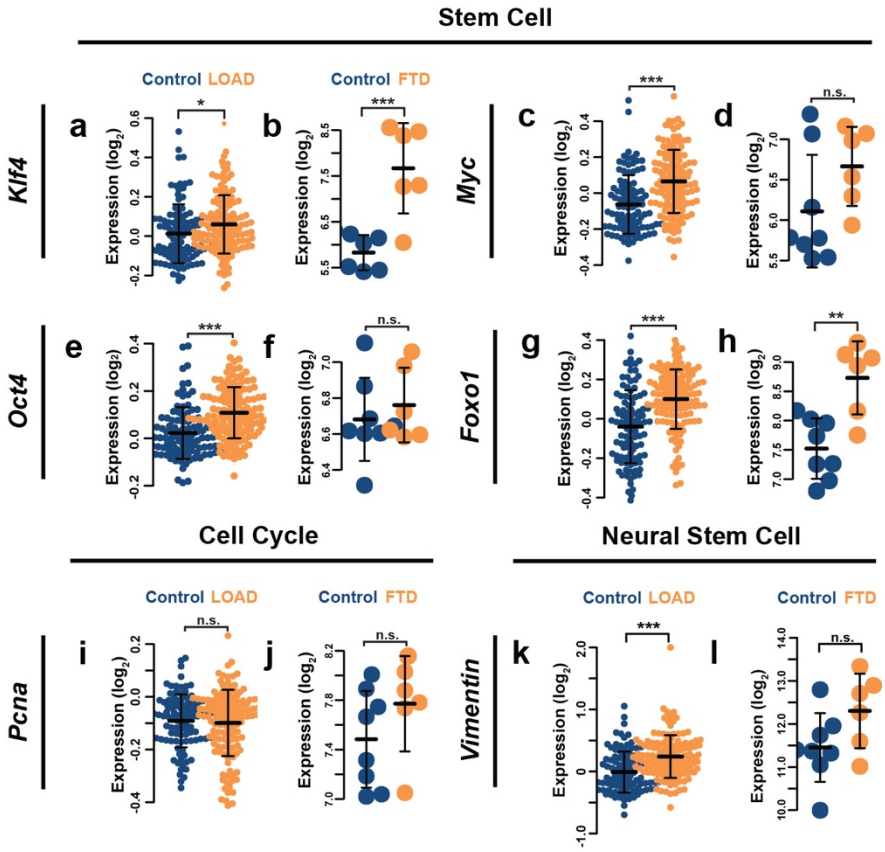

Figure 3-21 Stem cell gene expression in human dementia.

(**a-n**) Beeswarm plots showing expression of *Klf4* (**a,b**), *Myc* (**c,d**), *Oct4* (**e,f**), *Foxo1* (**g,h**), *PCNA* (**i,j**) and *Vimentin* (**k,l**) in control (blue) versus LOAD prefrontal cortex[29] (**a,c,e,g,i,k,** orange), or control (blue) versus FTD-progranulin frontal cortex[30] (**b,d,f,h,j,l,** orange). Values represent the $\log_2$ expression of each patient and bars represent mean ± s.d., *$P < 0.05$, **$P < 0.01$, ***$P < 0.001$, n.s.: not significant.

CHAPTER 4:

The Inhibition of LSD1 Via Sequestration Contributes to Tau-mediated Neurodegeneration

Amanda K. Engstrom, Alicia C. Walker, Rohitha A. Moudgal, Dexter A. Myrick, Stephanie M. Kyle, David J. Katz

This Chapter is from a manuscript that is under review at Review Commons

4.1 Abstract

Tauopathies are a class of neurodegenerative diseases associated with pathological tau. However, the mechanism through which tau contributes to neurodegeneration remains unknown. Previously, our lab implicated the histone demethylase LSD1 in tau-induced neurodegeneration by showing that LSD1 localizes to pathological tau aggregates in Alzheimer's disease cases, and that it is continuously required for the survival of hippocampal and cortical neurons in mice. Here, we utilize the P301S tauopathy mouse model to demonstrate that pathological tau can exclude LSD1 from the nucleus in neurons. In addition, we show that reducing LSD1 in these mice is sufficient to highly exacerbate tau-mediated neurodegeneration. Finally, we find that overexpressing LSD1 in the hippocampus of tauopathy mice, even after pathology has formed, is sufficient to significantly delay neurodegeneration. These results suggest that inhibiting LSD1 via sequestration contributes to tau-mediated neurodegeneration. Thus, LSD1 is a promising therapeutic target for tauopathies such as Alzheimer's disease.

4.2 Introduction

Tauopathies such as corticobasal degeneration, progressive supranuclear palsy, and frontotemporal lobar degeneration with tau inclusions are neurodegenerative diseases pathologically defined by different forms of tau positive intraneuronal deposits [2-5,222]. In addition to these primary tauopathies, neuropathological observations of postmortem Alzheimer's disease (AD) brains show the presence neurofibrillary tangles (NFTs) of hyperphosphorylated tau protein, as well as plaques containing β-amyloid (Aβ) peptide [28,33,34,223]. AD is the leading cause of age-related dementia, resulting from neuronal cell death in the frontal and temporal cortices, as well as the hippocampus [223]. As dementia progresses, the spatial pattern of tau pathology

highly correlates with the level of cognitive impairment [32,224-226]. In addition, Aβ oligomers and/or plaques can enhance tau pathology in various mouse models [227,228], and there is increasing evidence that accumulation of Aβ plaques can contribute to tau pathology [4,42,229]. The most well-defined physiological role of tau is in stabilizing microtubules, particularly in neuronal axons [3]. However, in the pathological state, tau becomes aberrantly phosphorylated [3,230,231], truncated [2,222], and aggregates into oligomers and larger insoluble filaments [18,232]. This pathology is thought to trigger synaptic loss, dramatic genome-wide expression changes, increased inflammatory response, and neuronal cell death [233-236]. These data suggest that pathological tau may be a downstream mediator of the neurotoxic effects leading to neuronal degeneration in AD.

Previously, our lab demonstrated that deleting the histone demethylase *Lsd1* in adult mice leads to significant neuronal cell death in the hippocampus and cortex with associated learning and memory defects [173]. In this mouse model, loss of *Lsd1* induces genome-wide expression changes that significantly overlap with those observed in the brains of postmortem human AD cases, but not other neurodegenerative diseases, such as Parkinson's disease or amyotrophic lateral sclerosis (ALS). Consistent with this overlap, we observed LSD1 protein mislocalized to cytoplasmic NFTs, but not associated with Aβ plaques in AD cases or Lewy bodies of α-synuclein in Parkinson's disease cases [173]. These data highlight the requirement for LSD1 in neuronal survival and suggest that the nuclear function of the histone demethylase LSD1 could be disrupted by mislocalization to pathological tau.

To investigate how LSD1 may contribute to tau-mediated neurodegeneration, we utilized the PS19 P301S tauopathy mouse model (hereafter referred to as PS19 Tau). PS19 Tau mice express a P301S mutated form of the human tau protein, originally identified in a frontotemporal dementia with parkinsonism (FTDP-17) patient, driven by the prion promoter throughout the

nervous system[49]. When expressed in mice, the P301S tau protein is prone to hyperphosphorylation and somatodendritic aggregation, without the presence of Aβ plaques. PS19 Tau mice develop a heavy pathological tau burden and have been well characterized for the temporal progression of tau pathology and disease-related phenotypes [237,238]. However, the mechanism of neuronal cell death caused by pathological tau is still unknown.

Here, we provide functional data that the inhibition of LSD1 function contributes to tau induced neurodegeneration. We demonstrate in PS19 Tau mice that pathological tau sequesters LSD1 in the cytoplasm of neurons throughout the brain. This results in depletion of LSD1 from the nucleus. Additionally, we provide genetic and molecular evidence that pathological tau contributes to neurodegeneration by disrupting LSD1. Finally, we show that overexpressing LSD1 in hippocampal neurons is sufficient to suppress neuronal cell death even after pathological tau has formed. We propose that pathological tau contributes to neuronal cell death by sequestering LSD1 in the cytoplasm, depleting the nuclear pool of LSD1 that is required for neuronal survival.

4.3 Results

4.3.1 Tau pathology depletes LSD1 from the nucleus in the PS19 Tau mouse

Previously, we showed in human AD cases that LSD1 protein inappropriately colocalizes with NFTs in the cell body of hippocampal and cortical neurons, while in unaffected controls LSD1 was properly localized exclusively to the nucleus [173]. However, because neurons in AD cases with intracellular NFTs presumably die and are cleared, it was difficult to determine whether tau prevents LSD1 from localizing to the nucleus in a dying neuron. To address this possibility, we performed LSD1 immunofluorescence on 12 month old PS19 Tau mice, which

have significant tau pathology[49]. Because PS19 Tau mice undergo neurodegeneration over a shortened period, there are more neurons undergoing neurodegeneration at any given time point. Thus, we reasoned that it may be possible to observe LSD1 depletion from the nucleus. Similar to what we observe in humans, LSD1 protein in 12 month old Wild Type mice was localized to the nucleus of neurons in the cerebral cortex (Figure 4-1A-C) and the hippocampus (Figure 4-2A-C). However, in 12 month old PS19 Tau mice, LSD1 protein was sequestered in the cytoplasm and depleted from the nucleus both in the cerebral cortex (Figure 4-1D-F) and the hippocampus (Figure 4-2D-F). These are both regions where we observe substantial cytoplasmic tau pathology (Figure 4-1G-I; Figure 3-2G-I). Similarly, in other brain regions that accumulate tau pathology, such as the thalamus and amygdala, LSD1 was localized to the nucleus in 12 month old Wild Type control mice (Figure 4-2J-O), but abnormally localized to the cytoplasm in PS19 Tau mouse littermates (Figure 4-2P-U). Overall, we observed sequestration of LSD1 in 6 out of 7 mice analyzed. In each of the 6 mice, there were varying levels of sequestration ranging from LSD1 found in both the nucleus and cytoplasm (Figure 4-2V-X), to depletion from the nucleus (Figure 4-2Y-DD).

4.3.2 Reduction of LSD1 increases the mouse tauopathy phenotype

If the presence of pathological tau in the cytoplasm is leading to neuronal cell death through the sequestration and nuclear depletion of LSD1, we would expect that lowering the overall levels of LSD1 would accelerate depletion and exacerbate the progression of disease. To test this, we made PS19 Tau mice heterozygous for *Lsd1* (hereafter referred to as PS19;$Lsd1^{\Delta/+}$, Figure 4-3A). *Lsd1* heterozygotes (hereafter referred to as $Lsd1^{\Delta/+}$) have a functioning copy of *Lsd1* and do not have phenotypes associated with LSD1 loss of function [166,239,240]. Thus, *Lsd1*

heterozygosity does not completely compromise LSD1 function. Instead mice that are heterozygous for *Lsd1* are sensitized to mechanisms affecting LSD1 localization and function. Consistent with this, we observed a 30% reduction in transcript levels (Figure 4-3B) and a 35% reduction in protein levels (Figure 4-3C,D) in $Lsd1^{\Delta/+}$ mice compared to their $Lsd1^{+/+}$ littermates. Surprisingly, PS19 Tau mice have a 20% increase in LSD1 protein levels compared to $Lsd1^{+/+}$ littermates. Nevertheless, consistent with the reduction in LSD1 that we observe in $Lsd1^{\Delta/+}$ mice, PS19;$Lsd1^{\Delta/+}$ mice have a similar 26% reduction in transcript levels (Figure 4-3B) and a 31% reduction in protein levels (Figure 4-3C,D) compared to PS19 Tau littermates. In addition, all genotypes were born at normal Mendelian ratios with equal male/female ratios.

As expected, $Lsd1^{\Delta/+}$ mice had normal survival (Figure 4-4A). In contrast, PS19 Tau mice had a reduced overall survival (Figure 4-4A)[49]. When one copy of *Lsd1* was removed from PS19 Tau mice, their lethality was significantly exacerbated (P-value = 0.0017, Figure 4-4A). As expected, there was little effect on the onset of reduced viability. The initial decline in the survival of PS19;$Lsd1^{\Delta/+}$ mice started only slightly earlier than PS19 Tau mice, after the appearance of pathological tau in neurons (Figure 4-9K-M)[49]. This suggests that pathological tau may have to be present before *Lsd1* heterozygosity has deleterious effects. Subsequently, PS19;$Lsd1^{\Delta/+}$ mice had a 14% reduction in median lifespan compared to PS19 Tau mice and reached median survival 44 days earlier then PS19 Tau mice. In addition, there was a further exacerbation of reduced lifespan as pathology became more severe. PS19;$Lsd1^{\Delta/+}$ mice reached the point when there was only 10% of the population remaining 83 days earlier than PS19 Tau mice, and all but one of the last 25% of PS19;$Lsd1^{\Delta/+}$ mice died between 11.5-13.5 months, compared to 13.5-19 months in PS19 Tau mice. As a result, 28% of PS19 Tau mice were still alive after all but one of the PS19;$Lsd1^{\Delta/+}$ mice had died (Figure 4-4A).

PS19 Tau mice develop paralysis starting with hind limb clasping which progresses until they are unable to feed[49]. In our hands, PS19 Tau mice displayed intermittent hind limb clasping starting at approximately 6 months of age. At 12 months, these mice had a severe clasp, but were still mobile. This is delayed compared to what was originally reported by Yoshiyama and colleagues[49]. PS19;*Lsd1*$^{\Delta/+}$ mice also displayed intermittent hind limb clasping beginning at approximately 6 months of age. However PS19;*Lsd1*$^{\Delta/+}$ mice became terminally paralyzed at a faster rate compared to PS19 Tau mouse littermates. At 12 months, when PS19 Tau mice were still mobile, PS19;*Lsd1*$^{\Delta/+}$ mice were severely paralyzed and typically terminal. To quantitatively assess paralysis we performed rotarod and grid performance tests. In the rotarod, we assessed the ability of the mice to stay on the rotating rod (latency to fall) (Figure 4-4B), the speed of the rod at which they fall off the rotarod (rotations per minute) (Figure 4-4C), and the total distance traveled (Figure 4-4D). All genotypes performed the same at 6 months and 8 months (Figure 4-4B-D). However, at 10 months, when PS19 Tau mice still performed normally, PS19;*Lsd1*$^{\Delta/+}$ mice had a significant deficit in mobility (P-value < 0.01, Figure 4-4B,C). A deficit in PS19;*Lsd1*$^{\Delta/+}$ mice was also observed at 10 months in the total distance traveled (Figure 4-4D) and in grid performance testing (Figure 4-5A), though neither were statistically significant.

To further investigate the exacerbation of paralysis we examined the spinal cord motor neurons. Healthy motor neurons from *Lsd1*$^{+/+}$ control mice express LSD1 (Figure 4-5B-D) and are classically identified by circular nuclei at the center of a large cell body. In contrast to the healthy motor neurons we observed in 12 month old PS19 Tau mice (Figure 4-5E), many of the motor neurons in PS19;*Lsd1*$^{\Delta/+}$ mice at 12 months had abnormal morphology, with the nucleus skewed to the edge of the cell body (Figure 4-5Evs.F) and a ballooned cell body (Figure 4-5F). Within the cell body we found aberrant hyperphosphorylated NFH (heavy chain neurofilament),

which is a sign of activated neuronal stress pathways (Figure 4-5Gvs.H) [241,242]. This abnormal morphology is highly reminiscent of a well-established process known as chromatolysis, which is characterized by swelling of the neuronal cell body, disruption of Nissl granules, and pyknotic or shrunken nuclei abnormally skewed to the edge of the cell body [243,244]. Chromatolysis, which is linked to neuronal stress and often leads to apoptosis [244], has been observed in AD and other neurodegenerative diseases [243,245-247].

4.3.3 Reduction of LSD1 exacerbates PS19 Tau neurodegeneration

In addition to accelerating the paralysis phenotype, reducing the level of *Lsd1* in PS19 Tau mice exacerbated neuronal cell death in the brain. At 6 months and 8 months, we observed no difference between genotypes in the overall morphology in the hippocampus (Figure 4-6A-H) based on histological analysis. There was also no difference between $Lsd1^{+/+}$ and $Lsd1^{\Delta/+}$ mice at 10 months or 12 months (Figure 4-7A,B; Figure 4-6I,J,M,N; Figure 4-8A,B,E,F,I,J,M,N). At 10 months, PS19 Tau mice had very little cell loss in the hippocampus compared to $Lsd1^{+/+}$ and $Lsd1^{\Delta/+}$ control mice (Figure 4-6I-K, M-O). In contrast, at 10 months, PS19;$Lsd1^{\Delta/+}$ mice had dramatic cell loss both in the CA1 region of the hippocampus and throughout the posterior hippocampus (Figure 4-6L,P). At 12 months, the PS19 Tau mice had a slight decrease in CA1 and CA3 neurons spanning the hippocampal pyramidal cell layer compared to $Lsd1^{+/+}$ control mice (17% and 19.4% respectively, Fig. 3A,B; Fig. S5 A-C, E-G). In comparison, PS19;$Lsd1^{\Delta/+}$ mice had a 52% and 54% decrease in the CA1 and CA3 respectively (Figure 4-7A,B; Figure 5-8D,H) compared to $Lsd1^{+/+}$ control mice. This resulted in decreased overall brain size (Figure 4-7C) and brain weight (Figure 4-7D) in PS19;$Lsd1^{\Delta/+}$ mice compared to PS19 Tau and $Lsd1^{\Delta/+}$

mouse littermates. Additionally, at 12 months there were increased levels of cell loss in the Dentate Gyrus (Figure 4-8I-L), and throughout the posterior hippocampus (Figure 4-8M-P).

Along with the histology, we monitored the progression of neuronal cell death in the same individual over time by performing magnetic resonance imaging (MRI) at 6 months and again at 10 months. At 6 months, there was no sign of cell loss or ventricular dilatation in *Lsd1*$^{\Delta/+}$, PS19 Tau, or PS19;*Lsd1*$^{\Delta/+}$ mice (Figure 4-7E-G). However, at 10 months the MRI showed that there was dramatic ventricular dilatation in PS19;*Lsd1*$^{\Delta/+}$ mice, as evidenced by high-intensity areas in T2- weighted imaging, with substantial hippocampal and neocortical atrophy (Figure 4-7Jvs.H). At this timepoint, PS19 Tau mice had some ventricular dilatation and hippocampal atrophy throughout the hippocampus (Figure 4-7I), but much less than PS19;*Lsd1*$^{\Delta/+}$ mice (Figure 4-7J).

4.3.4 Tau pathology is not effected by change in LSD1 levels

Since LSD1 is a chromatin regulator, it is possible that reducing LSD1 protein levels affects the PS19 Tau transgene. However, we confirmed that there was no difference between PS19 Tau mice and PS19;*Lsd1*$^{\Delta/+}$ mice in the endogenous mouse *Mapt* RNA expression, nor in the human P301S MAPT transgene expression (Figure 4-9A). It is also possible that LSD1 affects tau pathology. To test this, we performed immunohistochemistry staining for a hyperphosphorylated form of tau (AT8). As expected, we did not observe any AT8 positive staining in *Lsd1*$^{\Delta/+}$ at 6, 8, or 10 months (Figure 4-9B,E,H). Additionally, we observed very little AT8 positive immunoreactivity at 6 months in both PS19 Tau or PS19;*Lsd1*$^{\Delta/+}$ mice (Figure 4-9C,D). At 8 months both PS19 Tau and PS19;*Lsd1*$^{\Delta/+}$ mice had low but consistent levels of AT8 positive immunoreactivity (Figure 4-9F,G), and by 10 months both PS19 Tau and PS19;*Lsd1*$^{\Delta/+}$

mice developed the same high level of AT8 positive tau immunoreactivity (Figure 4-9I,J). This was consistent throughout both the CA1 and CA3 regions of the hippocampus and the cerebral cortex (Figure 4-9K-M). We also did not observe any difference between PS19 Tau mice and PS19;*Lsd1*$^{\Delta/+}$ mice when assaying PHF1 (an alternative phospho-tau antibody) immunoreactivity in the CA1 region of the hippocampus at 8 months (Figure 4-10A-C, G) and 10 months (Figure 4-10D-F, G), nor in the CA3 region of the hippocampus or the cerebral cortex at 8 and 10 months (Figure 4-10H,I).

4.3.5 The interaction between tau pathology and LSd1 inhibition is specific

To test the specificity of the functional interaction between tau pathology and LSD1, we investigated the overlap in the effected molecular pathways associated with both pathological tau and *Lsd1* heterozygosity. To address this, we performed RNA sequencing on the hippocampus of 9 month *Lsd1*$^{+/+}$, *Lsd1*$^{\Delta/+}$, PS19 Tau, and PS19;*Lsd1*$^{\Delta/+}$ littermates. As opposed to analyzing transcriptional changes at the terminal stage of disease, this time point allows us to assess molecular changes prior to the onset of neuronal cell death. This is also the time point that we observed the earliest signs of exacerbation of paralysis in PS19;*Lsd1*$^{\Delta/+}$ mice. Because of this early stage in the progression of the disease, we would not expect dramatic changes in transcription overall. Nevertheless, if tau pathology is inhibiting LSD1 function, we would expect that the genome-wide expression changes induced by tau might be exacerbated by a reduction in LSD1. The RNA-seq analysis detected 54 significant gene expression changes in PS19 Tau mice compared to *Lsd1*$^{+/+}$ (Figure 4-11A,B), and 271 significant gene expression changes in PS19;*Lsd1*$^{\Delta/+}$ mice compared to *Lsd1*$^{+/+}$ (Figure 4-11C,D). Importantly, *Lsd1*$^{\Delta/+}$ mice had only 4 gene expression changes observed genome-wide (Figure 4-11E,F), indicating that the

partially reduced level of LSD1 expression had very little effect on transcription on its own. This is consistent with the lack of phenotype in these animals.

We first examined the relationship between tau-induced expression changes and the effects of *Lsd1* heterozygosity by comparing the transcriptional changes observed in PS19 Tau mice with PS19;$Lsd1^{\Delta/+}$ mice. In PS19 Tau mice that do not yet have significant neurodegeneration, we identified 54 genes (36 up and 18 down) that were differentially expressed. Of these 54 genes, 50 were similarly deregulated in PS19;$Lsd1^{\Delta/+}$ mice (93%). In addition, amongst the 50 genes changed in the same direction, 36 (72%) had exacerbated expression in PS19;$Lsd1^{\Delta/+}$ mice compared to PS19 Tau mice (Figure 4-12A). Therefore we see the similar gene expression changes with severity increased when LSD1 levels are reduced. Based on this overlap, we further compared the expression changes between PS19 Tau mice and PS19;$Lsd1^{\Delta/+}$ mice genome-wide. Amongst the transcripts that were changed in both PS19 Tau mice and PS19;$Lsd1^{\Delta/+}$ mice compared to $Lsd1^{+/+}$ mice, 71% changed in the same direction (either up or down). Consistent with this overlap in gene expression, Gene Set Enrichment Analysis demonstrated that the pathways that are affected in both PS19 Tau mice and PS19;$Lsd1^{\Delta/+}$ mice are very similar (Figure 4-11G-J). However, the genes affected in both sets of mice tended to be further exacerbated in PS19;$Lsd1^{\Delta/+}$ mice compared to PS19 Tau mice. Amongst the 71% of genes that changed in the same direction in both PS19 Tau mice and PS19;$Lsd1^{\Delta/+}$ mice, 76% of these transcripts had a higher fold-change in PS19;$Lsd1^{\Delta/+}$ mice compared to PS19 Tau mice (Figure 4-12B).

4.3.6 Overexpression of LSD1 rescues neurodegeneration in PS19 Tau mice

Our data demonstrate that reduction of LSD1 protein exacerbates the tauopathy phenotype in PS19 Tau mice. Based on this, we considered the possibility that overexpression of LSD1 might counter the loss of LSD1 from the nucleus and protect against neurodegeneration in PS19 Tau mice. To address this possibility, we injected PS19 Tau mice with a neuronal specific virus (AAV-DJ driven by the synapsin promoter) expressing either the full length LSD1 protein with an N-terminal HA tag (hereafter referred to as PS19- LSD1 inj) or a control virus expressing only the HA tag (hereafter referred to as PS19- HA inj). Additionally, to control for the effects of viral injection, we injected Wild Type littermates with the HA only expressing virus (hereafter referred to as WT- HA inj). All injections were performed directly into the hippocampus at 8-8.5 months, when tau pathology is already present throughout the nervous system. Immunolabeling for the HA tag demonstrated that the virus is specific to NeuN+ neurons (Figure 4-13A-D), with no HA expression observed in IBA+ microglia (Figure 4-13E-H), or GFAP+ astrocytes (Figure 4-13I-L). It also confirmed that virally expressed LSD1 is nuclear (Figure 4-13M) and confined to the hippocampus (Figure 4-13N). After 3 months of overexpression, 11-11.5 month old mice were euthanized, and the brains were analyzed. Injections resulted in a ~6-fold increase in expression of LSD1 in the hippocampus compared to endogenous LSD1 in the PS19- HA inj mice, but no increase in the cerebellum (Figure 4-13O,P). As expected, because the viral injections were restricted to the hippocampus, the mice injected with LSD1 still developed paralysis. This confirms that the tau transgene is expressed and functioning. Additionally, we did not observe a difference in total levels of AT8 positive tau immunoreactivity (Figure 4-13Q-T). Therefore, any modulation to the phenotype was not due to changes in tau pathology.

Injected mice were evaluated for cell death by neuronal cell counts in the hippocampus. Injection of LSD1 virus into the hippocampus of PS19 Tau mice rescued the neurodegeneration phenotype. At 11 months, compared to WT-HA inj control mice, 70% of the PS19-HA inj mice had hippocampal cell counts that were below the lowest WT-HA inj control, while none of the Tau mice injected with the LSD1 virus were below this level. Overall, we observed significantly more neurons (P-value <0.05) spanning the pyramidal cell layer (84% of WT- HA inj CA1 counts) compared to their PS19- HA inj littermates (59% of WT- HA inj CA1 counts), such that overall the neuronal cell count in PS19- LSD1 inj mice was not statistically different from the WT- HA inj (Figure 4-14A-D). Additionally, in the histological analysis we observed a large number of cells infiltrating the hippocampus in PS19- HA inj mice compared to WT- HA inj littermates (Figure 4-14Bvs.C). Marker analysis demonstrated that this was due to a strong inflammatory response, with a large increase in the number of GFAP+ astrocytes (Figure 4-15A-Cvs.D-F) and TRL2+ activated microglia (Figure 4-15J-Lvs.M-O, S-Vvs.W,Z, EE). Injection of PS19 Tau mice with LSD1 virus rescued this inflammatory response. For example, all but one (9 out of 10 analyzed) of the PS19- LSD1 inj mice had a reduction in the number of GFAP+ astrocytes (Figure 4-15G-Ivs.D-F) and TRL2+ activated microglia (Figure 4-15P-Rvs.M-O, AA-DDvs.W-Z, EE). Of note, the one PS19- LSD1 inj mouse where we did observe increased glial cells, similar to PS19- HA inj mice, had the lowest neuronal cell count (74% of WT- HA inj CA1 neurons). It is possible that this mouse was already undergoing neurodegeneration prior to the injection of the LSD1 overexpression virus.

Although the number of hippocampal neurons in PS19- LSD1 inj mice did not differ from WT- HA inj controls, in 6 of the 10 PS19- LSD1 inj mice we observed cells with abnormal blebbed nuclei at varying numbers throughout the hippocampus (Figure 4-14E). These abnormal

cells are rare in PS19- HA inj mice, which have a reduced overall number of cells in the pyramidal cell layer compared to WT- HA inj control mice. One possibility is that these abnormal cells with blebbing nuclei represent an intermediate state between a healthy neuron and a dying neuron that is prolonged by rescue via LSD1 overexpression. Interestingly, these abnormal cells also differed in the localization of HA-tagged LSD1. The four mice with normal nuclei had HA-tagged LSD1 protein localized uniformly throughout the nucleus (Figure 4-14F). In contrast, the six mice with abnormal nuclear blebbing had some HA-tagged LSD1 that was mislocalized to the cytoplasm (Figure 4-14G). This includes the one PS19- LSD1 inj mouse that had an elevated number of astrocytes and TRL2 positive microglia. Thus, the blebbing state correlates with when the viral produced LSD1 begins to be sequestered in the cytoplasm, similar to the endogenously produced LSD1.

4.4 Discussion

In this study we investigate a potential downstream mediator of tau pathology in neurodegenerative disease. We find that modulation of the chromatin modifying enzyme LSD1 can alter neurodegeneration in a tauopathy mouse model. Previously, we showed that LSD1 colocalizes with tau pathology in the cell body of neurons in AD cases [173]. This suggested that LSD1 might be disrupted in tauopathies such as AD, by being excluded from the nucleus. To address this directly, we utilize the PS19 tauopathy mouse model. In these mice, we find that LSD1 is sequestered in the cytoplasm, in some cases being completely depleted from the nucleus. This provides the first cytological evidence that pathological tau can prevent LSD1 from properly localizing to the nucleus in hippocampal and cortical neurons, where we have previously shown it is continuously required.

Based on the ability of pathological tau to sequester LSD1, we hypothesized that neuronal cell death may be due, at least partly, to LSD1 being sequestered in the cytoplasm and depleted from the nucleus. In this case, reducing LSD1 levels should make it easier for tau to deplete LSD1 from the nucleus, resulting in a faster progression of neurodegeneration and/or a more severe neurodegenerative phenotype. Importantly, LSD1 heterozygosity alone induces only 4 significant gene expression changes and does not lead to any neurodegeneration. This suggests that any effects observed in PS19;*Lsd1*$^{\Delta/+}$ mice are not simply due to LSD1 haploinsufficiency. Normally, PS19 Tau mice develop paralysis and neurodegeneration, along with reduced survival. In contrast, when we reduce LSD1 in the PS19 Tau mice, PS19;*Lsd1*$^{\Delta/+}$ mice die significantly earlier, most likely due to the increased rate of paralysis. Additionally, PS19;*Lsd1*$^{\Delta/+}$ mice have increased neuronal cell death and clearance in the hippocampus. This suggests that pathological tau functions through LSD1 to cause neurodegeneration *in vivo* in mice.

PS19;*Lsd1*$^{\Delta/+}$ mice have a 31% reduction in LSD1 protein levels compared to PS19 Tau mice from birth. This reduction should theoretically make mice sensitive to LSD1 depletion at any time. However, tau pathology starts at 6-8 months in PS19 Tau mice. As a result, if *Lsd1* heterozygosity is functioning by making it easier for pathological tau to deplete LSD1 from the nucleus, we would not expect to see any exacerbation until after pathological tau is present. The exacerbation of the PS19 Tau mouse neurodegenerative phenotype does not occur until after pathological human tau was present. This suggests that the effect of *Lsd1* heterozygosity requires the presence of pathological tau, placing LSD1 downstream of tau. Consistent with LSD1 being downstream of pathological tau, we found no evidence that *Lsd1* heterozygosity affects the expression of the tau transgene, or the buildup of pathological tau in PS19 Tau mice.

To test whether the functional interaction between pathological tau and reduced LSD1 is specific, we used RNA-seq to determine whether the downstream molecular pathways altered in PS19 Tau mice are exacerbated in PS19;*Lsd1*$^{\Delta/+}$ mice. This analysis was performed at the time of earliest signs of neuronal distress, allowing us to assess molecular changes prior to cell death and clearance. LSD1 heterozygosity induces only 4 significant expression changes. In addition, the pathways affected in both PS19 Tau mice and PS19;*Lsd1*$^{\Delta/+}$ mice are very similar. This suggests that reducing LSD1 did not induce any additional neurodegeneration pathways. In contrast, when LSD1 is reduced in PS19 Tau mice, the genome-wide expression changes induced by pathological tau are specifically exacerbated. This suggests that the functional interaction that we observe between pathological tau and reduced LSD1 is occurring through one downstream pathway.

Our previous data implicated LSD1 in the tau-mediated neurodegeneration pathway. Utilizing the PS19 Tau mouse model, we now show a functional interaction between pathological tau and LSD1. Importantly, because PS19 Tau mice do not have Aβ plaque accumulation, this functional interaction is specific to tau. Based on these data we propose the following model (Movie S4): in healthy hippocampal and cortical neurons, LSD1 is translated in the cytoplasm and transported into the nucleus where it is continuously required to repress inappropriate transcription. In tauopathy, pathological tau accumulates in the cytoplasm blocking LSD1 from nuclear import. This interferes with the continuous requirement for LSD1, resulting in neuronal cell death. Recently, it has been observed that the nuclear pore breaks down in AD [248-250]. It should be noted that this mechanism would potentially exacerbate the model that we propose.

This model makes a direct prediction: if tau is predominantly functioning through LSD1, then increasing the levels of LSD1 should rescue the tau-induced neurodegenerative phenotype. To address this, we overexpressed LSD1 in the hippocampal neurons of PS19 Tau mice. Overexpression of LSD1 specifically in hippocampal neurons rescues the neuronal cell death and limits the inflammatory response. This rescue is neuronal specific, suggesting that the functional interaction between LSD1 and tau is occurring in neurons. In addition, this rescue occurs despite there being no effect on tau aggregation. This negates the possibility that the tau transgene is simply not functioning when LSD1 is overexpressed. The ability of LSD1 overexpression to overcome tau-mediated neurodegeneration in the presence of pathological tau aggregates, provides further evidence that pathological tau is functioning through the inhibition of LSD1. Importantly, overexpressing LSD1 should not prevent it from being sequestered. Rather overexpressing LSD1 should make it more difficult for pathological tau to sequester all of the LSD1 protein, allowing some LSD1 to be transported to the nucleus. Thus, overexpressing LSD1 would be expected to temporarily rescue the ability of pathological tau to kill neurons. Consistent with this, LSD1 overexpression delays the effect of pathological tau rather than permanently rescuing. In 60% of the mice, the surviving neurons have abnormal morphology, and the overexpressed version of LSD1 is also sequestered. observation that neurons fail to maintain their morphology when the overexpressed LSD1 begins to be sequestered in the cytoplasm provides further support for the model that tau mediates neurodegeneration through the sequestration of LSD1. Nevertheless, our data suggest that overexpression of LSD1 cannot permanently overcome pathological tau. To permanently overcome pathological tau, it would likely be necessary to permanently disrupt the interaction between pathological tau and LSD1. This work is currently ongoing in the lab. Overall, our data establish LSD1 as a major

downstream effector of tau-mediated neurodegeneration. Based on these data, we propose that the LSD1 pathway is a potential late stage target for intervention in tauopathies, such as AD.

4.5 Figures

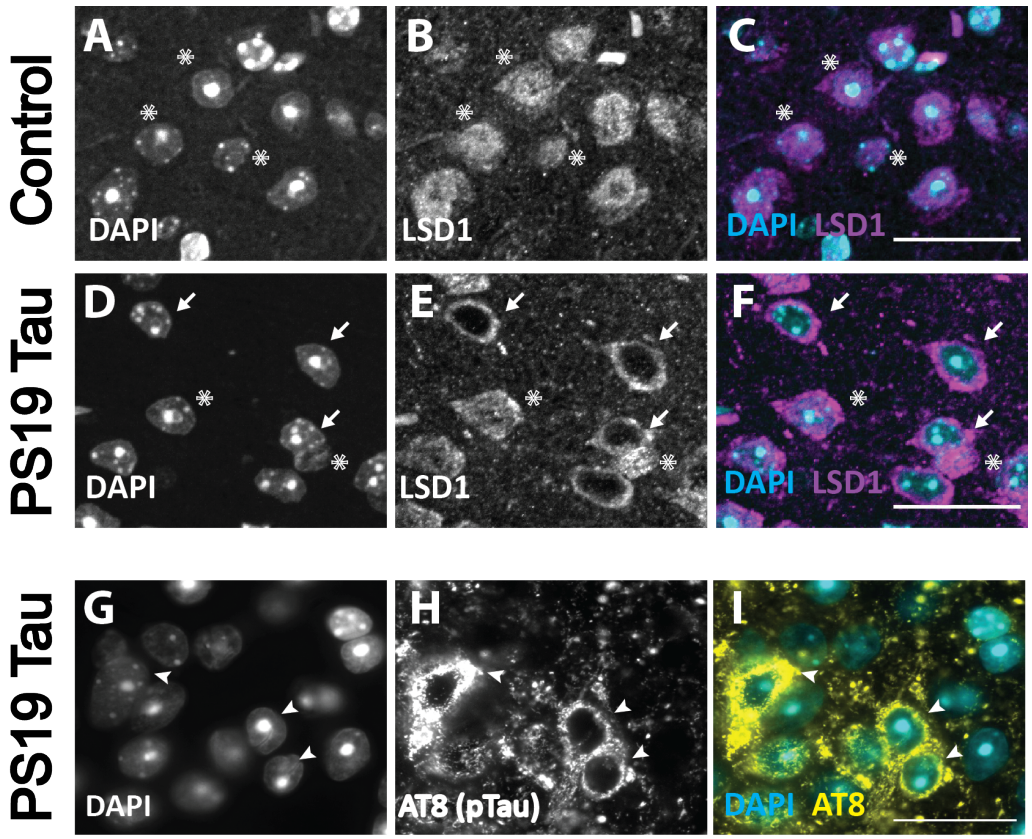

Figure 4-1 LSD1 sequestration and tau accumulation in PS19 Tau mice. A-C, Representative immunofluorescence of 12 month old control Wild Type mice showing DAPI (**A**), LSD1 (**B**), and merged (**C**) in the cerebral cortex where LSD1 is localized specifically to DAPI positive nuclei. **D-F**, Representative image of the cerebral cortex in 12 month old PS19 Tau mice. Staining for DAPI (**D**), LSD1 (**E**), and merged (**F**) shows that LSD1 is localized outside the nucleus, and depleted from the DAPI positive nucleus. Arrows denote cells where LSD1 is localized outside of the nucleus, and asterisks denote LSD1 localized specifically to the nucleus. **G-I,** Representative immunofluorescence of 12 month old PS19 Tau mouse with staining for DAPI (**G**), AT8 positive hyper-phosphorylated tau (**H**) and merge (**I**) where hyper-phosphorylated tau accumulates in the cytoplasm of the cell body. Arrowheads denote hyper-phosphorylated tau. Scale bars=25µm.

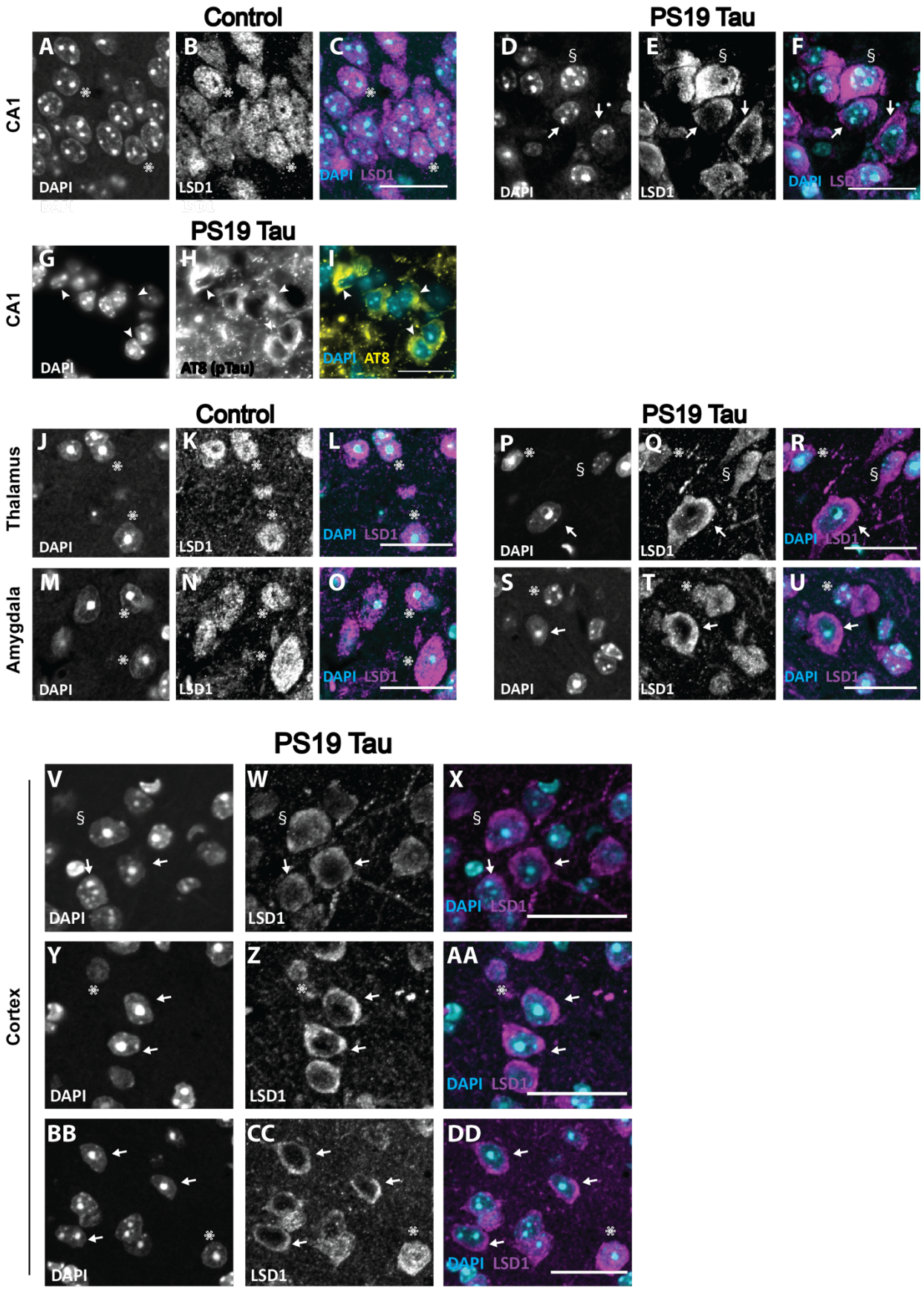
Control
PS19 Tau
CA1
A
B
C
D
E
F
DAPI
LSD1
DAPI LSD1
§
PS19 Tau
CA1
G
H
I
DAPI
AT8 (pTau)
DAPI AT8
Control
PS19 Tau
Thalamus
Amygdala
J
K
L
P
Q
R
M
N
O
S
T
U
PS19 Tau
Cortex
V
W
X
Y
Z
AA
BB
CC
DD

Figure 4-2 Sequestration of LSD1 in PS19 Tau mice. A-F, Representative immunofluorescence showing DAPI (**A,D**), LSD1 (**B,E**), and merged (**C,F**) images in the CA1 region of the hippocampus in 12 month old Wild Type (**A-C**) and PS19 mice (**D-F**). **G-I**, Representative immunofluorescence showing DAPI (**G**), AT8 positive hyper-phosphorylated tau (**H**), and merged (**I**) in the CA1 region of the hippocampus of 12 month old PS19 Tau mice showing hyper-phosphorylated tau accumulation in the cytoplasm of the cell bodies. Arrowheads denote hyper-phosphorylated tau. **J-U,** Representative immunofluorescence showing DAPI (**J,M,P,S**), LSD1 (**K,N,Q,T**), and merged (**L,O,R,U**) images in the thalamus (**J-L,P-R**) and amygdala (**M-O,S-U**). In 12 month old control Wild Type mice (**J-O**), LSD1 is localized specifically to the DAPI positive nuclei, but in 12 month old PS19 Tau mice (**P-U**) LSD1 is localized outside of the nucleus. **V-DD,** Additional examples of immunofluorescence showing DAPI (**V,Y,BB**), LSD1 (**W,Z,CC**), and merged (**X,AA,DD**) of the cerebral cortex of 12 month old PS19 Tau mice. Arrows denote cells where LSD1 is localized outside of the nucleus, asterisks denote LSD1 localized specifically to the nucleus, and § denotes cells where LSD1 is both nuclear and cytoplasmic. *n*=7 mice analyzed (images representative of 6 of the 7 mice analyzed). Scale bars=25μm.

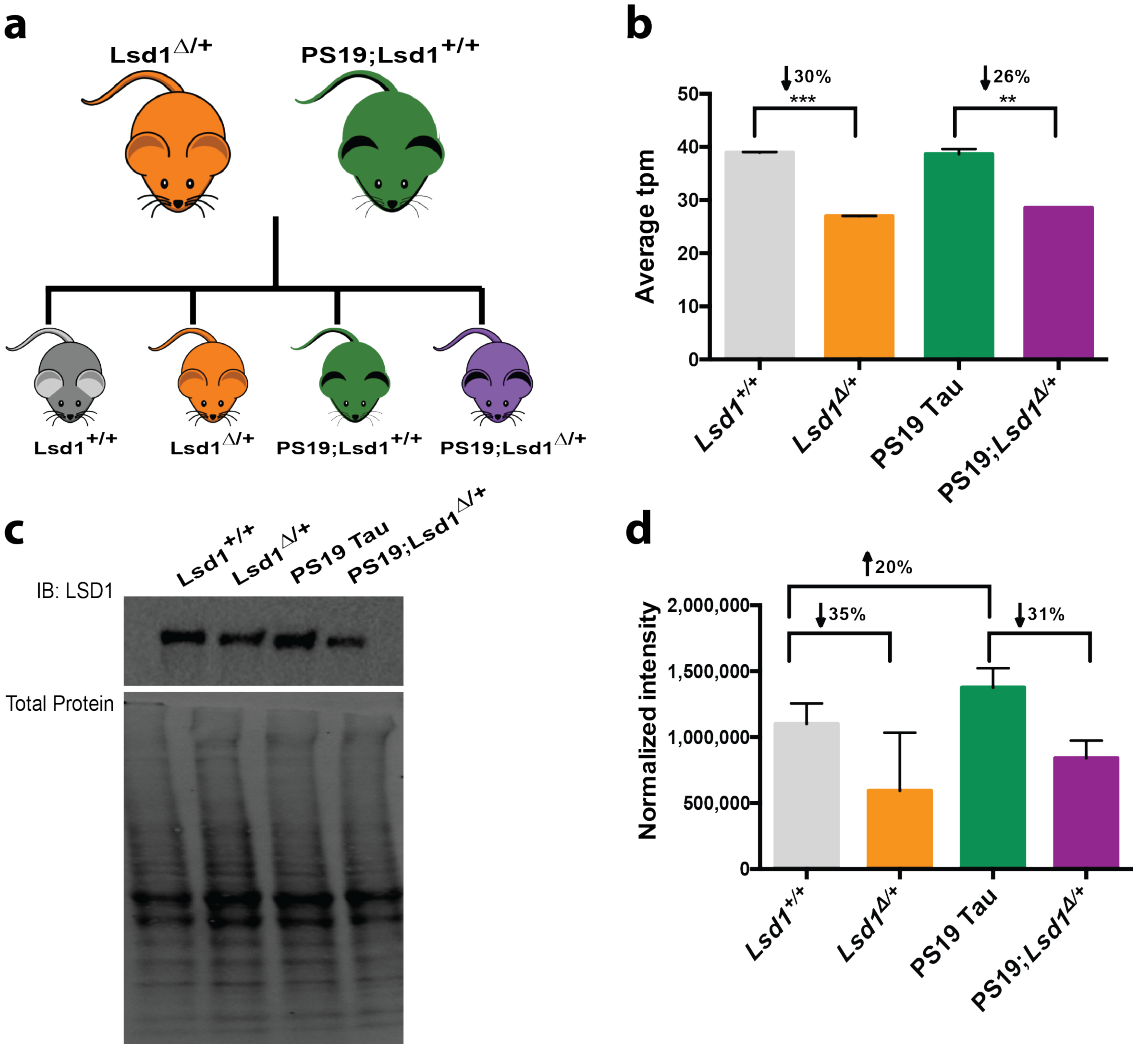

Figure 4-3 Generation of PS19 Tau mice with reduced levels of LSD1. a, PS19 Tau mice carrying the P301S human tau transgene that are wild-type for *Lsd1* were crossed with *Lsd1* heterozygous mice. These crosses generated four genotypes: Wild Type mice ($Lsd1^{+/+}$, grey), *Lsd1* heterozygous mice ($Lsd1^{\Delta/+}$, orange), PS19 Tau mice that are wild-type for *Lsd1* (PS19;$Lsd1^{+/+}$ referred to as PS19 Tau, green), and PS19 Tau mice that are heterozygous for *Lsd1* (PS19;$Lsd1^{\Delta/+}$, purple). Colors designated here are maintained throughout all figures. **b,** Average transcripts per million (tpm) from RNA-sequencing of *Lsd1* expression in the hippocampus of $Lsd1^{+/+}$, $Lsd1^{\Delta/+}$, PS19 Tau, and PS19;$Lsd1^{\Delta/+}$ mice. $Lsd1^{\Delta/+}$ mice had a 30% reduction in expression compared to $Lsd1^{+/+}$ mice, and PS19;$Lsd1^{\Delta/+}$ had a 26% reduction in

expression compared to PS19 Tau mice. Values are mean ± SD (*n*=2, one-way analysis of variance (ANOVA) **P<0.01, ***P<0.005). **c,** Representative image of protein levels in the brain of *Lsd1*$^{+/+}$, *Lsd1*$^{\Delta/+}$, PS19 Tau, and PS19;*Lsd1*$^{\Delta/+}$ mice from LSD1 immunoblot and corresponding total protein blot. **d,** Quantification of immunoblot for LSD1 normalized to total protein loaded per sample as represented in **Figure 4-3c**. Compared to *Lsd1*$^{+/+}$ mice, *Lsd1*$^{\Delta/+}$ mice had a 35% reduction and PS19 Tau mice had 20% increase in LSD1 protein levels. PS19; *Lsd1*$^{\Delta/+}$ mice had a 31% reduction in LSD1 protein level compared to PS19 Tau mice. Values are mean ± SD (*n*=3, one-way analysis of variance (ANOVA)).

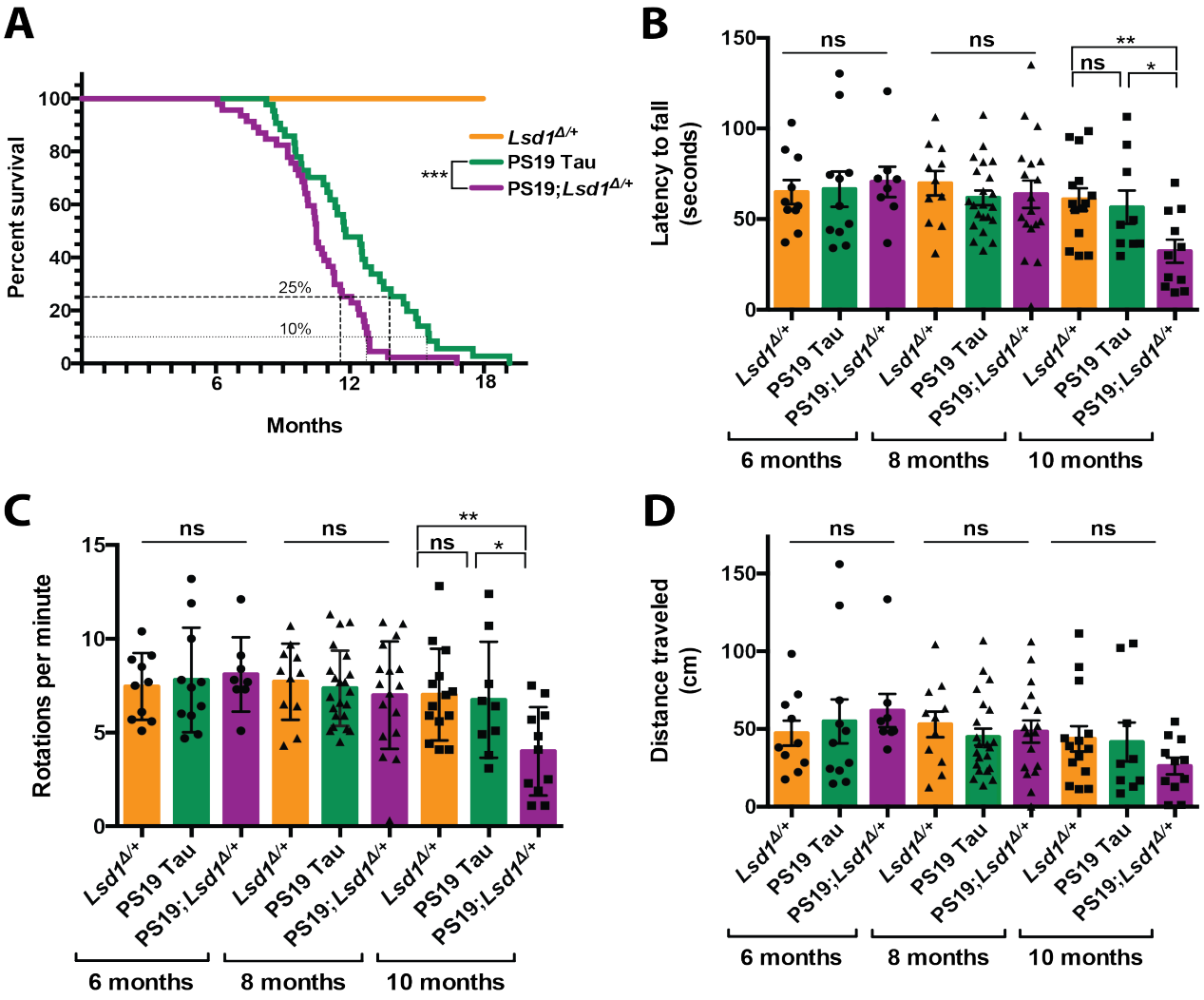

Figure 4-4 Reduction of *Lsd1* exacerbates the PS19 Tau mouse paralysis phenotype. A, Lifespan curve showing that no *Lsd1*$^{\Delta/+}$ mice died before 18 months (orange, *n*=20). PS19;*Lsd1*$^{\Delta/+}$ mice (purple, *n*=44) have a significant reduction in survival compared to PS19 Tau mice with wild-type levels of *Lsd1* (green, *n*=37)(Log-rank Mantle-Cox test ***P<0.005). **B-D**, Rotarod testing of latency to fall (in seconds) (**B**), rotations per minute (when the mouse fell) (**C**), and distance traveled (in centimeters) (**D**) for mice at age 6, 8 and 10 months. *Lsd1*$^{\Delta/+}$ (orange, *n*=10,11,14), PS19 Tau (green, *n*=11,22,9), and PS19;*Lsd1*$^{\Delta/+}$ (purple, *n*=8,17,11). Values are mean ± SEM (two-way analysis of variance (ANOVA) with Tukey's post hoc test *P<0.05 **P<0.01, ns=not significant).

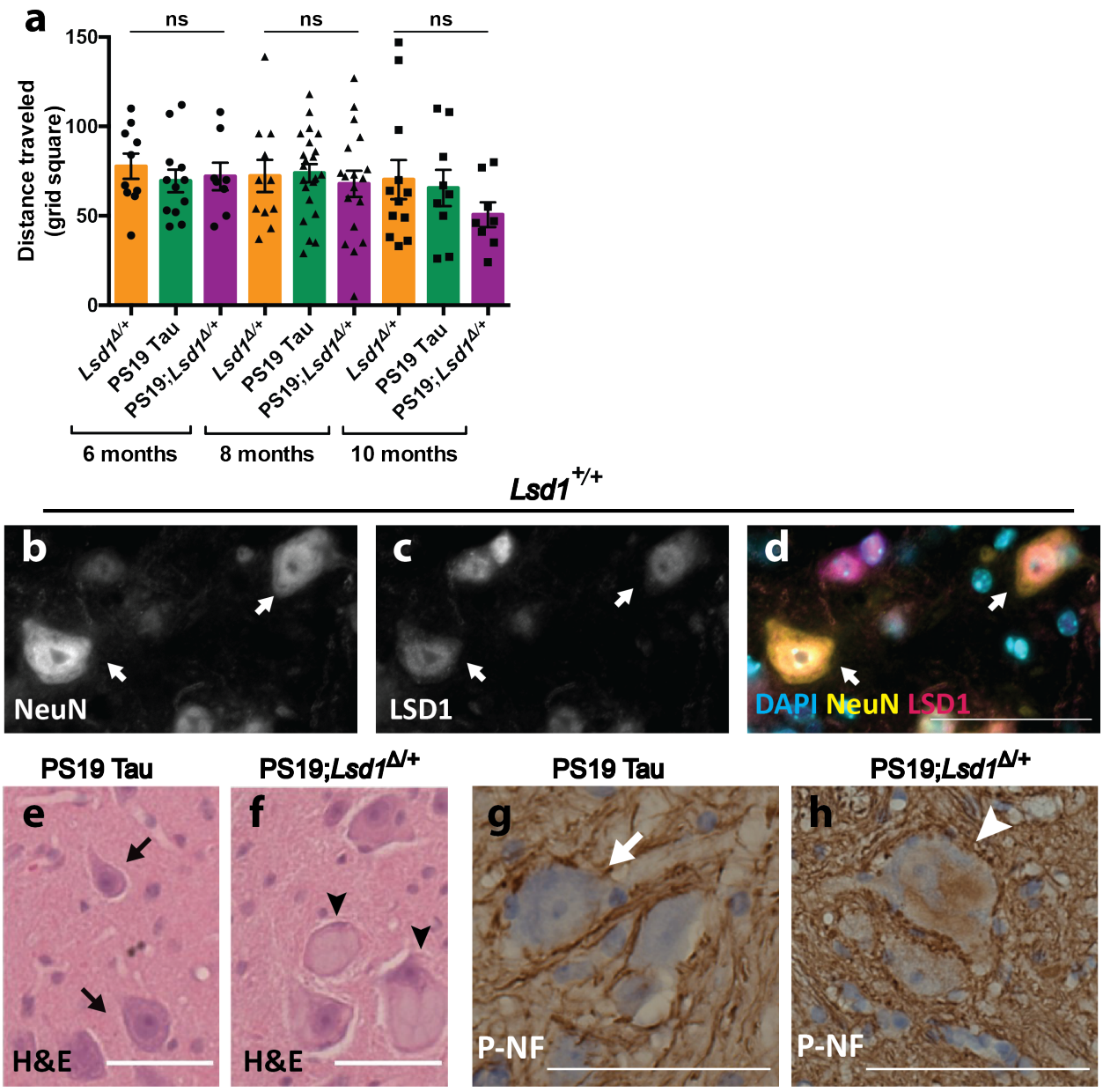

Figure 4-5 Reduction of *Lsd1* affects spinal cord in PS19 Tau mice. a, Grid performance test measuring the distance traveled (grid squares traversed) with both forelimbs and hindlimbs in 6, 8, and 10 month old mice. *Lsd1*$^{\Delta/+}$ (orange, *n*=10,11,12), PS19 Tau (green, *n*=12,22,9), and PS19;*Lsd1*$^{\Delta/+}$ (purple, *n*=8,18,8). Values are mean ± SEM (two-way analysis of variance (ANOVA) with Tukey's post hoc test. ns=not significant). **b-d,** Immunofluorescence staining of NeuN (**b**), LSD1 (**c**), and merged with DAPI (**d**) in spinal cord motor neurons of 12 month old

Lsd1$^{+/+}$ control mice. **e,f,** Representative image of hematoxylin and eosin (H&E) staining of motor neurons in 12 month old PS19 Tau mice (**e**) and PS19;*Lsd1*$^{\Delta/+}$ (**f**) littermates. **g,h,** Representative image of immunohistochemistry staining for phospho-nuerofilament (brown) counterstained with DAPI (blue) in the motor neurons of 12 month old PS19 Tau mice (**g**) and PS19;*Lsd1*$^{\Delta/+}$ (**h**) littermates. Arrows denote healthy motor neurons. Arrowheads denote abnormal motor neurons. Scale bars=50μm.

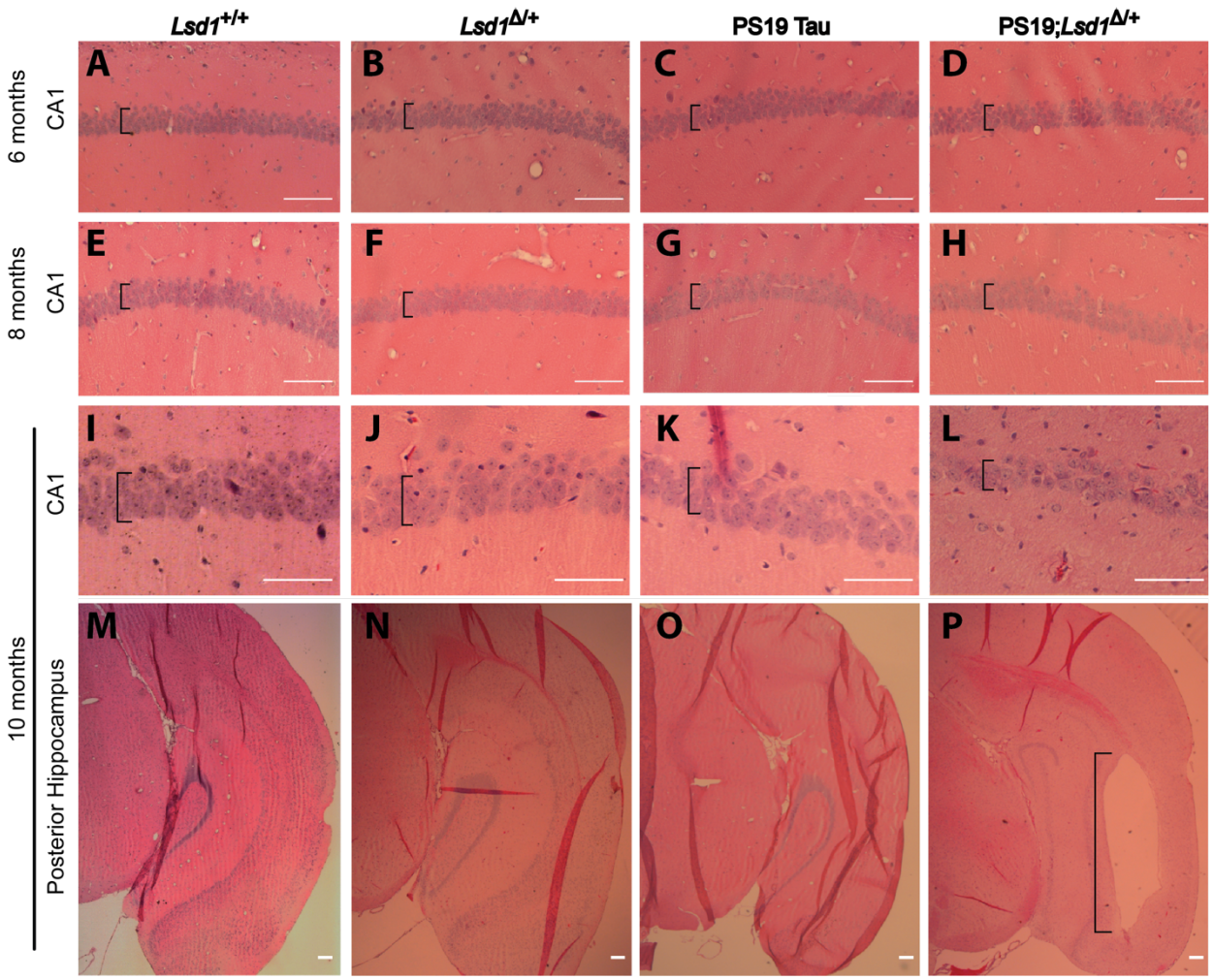

Figure 4-6 There is no exacerbation of neurodegeneration in PS19 Tau mice with reduced *Lsd*1 until 10 months of age. a-p, Representative image of H&E staining of *Lsd1*$^{+/+}$ (**a,e,i,m**), *Lsd1*$^{\Delta/+}$ (**b,f,j,n**), PS19 Tau (**c,g,k,o**), and PS19;*Lsd1*$^{\Delta/+}$ (**d,h,l,p**) littermates at 6 months (**a-d**), 8 months (**e-h**) and 10 months (**i-p**) in the CA1 (**a-l**) and posterior hippocampus (**m-p**). Brackets denote thickness of pyramidal layer of the CA1 (**a-l**), and region of cell clearance in posterior hippocampus (**p**). Scale bars=50μm.

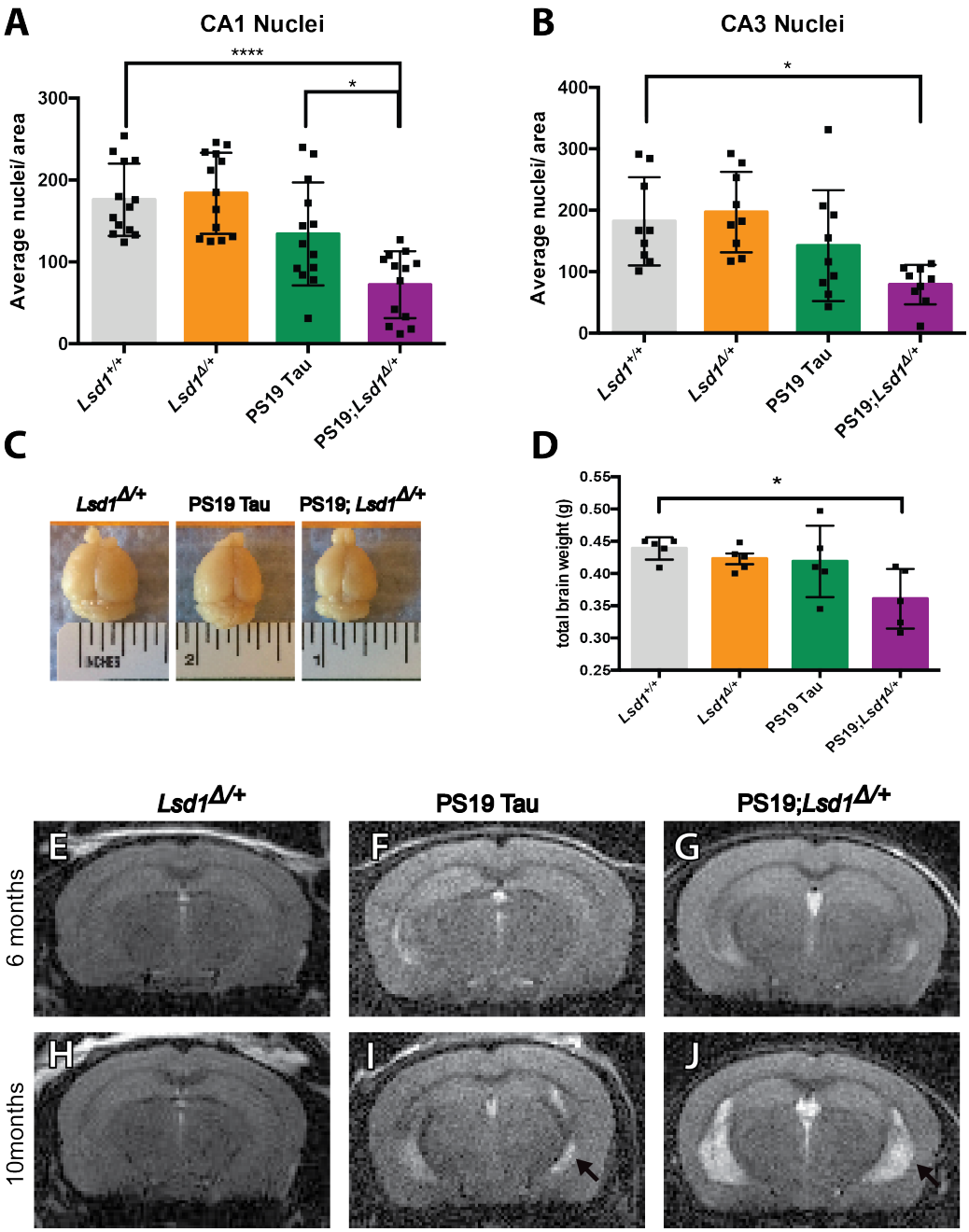

Figure 4-7 Reduction of *Lsd1* exacerbates neurodegeneration in PS19 Tau mice. A,B, Average nuclei per area in the CA1 (**A**) and CA3 (**B**) regions of the hippocampus in 12 month old *Lsd1*$^{+/+}$, *Lsd1*$^{\Delta/+}$, PS19 Tau, and PS19;*Lsd1*$^{\Delta/+}$ mice. Quantification from histology represented in **Figure 4-8A-H**. Values are mean ± SD (**A**, *n*=13 & **B,** *n*=9). **C,** Representative image of the brains of 12 month old *Lsd1*$^{\Delta/+}$, PS19 Tau, and PS19;*Lsd1*$^{\Delta/+}$ littermates. **D,** Total

brain weight of 12 month old littermates represented in **Fig. 3C.** Values are mean ± SD (*n*=5). For all graphs: one-way analysis of variance (ANOVA) with Tukey's post hoc test (two-sided) *P<0.05,****P<0.001. **E-J,** Representative image of T2- weighted RARE coronal MRI taken from 6 months (**E-G**) and 10 months (**H-jJ**) of age in *Lsd1*$^{\Delta/+}$ (**E,H**), PS19 (**F,J**), and PS19;*Lsd1*$^{\Delta/+}$ (**G,J**) mice (*n*=3). Arrow denotes region of hippocampal atrophy.

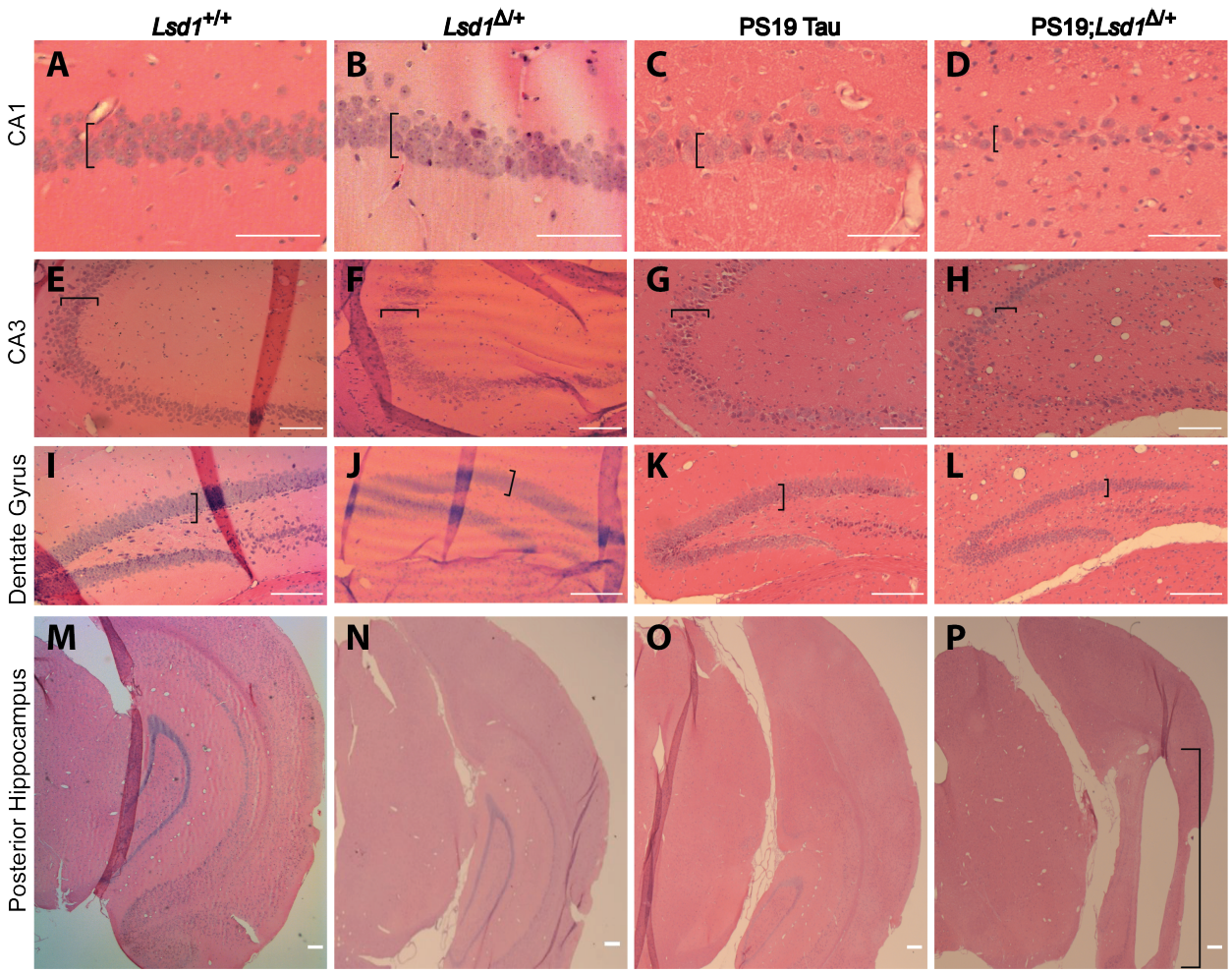

Figure 4-8 Increased neurodegeneration throughout the hippocampus and cortex of 12 month old mice. a-p, H&E staining of 12 month old *Lsd1*$^{+/+}$ (**a,e,i,m**), *Lsd1*$^{\Delta/+}$ (**b,f,j,n**), PS19 Tau (**c,g,k,o**), and PS19;*Lsd1*$^{\Delta/+}$ (**d,h,l,p**) littermates in the CA1 (**a-d**) and CA3 (**e-h**) regions of the hippocampus, the dentate gyrus (**i-l**), and the posterior hippocampus (**m-p**). Brackets denote thickness of pyramidal layer of the CA1 (**a-d**), CA3 (**e-h**), the granule cell layer of the Dente Gyrus (**i-l**), and region of cell clearance in posterior hippocampus (**p**). Scale bars=50μm.

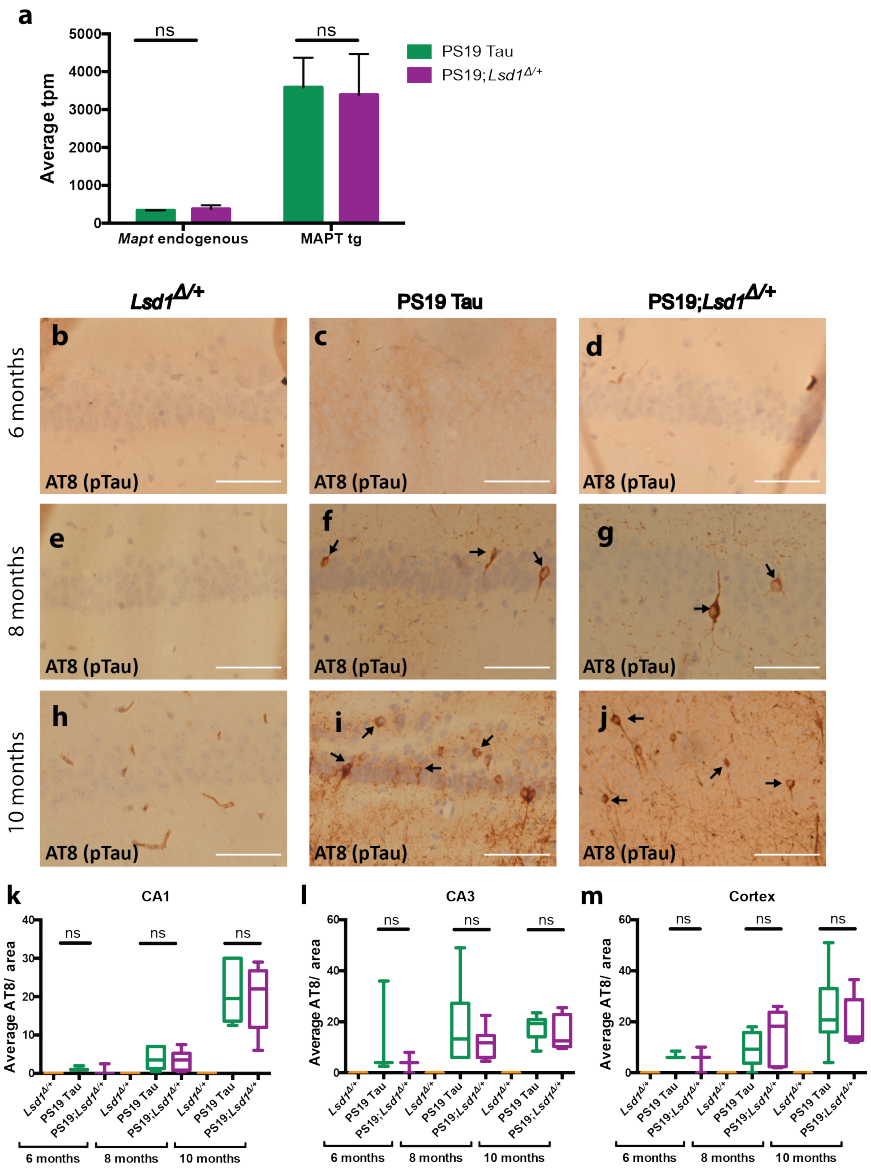

Figure 4-9 Reduction of *Lsd1* does not affect AT8 positive tau pathology. a, Average transcripts per million (tpm) from RNA sequencing of endogenous MAPT and the expression of the human P301S MAPT transgene in the hippocampus of PS19 Tau, and PS19; $Lsd1^{\Delta/+}$ mice. Values are mean ± SD (n=2). **b-j,** Representative image of immunohistochemistry staining of phosphorylated tau (AT8 antibody) of the CA1 region of the hippocampus in $Lsd1^{\Delta/+}$ (**b,e,h**) , PS19 Tau (**c,f,i**), and PS19;$Lsd1^{\Delta/+}$ (**d,g,j**) littermates at 6 months (**b-d**), 8 months (**e-g**), and 10 months (**h-j**). Arrows denote AT8 positive immunoreactivity. Scale bars=50µm. **k-m,**

Quantification of the average AT8 positive tau immunoreactivity per area from histology represented in **Figure 4-9b-j** in the CA1 (**k**) and CA3 (**l**) regions of the hippocampus, and the cerebral cortex (**m**) (6 months *n*=3, 8 months *n*=6, and 10 months *n*=6, box plot edges are 25th and 75th percentile, central line is the median, and whiskers are max and min). For all graphs: one-way analysis of variance (ANOVA) with Tukey's post hoc test (two-sided), ns=not significant.

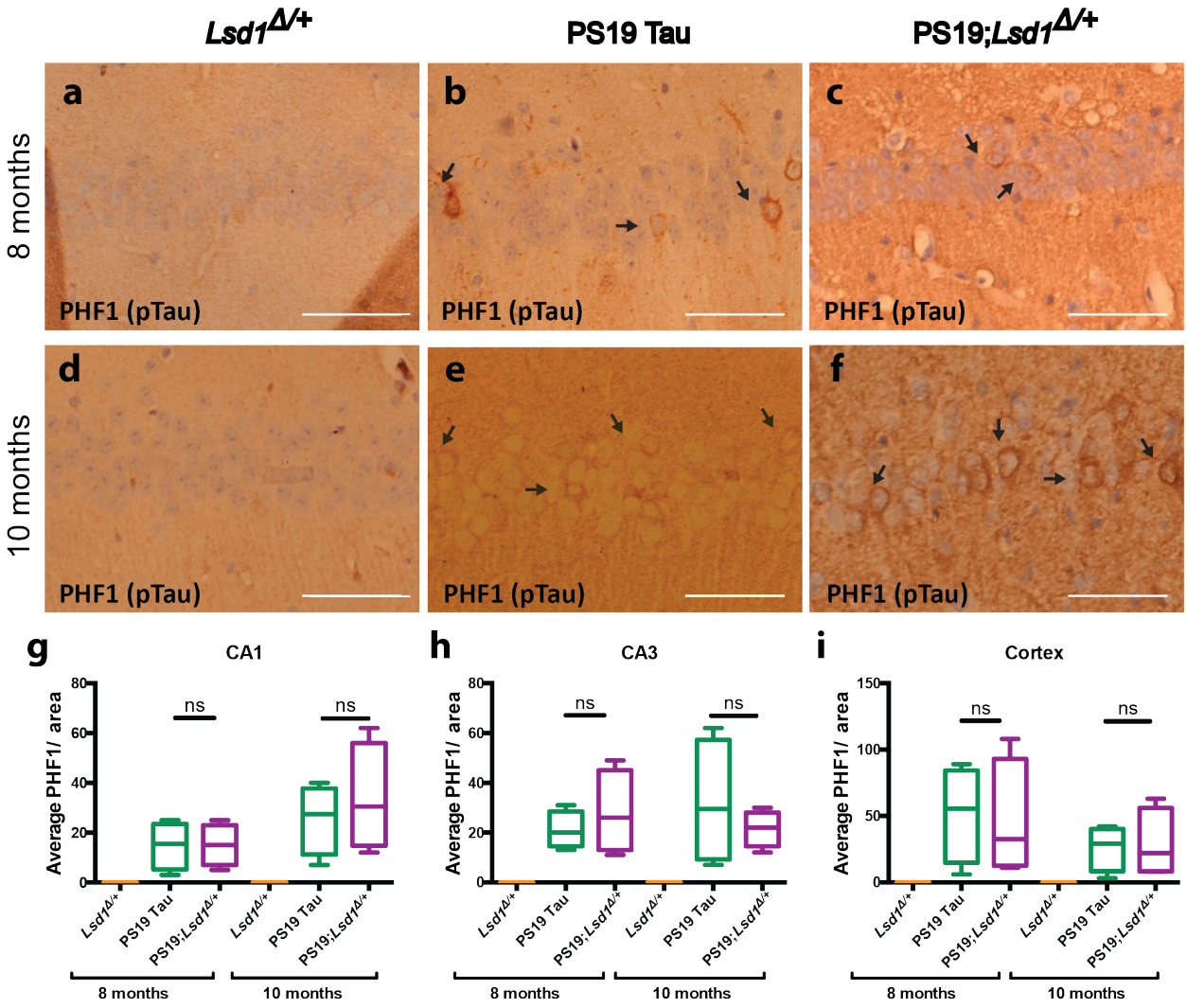

Figure 4-10 Reduction of *Lsd1* does not affect PHF1 positive tau pathology. a-f, Representative image of immunohistochemistry staining of PHF1 in the CA1 region of the hippocampus in *Lsd1*$^{\Delta/+}$ (**a,d**), PS19 Tau (**b,e**), and PS19;*Lsd1*$^{\Delta/+}$ (**c,f**) littermates at 8 months (**a-c**) and 10 months (**d-f**). Arrows denote PHF1 positive immunoreactivity. Scale bars=50μm. **g-i,** Quantification of average PHF1 positive tau immunoreactivity per area from histology represented in Figure **4-10a-f** in the CA1 (**g**) and CA3 (**h**) regions of the hippocampus, and the cerebral cortex (**i**) (*n*=4 box plot edges are 25th and 75th percentile, central line is the median, and whiskers are max and min). For all graphs: one-way analysis of variance (ANOVA) with Tukey's post hoc test (two-sided), ns=not significant.

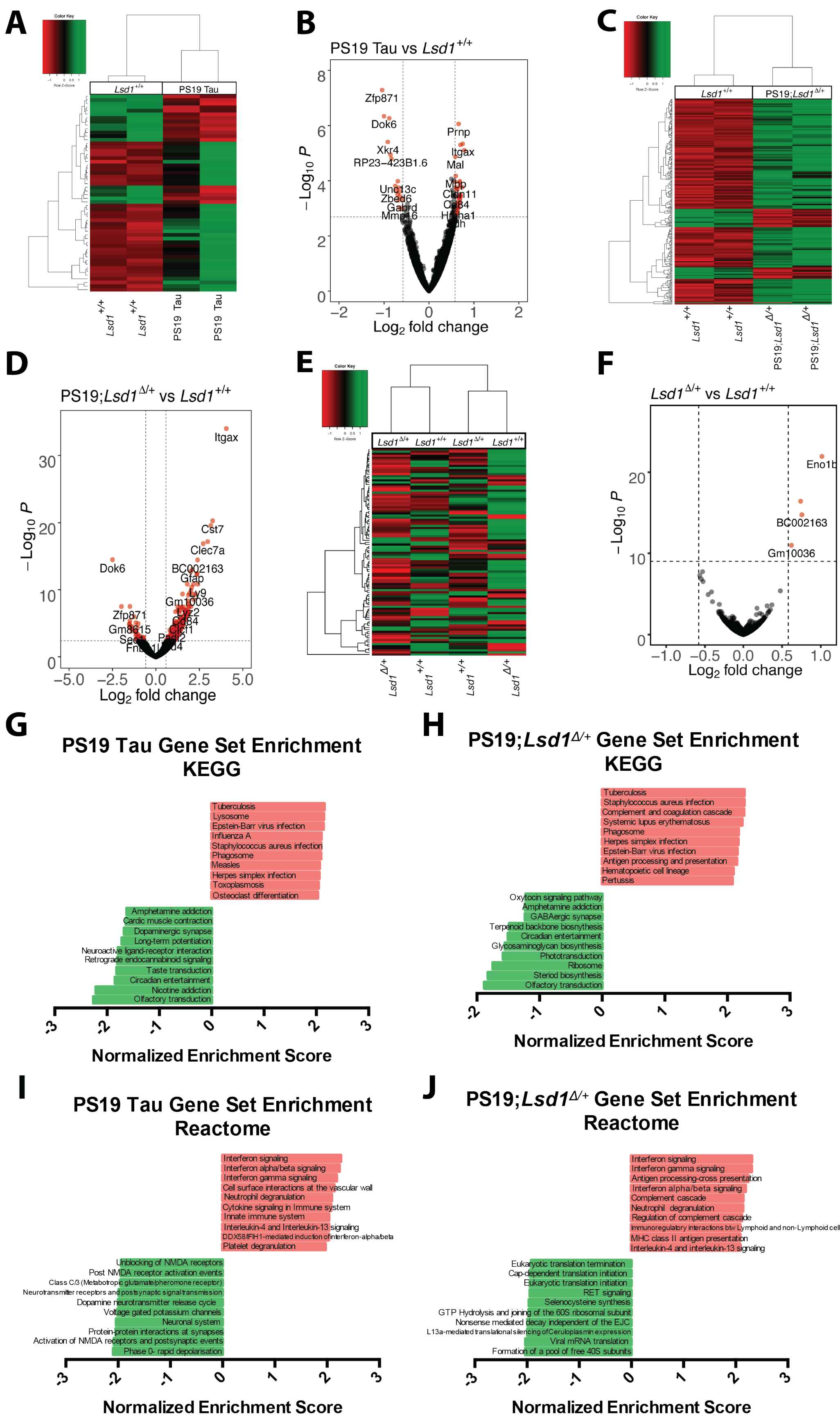
A
Lsd1+/+
PS19 Tau
B
PS19 Tau vs Lsd1+/+
Zfp871
Dok6
Xkr4
RP23−423B1.6
Unc13c
Zbed6
Gabrd
Mmp16
Prnp
Itgax
Mal
Mbp
Cldn11
Cd84
Hapa1
− Log10 P
Log2 fold change
C
Lsd1+/+
PS19;Lsd1Δ/+
D
PS19;Lsd1Δ/+ vs Lsd1+/+
Itgax
Cst7
Clec7a
BC002163
Gfap
Ly9
Gm10036
Dok6
Zfp871
Gm8615
− Log10 P
Log2 fold change
E
Lsd1Δ/+
Lsd1+/+
F
Lsd1Δ/+ vs Lsd1+/+
Eno1b
BC002163
Gm10036
− Log10 P
Log2 fold change
G
PS19 Tau Gene Set Enrichment
KEGG
Tuberculosis
Lysosome
Epstein-Barr virus infection
Influenza A
Staphylococcus aureus infection
Phagosome
Measles
Herpes simplex infection
Toxoplasmosis
Osteoclast differentiation
Amphetamine addiction
Cardiac muscle contraction
Dopaminergic synapse
Long-term potentiation
Neuroactive ligand-receptor interaction
Retrograde endocannabinoid signaling
Taste transduction
Circadian entertainment
Nicotine addiction
Olfactory transduction
Normalized Enrichment Score
H
PS19;Lsd1Δ/+ Gene Set Enrichment
KEGG
Tuberculosis
Staphylococcus aureus infection
Complement and coagulation cascade
Systemic lupus erythematosus
Phagosome
Herpes simplex infection
Epstein-Barr virus infection
Antigen processing and presentation
Hematopoietic cell lineage
Pertussis
Oxytocin signaling pathway
Amphetamine addiction
GABAergic synapse
Terpenoid backbone biosynthesis
Circadian entertainment
Glycosaminoglycan biosynthesis
Phototransduction
Ribosome
Steriod biosynthesis
Olfactory transduction
Normalized Enrichment Score
I
PS19 Tau Gene Set Enrichment
Reactome
Interferon signaling
Interferon alpha/beta signaling
Interferon gamma signaling
Cell surface interactions at the vascular wall
Neutrophil degranulation
Cytokine signaling in Immune system
Innate immune system
Interleukin-4 and Interleukin-13 signaling
DDX58/IFIH1-mediated induction of interferon-alpha/beta
Platelet degranulation
Unblocking of NMDA receptors
Post NMDA receptor activation events
Class C/3 (Metabotropic glutamate/pheromone receptor)
Neurotransmitter receptors and postsynaptic signal transmission
Dopamine neurotransmitter release cycle
Voltage gated potassium channels
Neuronal system
Protein-protein interactions at synapses
Activation of NMDA receptors and postsynaptic events
Phase 0- rapid depolarisation
Normalized Enrichment Score
J
PS19;Lsd1Δ/+ Gene Set Enrichment
Reactome
Interferon signaling
Interferon gamma signaling
Antigen processing-cross presentation
Interferon alpha/beta signaling
Complement cascade
Neutrophil degranulation
Regulation of complement cascade
Immunoregulatory interactions b/w Lymphoid and non-Lymphoid cell
MHC class II antigen presentation
Interleukin-4 and interleukin-13 signaling
Eukaryotic translation termination
Cap-dependent translation initiation
Eukaryotic translation initiation
RET signaling
Selenocysteine synthesis
GTP Hydrolysis and joining of the 60S ribosomal subunit
Nonsense mediated decay independent of the EJC
L13a-mediated translational silencing of Ceruloplasmin expression
Viral mRNA translation
Formation of a pool of free 40S subunits
Normalized Enrichment Score

Figure 4-11 Differential expression in 9 month old *Lsd1*$^{\Delta/+}$, PS19 Tau, and PS19;*Lsd1*$^{\Delta/+}$ hippocampus. A,C,E, Heatmap of differentially expressed RNA-seq transcripts between *Lsd1*$^{+/+}$ and PS19 Tau (**A**), PS19; *Lsd1*$^{\Delta/+}$ (**C**), and *Lsd1*$^{\Delta/+}$ (**E**) mouse hippocampus. Samples are hierarchically clustered by relative expression of differentially expressed transcripts. Relative higher (red) and lower (green) expression is indicated. **B,D,F,** Volcano plot of $\log_2$ fold-changes in gene expression (x-axis) by statistical significance ($-\text{Log}_{10}$ P-value; y-axis) in PS19 Tau (**B**), PS19; *Lsd1*$^{\Delta/+}$ (**D**), and *Lsd1*$^{\Delta/+}$ (**F**) compared to *Lsd1*$^{+/+}$ mouse hippocampus. Each dot represents a transcript, and the dotted line represents a significance $\log_2$ fold change cut off of 0.5. **G-J,** Histogram of Gene Set Enrichment Analysis compared to KEGG pathways (**G,H**) and the Reactome (**I,J).** The top ten most enriched (red) and depleted (green) gene sets in the PS19 Tau (**G,I**) and PS19; *Lsd1*$^{\Delta/+}$ (**H,J**) are shown with normalized enrichment scores.

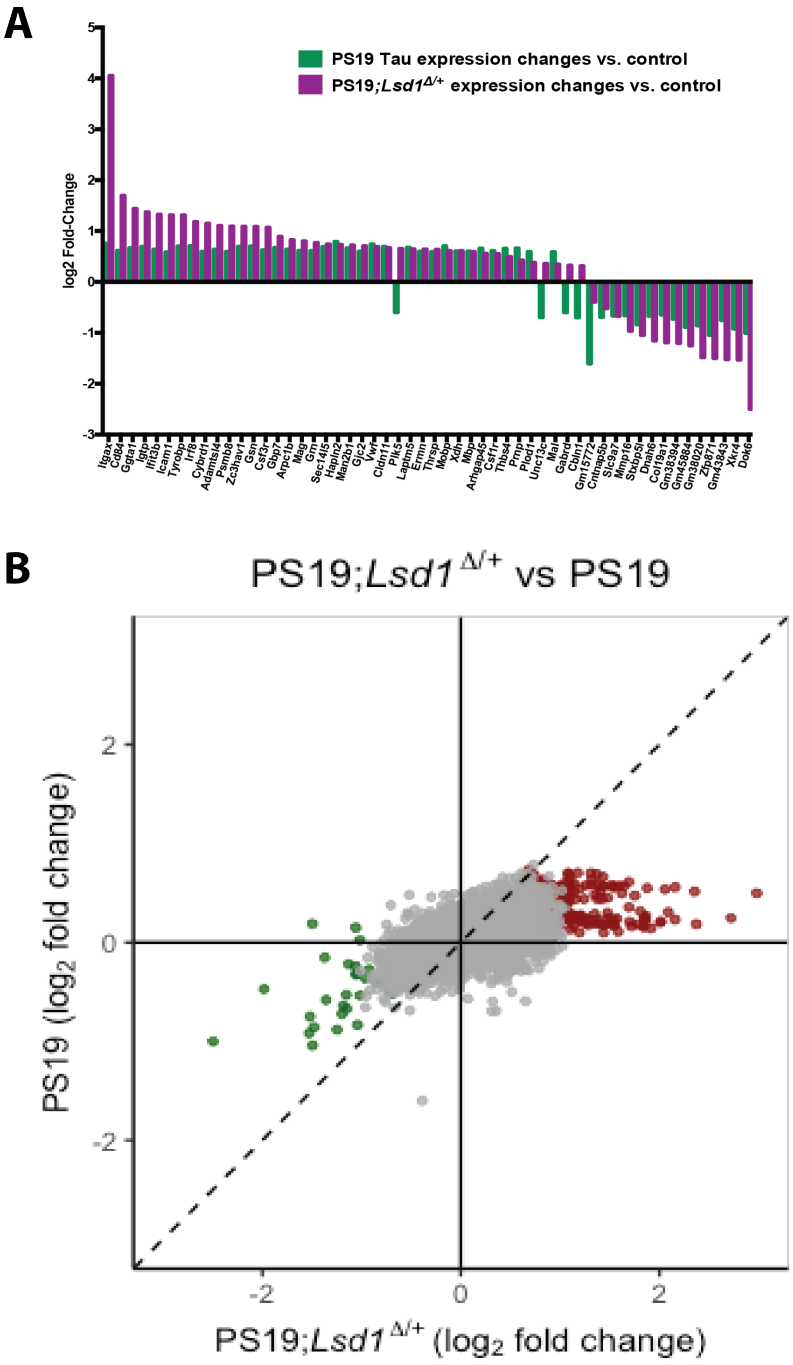

Figure 4-12 Molecular overlap between loss of LSD1 function and tauopathy. A, Histogram (log_2 fold change) of the 54 genes that have significant changes in expression in the PS19 Tau mouse (green) and their corresponding expression changes in the PS19;*Lsd1*$^{\Delta/+}$ mouse (purple). **B,** Scatter plot showing the correlation between the genome-wide log_2 fold change in gene

expression between PS19 Tau and PS19;*Lsd1*$^{\Delta/+}$. The most significantly changed genes in PS19;*Lsd1*$^{\Delta/+}$ mouse are shown in red (upregulated) and green (downregulated). All other genes are shown in grey. Dotted line represents 1:1 relationship between gene expression changes in PS19 Tau vs. PS19;*Lsd1*$^{\Delta/+}$. Exacerbated genes fall to the right of the dotted line in the positively correlated quadrant and to the left of the dotted line in the negatively correlated quadrant. Genes with correlated expression changes are found in the top right and bottom left quadrants, while genes that do not correlate are found in the opposite quadrants.

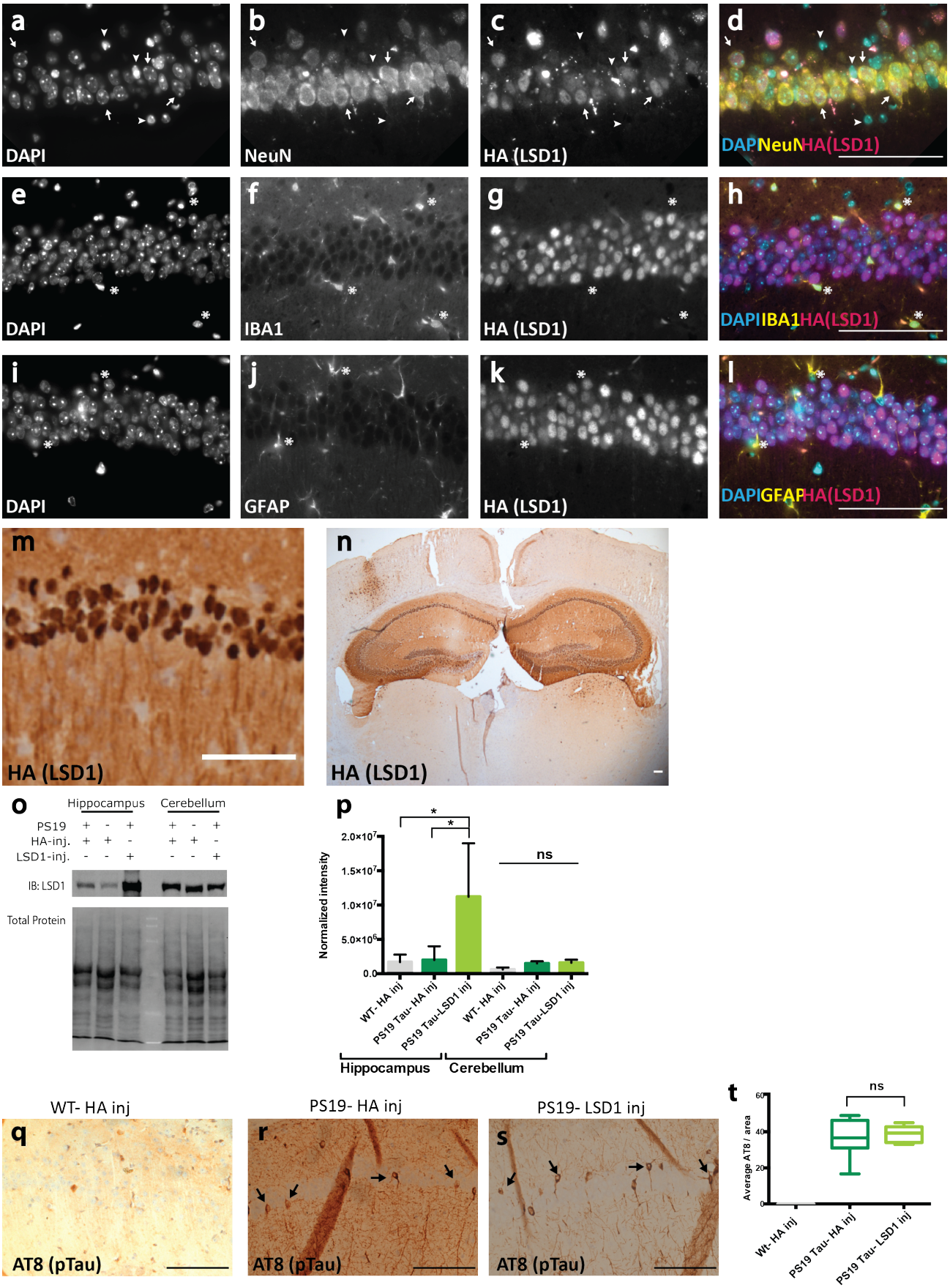
a
DAPI
b
NeuN
c
HA (LSD1)
d
DAPNeuNHA(LSD1)
e
DAPI
f
IBA1
g
HA (LSD1)
h
DAPIIBA1HA(LSD1)
i
DAPI
j
GFAP
k
HA (LSD1)
l
DAPIGFAPHA(LSD1)
m
HA (LSD1)
n
HA (LSD1)
o
Hippocampus
Cerebellum
PS19 + - + + - +
HA-inj. + + - + + -
LSD1-inj. - - + - - +
IB: LSD1
Total Protein
p
Normalized intensity
2.0×10^7
1.5×10^7
1.0×10^7
5.0×10^6
0.0
*
*
ns
WT- HA inj
PS19 Tau- HA inj
PS19 Tau-LSD1 inj
WT- HA inj
PS19 Tau- HA inj
PS19 Tau-LSD1 inj
Hippocampus
Cerebellum
WT- HA inj
PS19- HA inj
PS19- LSD1 inj
q
AT8 (pTau)
r
AT8 (pTau)
s
AT8 (pTau)
t
ns
Average AT8 / area
60
40
20
0
Wt- HA inj
PS19 Tau- HA inj
PS19 Tau- LSD1 inj

Figure 4-13 LSD1 overexpression in hippocampal neurons of PS19 Tau mice. a-d, Representative immunofluorescence labeling in a WT- HA inj mouse showing DAPI (**a**), NeuN (**b**), HA (which represents the LSD1 virus, hereafter denoted as HA(LSD1)) (**c**), and merged (**d**). Viral produced LSD1 is present in NeuN+ neurons. Arrows denote NeuN+ cells that have HA expression. Arrowheads denote cells that lack NeuN staining and also lack HA expression. **e-h,** Representative immunofluorescence labeling showing DAPI (**e**), IBA1 (**f**), HA(LSD1) (**g**), and merged (**h**). Asterisks denote cells stained positive for IBA1 (**e-h**), which lack HA expression. **i-l,** Representative immunofluorescence labeling showing DAPI (**i**), GFAP (**j**), HA(LSD1) (**k**), and merged (**l**) images. Asterisks denote cells stained positive for GFAP (**i-l**), which lack HA expression. **m-n,** Immunohistochemistry staining for HA(LSD1) showing expression localized to the nucleus of neurons (**m**) specifically within the hippocampus (**n**). **o,** Representative image of immunoblot for LSD1 protein and corresponding total protein blot in the hippocampus versus the cortex of mice injected with either LSD1 or HA only expressing virus. **p,** Quantification of immunoblot for LSD1 normalized to total protein loaded per sample as represented in **Figure 4-13o** shows overexpression in the hippocampus, but not the cortex. Values are mean ± SD (n=3, one-way analysis of variance (ANOVA) with Tukey's post hoc test (two-sided), *P<0.05, ns=not significant. **q-r,** Representative image of immunohistochemistry staining of phosphorylated tau (AT8 antibody) in the CA1 region of the hippocampus in 11 month old WT- HA inj (**q**), PS19-HA inj (**r**), and PS19- LSD1inj (**s**) mice. Arrows denote AT8 positive immunoreactivity. Scale bars=50μm. (**t**) Quantification of average AT8 positive tau immunoreactivity per area. Box plot edges are 25th and 75th percentile, central line is the median, and whiskers are max and min (n=8, one-way analysis of variance (ANOVA) with Tukey's post hoc test (two-sided), ns=not significant).

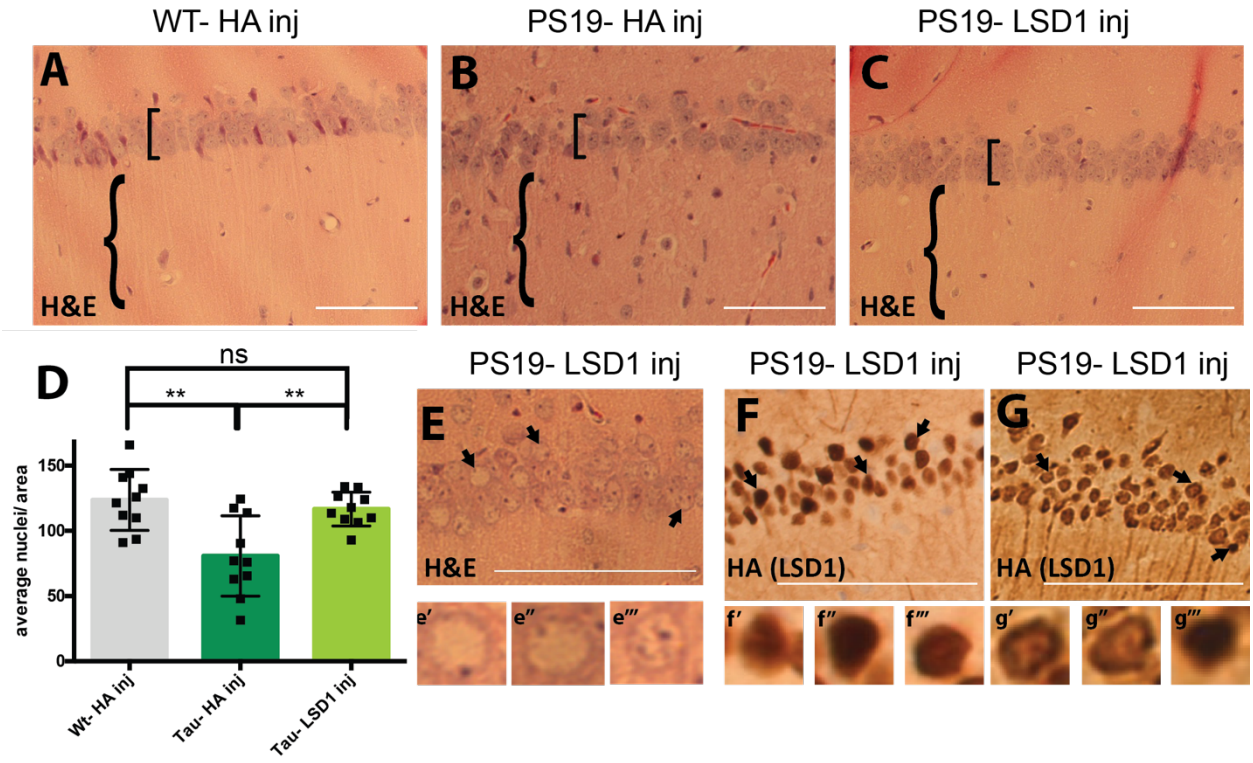

Figure 4-14 LSD1 overexpression rescues the neurodegenerative phenotype in the hippocampus of 11 month old PS19 Tau mice. A-C, Representative image of H&E stained CA1 region of the hippocampus of 11 month old Wild Type mice injected with HA control virus (WT- HA inj) (**A**), PS19 Tau mice injected with HA control virus (PS19- HA inj) (**B**), and PS19 Tau mice injected with *Lsd1* overexpressing virus (PS19- LSD1 inj) (**C**). Square brackets denote thickness of pyramidal layer of the CA1 of the hippocampus and curvy brackets denote hippocampal region with or without infiltrating cells. **D,** Quantification of the average number of nuclei in the pyramidal layer of the hippocampus per area per mouse from histology represented in **Fig. 5A-C**. Values are mean ± SD (n=10, one-way analysis of variance (ANOVA) with Tukey's post hoc test, **p<0.01, ns=not significant). **E,** Representative H&E of PS19- LSD1 inj mouse with abnormal nuclei blebbing in the CA1 region of the hippocampus. **E'-E''',** High magnified image of cells denoted by arrows in **Figure 4-14E** of individual nuclei that are either abnormally blebbed (**E', E"**) or normal (**E'''**). **F,G,** Immunohistochemistry staining of

HA(LSD1) in 11 month PS19- LSD1 inj mice. HA is either localized specifically to the nucleus in all nuclei (**F**) or in only a few nuclei while it is partially sequestered in the cytoplasm in others (**G**). **F'-F''',** High magnified image of cells denoted by arrows in **Figure 4-14F** of nuclear HA localization in individual nuclei. **G'-G''',** High magnified image of cells denoted by arrows in **Figure 4-15G** of individual nuclei with HA(LSD1) either sequestered to the cytoplasm (**G', G"**) or confined to the nucleus (**G'''**). Scale bars=50μm.

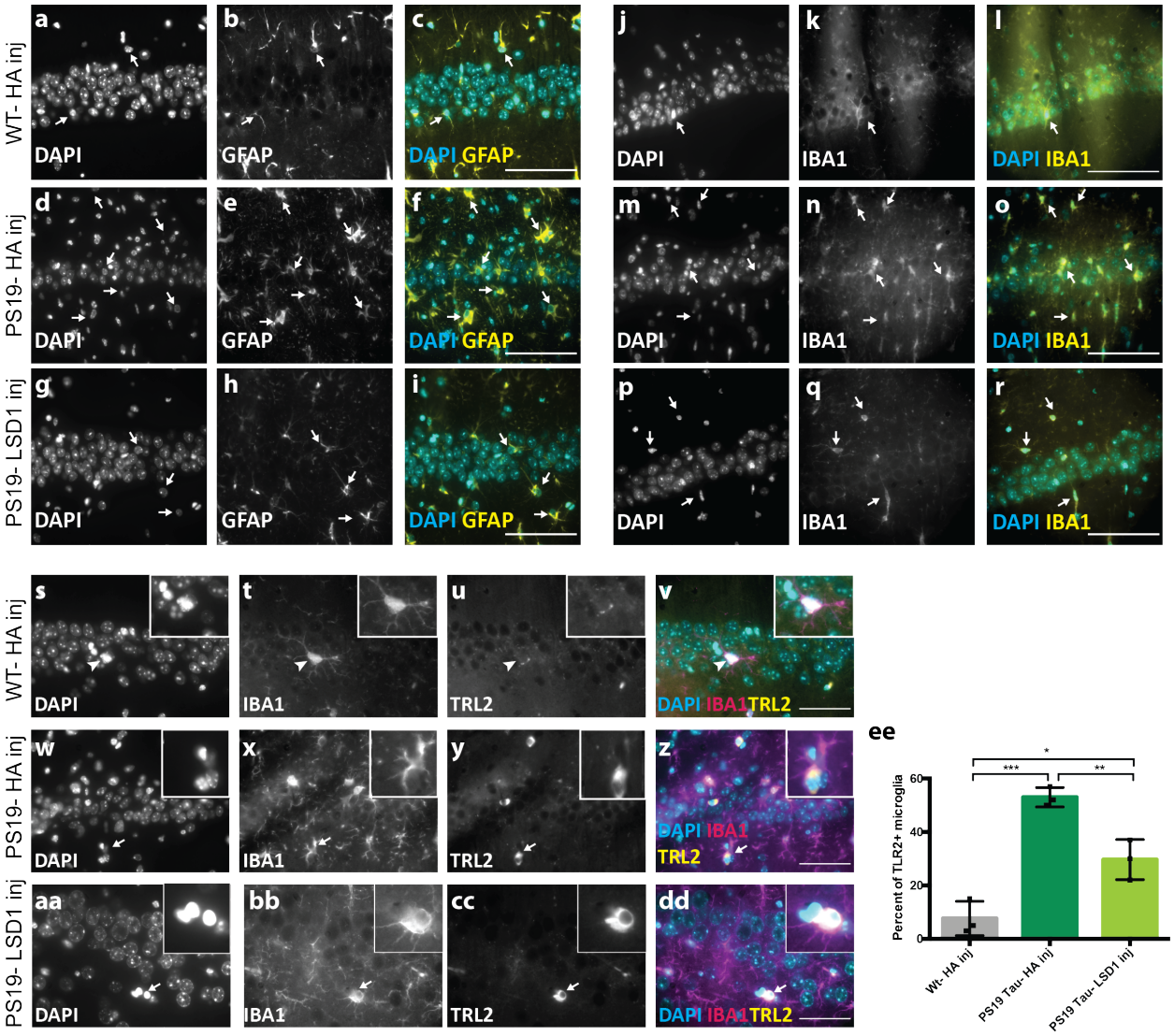

Figure 4-15 LSD1 overexpression reduces the gliosis in PS19 Tau mice. a-i, Representative immunofluorescence showing DAPI (**a,d,g**), astrocyte marker GFAP (**b,e,h**), and merged (**c,f,i**) images in WT- HA inj (**a-c**), PS19- HA inj (**d-f**), and PS19- LSD1 inj (**g-i**). Arrows denote GFAP+ astrocytes. **j-r,** Representative immunofluorescence showing DAPI (**j,m,p**), microglia marker IBA1 (**k,n,q**), and merged (**l,o,r**) images in WT- HA inj (**j-l**), PS19-HA inj (**m-o**), and PS19- LSD1 inj (**p-r**). Arrows denote IBA1+ microglia. **s-dd,** Representative immunofluorescence labeling showing DAPI (**s,w,aa**), microglia marker IBA1 (**t,x,bb**), activated microglia marker TRL2 (**u,y,cc**), and merged (**v,z,dd**) images in WT-Ha inj (**s-v**), PS19-HA inj

(**w-z**), and PS19-LSD1 inj (**aa-dd)**. Inset of microglia that is IBA1 positive but TRL2 negative (**s-v,** denoted by arrowhead) or both IBA1 and TRL2 positive (**w-dd**, denoted by arrow). All images are from the CA1 region of the hippocampus Scale bars=50μm. **ee,** Quantification of the percentage of microglia that are TRL2+ in WT- HA inj, PS19- HA inj, and PS19- LSD1 inj mice represented in **Figure 4-15s-dd**. Values are mean ± SD are (*n*=3, one- way analysis of variance (ANOVA) with Tukey's post hoc test, *p<0.05, **p<0.01, ***p<0.005).

CHAPTER 5:

Interaction of pathological tau and LSD1 through the N-terminal disordered domain

5.1 Introduction

The microtubule binding protein, tau has been well characterized as the driving pathology for tauopathies. However, the molecular mechanism of how tau pathology contributes to neuronal cell loss is incompletely understood. Tau becomes hyperphosphorylated and a misfolding event leads to the formation of tau oligomers. Accumulation of tau oligomers eventually form into the intracellular neurofibrillary tangles (NFTs) which are observed in the postmortem brain of tauopathies cases[9]. This pathology is thought to trigger synaptic loss, dramatic genome-wide expression changes, increased inflammatory response, and neuronal cell death[4]. Aggregated human tau has been shown to exhibit prion disease properties, in which misfolding and subsequent aggregation can induce further misfolding of both tau[38,40]. Furthermore, it has been shown that introduction of aggregated human tau into the brains of young P301S mice not yet exhibiting tau pathology induces the rapid onset of tau aggregation[41].

In AD, NFTs are composed of paired helical filaments (PHF) of the tau protein. The conversion from unaffected tau into PHFs is a multi-step process and is based on the innate structure of the tau protein. Native tau is classified as an intrinsically disordered protein (IDP) (Figure 5-1A). IDPs have very little stable secondary or tertiary structure in their free form. This provides structural flexibility to bind with multiple partners and the binding to other proteins typically stabilizes the disordered nature of IDPs[251-253]. For example, tau has the ability to interact with various tubulins. In addition, posttranslational modifications, such as phosphorylation may modulate the conformational freedom that tau would normally have by altering the binding-folding events to induce conformational changes. These conformational shifts aid in the formation of PHF and exposes the protein to new binding partners[14,252]. Interestingly, tau has been shown to interact with the disordered domains of other proteins, such

as the small nuclear ribonucleoprotein U1-70K. In AD cases it was shown that, tau co-aggregates with the C-terminal low complexity domain of U1-70K[254]. These data raise the possibility that tau PHFs could interact with other IDPs or even low complexity domains of other proteins.

Previously, our lab has implicated the histone demethylase LSD1 as a significant downstream mediator of the tau neurodegenerative pathway. LSD1 specifically removes mono- and di-methylation from lysine 4 on histone 3 (H3K4me/me2), and is required to suppress the stem cell program during differentiation in mouse embryonic stem cells[84,165]. In multiple paradigms, LSD1 has been shown to be a transcriptional repressor that facilitates cell fate transitions. Interestingly, in mammals, LSD1 continues to be expressed throughout adulthood, even in terminally differentiated cells such as neurons. Deletion of *Lsd1* in adult mice leads to significant neuronal cell death in the hippocampus and cortex with associated learning and memory defects, as well as genome-wide expression changes that significantly overlap with those observed in the brains of postmortem human AD cases. Additionally, in postmortem brains of AD cases, we observed LSD1 protein mislocalized to cytoplasmic NFTs[173]. In this thesis, we further demonstrate that tau can sequester LSD1 in the cytoplasm and that manipulating LSD1 can modulate tau-induced neurodegeneration. These data implicate the inhibition of LSD1 as the downstream mediator of tau aggregation.

LSD1 is highly structured, and is thought to have completely ordered functional domains. However, human LSD1 also has an 172 amino acid intrinsically disordered N-terminal domain (Figure 5-1B)[84]. This domain has no known function except for containing the six amino acid nuclear localization sequence (NLS) that is known to interact with importin-α and be required for proper nuclear localization[255]. In particular, the N-terminal disordered domain is known to be dispensable for H3K4 demethylation, forming a secondary structure and interacting with known

associated complex members, such as CoREST[256]. Since it has been shown that tau can interact with the unstructured region of other proteins, we hypothesized that LSD1's intrinsically disordered N-terminal domain is interacting with tau aggregates and blocking the NLS from being recognized and imported into the nucleus. In order to address this, we first investigated what is known about the N-terminal domain of LSD1. The LSD1 protein is evolutionarily conserved from *S.pombe* to mammals (Figure 5-1C). However, the N-terminal disordered domain, present in *Drosophia* and mammals, is only partially conserved (Figure 5-1D)[84]. The lack of this domain in other organisms, such as *C. elegans, S. pombe* and *Arabidopsis* suggests that LSD1 can function without it *in vivo*. Additionally, all *in vitro* studies on LSD1 have been performed using an N-terminally truncated clone. Considering these findings, we predicted that removing the N-terminal domain of LSD1 might inhibit LSD1's interaction with tau without disrupting the *in vivo* function.

With this consideration, we proposed to interrogate a potential interaction between tau and the disordered domain of LSD1 in two complementary experiments. First, we utilized the same overexpression paradigm of injecting aged PS19 Tau mice in the hippocampus, but here we utilized an N-terminally truncated LSD1 virus (LSD1ΔN). The viral construct used for these experiments has the NLS added back to the N-terminus of the protein to allow for nuclear import. This approach will allow us to interrogate if LSD1ΔN is capable of entering the nucleus and avoid sequestration by tau, as well as determine if the truncated LSD1ΔN protein is functional in the hippocampus. Because the viral injection approach can only influence neurodegeneration in the hippocampus and does not block degeneration throughout the rest of the CNS, injected PS19 Tau mice still develop paralysis and die at the same rate as un-injected

tauopathy mice. This limits our ability to observe the viral product's localization and effects on cell death beyond the onset of paralysis.

For our second approach we generated the N-terminally truncated LSD1 protein at the endogenous locus in mouse and crossed these mice into the PS19 Tau mouse background. We predicted that the truncated protein would no longer be sequestered by pathological tau, allowing LSD1ΔN to enter the nucleus unencumbered. Because *Lsd1* heterozygous mice are phenotypically wildtype, we hypothesized that one copy of *Lsd1ΔN* would be enough to maintain the nuclear pool of LSD1, despite tau-mediated sequestration of the full-length copy. By comparing neurodegeneration of the PS19 Tau mice with those that are heterozygous for *Lsd1ΔN*, we can determine tau functions through the N-terminal domain of LSD1 to induce neurodegeneration. If this is the case, the N-terminal domain of LSD1 could provide a novel therapeutic target for tauopathies, such as Alzheimer's disease.

5.2 Results

5.2.1 Overexpression of LSD1ΔN rescues neurodegeneration more completely than full length LSD1

Previously we showed that overexpression of the full length LSD1 protein in the hippocampus of PS19 Tau mice can rescue neurodegeneration after the onset of tau pathology. There was no cell loss of hippocampal neurons in LSD1 injected PS19 Tau mice at 11 months. However, this rescue was not permanent and in some cases we observed abnormal nuclear blebbing corresponding to the observation of HA-tagged LSD1 localized to the cytoplasm. Based on this, we hypothesized that the full length LSD1 protein was continuing to be sequestered and could only overcome the nuclear depletion of LSD1 temporarily. Here, we assessed whether

overexpression of N-terminally truncated LSD1 in PS19 Tau mice would recapitulate this rescue or possibly result in more effective or long-term rescue. For this, we performed the same viral injection experiments described in Chapter 4 using an N-terminally truncated LSD1 construct (Figure 5-2A). Briefly, we injected PS19 Tau mice with a neuronal specific virus (AAV-DJ driven by the synapsin promoter) expressing either the full length LSD1 protein with an N-terminal HA tag (hereafter referred to as PS19- LSD1 inj), control virus expressing only the HA tag (hereafter referred to as PS19- HA inj), and the N-terminally truncated LSD1 (hereafter referred to as PS19- LSD1ΔN inj). Additionally, to control for the effects of viral injection, we injected Wild Type littermates with the HA only expressing virus (hereafter referred to as WT-HA inj). All injections were performed directly into the hippocampus at 8-8.5 months, when tau pathology is already present throughout the nervous system.

At this time, with only preliminary numbers, we have analyzed and pooled all cohorts where the injections have been validated to be successful. At a later date we may be able to sub categorize the cohorts based on age of post-injection analysis. Since we are only injecting the hippocampus, the PS19 Tau mice still reach terminally paralysis. This typically occurs at 12 months, but can occur as early as 8 months. For this analysis, mice range from 9-13 months old. Injected mice were evaluated for cell death by neuronal cell counts in the hippocampus. As expected, there was significant neuronal cell death in PS19- HA inj mice compared to WT- HA inj (Figure 5-2B,C,F; $p=0.0002$). Continued from our data in Chapter 4, we show a statistically significant rescue of the neuronal cell death in PS19 Tau mice injected with full length LSD1 (Figure 5-2B,D,F; $p=0.0002$). Similar to what we documented previously, compared to WT-HA inj control mice, 58% (10 of 17) of the PS19-HA inj mice had hippocampal cell counts that were below the lowest WT-HA inj control, while only 1 of the 12 PS19- LSD1 inj mice (8%) were

below this level. For PS19- LSD1ΔN inj mice, the overall neuronal cell count was not statistically different from the WT- HA inj mice (Figure5-2B,E,F;p=0.0002). This suggests that the PS19- LSD1ΔN inj mice may be rescued, similar to full length PS19- LSD1 inj. However, the neuronal cell counts in PS19- LSD1ΔN inj are also not statistically significant from the PS19- HA group ($p = 0.7692$, comparing means of the PS19- LSD1ΔN inj group to the PS19- HA inj group). This indicates that the rescue may not be as robust as the rescue observed in full length PS19- LSD1 inj. Nevertheless, it is promising to note that only 2 out of the 6 PS19- LSD1ΔN inj mice were below the lowest WT-HA inj control (33%) and the cohort of mice with the most significant neuronal cell death in PS19- HA inj mice is clearly absent in PS19- LSD1ΔN inj mice. Although this work is ongoing, the results indicate that 1) N-terminally truncated LSD1 construct rescues neurodegeneration in PS19 Tau mice, and 2) it is possible that the N-terminal domain has a minor function that is compromising the rescue.

For the comparison of whether the N-terminally truncated LDS1 rescues better than the full length protein, more cohorts of older aged mice will need to be evaluated. However, to get an early indication, we can evaluate the blebbing that was previously observed in over half of rescued PS19- LSD1 inj mice. In Chapter 4, we proposed these neurons with blebbing nuclei represented an intermediate state between a healthy neuron and a dying neuron that is prolonged by the overexpression of LSD1 from the virus. In these cohorts, we observed the same ~60% of PS19- LSD1 inj mice exhibit blebbing in the CA1, while there was no blebbing observed in the CA1 of PS19- LSD1ΔN inj mice (Figure 5-3A-D). This was true in the mice analyzed at both 10 months (Figure 5-3A,B) and one year (Figure 5-3C,D). Furthermore, when investigating blebbing throughout the hippocampus, only 38% of PS19- LSD1ΔN inj mice had blebbing outside of the CA1. In comparison, we observed CA1 blebbing in most of the PS19- LSD1 inj

mice and blebbing in other regions of the hippocampus as well as other brain regions in 100% of PS19- LSD1 inj mice (Figure 5-3E). The comparative lack of blebbing in the PS19- LSD1ΔN inj mice raises the possibility that neurons still present when PS19 mice are rescued with the N-terminally truncated LSD1 construct are healthier or more functional than those rescued by the full length protein.

5.2.2 Removal of the N-terminal domain aids in LSD1 nuclear localization in the presence of pathological tau

When PS19 Tau mice are injected with full length LSD1 protein, this protein begins to be sequestered into the cytoplasm at around 11-12 months of age. To determine if deleting the N-terminal disordered domain is sufficient to allow LSD1 to properly localize to the nucleus even in the presence of pathological tau aggregates, we examined the localization of LSD1 protein produced from the N-terminally truncated LSD1 construct via the HA tag. In controls injected with the full length protein, all of the mice that had CA1 blebbed nuclei showed HA-tagged LSD1 that mislocalzied to the cytoplasm (Figure 5-4A,C). In contrast, PS19- LSD1ΔN inj mice show persistent nuclear HA staining. This is consistent with the lack of blebbed nuclei (Figure 5-4C). Even in the oldest PS19- LSD1ΔN inj mouse analyzed at 12.3 months of age (Figure 5-4D), we did not observe blebbing or HA-tagged LSD1 mislocalization. This suggests that LSD1ΔN evades tau aggregates to be successfully imported into the nucleus.

5.2.3 Heterozygous removal of the N-terminal domain modulates the PS19 Tau mouse phenotype

Viral expression of the N-terminally truncated LSD1 protein preliminarily showed that removal of this domain increases the ability of LSD1 to localize to the nucleus even in the presence of tau pathology, and eliminates the blebbing phenotype observed in full length LSD1 overexpression. However, data from the viral rescue experiments also suggested that the N-terminal domain may be required for the maximum function of LSD1. To further address the function of the N-terminal disordered domain *in vivo*, we generated a novel mouse line with an exon 1 deletion of *Lsd1* at the endogenous locus (hereafter referred to as $Lsd1^{\Delta N/+}$). As with the virally expressed protein, the NLS was inserted back into the $Lsd1^{\Delta N/+}$ construct. However, the mouse model is not identical to the viral expression construct, as the mouse maintains all of exon 2, which includes a small portion of the disordered domain (21 amino acids). Importantly, the new *Lsd1* mouse allele also retains all the intronic regulatory elements between exon 1 and 2 (Figure 5-5A). Based on the preliminary virus data, we hypothesized that the $Lsd1^{\Delta N/+}$ variant would be resistant to sequestration by cytoplasmic tau aggregates and therefore increase the nuclear pool of LSD1. *Lsd1* heterozygous mice do not have a neurodegenerative phenotype. Therefore, even if the N-terminal disordered domain is required for LSD1 function, the one full length copy of LSD1 should be sufficient to bypass any potential embryonic lethality. This would enable us to still determine whether having one copy of *Lsd1* with the N-terminal deletion that can still be transported into the nucleus can rescue tau-mediated neurodegeneration. Importantly, from the viral experiments, we know that the N-terminal deleted version of LSD1 is at least mostly functional in degenerating neurons of the brain.

$Lsd1^{\Delta N/+}$ mice were crossed with PS19 Tau mice (Figure 5-5B), generating four experimental genotypes at: Wild Type ($Lsd1^{+/+}$), $Lsd1^{\Delta N/+}$, PS19 Tau, and PS19;$Lsd1^{\Delta N/+}$. Thus far, the ratio of the four genotypes that we have obtained is not completely equal, $Lsd1^{+/+}$ made

up 32% of mice, *Lsd1*$^{\Delta N/+}$ made up 19.5%, PS19 Tau made up 33.5%, and PS19;*Lsd1*$^{\Delta N/+}$ made up 15%. It is possible that there is a slight selection against the *Lsd1*$^{\Delta N/+}$ allele, but this will have to continue to be monitored. If the N-terminal disordered domain is dispensable for LSD1 functionality and is required for sequestration by pathological tau, we would anticipate a complete rescue of the PS19 Tau phenotype. However, it is possible that the N-terminal domain is required for LSD1 function. In this case, we would expect varying phenotypes based on the degree to which the domain contributes to enzymatic function or loci targeting. If the N-terminal disordered domain is entirely required for LSD1 function, we would anticipate PS19;*Lsd1*$^{\Delta N/+}$ mice to have an exacerbated neurodegeneration phenotype that is similar to PS19 Tau mice with reduced LSD1 (PS19;*Lsd1*$^{\Delta/+}$, see Chapter 3). In that case, the truncated product from the *Lsd1ΔN* allele would be entirely compromised and no better than a null allele. If the N-terminal disordered domain is partially required for LSD1 function and the *Lsd1ΔN* allele is hypomorphic, then we might expect PS19;*Lsd1*$^{\Delta N/+}$ mice to have a phenotype slightly better or worse than PS19 Tau mice, depending on the degree to which truncation affects LSD1's functionality, combined with the disordered domain's requirement for association with pTau.

Thus far in overall lifespan, *Lsd1*$^{\Delta N/+}$ (red) have the same survival was *Lsd1*$^{+/+}$ mice. This is similar to what we found for *Lsd1*$^{\Delta/+}$ mice in Chapter 3. PS19;*Lsd1*$^{\Delta N/+}$ mice (yellow) appear to have a survival phenotype intermediate between PS19 Tau mice (green) and tau mice that are heterozygous for an *Lsd1* loss of function allele (purple; data taken from Figure 4-4A) (Figure 5-6A). This suggests that the *Lsd1*$^{\Delta N/+}$ allele may be hypomorphic for LSD1 function. However, this experiment is ongoing, and a survival curve is only truly informative once the entire population is deceased. Therefore we have also plotted all the remaining living mice >11 months old on top of all mice that reached terminal paralysis and died (dots in red) (Figure 5-6B). This

figure more legibly represents the remainder of the colony. Interestingly, the PS19;*Lsd1*$^{\Delta N/+}$ mice that died were all younger then 10 months and the few mice that lived past 10 months are all still alive. This raises the possibility that there ultimately may be a bimodal distribution.

When *Lsd1* was reduced in the PS19 Tau mice the exacerbated effect on survival was due to an increase in the progression of paralysis. Although we have not yet performed quantitative analysis of paralysis (i.e. rotarod, grid performance) in the PS19;*Lsd1*$^{\Delta N/+}$ animals, we did record the age at clasp onset for all mice during weekly monitoring. Figure 5-6C shows age at clasp onset (black dots), or current age for mice that have no paralysis phenotype (blue dots, y = current age), for all living PS19 Tau and PS19;*Lsd1*$^{\Delta N/+}$ mice >11 months. All of the longest-lived PS19;*Lsd1*$^{\Delta N/+}$ mice show no sign of paralysis, despite being older than one year of age. There are still PS19 Tau mice of similar age that do not have a clasp, so perhaps this is part of the normal distribution. Nevertheless, it is intriguing that certain animals remain unaffected into old age. This is potentially consistent with a bimodal distribution of the paralysis phenotype. Taken together, the survival curve and the paralysis phenotypes indicate that there could ultimately be a population of PS19;*Lsd1*$^{\Delta N/+}$ mice that are resistant to tau-mediated neurodegeneration. However, quantitative analysis at multiple time points, as well as further analysis of the full population of mice is necessary to confirm the effects that the N-terminal truncation has on paralysis and neurodegeneration.

5.2.4 Homozygous loss of the N-terminal domain of LSD1

Preliminary data suggests that the *Lsd1*$^{\Delta N/+}$ allele may be hypomorphic, which could potentially result in the subtle effect on survival. *Lsd1*$^{-/-}$ mice are embryonic lethal, arresting at E5.5 and are resorbed by E7.5 [98,162]. Therefore, if LSD1's N-terminal disordered domain is

functionally required, then we might not be expect to be able to obtain mice that are homozygous for the *Lsd1*$^{\Delta N}$ allele. Similar to the cross described above, we crossed *Lsd1*$^{\Delta N/+}$ mice with PS19;*Lsd1*$^{\Delta N/+}$ mice. These crosses will generate six genotypes: wildtype, PS19 Tau, *Lsd1*$^{\Delta N/+}$, PS19;*Lsd1*$^{\Delta N/+}$, *Lsd1*$^{\Delta N/\Delta N}$, and PS19;*Lsd1*$^{\Delta N/\Delta N}$ (Figure 5-7A). In order to be able to distinguish between heterozygotes and homozygotes, we need to be able to detect the wild-type *Lsd1* band. We are currently in the process of optimizing a new PCR genotyping reaction that will enable us to do so. Once that reaction is functioning, we will be able to determine if *Lsd1*$^{\Delta N/\Delta N}$ mice are viable, and whether they have any phenotype. So far, these crosses have repeatedly generated large litters (9+ pups), which decreases the likelihood that any genotype is embryonic lethal. Furthermore, we have not observed perinatal lethality in these progeny. As a result, we expect that mice that are homozygous for the N-terminal *Lsd1* allele will be viable.

5.3 Discussion

Tauopathies are molecularly characterized by the presence of aberrantly hyperphosphorylated tau protein that forms aggregates within the cell body of neurons. This is thought to lead to neuronal cell death. To date, many factors that contribute to tau aggregation, neuronal dysfunction, and neuronal cell death have been uncovered. However the complete downstream mechanism of tau-mediated neurodegeneration is poorly understood. Previously, we showed that modulation of the histone demethylase LSD1 can alter neurodegeneration in a tauopathy mouse model. We produced the first cytological evidence that pathological tau can prevent LSD1 from properly localizing to the nucleus in neurons, thereby inhibiting its required function to maintain proper transcription. Additionally, we showed that overexpression of LSD1 directly into the hippocampus of neurons can rescue the tau-mediated neurodegeneration, but

only temporarily. Eventually, the exogenous LSD1 becomes sequestered. Our ongoing work looks to address the *in* vivo interaction between LSD1 and pathological tau and address how to avoid the ongoing sequestration of LSD1.

Based on studies that have implicated tau's intrinsic disorder in its association with the disordered domains of other proteins, we predicted that tau associates with LSD1's N-terminal disordered domain, blocking the NLS of LSD1. This would inhibit the interaction between LSD1 and the importin proteins, causing LSD1 to be sequestered in the cytoplasm. If this is the case, then removal of LSD1's disordered domain should prevent sequestration by tau, resulting in persistent nuclear localization, despite the presence of tau pathology. Excitingly, when the LSD1ΔN virus was expressed into 8 month old PS19 Tau mice, we observed improved persistence in the nuclear localization of exogenous LSD1ΔN compared to the full length LSD1 exogenous protein. This persistence lasted as late as one year of age (4 months post viral injection). At this time point almost all mice injected with full length LSD1 show sequestration of the exogenous protein. These data support the hypothesis that the N-terminal domain of LSD1 is required for the interaction between LSD1 and tau. If this is the case, then interfering with this pathological interaction could significantly help AD patients therapeutically.

In addition to the increased nuclear persistence of the LSD1ΔN virus, we demonstrated that overexpression of LSD1ΔN eliminates the degenerating population consistently seen in age-matched samples of PS19- HA animals. This rescue, suggests that N-terminally deleted LSD1 is functional in hippocampal neurons, at least when overexpressed. Additionally, in full length PS19-LSD1 inj mice, many hippocampal neurons have an abnormal blebbing phenotype, even at 11 months and younger. In contrast, there is relatively little blebbing in the hippocampus overall, and no blebbing in the CA1, when PS19 mice are injected with the *Lsd1ΔN* construct. We

propose that the nuclear blebbing is an intermediate stage of cell death due to prolonged survival. If this is the case, the relative lack of blebbing points to an improved rescue by overexpression of the N-terminal truncated LSD1. However, we do not currently have evidence that overexpressed LSD1ΔN rescues cell death longer than full length (past 12 months) because the experiments are currently ongoing and limited by the death of these mice due to spinal cord paralysis.

Within our mouse colony, initially we have observed that the majority of PS19;*Lsd1*$^{\Delta N/+}$ mice have paralysis. The presence of this phenotype could be interpreted in a number of ways: 1) the exclusive deletion of exon 1 left enough of the disordered domain remaining to allow for interaction with and sequestration by tau; 2) the N-terminal disordered domain, specifically the sequence encoded by exon 1, is partially required for LSD1 functionality *in vivo*; or 3) the domain encoded by exon 1 is not the mechanism through which LSD1 is sequestered in the PS19 Tau mouse. Currently, there are three old (>400 days) PS19;*Lsd1*$^{\Delta N/+}$ mice living with no sign of paralysis. While there is a PS19 Tau mouse of the same age that has yet to show a clasp, we feel confident that this animal will eventually develop paralysis. It is possible that the PS19;*Lsd1*$^{\Delta N/+}$ mice will show the same stochasticity as the PS19 Tau mice; however, it is also possible that these mice will never develop paralysis. This preliminary result indicates that PS19;*Lsd1*$^{\Delta N/+}$ mice may be bimodally distributed, in that most will undergo some degree of neurodegeneration that is perhaps exacerbated due to the function of the disordered domain, while some mice may remain phenotypically wildtype and have a normal lifespan. This would be because they have stochastically avoided the reduced function associated with loss of the disordered domain, and are able to benefit from the ability of the truncated LSD1 to avoid association with tau aggregates.

Overall, PS19;*Lsd1*$^{\Delta N/+}$ mice show a survival phenotype that is intermediate between PS19 Tau and PS19 Tau mice that are heterozygous for *Lsd1* deletion. The fact that the PS19;*Lsd1*$^{\Delta N/+}$ mice show a worse survival phenotype than PS19 Tau mice with two normal copies of *Lsd1* suggests that LSD1ΔN is functionally compromised compared to the full-length protein. However, because PS19;*Lsd1*$^{\Delta N/+}$ mice appear to have a better survival phenotype than PS19;*Lsd1*$^{-/+}$ animals, we argue that LSD1ΔN retains partial functionality *in vivo*.

This finding is consistent with the observation that full length LSD1 potentially rescues slightly better than the *Lsd1ΔN* version (based on neuronal cell count). In this case the possibility that a hypomorphic allele can rescue at all may only be due to the viral expression, which results in 6-fold overexpression compared to endogenous level. This abundance of partially functioning LSD1 could be compensatory, facilitating the elimination of the degenerating population we observed in the viral injection experiment. Conversely, when the hypomorphic allele is expressed at endogenous levels in the mouse model, we can observe the consequences of its functional shortcomings in the form of paralysis and shortened survival.

Combined with our evidence that truncated LSD1 is resistant to sequestration by tau, the argument that *Lsd1ΔN* is a hypomorphic allele potentially further explains the bimodal pattern of paralysis observed in the PS19;*Lsd1*$^{\Delta N/+}$ mice. This is because the neuronal cell death and paralysis would be explained by a combination of 1) the amount of LSD1ΔN versus full length LSD1 any cell is producing, 2) the tau burden in that animal, and 3) how the loss of the N-terminal disordered domain ultimately affects LSD1 function. As an epigenetic enzyme with a wide array of target loci, it is possible that LSD1's disordered domain is necessary for binding to certain targets or interacting partners, particularly in the case of transcriptional condensates at highly specific genomic loci. It has been proposed that chromatin could be in a form of phase

separation and the disordered domains of chromatin proteins have been suggested to enable these proteins access to the phase separated compartments. This is similar to RNA binding proteins which interact with cytoplasm granules, through their disordered domains[257]. If removal of the N-terminal disordered domain *in vivo* precludes LSD1 from accessing or interacting with regions of chromatin that are in this state, then we would observe LSD1 failing to demethylate at a few specific targets as opposed to a global decrease in methylation. Therefore, it is possible that moving forward we will continue to observe a bimodal distribution of mice that die early of paralysis, and mice that appear phenotypically normal and are long-lived. If this is the case, we might anticipate that homozygosity of the N-terminal deletion would exacerbate this bimodal distribution, where some homozygotes become terminal even younger than their heterozygous counterparts and some remain unaffected. In the affected animals, neurons would accumulate transcription-coupled H3K4me2 on the loci where truncated LSD1 cannot demethylate. This would lead to inappropriate transcription of those loci, as well as further accumulation of active epigenetic modifications. This would result in disruption of the cell's transcriptional program, leading to its dysfunction or death.

Alternatively, it is possible that the N-terminal domain aids in efficiency or somewhat contributes to general function of the LSD1. In this case, homozygotes in the PS19 Tau background would show an improved phenotype compared to heterozygotes because now both copies would avoid sequestration and increase nuclear levels of LSD1. Despite the partial loss of function in LSD1ΔN, persistent nuclear localization despite aggregation of tau could allow for LSD1 to demethylate targets most crucial to cell survival, creating improved paralysis and survival phenotypes. Our preliminary data from the PS19;*Lsd1*$^{\Delta N/+}$ colony only allow for speculation at this time. The function of the N-terminal domain can be further studied in the

homozygous *Lsd1*$^{\Delta N/\Delta N}$ mice outside of its role in the PS19 Tau mouse. This ongoing work will aid in our understanding of both the *in vivo* interaction between LSD1 and pathological tau as well as the function, if there is one, of the N-terminal domain of mammalian LSD1.Through our investigation of the interaction between pathological tau and N-terminal domain of LSD1 we can target the specific interaction in order to restore LSD1 function in tauopathies. Additional discussion of how this mechanism could be targeted is detailed in the discussion chapter.

5.4 Figures

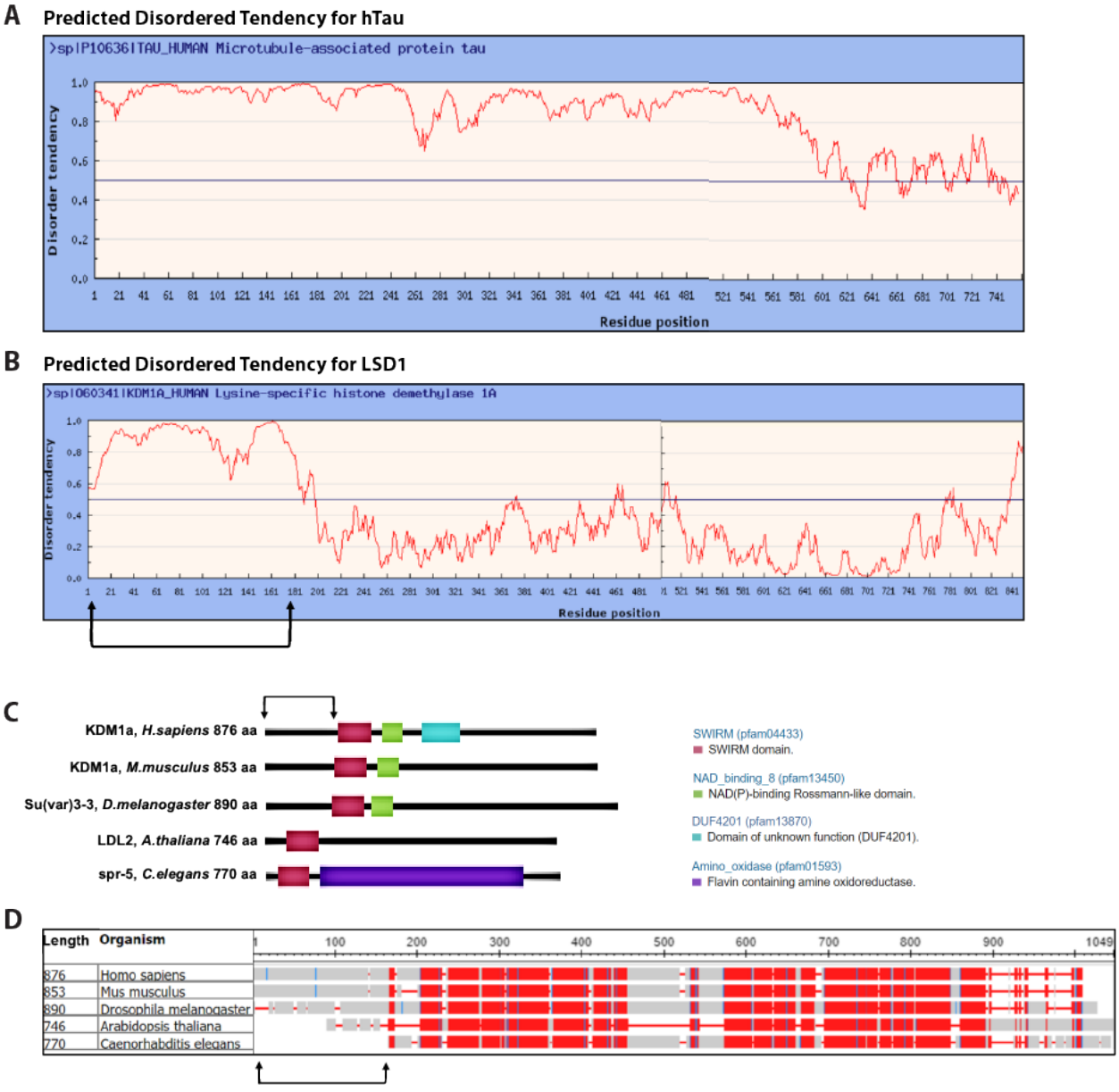

Figure 5-1 LSD1 contains an intrinsically disordered domain which is partially conserved. **A, B,** Disorder frequency by amino acid residue of human proteins showing that tau is a highly disordered protein with very little secondary structure (**A**) and LSD1 is highly ordered, apart from the 172 amino acid intrinsically disordered N-terminal domain (**B**). Figure generated at http://iupred.elte.hu/ courtesy of Dr. David J. Katz and Dr. Stephanie M. Kyle. **C,** Cartoon

depiction of the structure of LSD1 homologs. N-terminal intrinsically disordered domain is conserved across humans, mice, and flies. This figure was generated at https://www.ncbi.nlm.nih.gov/homologene courtesy of Alicia Walker **D,** NCBI blastP multiple sequence alignment showing detailed primary structure of LSD1 homologs. This figure was generated using https://www.ncbi.nlm.nih.gov/projects/msaviewer/ courtesy of Alicia Walker. Brackets denote N-terminally unstructured domain of LSD1.

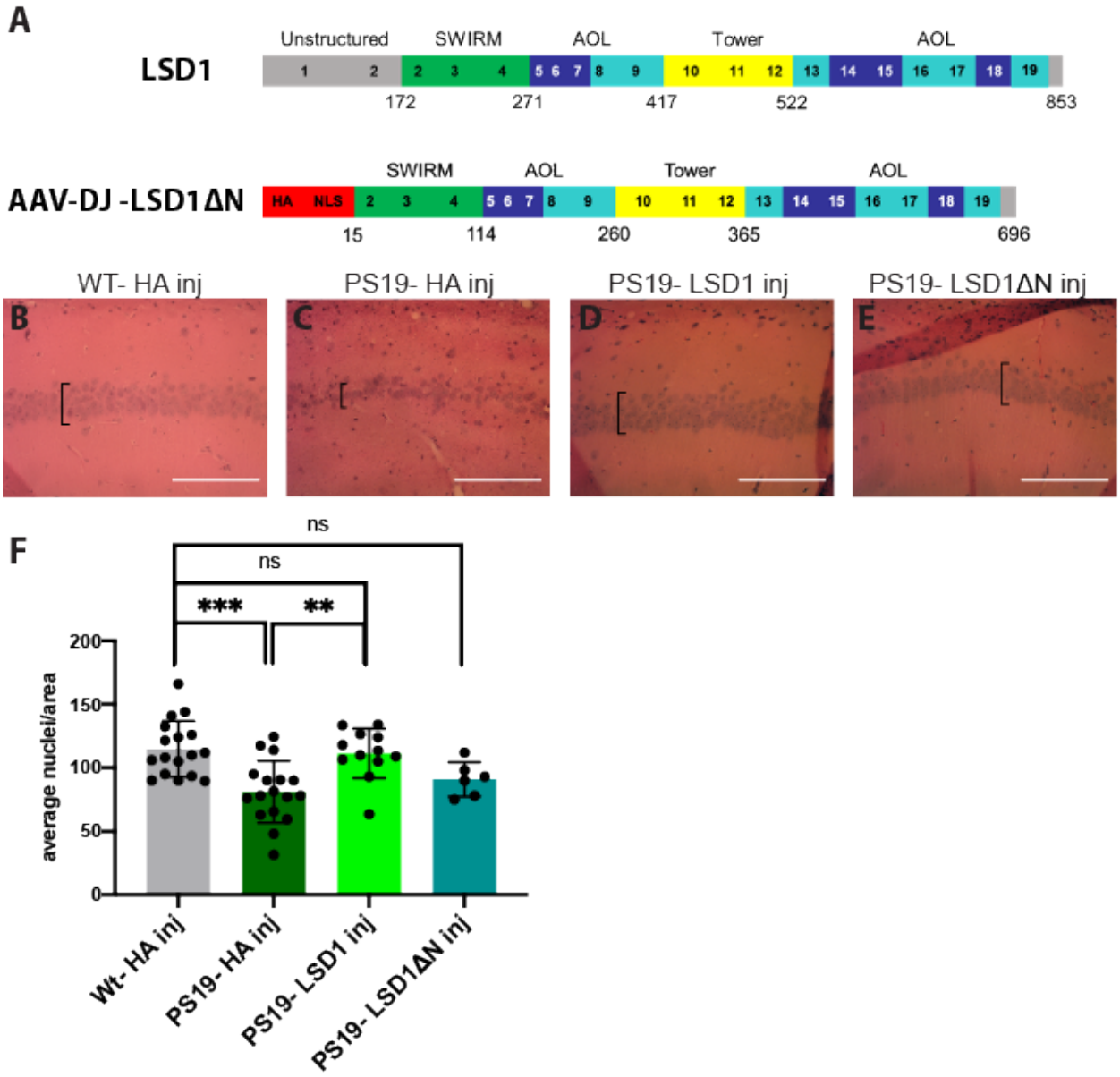

Figure 5-2 N-terminal domain of LSD1 is not required for survival in PS19 Tau mice. A, Cartoon depiction of the LSD1 with the functional domains and corresponding amino acid number. **LSD1** is the endogenous mouse protein and **AAV-DJ-LSD1 ΔN** shows the N-terminally truncated protein with a the HA-tag and nuclear localization sequence inserted. **B-E,** Representative image of H&E stained CA1 region of the hippocampus of WT- HA inj mouse aged 11.4 months (**B**), PS19- HA inj mouse aged 11.7 months (**C**), PS19- LSD1 inj mouse aged 10.8 months, **(D)** PS19- LSD1ΔN inj mouse aged 10.8 months (**E**). Square brackets denote

thickness of pyramidal layer of the CA1 of the hippocampus. Scale bars= 50μm. **F,** Quantification of the average number of nuclei in the pyramidal layer of the hippocampus per area per mouse from histology represented in **Fig. 5-2B-E**. Values are mean ± SD. WT- HA inj *n=17*, PS19- HA inj *n=17*, PS19- LSD1 inj *n=13*, PS19- LSD1ΔN inj *n=6*. Values are mean ± SD (one-way analysis of variance (ANOVA) with Tukey's post hoc test, ***p=0.0002, **p=0.0079, ns=not significant.

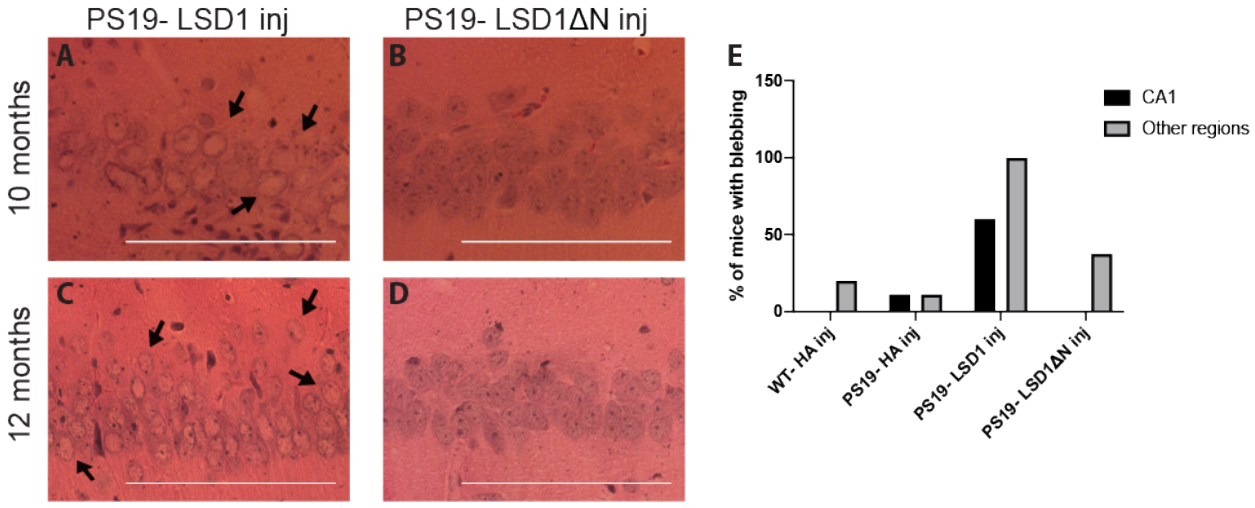

Figure 5-3 Removal of the N-terminal domain of LSD1 rescues nuclear blebbing when overexpressed in PS19 Tau mice. A-D, Representative image of H&E stained CA1 region of the hippocampus showing blebbing in PS19- LSD1 inj mice (**A,C)** analyzed at both 10 months (**A**) and 12 months (**B**) but no blebbing in PS19- LSD1ΔN inj mice (**B,D)** analyzed at both 10 months (**B**) and 12 months (**D**). Scale bars= 50µm. **E,** Quantification of the percentages neurons in each mouse condition where blebbing was observed in either the CA1 (black bars) or throughout other brain regions, but not in CA1 (grey). None of the PS19- LSD1ΔN inj mice show CA1 blebbing, even past 1 year of age **(D)**.

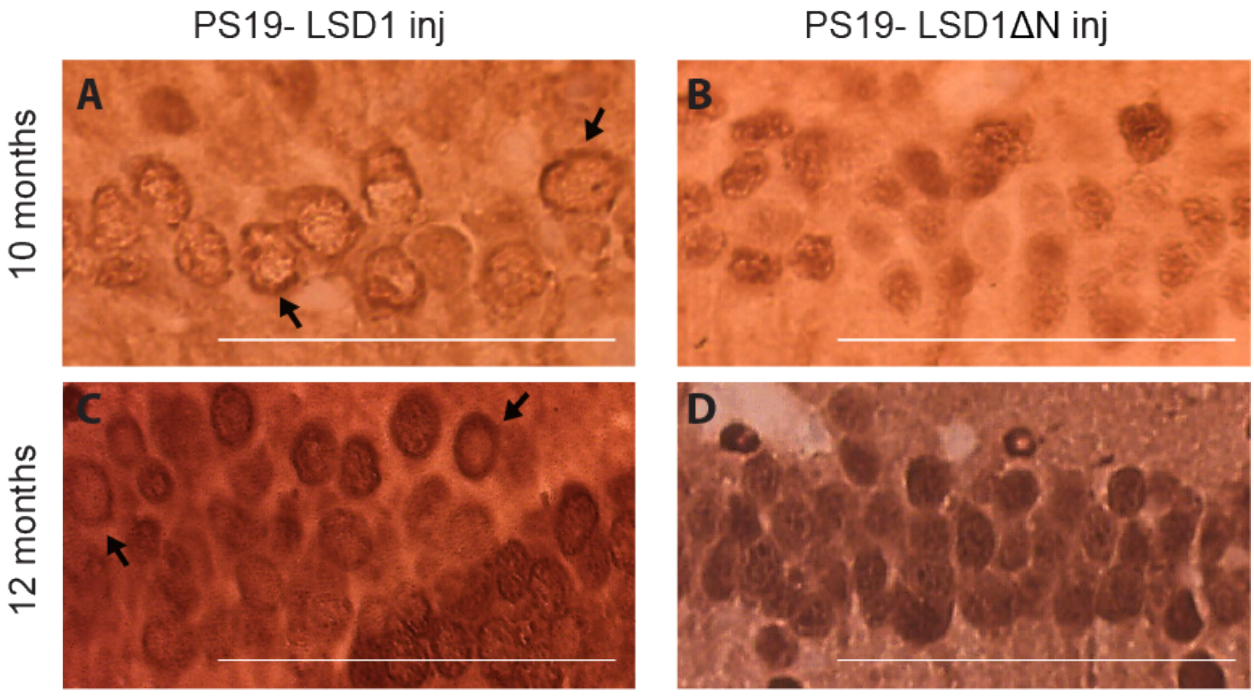

Figure 5-4 LSD1ΔN virus remains nuclear at the timepoint when the full length LSD1 is sequestered. A-D, Representative image of immunohistochemistry staining of HA(LSD1 in the CA1 region of the hippocampus showing sequestration of exogenous LSD1 tagged with HA (**A,C)** analyzed at both 10 months (**A**) and 12 months (**C**) but in PS19- LSD1ΔN inj mice (**B,D)** exogenous LSD1ΔN is localized to the nucleus analyzed at both 10 months (**B**) and 12 months (**D**). Arrows denote HA staining is sequestered and excluded from the nucleus. Scale bars= 50µm.

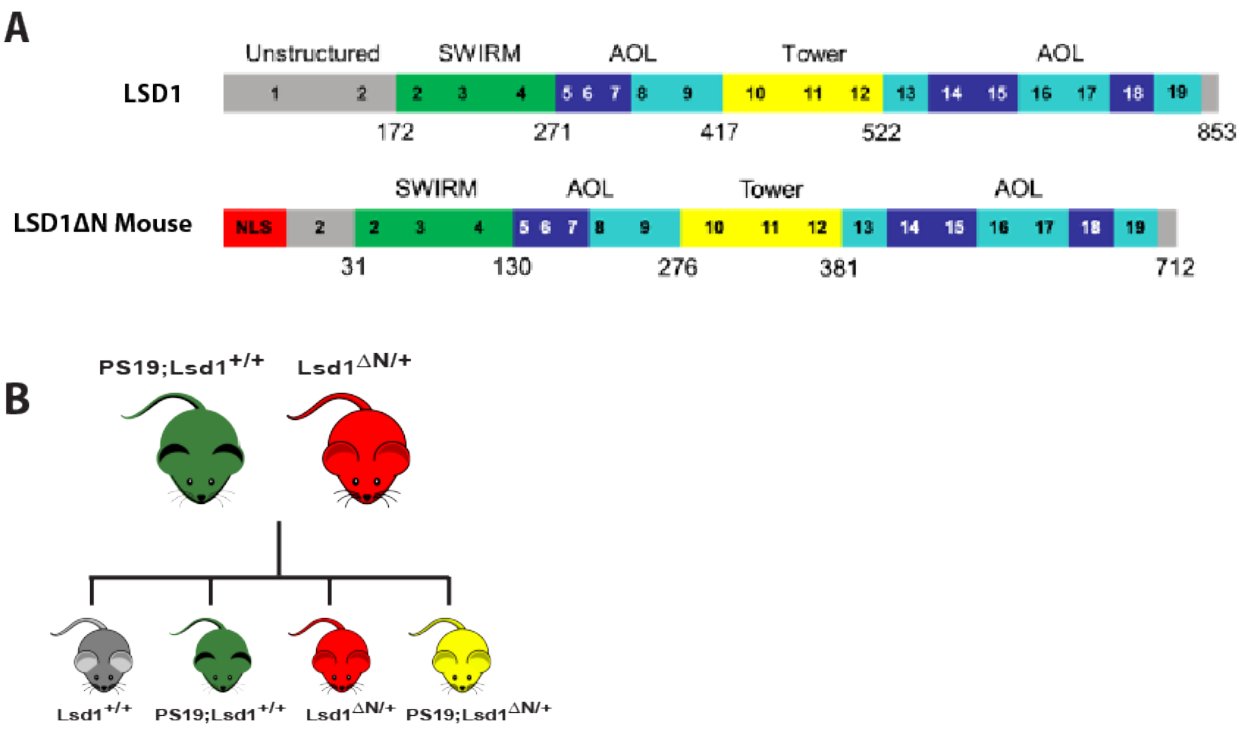

Figure 5-5 Generation of tauopathy mice heterozygous for the exon 1 deletion of *Lsd1*. A, Cartoon depiction of the LSD1 with the functional domains and corresponding amino acid number. **LSD1** is the endogenous mouse protein and **LSD1ΔN Mouse** shows the N-terminally truncated protein produced by the *Lsd1ΔN* allele in the mouse with the NLS inserted. **B,** PS19 Tau mice that are wild-type for *Lsd1* were crossed with *Lsd1ΔN* heterozygous mice. These crosses generated four genotypes: Wild Type mice ($Lsd1^{+/+}$, grey), PS19 Tau (green), $Lsd1^{\Delta N/+}$ (red), and PS19;$Lsd1^{\Delta N/+}$ (yellow). Colors designated here are maintained throughout all figures.

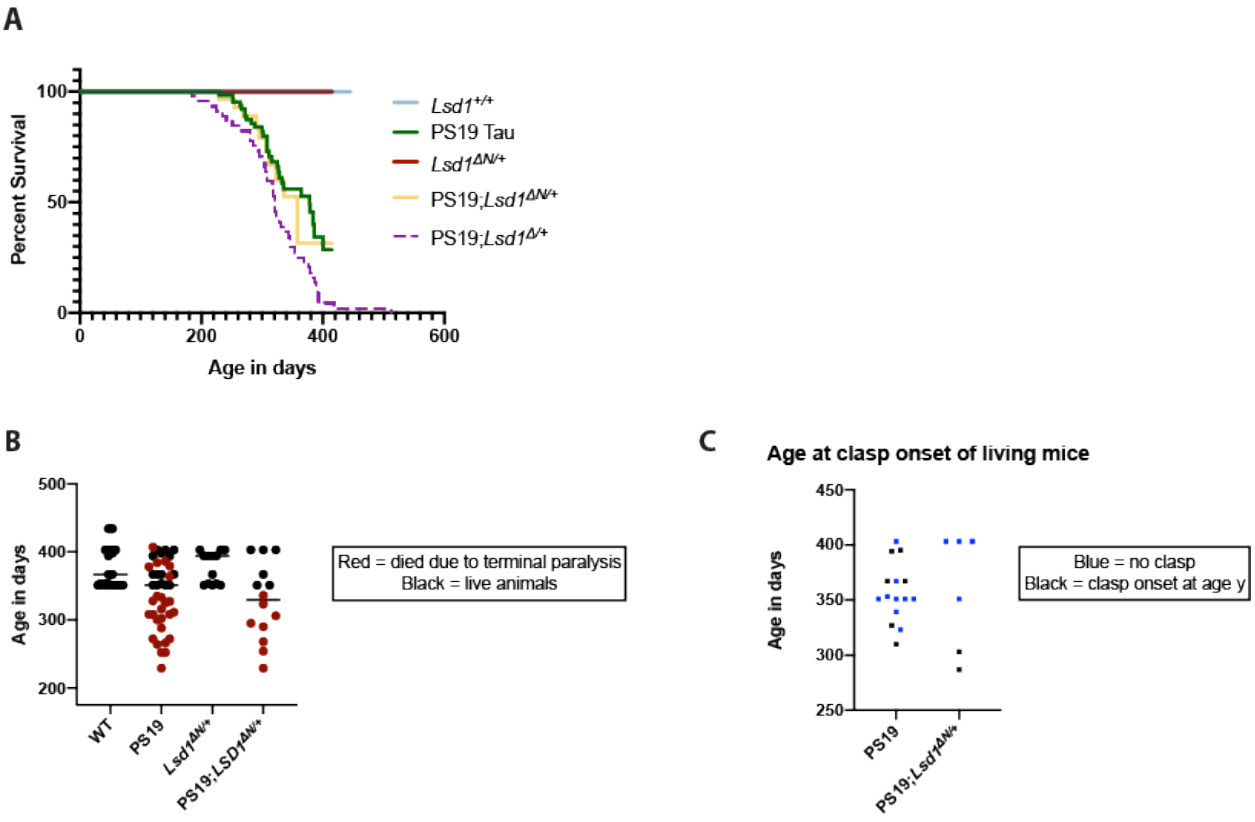

Figure 5-6 *Lsd1*$^{\Delta N/+}$ allele has a hypomorphic-like effect on the tauopathy phenotype. A, Ongoing lifespan curve showing that *Lsd1*$^{\Delta N/+}$ mice (red, *n=34*) have the same survival as Wild Type mice (blue, *n=66*). PS19 Tau (green, *n=66*), PS19;*Lsd1*$^{\Delta N/+}$ (yellow, *n=28*), and PS19;*Lsd1*$^{\Delta/+}$ (purple dotted line taken from **Figure 4-4**, *n=44*) mice have reduced survival. **B,** Remaining living mice >11 months old in the same colony merged with the mice that have died (red dots) **C,** Age at clasp onset of living mice >11 months only. Black points represent animals living with hindlimb paralysis and show y = age at clasp onset, blue points represent animals without a clasp and show y = current age in days. PS19 *n=15* and PS19;*Lsd1*$^{\Delta N/+}$ *n=6*.

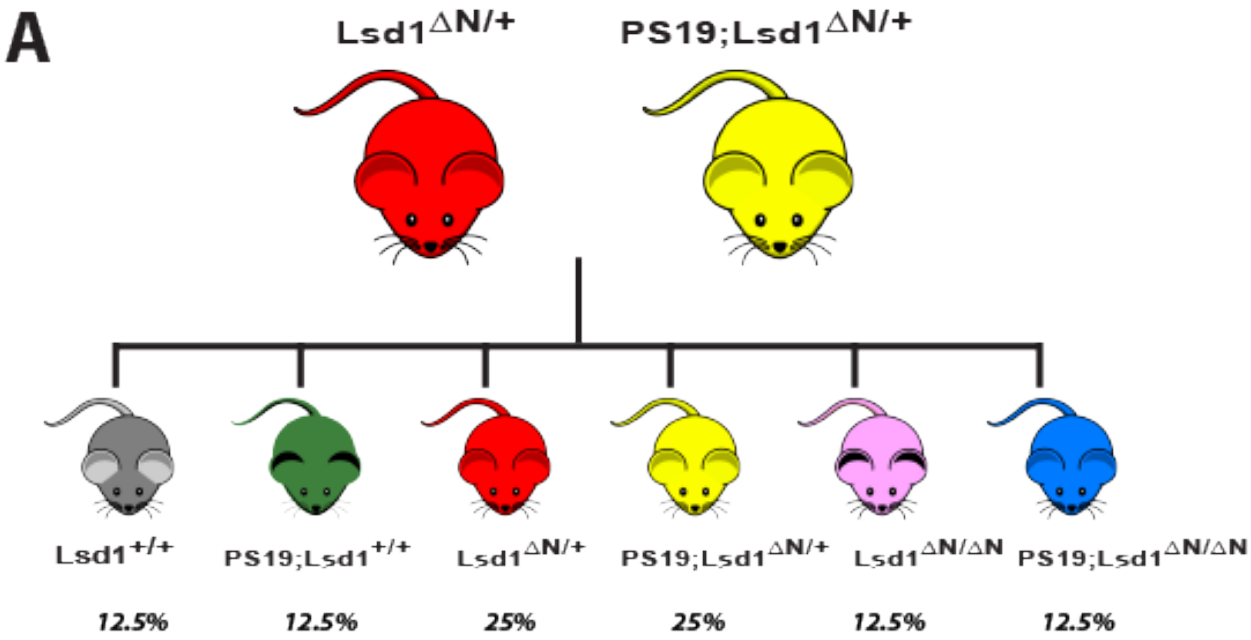

Figure 5-7 Generation of tauopathy mice homozygous for the exon 1 deletion of *Lsd1*. A, PS19 Tau mice that are heterozygous for the *Lsd1ΔN* allele were crossed with *Lsd1ΔN* heterozygous mice. These crosses are expected to yield six experimental genotypes (with an expected Mendelian ratio): Wild Type mice ($Lsd1^{+/+}$, grey, 12.5%) , PS19 Tau (green, 12.5%), $Lsd1^{\Delta N/+}$ (red, 25%), and PS19;$Lsd1^{\Delta N/+}$ (yellow, 25%), $Lsd1^{\Delta N/\Delta N}$ (pink, ~12.5%), PS19;$Lsd1^{\Delta N/\Delta N}$ (blue, ~12.5%).

CHAPTER 6:

Discussion

Each section of this discussion contains a summary of the conclusions from the previous chapters that correspond with the section topic.

6.1 LSD1 is continuously required for neuronal maintenance

In this dissertation, we have shown that LSD1 is required for neuronal maintenance and survival. Through this work we argue that normally, LSD1 maintains terminally differentiated neurons, and prevents the activation of common neurodegenerative pathways, by continuously repressing the transcription of inappropriate genes. Consequently, when LSD1 function is impaired, either through deletion of *Lsd1* or through cytoplasm sequestration by pathological aggregates, neurons undergo cell death, which results in learning and memory defects and dementia in human patients.

Inducible deletion of *Lsd1* in adult mice leads to widespread neurodegeneration throughout the cerebral cortex and hippocampus as well as terminal motor paralysis. In addition, global gene expression changes in the hippocampus highly correlate with those documented in human cases of late-onset Alzheimer's disease (LOAD)[192] and Frontotemporal Dementia with progranulin mutation (FTP-progranulin)[193]. The transcriptional changes may not be surprising at first, as you would expect that a signature of neuronal cell death would be shared amongst these diseases. However, it is surprising that the expression changes of a complex human disease can be recapitulated by deletion of a single gene. Additionally, these changes appear to be specific to LOAD and FTD-progranulin, as the overlap in expression between *Lsd1* deletion mice and Parkinson's disease, Huntington's disease, or sporadic FTD was not significant. This lack of similarity with other neurodegenerative diseases suggests that the overlap observed with LOAD and FTD-progranulin is being driven by a shared mechanism, rather than a common neurodegeneration signature.

Consistent with this idea, there are enrichments and depletions of gene ontologies in *Lsd1* deletion mice that have been implicated in these diseases. Several pathways were identified such

as a reduction in the oxidative phosphorylation pathway as well as a reduction in synaptic transmission. Interestingly, there is a dramatic upregulation of genes involved in neuroinflammation and the inflammatory complement cascade, both of which have been implicated in neurodegenerative diseases such as Alzheimer's disease (AD)[192,258,259]. The majority of genes in the neuroinflammatory pathway are involved in microglial activation. The complement cascade is required during early postnatal development for the deletion of supernumerary weak synapses and axons by microglia phagocytosis. This pruning by the complement cascade is required for properly refining the connective landscape of neurons[213,260]. Identification of the developmentally-regulated complement cascade in AD molecular pathology has raised the possibility that microglia do not merely act passively to clear cells that have undergone neurodegeneration. Instead microglia may function actively to aberrantly clear synapses and axons of living neurons. The aberrant upregulation of the complement cascade due to deletion of *Lsd1,* and in AD patients, poses an interesting question of how neurons and microglia are connected during neurodegeneration.

Our data suggests that the neuronal cell loss observed in *Lsd1* deletion mice is cell autonomous. First, although LSD1 protein is lost from all hippocampal and cortical neurons that undergo neuronal cell death, LSD1 persists in both astrocytes and oligodendrocytes when neurons are dying in *Lsd1* deletion mice. In addition, we found that LSD1 protein is not present in microglia. To confirm cell autonomy, we performed clonal analysis. To perform the clonal analysis, we induced deletion of *Lsd1* in mice using a single low dose tamoxifen injection. This resulted in a much lower level of *Lsd1* deletion then the standard protocol. Nonetheless, the few neuronal nuclei that lack LSD1 still undergone neurodegeneration. Taken together, these results

suggest that the neuronal cell death that we are observing in *Lsd1* deletion mice is due to loss of LSD1 function cell autonomously within the neuron.

Although *Lsd1* deletion functions cell autonomously, this does not preclude the involvement of external factors and other cell types in the neurodegenerative mechanism. Recently, genomic techniques including genome-wide association studies, integrated network analyses, and RNA-sequencing of AD cases and mouse models have pointed to a role for microglia and the complement cascade in AD etiology. From our work, we have shown that in addition to the increased inflammatory transcriptional signature, there is a strong reactive gliosis response in the hippocampus and cortex the brain of *Lsd1* deletion mice. Additionally, we observe that the dying neurons that are still present in the brain have lost all of their axons and dendrites. Given the role of the complement cascade in developmentally-regulated pruning, perhaps the aberrant activation of the complement cascade is orchestrating the synaptic and axonal loss observed in *Lsd1* deletion mice. It has been difficult to interrogate the dynamic process of synapse and axon loss during neurodegeneration in current animal models of AD because modest neuronal cell death occurs over many months. Thus dying neurons are rare and typically cleared before they can be observed. However, unlike other mouse models of neurodegeneration, *Lsd1* deletion mice consistently and rapidly produce near complete hippocampal neuronal cell death, and this neurodegeneration has striking similarities to AD. This allows us to utilize this model to investigate the mechanisms of AD neurodegeneration more easily. Specifically, the *Lsd1* mouse model can be used to interrogate the complex relationship between the increased immune response, the activation of the complement cascade, and the loss of axons and dendrites from degenerating neurons. There are multiple ways we can approach this question. Thus far we have started pursuing a few. All will involve the use of the *Lsd1* deletion

mouse. Importantly, since the neurons in *Lsd1* deletion mice degenerate rapidly and coordinately, we can interrogate these questions by observing the cell death as it is occurring.

The first approach utilizes an *ex-vivo* system, hippocampal slice culture. In order to observe live neurons we crossed *Lsd1*^{CAGG} mice with *Thy1*-GFP mice. *Thy1*-GFP mice provide a strong 'Golgi staining-like" marker of hippocampal axons, dendrites, and cell bodies, with only a small number of neurons being labeled[261]. This allows these labeled neurons to be observed among the rest. *ex-vivo* slice cultures are taken after *Lsd1* has been deleted in the mouse and then monitored by confocal live-imaging. This approach allows us to track the cell death and observe if the loss of axons and dendrites is a progressive process. During the process of neuronal cell death in *Lsd1* mice, we observed that the nuclei become highly condensed, referred to as pyknotic. By live imaging the neuronal cell death in slice culture, it also allows us to determine the timing of when the nuclei become pyknotic in relation to the loss of axons and the onset of neuronal cell death. Up to this point, the mice have been crossed and the colony is easily maintained, hippocampal slices are kept alive in culture, and we can image the Thy1-GFP neurons. However, surprisingly the hippocampal slices where *Lsd1* has been deleted do not undergo cell death. This is despite the fact that we observe LSD1 protein lost from the hippocampal neurons. This surprising result raised a few critical questions: What is different in the *ex-vivo* hippocampus? Is there something present in the *Lsd1* deletion mice that is missing in the slice cultures? One key component that is missing is the peripheral nervous system. The hippocampal slice cultures do not have the ability for the microglia to invade into the hippocampus. It is possible that as the complement cascade is aberrantly activated in response to *Lsd1* deletion, this recruits the microglial response. In the *ex-vivo* system, neurons may be activating the complement cascade, but the microglia are not able to respond. Therefore, despite

the “activation” of the cell death mechanism present from *Lsd1* deleted neurons, the “response” from microglia is not present. There are a few ways to address this. First, we can confirm that the neuronal response is not effected by the change to an *ex-vivo* system. This can be done by RNA-seq analysis of the hippocampal slice culture, or through RT-qPCR. The most important signature would be to look at the components of the complement cascade and neuroinflammation to determine how this has changed. Additionally, it would be interesting to re-introduce elements to the slice system that could activate the few microglia that are present, or to co-culture the system with activated microglia.

An alternative approach would be to utilize the *Lsd1* deletion mouse and determine the role of the microglia *in vivo*. To do this, we will treat the mice with the microglial inhibitor PLX3397. PLX3397 is a CSF1 inhibitor, which when administered to adult mice, depletes ~90% of microglia[262]. PLX3397 administration in adult mice has no effect on motor function, or on cognitive and memory function. Nor does it affect the blood brain barrier, or the number of neurons, oligodendrocytes, or astrocytes. If the action of microglia is required for neuronal cell death after deletion of *Lsd1* we would expect that treatment with this inhibitor will rescue or ameliorate the neurodegenerative phenotype. These experiments are currently under way.

The second approach to examining the relationship of the immune system to the loss of axons and dendrites in our *Lsd1* mice is to employ *in vivo* imagining of a live mouse. This procedure requires a cranial window surgery and two-photon imaging of the brain[263]. For this, we needed to optimize the protocols for performing the surgeries and imagining. The cranial window surgery technique, while more complex than the viral vector infusions, is a standard surgery routinely performed in many labs. Therefore we are in the process of adopting it in the lab. Prior to cranial window surgery, mice that express the *Thy1-GFP* will be tamoxifen injected

in order to delete *Lsd1.* After roughly 5 weeks post injection we would expect to see effects on the neurons. At that point we can image the mice through the cranial window to observe the GFP labeled neurons in the outer layers of the cortex. Since we observe cell death throughout the cortex, we expect that the window on the surface of the brain should capture dying neurons. Using time-lapse live-imaging to observe the cell death via the cranial window, we can determine if the neurodegeneration is an active or passive process, and what happens to the labeled axons and dendrites. Although imaging via a cranial window is a challenging technique, this will allow us to remove any artifacts from the *ex-vivo* system. Thus far, we have fabricated a special immobilization device to hold the anesthetized mice in place for two-photon imaging. We have also obtained the necessary components to carry out the protocol.

6.2 LSD1 represses the stem cell program in terminally differentiated neurons

One important consideration is the function of LSD1 in neurons. In Chapter 3 of this study we show that stem cell gene transcription is ectopically reactivated in the absence of LSD1. Although robust reactivation occurred in neurons, it remains unclear whether this requirement for stem cell gene repression is neuronal specific or more general. Indeed, if the requirement is general, it would dramatically change our view of differentiation. The current view, established by Conrad Waddington, describes cells in a developing embryo as being like a ball rolling down a hill[264]. Each starts at the top (undifferentiated), then descends due to gravity, making path choices in the form of valleys (cell fate choices), until it ultimately reaches the bottom of the hill (terminally differentiated), where it can never return to the top (undifferentiated state). This analogy is accurate for natural development. However, several experiments have challenged this idea terminal differentiation. Somatic cell nuclear transfer[265,266]

and inducible pluripotency reprogramming[211] revert a differentiated cell or nucleus back into a completely undifferentiated state. In both of these experiments, the donor cells or nuclei contain all the genetic information necessary to produce an organism. The chromatin must be epigenetically reprogrammed to both silence the differentiated cell fate program and activate the undifferentiated program. These experiments present an enormous shift in the developmental paradigm, because they suggest that terminal differentiation can be overcome, albeit in artificial systems. Nevertheless, they demonstrated that the widely held view of differentiation was incomplete.

Conversely, if this is a neuronal specific phenomenon, it raises many questions as to why neurons maintain such a propensity to reactivate stem cell gene transcription. This would be quite striking for a cell type that is considered to be highly differentiated, including post-mitotic status, complex structure and asymmetry. Future experiments could aim to determine whether the reactivation of stem cell gene transcription contributes to the observed neuronal cell death in the absence of LSD1. During the course of inducible pluripotency reprogramming, the four Yamanaka factors (OCT4, c-MYC, SOX2 and KLF4)[267] each bind to the promoter of p53. It is thought that through this binding, tumor suppressor pathways are activated, leading to apoptosis. This mechanism is a potential explanation of the relatively low efficiency of inducible pluripotency reprogramming. Therefore, it is possible that stem cell gene reactivation when LSD1 is lost triggers apoptotic pathways by activation of p53. If this is the case, deletion of the Yamanaka factors or p53 along with LSD1 should rescue the LSD1-mediated neurodegeneration phenotype. Consistent with these ideas, we have shown that there is an upregulation of pluripotency factor expression in post-mortem AD and FTD brain samples relative to controls.

This raises the exciting possibility that human neurodegeneration could occur through the loss of neuronal cell fate.

6.3 LSD1 interacts with specific pathological aggregates

In this study we discovered that LSD1 co-localizes with hyperphosphorylated tau (pTau) aggregates in AD patients. This was surprising because few proteins have been shown histologically to interact with intracellular tau pathology. The standard nonbiased method for identifying interacting proteins is mass spectrometry on the detergent insoluble fragment from brain tissue homogenates. Since pTau and Aβ plaques are detergent insoluble, the proteins that have a strong interaction with these pathologies should then be detected by mass spectrometry. However, this method will not identify more "loosely" associated proteins that may not maintain their interaction after the neuron has been engulfed and the tau aggregates are free in extra cellular space. Mass spectrometry has been used to identify candidate proteins that are present in the insoluble fraction. However of these potential interactors, only one protein, U1-70K, was shown to colocalize with intracellular pTau[221]. Of course this failure to validate the mass spectrometry results could be due to the requirement of antibody detection, which varies based on the protein of interest. Nonetheless, it is clear that novel proteins that colocalize with pathological tau aggregates in AD are quite rare.

The observation that LSD1 colocalizes with pTau in AD suggests that the proteins are physically interacting. However, whether this interaction is direct or indirect remains to be determined. The observation that LSD1 colocalizes with pTau in the cytoplasm suggested to us that the nuclear pool of LSD1 could be depleted. There are multiple approaches that could aid in addressing this question. First, is the genetic approach where we modulated the

neurodegenerative phenotype in a tauopathy mouse model by altering the levels of LSD1. These experiments are described in Chapter 4, and further discussed below. Second, is a cell biological approach. In the tauopathy mouse model we observed LSD1 protein being sequestered in the cytoplasm, and in most cases completely depleted from the nucleus. LSD1 has two nuclear localization sequences that have been well characterized and function to transport LSD1 into the nucleus. Since LSD1 is synthesized in the cytoplasm by the ribosome and transported directly into the nucleus, it would rarely encounter tau, a cytoskeleton protein in axons. We believe that under normal conditions, LSD1 and tau do not interact. It is only when tau is aberrantly forming aggregates in the cell body that they have the opportunity to interact. Thus, this aberrant interaction only occurs in the neurons with tau pathology. However, when pathological tau is present in the cell body, the interactions between pathological tau and LSD1 masks the NLS. This prevents the importin complex from recognizing LSD1 and translocating it to the nucleus. As a result, the nuclear pool becomes depleted and essentially becomes like a *Lsd1* deletion neuron.

There are limitations to working *in vivo*, and an alternative approach for understanding the relationship between LSD1 and pTau is to explore their colocalization biochemically. The observation that LSD1 and pTau colocalize in human AD suggests these proteins physically interact, though whether this interaction is direct or indirect is completely unknown. Notably, LSD1 was not identified as one of the proteins enriched in the insoluble fraction of AD patient brain lysates in a recent study[221]. However, it is possible that the interaction between LSD1 and pTau is disrupted by detergent treatment and therefore prevents the detection of LSD1 in the insoluble fraction. Co-immunoprecipitation experiments from homogenates of AD patient brains or mouse models could provide insight into the nature of LSD1 and pTau colocalization.

However, if LSD1 only interacts with pTau intracellularly, then it may not be possible to detect the interaction. In addition, experiments of insoluble proteins are particularly difficult and there are many technical factors that could result in false negative results. To partially circumvent these issues, one experiment that we are planning is to determine the fraction of LSD1 that is present in the nuclear versus cytoplasmic fractions of AD cases. This will allow us to quantitatively determine how much of the LSD1 protein is inappropriately sequestered in the cytoplasm at different stages in the progression of the disease.

In addition to tissue homogenate from AD patients, we also have access to tissue that we can stain for LSD1. We previously showed that there is colocalization between LSD1 and pTau via standard wide-field microscopy. However, we can further investigate the colocalization via super resolution Structure Illumination Microscopy (SIM). SIM is a widefield technique in which a grid pattern is generated through interference diffraction orders and superimposed on the tissue while capturing images. The grid pattern is shifted or rotated between captures of the same image and then reconstructed into an image that has a lateral resolution of roughly 200nm, approximately twice that of diffraction-limited imagining[268]. SIM can be readily applied to samples that are prepared for conventional fluorescence microscopy. Therefore, with only a few optimization steps we can use similar staining protocols that have been used in the lab previously. Employing SIM may allow us to better determine the spatial relationship between LSD1 and pTau.

Many questions remain regarding the interaction of LSD1 and pTau in AD. For example, what form of tau does LSD1 interact with? One of the ways to address this is to look at the colocalization of LSD1 in other tauopathies. Tauopathies differ is in the isoform of tau that the aggregates are composed of. In AD, aggregates are composed of both the 3R and 4R isoform[21].

However most tauopathies only contain one or the other. Therefore if LSD1 did have a specific isoform that it interacted with, we would not be able to detect that bias. The PS19 Tau mouse that we utilized for our *in vivo* studies harbors the P301S mutation that was identified from an FTD-Tau patient with a tau mutation in the 4R isoform. Since LSD1 colocalizes with pTau in these mice, it suggests that LSD1 interacts with at least the 4R isoform. We have received tissue from the Emory Brain Bank for FTD-tau patients with Pick's disease, Corticobasal degeneration (CBD), Progressive supranuclear palsy (PSP), and FTDP-17 with tau mutations. Aggregates in Pick's disease are composed of the 3R isoform, while aggregates from CBD and PSP are composed of the 4R isoform[21]. The isoform of tau in cases of FTDP-17 with tau mutations is patient dependent. This allows us to investigate a different combination of the tau isoform in aggregates. In addition, since these tauopathies have different brain region specificities, examining LSD1 in these different diseases may shed light on what brain region most effected.

Another piece of evidence that might suggest LSD1 is truly related to human dementia would be to examine extremely rare cases with neurofibrillary tangles but no dementia. Neurofibrillary tangles have a higher correlation with disease severity than Aβ plaques[32], suggesting they may play a more important role in the development of the disease. However, in extremely rare cases, neurofibrillary tangles have been observed in healthy elderly brains from patients without cognitive impairment[269]. If LSD1 mislocalization with pTau is part of the etiology of AD, then some of these rare cases might show an absence or reduction of LSD1 colocalization with pTau. This might provide further evidence that cognitive impairment only occurs when LSD1 is colocalized with pTau.

When considering the role of LSD1 in neurodegeneration, the majority of my focus has been on the interaction between LSD1 and pathological tau. However, as shown in Chapter 3,

LSD1 colocalizes with TDP-43 inclusions, and the RNA-seq data suggests that the deletion of *Lsd1* is sufficient to recapitulate the transcriptional observed in FTD-progranulin cases. In addition to FTD-tau, FTD can also be due to aggregates of Tar DNA binding protein 43 (TDP-43), FTD-TDP43[218]. Just as we are able to exacerbate the tauopathy phenotype by reducing LSD1 and rescue the neurodegeneration through over expression of LSD1, it may be possible to modulate the TDP-43 phenotype. Transgenic TDP-43 mice can develop cytoplasmic aggregates within neurons of the brain and the spinal cord. In these mice the onset of the paralysis and reduction in survival is much faster than in the PS19 Tau mice. Therefore, rather than exacerbating the phenotype, we will directly attempt to rescue it. For these experiments, we would like to test an alternative method for LSD1 overexpression. Rather than inject LSD1 directly into the hippocampus of adult mice, we would inject the LSD1 virus into pups via tail vain injection. This would allow for the virus to be expressed throughout the body, including spinal cord motor neurons. Of course we would need to control for any effects of LSD1 overexpression during development, as upregulation of LSD1 has been implicated in multiple forms of cancer[52]. Nonetheless, viral overexpression of LSD1 throughout the mouse may allow us to overcome the paralysis issue that we face when we only overexpressed LSD1 in the hippocampus of PS19 Tau mice. If overexpressing LSD1 in TDP-43 mice rescued or temporarily rescued the neurodegeneration phenotypes in TDP-43 mice, it would indicate that TDP-43 may also be functioning through the sequestration of LSD1. In this case, comparing the sequestration between the Tau P301S and TDP-43 mouse models may provide insight into the mechanism of the interaction based.

6.4 Reduction of LSD1 specifically exacerbates the tauopathy disease pathway

Based on the ability of pathological tau to deplete the nuclear pool of LSD1, we hypothesized that neuronal cell death may be due, at least partly, to LSD1 being sequestered by tau. In this case, reducing LSD1 levels should make it easier for tau to deplete LSD1 from the nucleus, resulting in a faster progression of neurodegeneration and/or a more severe neurodegenerative phenotype. Importantly, LSD1 is not haploinsufficient. Mice that are heterozygous for *Lsd1* (*Lsd1*$^{\Delta/+}$) have been used as controls for many different studies[166,239,240], and in our hands we do not observe any neurodegeneration or other neurological phenotypes in these mice (seizers, behavioral abnormalities etc.). In addition, we show that *Lsd1*$^{\Delta/+}$ mice have wildtype lifespan, no deficit in rotarod or grid performance, and normal neuronal cell counts. Most importantly, LSD1 heterozygosity alone induces only 4 significant gene expression changes. This suggests that any effects observed in PS19 Tau mice with reduced *Lsd1* (PS19;*Lsd1*$^{\Delta/+}$) are not simply due to LSD1 haploinsufficiency.

PS19 Tau mice with wildtype levels of LSD1 develop paralysis and neurodegeneration, along with reduced survival. When we reduce LSD1 in the PS19 Tau mice, PS19;*Lsd1*$^{\Delta/+}$ mice die significantly earlier, most likely due to the increased rate of paralysis. Additionally, PS19;*Lsd1*$^{\Delta/+}$ mice have increased neuronal cell death and clearance in the hippocampus. This suggests that pathological tau functions through LSD1 to cause neurodegeneration *in vivo* in mice. Importantly, the exacerbation of the PS19 Tau mouse neurodegenerative phenotype does not occur until after pathological human tau is present. This suggests that, although PS19 Tau mice have reduced LSD1 from birth, the effect of *Lsd1* heterozygosity requires the presence of pathological tau, placing LSD1 downstream of tau. Consistent with LSD1 being downstream of

pathological tau, we find no evidence that *Lsd1* heterozygosity affects the expression of the tau transgene, or the buildup of pathological tau in PS19 Tau mice.

In addition to exacerbating the PS19 Tau phenotype, we show that the functional interaction between pathological tau and reduced LSD1 is specific. Pathway analysis from the transcriptional changes in the hippocampus of PS19;*Lsd1*$^{\Delta/+}$ and PS19 Tau mice show that the same pathways are affected. This suggests that LSD1 enhances the tauopathy pathway rather than inducing any new neurodegenerative mechanisms. Additionally, the genome-wide expression changes induced by pathological tau are specifically exacerbated in the PS19;*Lsd1*$^{\Delta/+}$ mice. This suggests that the functional interaction that we observe between pathological tau and reduced LSD1 is occurring through the tau pathway. This analysis was performed at the time of the earliest signs of neuronal distress, allowing us to assess molecular changes prior to cell death and clearance. Therefore, the expression changes in the PS19 Tau and PS19;*Lsd1*$^{\Delta/+}$ may only be a small subset of those observed in the *Lsd1* deletion mouse or in AD cases, which were taken after large levels of cell death. It could, however, be interesting to do a few other comparisons. First, it would be interesting to see if there are transcriptional changes in the hippocampus of *Lsd1* deletion mice at an earlier stage, such as 3-4 weeks post tamoxifen injection. This was at a time when there were learning and memory defects observed, but not yet paralysis, which could be more similar to the nine month time point of PS19 Tau and PS19;*Lsd1*$^{\Delta/+}$ mice. Additionally, performing RNA-seq on PS19 Tau and PS19;*Lsd1*$^{\Delta/+}$ mice at one year, a more terminal stage, would be interesting to compare to the human AD dataset and the *Lsd1* deletion mice. Based on our model, we would expect that at a more terminal stage, the PS19;*Lsd1*$^{\Delta/+}$ mice, which have a much more severe form of neurodegeneration than PS19 Tau mice, would have gene expression changes that are highly similar to AD cases.

Together these data argue that there is a specific, functional interaction between LSD1 and pathological tau in the mouse model of tauopathy. Nevertheless, there are two additional questions that remain. The first is whether Aβ plaques also function through the tau LSD1 pathway. There are a number of papers that have provided evidence that Aβ plaques can induce the formation of pathological tau[229]. If Aβ plaques primarily work by inducing tau pathology, we would expect that modulating LSD1 would be able to alter neurodegeneration in the Aβ mouse model. One way to address this would be to introduce the same paradigm into mice with the transgene containing mutations associated with familial Alzheimer's disease[270] (3xTg- APP Swedish mutation, and PSEN1 M146V, and the tau mutation). A second remaining question involves an additional observation that did not follow up on. At the transcriptional level, *Lsd1* heterozygosity results in a reduction of roughly 30% and a similar 35% reduction of LSD1 protein. PS19 Tau mice have wildtype levels of *Lsd1* transcripts, but a 20% increase in LSD1 protein compared to wildtype. *Lsd1* heterozygosity in the PS19 Tau mice results in the same 30% decrease relative to the PS19 Tau level, such that there is only 14% decrease in PS19;$Lsd1^{\Delta/+}$ mice compared to wildtype. There are many potential explanations for this observation. The most basic explanation is that we only tested three mice, and this is part of the natural variation caused by analyzing bulk brain tissue. Alternatively, the explanation could be related to the sequestration of the protein in the cytoplasm. Perhaps as LSD1 is being sequestered by pathological tau, the protein is not turning over as quickly. Based on the many weeks required for LSD1 deletion to result in a complete loss of the protein, we know that the turn-over rate of LSD1 is very slow in neurons. Perhaps as LSD1 is being sequestered in the cytoplasm by pathological tau, it is not able to be degraded at the normal rate. To test this hypothesis, we could perform a pulse-chase experiment to determine the rate of protein turnover. This could be done

in a cell culture model of tau aggregation using cells that are heterozygous for *Lsd1*. However, setting up a neuronal culture model is not trivial, and the turnover rate of proteins in culture may not reflect *in vivo*. Alternatively, this could be done *in vivo* by feeding the mice isotopically labeled diets, but again these experiments are technically challenging.

6.5 Intervention via LSD1 overexpression or disruption the LSD1-tau interaction

Our model states that LSD1 is functionally inhibited due to tau aggregates sequestering LSD1 in the cytoplasm and depleting the nuclear pool where it is required. Reducing the levels of LSD1 in the tauopathy mouse exacerbated the neurodegenerative phenotype. Based on our previous data, our model makes a direct prediction: if tau is predominantly functioning through LSD1, then increasing the levels of LSD1 should rescue the tau-induced neurodegenerative phenotype. To address this, we overexpressed LSD1 in the hippocampal neurons of PS19 Tau mice. We determined that the virally expressed LSD1, which was fused with an HA tag, is only expressed in neurons and localizes to the nucleus. Overexpression of LSD1 specifically in hippocampal neurons rescues the neuronal cell death and limits the inflammatory response. This rescue is neuronal specific, suggesting that the functional interaction between LSD1 and tau is occurring in neurons. In addition, this rescue occurs despite there being no effect on tau aggregation. The ability of LSD1 overexpression to overcome tau-mediated neurodegeneration in the presence of pathological tau aggregates, provides further evidence that pathological tau is functioning through the inhibition of LSD1. Based on this evidence it may be possible to therapeutically intervene in tauopathies, such as AD, after symptoms have started by modulating the LSD1 pathway.

Another important prediction from our model is that the virally overexpressed LSD1 does not prevent it, or the endogenous LSD1, from being sequestered. Thus, although overexpressing LSD1 should make it more difficult for pathological tau to sequester all of the LSD1 protein, allowing some LSD1 to be transported to the nucleus over a longer period of time, we would not expect it to permanently rescue. Consistent with this, LSD1 overexpression temporarily rescues neurons, delaying the effect of pathological tau rather than permanently rescuing. At 11 months, there is no decrease in the number of neurons in the CA1, however in 60% of the mice, the surviving neurons have abnormal morphology, and the overexpressed version of LSD1 is also sequestered. Our observation that neurons fail to maintain their morphology when the overexpressed LSD1 begins to be sequestered in the cytoplasm provides further support for the model that tau mediates neurodegeneration through the sequestration of LSD1. When considering intervention for human patients, it is possible that simply overexpressing LSD1 will be enough to delay the onset of AD for years. Nevertheless, to permanently overcome pathological tau it will likely be necessary to permanently disrupt the interaction between pathological tau and LSD1.

In considering the mechanism of the interaction between tau and LSD1, we hypothesized that the N-terminal disordered domain of LSD1 could be interacting with the disordered tau protein. Tau has previously been shown to interact with the RNA binding protein, U170K, through the disordered region of each protein[254]. Similarly, LSD1 has a 172 amino acid unstructured domain at the N-terminus of the otherwise fully structured protein. This domain has no known function, and all *in vitro* studies of LSD1 have been done without the domain present. However, the N-terminal disordered domain does contain the nuclear localization sequence (NLS). This sequence is required for import into the nucleus through the nuclear pore. We

predicted that tau associates with LSD1's N-terminal disordered domain, blocking LSD1's NLS and inhibiting interaction with importin proteins. If this is the case, then removal of LSD1's disordered domain would prevent sequestration by tau, resulting in persistent nuclear localization despite the presence of tau pathology. To do this, we injected PS19 Tau mice with an N-terminally truncated LSD1 virus (LSD1ΔN), with the NLS and an HA-tag added. With the LSD1ΔN virus, we observed improved persistence in the nuclear localization compared to the full length LSD1exogenous protein. This persistence lasted as late as one year of age (4 months post viral injection). At this time point almost all mice injected with full length LSD1 show sequestration of the exogenous protein. These preliminary data argue that removal of LSD1's N-terminal disordered domain aids in the proper localization of LSD1 in the presence of tau aggregates. These data also strongly support the claim that the N-terminal domain for LSD1 could be required for the interaction between LSD1 and tau. However there is ongoing work in order to be able to fully argue this. For example, we demonstrated that overexpression of LSD1ΔN eliminates the degenerating population consistently seen in age-matched samples of PS19- HA animals at 11-months. This suggests that LSD1ΔN effectively rescues at this time point. However, we do not currently have evidence that overexpressed LSD1ΔN rescues cell death longer than full length (past 12 months), because these experiments are currently ongoing and dependent on the timing of spinal cord paralysis. What we have consistently observed is that the abnormal blebbing phenotype that was seen in the full length LSD1 virus is not present in the LSD1ΔN injected mice. If the blebbing morphology is a sign of cellular distress or prolonged cell death, the relative lack of blebbing may indicate an improved rescue by overexpression of truncated LSD1, but this remains to be further investigated. Regardless, the preliminary evidence indicates that the N-terminal disordered domain is responsible for the interaction with

pathological tau. To test this directly, we are creating a construct in which the NLS is moved to the C-terminus of LSD1. If the NLS is being blocked by the association of LSD1's disordered domain with aggregates of tau, then we would expect this modified version of LSD1 to continue to localize to the nucleus even in the presence of tau aggregates. Additionally, biochemical analysis could support this hypothesis. Determining the physical interaction between these proteins is an important missing piece to this mechanism. However it can be technically challenging. In section 6.2, I have described approaches to circumvent these challenges. Another way to investigate if the N-terminal domain of LSD1 is required for interaction with tau would be to assess the ability of AD brain homogenate to induce the aggregation of LSD1 truncation constructs. To address this, we could isolate the tau-containing sarkosyl-insoluble fraction from AD brain samples and add it to mice containing tagged versions of truncated LSD1 constructs.

The N-terminal disordered domain of LSD1 is a promising therapeutic target for tauopathies such as AD. However there is a concern that the disordered domain may have at least a minor function *in vivo*. There are two ways to target the LSD1 pathway in tauopathies without interfering with the endogenous LSD1 protein. The first would be to use a peptide of the disorder domain. If the disordered domain is responsible for interacting with tau, it is possible that the N-terminal domain peptide would "coat" the interacting epitope of pathological tau. This might block the full length protein from interacting with pathological tau and allow it to enter the nucleus. However, the amount of N-terminal peptide would most likely need to be relatively high. This is also making the assumption that the N-terminal domain truly "sticks" to tau and would remain there to block the full length protein from being sequestered.

The second approach would be to bypass the interaction between LSD1 and tau by targeting the downstream transcriptional changes. To do this, we are carrying out a chemical

screen of LSD1 agonists in *C.elegans*. In *C. elegans*, *Lsd1* and *Met-2*, a H3K9 methyltransferase, act synergistically to silence germline transcription during the transition from gamete to zygote. Previously, our lab demonstrated that loss of the *Lsd1* pathway in an *Lsd1;Met-2* double mutant results in a developmental delay and ultimately complete sterility due to a failure to repress transcription of germline genes in somatic lineages. To identify agonists of the *Lsd1* pathway, our lab is utilizing a high-throughput *C. elegans* drug screen to identify compounds that reverse the developmental delay and sterility of *Lsd1;Met2* mutants. This work has already started in the lab in collaboration with the Emory Chemical Biology Discovery Center. We have selected an initial 5,000 compounds to carry out a pilot screen, and could eventually screen a whole chemical library of ~100,000 compounds. In addition, we have identified some candidate compounds based on genes that suppress the *Lsd1;Met2* phenotypes via RNA interference. Successful drugs are expected to antagonize the loss of *Lsd1* by elevating expression of *Lsd2*, a conserved homologue of *Lsd1*, or by reverting chromatin structure through inhibition of an aberrant chromatin activator. Although our research efforts are underway to understand how LSD1 localizes to pathological tau aggregates and how LSD1 functions mechanistically to prevent neurodegeneration, this drug screening approach allows us to circumvent that. The results from this screen will also provide insight into the mechanism of LSD1 function and will guide our future research. Thus, with this drug screen we will be able to simultaneous search for a therapeutic target while continuing to investigate the cellular mechanism of tau-mediated neurodegeneration.

6.6 Investigating the function of the N-terminal domain of LSD1 *in vivo*

We propose that the disordered domain of LSD1 is necessary for its interaction with pathological tau. Injection of a truncated version of the LSD1 protein allows us to specifically interrogate whether the disordered domain is required for mislocalization to pathological tau. In addition it could potentially shed light on the function of this domain by determining if there is a better rescue of the hippocampal neurons compared to full length. However the analysis is dependent on the timing of paralysis, which is not being altered in this experiment. Therefore, to determine the function of the N-terminal disordered domain in tau-mediated neurodegeneration, we truncated the N-terminal of *Lsd1* at the endogenous locus and crossed this allele into the PS19 Tau mouse background. We predicted that the truncated protein will no longer be sequestered by pathological tau, allowing LSD1ΔN to enter the nucleus unencumbered. Because *Lsd1* heterozygous mice are phenotypically wildtype, we predicted that one copy of *Lsd1ΔN* would be sufficient to maintain the nuclear pool of LSD1, despite tau-mediated sequestration of the full-length copy. Other than containing the nuclear localization sequence (NLS), the function of the N-terminal domain is unknown. LSD1 is evolutionarily conserved from from *S.pombe* to mammals, but the N-terminal disordered domain is only present in *Drosophila* and mammals. Additionally, all *in vitro* studies of LSD1 have been performed using an N-terminally truncated clone. Nevertheless, the function of the N-terminal disordered domain had never been tested *in vivo* in mice.

Within our mouse colony, initially we observed that the majority of PS19;$Lsd1^{\Delta N/+}$ mice have paralysis. The presence of this phenotype could be interpreted in a number of ways. First it is important to note that the $Lsd1^{\Delta N/+}$ is not the same construct as the LSD1ΔN virus. They differ in the amount of the LSD1 protein that is deleted. In the mouse, we have only deleted exon 1 of *Lsd1*. Therefore $Lsd1^{\Delta N/+}$ mice maintain all the intragenic regulatory elements after exon 1, and

all of exon 2 which contains a small portion of the disordered domain (21 amino acids). Therefore the first interpretation of the paralysis in PS19;*Lsd1*$^{\Delta N/+}$ mice could be that the exclusive deletion of exon 1 left enough of the disordered domain remaining to allow for sequestration by tau. Previously, it was shown that pathological tau interacts with the splicing protein U170K. U170K has two disordered regions, but only one of those specific regions is required[254]. The N-terminally disordered region of LSD1 is roughly 20% of the protein, and similar to U170K, this region can be divided into two somewhat distinct disordered sections. One potential interpretation of the difference between our viral result and our *in vivo* results, is that LSD1 does not require the entire disordered region to interact with pathological tau. Instead, only a section may be sufficient for the interaction with pathological tau. There are both *in vitro* and *in vivo* methods for addressing this. First is through the biochemical assays utilizing injections of the tau-containing sarkosyl-insoluble fraction from AD brain samples into mice (described in the previous section). Second is by distinguishing between the full length and the N-terminally truncated version of LSD1 *in vivo*. We can utilize two-different antibodies for LSD1; one of them targets the N-terminus while the other targets the C-terminus. We have tested these antibodies via western blot and validated that the N-terminal targeting antibody does not recognize an LSD1 construct with the N-terminus removed. This will allow us to monitor full length LSD1 protein versus N-terminally truncated LSD1 protein. If the N-terminal deletion enables LSD1 to properly localize to the nucleus, even in the presence of tau aggregates, we would expect the following. The C-terminus antibody, which recognizes both the full length and N-terminally truncated LSD1 protein, would show both nuclear and cytoplasmic staining, while the N-terminus antibody, which recognizes only the full length LSD1 protein, would be confined to the cytoplasm because of the sequestration by pathological tau.

The alternative interpretation of the preliminary data from our mouse colony is that the N-terminal disordered domain, specifically the sequence encoded by exon 1, is required for LSD1 functionality *in vivo*. If exon 1 is required for the entire function of LSD1, we would expect that the PS19;*Lsd1*$^{\Delta N/+}$ mice would have the same phenotype as the PS19;*Lsd1*$^{\Delta/+}$ mice, because the *Lsd1*$^{\Delta N}$ allele would be equivalent to the null allele. Additionally, if mice were homozygous for the *Lsd1*$^{\Delta N}$ allele they would be embryonic lethal. To determine whether this is the case, we have performed crosses to generate the *Lsd1*$^{\Delta N/\Delta N}$ mice. At this time we are genotyping these litters to determine if there are *Lsd1*$^{\Delta N/\Delta N}$ mice. We have not determined if there are *Lsd1*$^{\Delta N/\Delta N}$ mice yet. However, based on the large litter sizes (up to 9-11 pups in some litters) and very little perinatal lethality, we hypothesize that the *Lsd1*$^{\Delta N/\Delta N}$ mice are viable. Nevertheless, this work is ongoing, so it remains an open question. For example, even if the *Lsd1*$^{\Delta N/\Delta N}$ mice are viable, these mice could have cognitive or behavioral deficits in adulthood. This has been observed in other epigenetic regulatory enzymes and in mice that have a maternal loss of LSD1[163].

Currently, we do have data on the heterozygous removal of the N-terminal domain in the tau background. Our preliminary results indicate that PS19;*Lsd1*$^{\Delta N/+}$ mice, with the heterozygous removal of the N-terminal domain in the tau background, may be bimodally distributed. This bimodal distribution is formed by most of the mice undergoing neurodegeneration and having reduced survival, while a few remain phenotypically wildtype past 400 days old. Overall, PS19;*Lsd1*$^{\Delta N/+}$ mice show an intermediate survival phenotype that is reduced compared to PS19 Tau mice, but not as severe as PS19 Tau mice that are heterozygous for the *Lsd1* deletion. This suggests that the *Lsd1*$^{\Delta N}$ protein retains partial functionality *in vivo.* This result is consistent with the observation that the *Lsd1ΔN* viral expression constructs eliminates the most severe loss of

hippocampal neurons observed in PS19 Tau mice, but perhaps does not rescue quite as well as full length LSD1. In this case the possibility that a hypomorphic allele can rescue at all may only be due to the viral overexpression, which is 6-fold higher than the endogenous expression level. This abundance of partially functioning LSD1 could be compensatory, facilitating the elimination of the degenerating population we observed in the PS19 Tau mice. Conversely, when the hypomorphic allele is expressed at endogenous levels in the mouse model, we can observe the consequences of its functional shortcomings in the form of paralysis and shortened survival. We do not yet know what effect on neuronal survival is in the brains of PS19;*Lsd1*$^{\Delta N/+}$ mice, however the paralysis suggests that there is cell death or dysfunction in spinal cord motor neurons. Combined with our evidence that truncated LSD1 is impervious to sequestration by tau, the argument that *Lsd1ΔN* is a hypomorphic allele potentially further explains the bimodal pattern of paralysis observed in the PS19;*Lsd1*$^{\Delta N/+}$ mice. This is because the neuronal cell death and paralysis would be explained by a combination of 1) the amount of LSD1ΔN versus full length LSD1 any cell is producing, 2) the tau burden in that animal, and 3) how the loss of the N-terminal disordered domain ultimately affects LSD1 function.

As an epigenetic enzyme with a wide array of target loci, it is possible that LSD1's disordered domain is necessary for binding to certain targets or interacting partners. If removal of the N-terminal disordered domain *in vivo* precludes LSD1 from demethylating a few specific targets, it is possible that moving forward we will continue to observe a bimodal distribution of mice that die early of paralysis, and mice that appear phenotypically normal. If this is the case, we might anticipate that homozygosity of the N-terminal deletion in the tau background (PS19; *Lsd1*$^{\Delta N/\Delta N}$) would exacerbate this bimodal distribution. In the affected animals, neurons would accumulate transcription-coupled H3K4me2 on the loci where truncated LSD1 cannot

demethylate. This would lead to inappropriate transcription of those loci, as well as further accumulation of active H3K4 methylation. This would result in disruption of the cell's transcriptional program, leading to dysfunction or death. However, the stoichasticity of this affect would mean that sometimes mice would be able to bypass this detrimental effect. When this happens, it is possible that PS19; *Lsd1*$^{\Delta N/+}$ will show an improved phenotype compared to PS19 Tau mice because N-terminal truncated LSD1 would avoid sequestration and increase nuclear levels of LSD1. Despite the partial loss of function from the *Lsd1*$^{\Delta N}$ allele, persistent nuclear localization could allow for LSD1 to demethylate targets most crucial to cell survival, creating improved paralysis and survival phenotypes. If this is the case, we expect that it might be exaggerated in PS19; *Lsd1*$^{\Delta N/\Delta N}$ mice. Because of the ongoing nature of these experiments, our preliminary data from the PS19;*Lsd1*$^{\Delta N/+}$ colony only allow for speculation at this time. Nevertheless, the existence of multiple PS19;*Lsd1*$^{\Delta N/+}$ mice with no phenotype even after 400 days raises the exciting possibility that removal of LSD1's N-terminal disordered domain may be sufficient to allow some mice to be completely impervious to tau mediated neurodegeneration. If this is the case, it would represent a big step for therapeutic intervention in tauopathies such as AD.

6.7 Conclusions

Through my research, I have investigated the role of LSD1 in neurodegenerative disease and implicated LSD1 in the downstream mechanism of tau and TDP-43 mediated neurodegeneration. I have shown that LSD1 localizes inappropriately to tau and TDP-43 pathology in human dementia cases, and is sequestered away from the nucleus in the PS19 tauopathy mouse model. Loss of LSD1 in adult mice recapitulates many aspect of Alzheimer's

disease, including widespread neurodegeneration in the brain, learning and memory deficits, and global gene expression changes that highly correlated with AD cases. I have shown that the interaction between LSD1 and pathological tau is function *in vivo* by modulating the tauopathy phenotype in two ways: (1) reduction of LSD1 in PS19 Tau mice is sufficient to highly exacerbate the neurodegenerative phenotype and (2) overexpression of LSD1 in PS19 Tau mice, even after tau aggregates, blocks tau-mediated neurodegeneration. Together these data led to the following model: in healthy hippocampal and cortical neurons, LSD1 is translated in the cytoplasm and transported into the nucleus where it is continuously required to repress inappropriate transcription throughout the genome. In tau and TDP-43 mediated neurodegeneration, pathological forms of these proteins accumulate, sequestering LSD1 in the cytoplasm. This interferes with the continuous requirement for LSD1, resulting in neuronal cell death. Thus our work identifies a new epigenetic step in the AD and FTD pathways, and shows that manipulating this step can block the progression of neurodegeneration, even after pathological aggregates have formed.

We have elucidated a novel role for LSD1 in neurodegenerative disease, but perhaps the most interesting question is still unanswered; Why is an epigenetic regulator of cell fate required in terminally differentiate neuron? During development, LSD1 is required to remove H3K4 methylation at enhancers, which acts as a transcriptional memory. This is necessary for a cell to "forget" the transcriptional program from its previous state and move into the new transcriptional program of its differentiate state. If this is the role of LSD1 and H3K4me/me2, what is its requirement in cells that are no longer changing their transcriptional program into a new differentiated state? This will be an important ongoing investigation within the lab. However, the work presented here hints that the cell fate of neurons is not terminally differentiated. Deletion of

Lsd1 leads to ectopic expression of stem cell genes in differentiated adult neurons. Neurons appear to be the most sensitive to loss of LSD1, but it is unclear why. It is possible they are a more vulnerable cellular population due to their complex regulation and plasticity. Nonetheless, this observation suggests that the commonly held view of terminal differentiation may not quite be complete. Instead, there may be some capacity for expression of genes associated with the undifferentiated state to re-express. Enzymes such as LSD1 may be continually employed to prevent this from happening. This should continue to be investigated, and could lead to new breakthroughs in not only in the interaction between epigenetic regulation and neuron function, but also in treatments for tau-mediated neurodegeneration. This work has revealed an important and novel role for LSD1, and I hope to look back on this thesis work and appreciate that it made a major contribution to improving the lives of people with dementia.

REFERENCES

1 2019 Alzheimer's disease facts and figures. *Alzheimer's & Dementia* **15**, 321-387, doi:https://doi.org/10.1016/j.jalz.2019.01.010 (2019).

2 Orr, M. E., Sullivan, A. C. & Frost, B. A Brief Overview of Tauopathy: Causes, Consequences, and Therapeutic Strategies. *Trends in pharmacological sciences* **38**, 637-648, doi:10.1016/j.tips.2017.03.011 (2017).

3 Wang, Y. & Mandelkow, E. Tau in physiology and pathology. *Nat Rev Neurosci* **17**, 5-21, doi:10.1038/nrn.2015.1 (2016).

4 Holtzman, D. M. *et al.* Tau: From research to clinical development. *Alzheimers Dement* **12**, 1033-1039, doi:10.1016/j.jalz.2016.03.018 (2016).

5 Goedert, M., Wischik, C. M., Crowther, R. A., Walker, J. E. & Klug, A. Cloning and sequencing of the cDNA encoding a core protein of the paired helical filament of Alzheimer disease: identification as the microtubule-associated protein tau. *Proc Natl Acad Sci U S A* **85**, 4051-4055, doi:10.1073/pnas.85.11.4051 (1988).

6 Weingarten, M. D., Lockwood, A. H., Hwo, S. Y. & Kirschner, M. W. A protein factor essential for microtubule assembly. *Proceedings of the National Academy of Sciences of the United States of America* **72**, 1858-1862, doi:10.1073/pnas.72.5.1858 (1975).

7 Niblock, M. & Gallo, J. M. Tau alternative splicing in familial and sporadic tauopathies. *Biochem Soc Trans* **40**, 677-680, doi:10.1042/bst20120091 (2012).

8 Qian, W. & Liu, F. Regulation of alternative splicing of tau exon 10. *Neurosci Bull* **30**, 367-377, doi:10.1007/s12264-013-1411-2 (2014).

9 Ballatore, C., Lee, V. M. & Trojanowski, J. Q. Tau-mediated neurodegeneration in Alzheimer's disease and related disorders. *Nat Rev Neurosci* **8**, 663-672, doi:10.1038/nrn2194 (2007).

10 Morris, M., Maeda, S., Vossel, K. & Mucke, L. The many faces of tau. *Neuron* **70**, 410-426, doi:10.1016/j.neuron.2011.04.009 (2011).

11 Cheng, Y. & Bai, F. The Association of Tau With Mitochondrial Dysfunction in Alzheimer's Disease. *Frontiers in neuroscience* **12**, 163-163, doi:10.3389/fnins.2018.00163 (2018).

12 Sealey, M. A. *et al.* Distinct phenotypes of three-repeat and four-repeat human tau in a transgenic model of tauopathy. *Neurobiology of Disease* **105**, 74-83, doi:https://doi.org/10.1016/j.nbd.2017.05.003 (2017).

13 Teng, J. *et al.* Synergistic effects of MAP2 and MAP1B knockout in neuronal migration, dendritic outgrowth, and microtubule organization. *The Journal of cell biology* **155**, 65-76, doi:10.1083/jcb.200106025 (2001).

14 Hefti, M. M. *et al.* Tau Phosphorylation and Aggregation in the Developing Human Brain. *J Neuropathol Exp Neurol* **78**, 930-938, doi:10.1093/jnen/nlz073 (2019).

15 Barbier, P. *et al.* Role of Tau as a Microtubule-Associated Protein: Structural and Functional Aspects. *Frontiers in aging neuroscience* **11**, 204-204, doi:10.3389/fnagi.2019.00204 (2019).

16 Ando, K. *et al.* Stabilization of Microtubule-Unbound Tau via Tau Phosphorylation at Ser262/356 by Par-1/MARK Contributes to Augmentation of AD-Related Phosphorylation and Abeta42-Induced Tau Toxicity. *PLoS Genet* **12**, e1005917, doi:10.1371/journal.pgen.1005917 (2016).

17 Iqbal, K., Liu, F., Gong, C. X. & Grundke-Iqbal, I. Tau in Alzheimer disease and related tauopathies. *Current Alzheimer research* **7**, 656-664, doi:10.2174/156720510793611592 (2010).

18 Arendt, T., Stieler, J. T. & Holzer, M. Tau and tauopathies. *Brain Research Bulletin* **126**, 238-292, doi:https://doi.org/10.1016/j.brainresbull.2016.08.018 (2016).

19 Cheng-Xin, G., Grundke-Iqbal, I. & Iqbal, K. Targeting Tau Protein in Alzheimer's Disease. *Drugs & Aging* **27**, 351 (2010).

20 Bozeat, S., Gregory, C. A., Ralph, M. A. L. & Hodges, J. R. Which neuropsychiatric and behavioural features distinguish frontal and temporal variants of frontotemporal dementia from Alzheimer's disease? *Journal of Neurology, Neurosurgery & Psychiatry* **69**, 178-186, doi:10.1136/jnnp.69.2.178 (2000).

21 Boxer, A. L. *et al.* Frontotemporal degeneration, the next therapeutic frontier: molecules and animal models for frontotemporal degeneration drug development. *Alzheimers Dement* **9**, 176-188, doi:10.1016/j.jalz.2012.03.002 (2013).

22 Harciarek, M. & Jodzio, K. Neuropsychological differences between frontotemporal dementia and Alzheimer's disease: a review. *Neuropsychol Rev* **15**, 131-145, doi:10.1007/s11065-005-7093-4 (2005).

23 Mohandas, E. & Rajmohan, V. Frontotemporal dementia: An updated overview. *Indian journal of psychiatry* **51 Suppl 1**, S65-S69 (2009).

24 Gibbons, G. S. *et al.* Detection of Alzheimer Disease (AD)-Specific Tau Pathology in AD and NonAD Tauopathies by Immunohistochemistry With Novel Conformation-Selective Tau Antibodies. *Journal of neuropathology and experimental neurology* **77**, 216-228, doi:10.1093/jnen/nly010 (2018).

25 Arakhamia, T. *et al.* Posttranslational Modifications Mediate the Structural Diversity of Tauopathy Strains. *Cell* **180**, 633-644.e612, doi:https://doi.org/10.1016/j.cell.2020.01.027 (2020).

26 Kahlson, M. A. & Colodner, K. J. Glial Tau Pathology in Tauopathies: Functional Consequences. *Journal of experimental neuroscience* **9**, 43-50, doi:10.4137/JEN.S25515 (2016).

27 Strang, K. H., Golde, T. E. & Giasson, B. I. MAPT mutations, tauopathy, and mechanisms of neurodegeneration. *Laboratory Investigation* **99**, 912-928, doi:10.1038/s41374-019-0197-x (2019).

28 Duyckaerts, C., Delatour, B. & Potier, M.-C. Classification and basic pathology of Alzheimer disease. *Acta Neuropathologica* **118**, 5-36, doi:10.1007/s00401-009-0532-1 (2009).

29 Karran, E., Mercken, M. & Strooper, B. D. The amyloid cascade hypothesis for Alzheimer's disease: an appraisal for the development of therapeutics. *Nat Rev Drug Discov* **10**, 698-712 (2011).

30 Tanzi, R. E. The genetics of Alzheimer disease. *Cold Spring Harbor perspectives in medicine* **2**, a006296, doi:10.1101/cshperspect.a006296 (2012).

31 Ricciarelli, R. & Fedele, E. The Amyloid Cascade Hypothesis in Alzheimer's Disease: It's Time to Change Our Mind. *Current neuropharmacology* **15**, 926-935, doi:10.2174/1570159X15666170116143743 (2017).

32 Arriagada, P. V., Growdon, J. H., Hedley-Whyte, E. T. & Hyman, B. T. Neurofibrillary tangles but not senile plaques parallel duration and severity of Alzheimer's disease. *Neurology* **42**, 631-639, doi:10.1212/wnl.42.3.631 (1992).

33 Bloom, G. S. Amyloid-β and Tau: The Trigger and Bullet in Alzheimer Disease PathogenesisAmyloid-β and TauAmyloid-β and Tau. *JAMA Neurology* **71**, 505-508, doi:10.1001/jamaneurol.2013.5847 (2014).

34 Hardy, J. & Selkoe, D. J. The amyloid hypothesis of Alzheimer's disease: progress and problems on the road to therapeutics. *Science* **297**, 353-356, doi:10.1126/science.1072994 (2002).

35 Kung, H. F. The β-Amyloid Hypothesis in Alzheimer's Disease: Seeing Is Believing. *ACS Medicinal Chemistry Letters* **3**, 265-267, doi:10.1021/ml300058m (2012).

36 Morris, G. P., Clark, I. A. & Vissel, B. Inconsistencies and Controversies Surrounding the Amyloid Hypothesis of Alzheimer's Disease. *Acta Neuropathologica Communications* **2**, 135, doi:10.1186/s40478-014-0135-5 (2014).

37 Serrano-Pozo, A., Frosch, M. P., Masliah, E. & Hyman, B. T. Neuropathological alterations in Alzheimer disease. *Cold Spring Harbor perspectives in medicine* **1**, a006189-a006189, doi:10.1101/cshperspect.a006189 (2011).

38 Frost, B., Jacks, R. L. & Diamond, M. I. Propagation of tau misfolding from the outside to the inside of a cell. *J Biol Chem* **284**, 12845-12852, doi:10.1074/jbc.M808759200 (2009).

39 Guo, J. L. & Lee, V. M. Seeding of normal Tau by pathological Tau conformers drives pathogenesis of Alzheimer-like tangles. *J Biol Chem* **286**, 15317-15331, doi:10.1074/jbc.M110.209296 (2011).

40 Usenovic, M. *et al.* Internalized Tau Oligomers Cause Neurodegeneration by Inducing Accumulation of Pathogenic Tau in Human Neurons Derived from Induced Pluripotent Stem Cells. *J Neurosci* **35**, 14234-14250, doi:10.1523/jneurosci.1523-15.2015 (2015).

41 Boluda, S. *et al.* Differential induction and spread of tau pathology in young PS19 tau transgenic mice following intracerebral injections of pathological tau from Alzheimer's disease or corticobasal degeneration brains. *Acta Neuropathol* **129**, 221-237, doi:10.1007/s00401-014-1373-0 (2015).

42 Braak, H. & Braak, E. Frequency of Stages of Alzheimer-Related Lesions in Different Age Categories. *Neurobiology of Aging* **18**, 351-357, doi:https://doi.org/10.1016/S0197-4580(97)00056-0 (1997).

43 Braak, H. & Del Tredici, K. The pathological process underlying Alzheimer's disease in individuals under thirty. *Acta Neuropathol* **121**, 171-181, doi:10.1007/s00401-010-0789-4 (2011).

44 Braak, H., Thal, D. R., Ghebremedhin, E. & Del Tredici, K. Stages of the pathologic process in Alzheimer disease: age categories from 1 to 100 years. *J Neuropathol Exp Neurol* **70**, 960-969, doi:10.1097/NEN.0b013e318232a379 (2011).

45 Jankowsky, J. L. & Zheng, H. Practical considerations for choosing a mouse model of Alzheimer's disease. *Molecular neurodegeneration* **12**, 89-89, doi:10.1186/s13024-017-0231-7 (2017).

46 Hernández, F. *et al.* Differences in structure and function between human and murine tau. *Biochimica et Biophysica Acta (BBA) - Molecular Basis of Disease* **1865**, 2024-2030, doi:https://doi.org/10.1016/j.bbadis.2018.08.010 (2019).

47 Dujardin, S., Colin, M. & Buee, L. Invited review: Animal models of tauopathies and their implications for research/translation into the clinic. *Neuropathol Appl Neurobiol* **41**, 59-80, doi:10.1111/nan.12200 (2015).
48 Götz, J. *et al.* A Decade of Tau Transgenic Animal Models and Beyond. *Brain Pathology* **17**, 91-103, doi:10.1111/j.1750-3639.2007.00051.x (2007).
49 Yoshiyama, Y. *et al.* Synapse loss and microglial activation precede tangles in a P301S tauopathy mouse model. *Neuron* **53**, 337-351, doi:10.1016/j.neuron.2007.01.010 (2007).
50 Goodwin, L. O. *et al.* Large-scale discovery of mouse transgenic integration sites reveals frequent structural variation and insertional mutagenesis. *Genome Res* **29**, 494-505, doi:10.1101/gr.233866.117 (2019).
51 Sperfeld, A. D. *et al.* FTDP-17: an early-onset phenotype with parkinsonism and epileptic seizures caused by a novel mutation. *Ann Neurol* **46**, 708-715, doi:10.1002/1531-8249(199911)46:5<708::aid-ana5>3.0.co;2-k (1999).
52 Kozub, M. M., Carr, R. M., Lomberk, G. L. & Fernandez-Zapico, M. E. LSD1, a double-edged sword, confers dynamic chromatin regulation but commonly promotes aberrant cell growth. *F1000Research* **6**, 2016-2016, doi:10.12688/f1000research.12169.1 (2017).
53 To, T. K., Saze, H. & Kakutani, T. DNA Methylation within Transcribed Regions. *Plant physiology* **168**, 1219-1225, doi:10.1104/pp.15.00543 (2015).
54 Bird, A. P. CpG-rich islands and the function of DNA methylation. *Nature* **321**, 209-213, doi:10.1038/321209a0 (1986).
55 De Carvalho, D. D., You, J. S. & Jones, P. A. DNA methylation and cellular reprogramming. *Trends in cell biology* **20**, 609-617, doi:10.1016/j.tcb.2010.08.003 (2010).
56 Klose, R. J. & Bird, A. P. Genomic DNA methylation: the mark and its mediators. *Trends Biochem Sci* **31**, 89-97, doi:10.1016/j.tibs.2005.12.008 (2006).
57 Christopher, M. A., Kyle, S. M. & Katz, D. J. Neuroepigenetic mechanisms in disease. *Epigenetics Chromatin* **10**, 47, doi:10.1186/s13072-017-0150-4 (2017).
58 Sen, N. Epigenetic regulation of memory by acetylation and methylation of chromatin: implications in neurological disorders, aging, and addiction. *Neuromolecular Med* **17**, 97-110, doi:10.1007/s12017-014-8306-x (2015).
59 Torres-Berrío, A., Issler, O., Parise, E. M. & Nestler, E. J. Unraveling the epigenetic landscape of depression: focus on early life stress *Dialogues in clinical neuroscience* **21**, 341-357, doi:10.31887/DCNS.2019.21.4/enestler (2019).
60 Leonhardt, H., Page, A. W., Weier, H. U. & Bestor, T. H. A targeting sequence directs DNA methyltransferase to sites of DNA replication in mammalian nuclei. *Cell* **71**, 865-873, doi:10.1016/0092-8674(92)90561-p (1992).
61 Okano, M., Bell, D. W., Haber, D. A. & Li, E. DNA methyltransferases Dnmt3a and Dnmt3b are essential for de novo methylation and mammalian development. *Cell* **99**, 247-257, doi:10.1016/s0092-8674(00)81656-6 (1999).
62 Ito, S. *et al.* Tet proteins can convert 5-methylcytosine to 5-formylcytosine and 5-carboxylcytosine. *Science* **333**, 1300-1303, doi:10.1126/science.1210597 (2011).

63 Tahiliani, M. *et al.* Conversion of 5-methylcytosine to 5-hydroxymethylcytosine in mammalian DNA by MLL partner TET1. *Science* **324**, 930-935, doi:10.1126/science.1170116 (2009).

64 Cui, D. & Xu, X. DNA Methyltransferases, DNA Methylation, and Age-Associated Cognitive Function. *International journal of molecular sciences* **19**, 1315, doi:10.3390/ijms19051315 (2018).

65 Levenson, J. M. *et al.* Evidence that DNA (cytosine-5) methyltransferase regulates synaptic plasticity in the hippocampus. *J Biol Chem* **281**, 15763-15773, doi:10.1074/jbc.M511767200 (2006).

66 Luan, G. *et al. Adenosine Kinase Expression in Cortical Dysplasia With Balloon Cells: Analysis of Developmental Lineage of Cell Types*. Vol. 74 (2015).

67 Szulwach, K. E. *et al.* 5-hmC–mediated epigenetic dynamics during postnatal neurodevelopment and aging. *Nature Neuroscience* **14**, 1607-1616, doi:10.1038/nn.2959 (2011).

68 Guo, J. U., Su, Y., Zhong, C., Ming, G. L. & Song, H. Hydroxylation of 5-methylcytosine by TET1 promotes active DNA demethylation in the adult brain. *Cell* **145**, 423-434, doi:10.1016/j.cell.2011.03.022 (2011).

69 Pekny, M. & Nilsson, M. Astrocyte activation and reactive gliosis. *Glia* **50**, 427-434, doi:10.1002/glia.20207 (2005).

70 SanMiguel, J. M., Abramowitz, L. K. & Bartolomei, M. S. Imprinted gene dysregulation in a Tet1 null mouse model is stochastic and variable in the germline and offspring. *Development* **145**, doi:10.1242/dev.160622 (2018).

71 Berger, S. L. The complex language of chromatin regulation during transcription. *Nature* **447**, 407-412, doi:10.1038/nature05915 (2007).

72 Worcel, A., Han, S. & Wong, M. L. Assembly of newly replicated chromatin. *Cell* **15**, 969-977, doi:10.1016/0092-8674(78)90280-5 (1978).

73 Smith, S. & Stillman, B. Stepwise assembly of chromatin during DNA replication in vitro. *Embo j* **10**, 971-980 (1991).

74 Jenuwein, T. & Allis, C. D. Translating the histone code. *Science* **293**, 1074-1080, doi:10.1126/science.1063127 (2001).

75 Henikoff, S. & Smith, M. M. Histone variants and epigenetics. *Cold Spring Harb Perspect Biol* **7**, a019364, doi:10.1101/cshperspect.a019364 (2015).

76 Wang, Z. *et al.* Genome-wide mapping of HATs and HDACs reveals distinct functions in active and inactive genes. *Cell* **138**, 1019-1031, doi:10.1016/j.cell.2009.06.049 (2009).

77 Kouzarides, T. Chromatin modifications and their function. *Cell* **128**, 693-705, doi:10.1016/j.cell.2007.02.005 (2007).

78 Cote, J., Quinn, J., Workman, J. L. & Peterson, C. L. Stimulation of GAL4 derivative binding to nucleosomal DNA by the yeast SWI/SNF complex. *Science* **265**, 53-60, doi:10.1126/science.8016655 (1994).

79 Kwon, H., Imbalzano, A. N., Khavari, P. A., Kingston, R. E. & Green, M. R. Nucleosome disruption and enhancement of activator binding by a human SW1/SNF complex. *Nature* **370**, 477-481, doi:10.1038/370477a0 (1994).

80 Ausio, J., Dong, F. & van Holde, K. E. Use of selectively trypsinized nucleosome core particles to analyze the role of the histone "tails" in the stabilization of the nucleosome. *J Mol Biol* **206**, 451-463, doi:10.1016/0022-2836(89)90493-2 (1989).

81 Li, B., Carey, M. & Workman, J. L. The role of chromatin during transcription. *Cell* **128**, 707-719, doi:10.1016/j.cell.2007.01.015 (2007).

82 Lee, J. H. & Skalnik, D. G. CpG-binding protein (CXXC finger protein 1) is a component of the mammalian Set1 histone H3-Lys4 methyltransferase complex, the analogue of the yeast Set1/COMPASS complex. *J Biol Chem* **280**, 41725-41731, doi:10.1074/jbc.M508312200 (2005).

83 Dou, Y. *et al.* Physical association and coordinate function of the H3 K4 methyltransferase MLL1 and the H4 K16 acetyltransferase MOF. *Cell* **121**, 873-885, doi:10.1016/j.cell.2005.04.031 (2005).

84 Shi, Y. *et al.* Histone Demethylation Mediated by the Nuclear Amine Oxidase Homolog LSD1. *Cell* **119**, 941-953, doi:10.1016/j.cell.2004.12.012.

85 Greer, E. L. & Shi, Y. Histone methylation: a dynamic mark in health, disease and inheritance. *Nat Rev Genet* **13**, 343-357, doi:10.1038/nrg3173 (2012).

86 Seward, D. J. *et al.* Demethylation of trimethylated histone H3 Lys4 in vivo by JARID1 JmjC proteins. *Nat Struct Mol Biol* **14**, 240-242, doi:10.1038/nsmb1200 (2007).

87 Xiang, Y. *et al.* JARID1B is a histone H3 lysine 4 demethylase up-regulated in prostate cancer. *Proceedings of the National Academy of Sciences of the United States of America* **104**, 19226-19231, doi:10.1073/pnas.0700735104 (2007).

88 Cheng, J. *et al.* A role for H3K4 monomethylation in gene repression and partitioning of chromatin readers. *Molecular cell* **53**, 979-992, doi:10.1016/j.molcel.2014.02.032 (2014).

89 Tachibana, M. *et al.* G9a histone methyltransferase plays a dominant role in euchromatic histone H3 lysine 9 methylation and is essential for early embryogenesis. *Genes Dev* **16**, 1779-1791, doi:10.1101/gad.989402 (2002).

90 Schultz, D. C., Ayyanathan, K., Negorev, D., Maul, G. G. & Rauscher, F. J., 3rd. SETDB1: a novel KAP-1-associated histone H3, lysine 9-specific methyltransferase that contributes to HP1-mediated silencing of euchromatic genes by KRAB zinc-finger proteins. *Genes Dev* **16**, 919-932, doi:10.1101/gad.973302 (2002).

91 Lee, M. G. *et al.* Demethylation of H3K27 regulates polycomb recruitment and H2A ubiquitination. *Science* **318**, 447-450, doi:10.1126/science.1149042 (2007).

92 Xiang, Y. *et al.* JMJD3 is a histone H3K27 demethylase. *Cell Res* **17**, 850-857, doi:10.1038/cr.2007.83 (2007).

93 Rose, N. R. & Klose, R. J. Understanding the relationship between DNA methylation and histone lysine methylation. *Biochim Biophys Acta* **1839**, 1362-1372, doi:10.1016/j.bbagrm.2014.02.007 (2014).

94 Guan, J. S. *et al.* HDAC2 negatively regulates memory formation and synaptic plasticity. *Nature* **459**, 55-60, doi:10.1038/nature07925 (2009).

95 Morris, M. J., Mahgoub, M., Na, E. S., Pranav, H. & Monteggia, L. M. Loss of histone deacetylase 2 improves working memory and accelerates extinction learning. *J Neurosci* **33**, 6401-6411, doi:10.1523/JNEUROSCI.1001-12.2013 (2013).

96 Kim, M. S. *et al.* An essential role for histone deacetylase 4 in synaptic plasticity and memory formation. *J Neurosci* **32**, 10879-10886, doi:10.1523/JNEUROSCI.2089-12.2012 (2012).

97 Williams, S. R. *et al.* Haploinsufficiency of HDAC4 causes brachydactyly mental retardation syndrome, with brachydactyly type E, developmental delays, and behavioral problems. *Am J Hum Genet* **87**, 219-228, doi:10.1016/j.ajhg.2010.07.011 (2010).

98 Wang, J. *et al.* Opposing LSD1 complexes function in developmental gene activation and repression programmes. *Nature* **446**, 882-887, doi:10.1038/nature05671 (2007).

99 Maze, I., Noh, K.-M. & Allis, C. D. Histone regulation in the CNS: basic principles of epigenetic plasticity. *Neuropsychopharmacology : official publication of the American College of Neuropsychopharmacology* **38**, 3-22, doi:10.1038/npp.2012.124 (2013).

100 St Laurent, G., Wahlestedt, C. & Kapranov, P. The Landscape of long noncoding RNA classification. *Trends Genet* **31**, 239-251, doi:10.1016/j.tig.2015.03.007 (2015).

101 Hanly, D. J., Esteller, M. & Berdasco, M. Interplay between long non-coding RNAs and epigenetic machinery: emerging targets in cancer? *Philosophical transactions of the Royal Society of London. Series B, Biological sciences* **373**, 20170074, doi:10.1098/rstb.2017.0074 (2018).

102 Brockdorff, N. *et al.* The product of the mouse Xist gene is a 15 kb inactive X-specific transcript containing no conserved ORF and located in the nucleus. *Cell* **71**, 515-526, doi:10.1016/0092-8674(92)90519-i (1992).

103 Brown, C. J. *et al.* The human XIST gene: analysis of a 17 kb inactive X-specific RNA that contains conserved repeats and is highly localized within the nucleus. *Cell* **71**, 527-542, doi:10.1016/0092-8674(92)90520-m (1992).

104 Clemson, C. M., McNeil, J. A., Willard, H. F. & Lawrence, J. B. XIST RNA paints the inactive X chromosome at interphase: evidence for a novel RNA involved in nuclear/chromosome structure. *J Cell Biol* **132**, 259-275, doi:10.1083/jcb.132.3.259 (1996).

105 Tsai, M. C. *et al.* Long noncoding RNA as modular scaffold of histone modification complexes. *Science* **329**, 689-693, doi:10.1126/science.1192002 (2010).

106 Weick, E.-M. & Miska, E. A. piRNAs: from biogenesis to function. *Development* **141**, 3458-3471, doi:10.1242/dev.094037 (2014).

107 Pal, S. & Tyler, J. K. Epigenetics and aging. *Science advances* **2**, e1600584-e1600584, doi:10.1126/sciadv.1600584 (2016).

108 Gao, J. W. *et al.* DJ-1-Mediated protective effect of protocatechuic aldehyde against oxidative stress in SH-SY5Y cells. *J Pharmacol Sci* **115**, 36-44 (2011).

109 Fontan-Lozano, A. *et al.* Histone deacetylase inhibitors improve learning consolidation in young and in KA-induced-neurodegeneration and SAMP-8-mutant mice. *Mol Cell Neurosci* **39**, 193-201, doi:10.1016/j.mcn.2008.06.009 (2008).

110 Hargreaves, D. C., Horng, T. & Medzhitov, R. Control of inducible gene expression by signal-dependent transcriptional elongation. *Cell* **138**, 129-145, doi:10.1016/j.cell.2009.05.047 (2009).

111 Fischer, A., Sananbenesi, F., Mungenast, A. & Tsai, L. H. Targeting the correct HDAC(s) to treat cognitive disorders. *Trends Pharmacol Sci* **31**, 605-617, doi:10.1016/j.tips.2010.09.003 (2010).

112 Lu, T. *et al.* Gene regulation and DNA damage in the ageing human brain. *Nature* **429**, 883-891, doi:10.1038/nature02661 (2004).

113 Copray, S., Huynh, J. L., Sher, F., Casaccia-Bonnefil, P. & Boddeke, E. Epigenetic mechanisms facilitating oligodendrocyte development, maturation, and aging. *Glia* **57**, 1579-1587, doi:10.1002/glia.20881 (2009).

114 Unnikrishnan, A. *et al.* The role of DNA methylation in epigenetics of aging. *Pharmacol Ther* **195**, 172-185, doi:10.1016/j.pharmthera.2018.11.001 (2019).

115 Jones, M. J., Goodman, S. J. & Kobor, M. S. DNA methylation and healthy human aging. *Aging Cell* **14**, 924-932, doi:10.1111/acel.12349 (2015).

116 Horvath, S. & Raj, K. DNA methylation-based biomarkers and the epigenetic clock theory of ageing. *Nature Reviews Genetics* **19**, 371-384, doi:10.1038/s41576-018-0004-3 (2018).

117 Ciccarone, F. *et al.* Age-dependent expression of DNMT1 and DNMT3B in PBMCs from a large European population enrolled in the MARK-AGE study. *Aging cell* **15**, 755-765, doi:10.1111/acel.12485 (2016).

118 Liu, L. *et al.* Insufficient DNA methylation affects healthy aging and promotes age-related health problems. *Clinical Epigenetics* **2**, 349-360, doi:10.1007/s13148-011-0042-6 (2011).

119 Klein, C. & Westenberger, A. Genetics of Parkinson's disease. *Cold Spring Harbor perspectives in medicine* **2**, a008888-a008888, doi:10.1101/cshperspect.a008888 (2012).

120 Dickson, D. W. Parkinson's disease and parkinsonism: neuropathology. *Cold Spring Harbor perspectives in medicine* **2**, a009258, doi:10.1101/cshperspect.a009258 (2012).

121 Luca Lovrečić, A. M., Maja Zadel and Borut Peterlin (2015).

122 Xiong, Y. & Yu, J. Modeling Parkinson's Disease in Drosophila: What Have We Learned for Dominant Traits? *Frontiers in neurology* **9**, 228-228, doi:10.3389/fneur.2018.00228 (2018).

123 Liu, Y. *et al.* Emerging Role of Sirtuin 2 in Parkinson's Disease. *Frontiers in Aging Neuroscience* **11**, doi:10.3389/fnagi.2019.00372 (2020).

124 Harrison, I. F., Smith, A. D. & Dexter, D. T. Pathological histone acetylation in Parkinson's disease: Neuroprotection and inhibition of microglial activation through SIRT 2 inhibition. *Neuroscience letters* **666**, 48-57, doi:10.1016/j.neulet.2017.12.037 (2018).

125 Harrison, I. F. & Dexter, D. T. Epigenetic targeting of histone deacetylase: Therapeutic potential in Parkinson's disease? *Pharmacology & Therapeutics* **140**, 34-52, doi:https://doi.org/10.1016/j.pharmthera.2013.05.010 (2013).

126 Sharma, S. & Taliyan, R. Targeting histone deacetylases: a novel approach in Parkinson's disease. *Parkinson's disease* **2015**, 303294-303294, doi:10.1155/2015/303294 (2015).

127 Outeiro, T. F. *et al.* Sirtuin 2 Inhibitors Rescue α-Synuclein-Mediated Toxicity in Models of Parkinson's Disease. *Science* **317**, 516-519, doi:10.1126/science.1143780 (2007).

128 Masliah, E., Dumaop, W., Galasko, D. & Desplats, P. Distinctive patterns of DNA methylation associated with Parkinson disease: identification of concordant epigenetic changes in brain and peripheral blood leukocytes. *Epigenetics* **8**, 1030-1038, doi:10.4161/epi.25865 (2013).

129 Miranda-Morales, E. *et al.* Implications of DNA Methylation in Parkinson's Disease. *Frontiers in molecular neuroscience* **10**, 225-225, doi:10.3389/fnmol.2017.00225 (2017).

130 Pavlou, M. A. S. & Outeiro, T. F. in *Neuroepigenomics in Aging and Disease* (ed Raul Delgado-Morales) 363-390 (Springer International Publishing, 2017).
131 Kim, J. *et al.* A MicroRNA feedback circuit in midbrain dopamine neurons. *Science (New York, N.Y.)* **317**, 1220-1224, doi:10.1126/science.1140481 (2007).
132 Roser, A. E., Caldi Gomes, L., Schünemann, J., Maass, F. & Lingor, P. Circulating miRNAs as Diagnostic Biomarkers for Parkinson's Disease. *Frontiers in neuroscience* **12**, 625-625, doi:10.3389/fnins.2018.00625 (2018).
133 Leggio, L. *et al.* microRNAs in Parkinson's Disease: From Pathogenesis to Novel Diagnostic and Therapeutic Approaches. *International journal of molecular sciences* **18**, 2698, doi:10.3390/ijms18122698 (2017).
134 Wolf, R. C., Vasic, N., Schonfeldt-Lecuona, C., Ecker, D. & Landwehrmeyer, G. B. Cortical dysfunction in patients with Huntington's disease during working memory performance. *Hum Brain Mapp* **30**, 327-339, doi:10.1002/hbm.20502 (2009).
135 Imarisio, S. *et al.* Huntington's disease: from pathology and genetics to potential therapies. *Biochemical Journal* **412**, 191-209, doi:10.1042/bj20071619 (2008).
136 Albin, R. L. & Tagle, D. A. Genetics and molecular biology of Huntington's disease. *Trends in Neurosciences* **18**, 11-14, doi:https://doi.org/10.1016/0166-2236(95)93943-R (1995).
137 Myers, R. H. Huntington's disease genetics. *NeuroRX* **1**, 255-262, doi:10.1602/neurorx.1.2.255 (2004).
138 Lee, J., Hwang, Y. J., Kim, K. Y., Kowall, N. W. & Ryu, H. Epigenetic mechanisms of neurodegeneration in Huntington's disease. *Neurotherapeutics* **10**, 664-676, doi:10.1007/s13311-013-0206-5 (2013).
139 Bassi, S., Tripathi, T., Monziani, A., Di Leva, F. & Biagioli, M. Epigenetics of Huntington's Disease. *Adv Exp Med Biol* **978**, 277-299, doi:10.1007/978-3-319-53889-1_15 (2017).
140 Zsindely, N. & Bodai, L. Histone methylation in Huntington's disease: are bivalent promoters the critical targets? *Neural regeneration research* **13**, 1191-1192, doi:10.4103/1673-5374.235029 (2018).
141 Hu, Y. *et al.* Transcriptional modulator H2A histone family, member Y (H2AFY) marks Huntington disease activity in man and mouse. *Proceedings of the National Academy of Sciences* **108**, 17141-17146, doi:10.1073/pnas.1104409108 (2011).
142 Chen, K.-W. & Chen, L. Epigenetic Regulation of BDNF Gene during Development and Diseases. *International journal of molecular sciences* **18**, 571, doi:10.3390/ijms18030571 (2017).
143 Wang, F., Fischhaber, P. L., Guo, C. & Tang, T.-S. Epigenetic modifications as novel therapeutic targets for Huntington's disease. *Epigenomics* **6**, 287-297, doi:10.2217/epi.14.19 (2014).
144 Ryu, H. *et al.* ESET/SETDB1 gene expression and histone H3 (K9) trimethylation in Huntington's disease. *Proceedings of the National Academy of Sciences of the United States of America* **103**, 19176-19181, doi:10.1073/pnas.0606373103 (2006).
145 Vashishtha, M. *et al.* Targeting H3K4 trimethylation in Huntington disease. *Proceedings of the National Academy of Sciences of the United States of America* **110**, E3027-E3036, doi:10.1073/pnas.1311323110 (2013).

146 Horton, J. R. *et al.* Characterization of a Linked Jumonji Domain of the KDM5/JARID1 Family of Histone H3 Lysine 4 Demethylases. *The Journal of biological chemistry* **291**, 2631-2646, doi:10.1074/jbc.M115.698449 (2016).
147 Palop, J. J., Chin, J. & Mucke, L. A network dysfunction perspective on neurodegenerative diseases. *Nature* **443**, 768-773, doi:10.1038/nature05289 (2006).
148 Rademakers, R. & Rovelet-Lecrux, A. Recent insights into the molecular genetics of dementia. *Trends Neurosci* **32**, 451-461, doi:10.1016/j.tins.2009.05.005 (2009).
149 Francis, Y. I. *et al.* Dysregulation of histone acetylation in the APP/PS1 mouse model of Alzheimer's disease. *J Alzheimers Dis* **18**, 131-139, doi:10.3233/jad-2009-1134 (2009).
150 Govindarajan, N., Agis-Balboa, R. C., Walter, J., Sananbenesi, F. & Fischer, A. Sodium butyrate improves memory function in an Alzheimer's disease mouse model when administered at an advanced stage of disease progression. *J Alzheimers Dis* **26**, 187-197, doi:10.3233/jad-2011-110080 (2011).
151 Lu, X., Wang, L., Yu, C., Yu, D. & Yu, G. Histone Acetylation Modifiers in the Pathogenesis of Alzheimer's Disease. *Frontiers in cellular neuroscience* **9**, 226-226, doi:10.3389/fncel.2015.00226 (2015).
152 Yang, S.-S., Zhang, R., Wang, G. & Zhang, Y.-F. The development prospection of HDAC inhibitors as a potential therapeutic direction in Alzheimer's disease. *Translational neurodegeneration* **6**, 19-19, doi:10.1186/s40035-017-0089-1 (2017).
153 Gräff, J. *et al.* An epigenetic blockade of cognitive functions in the neurodegenerating brain. *Nature* **483**, 222-226, doi:10.1038/nature10849 (2012).
154 Frost, B., Hemberg, M., Lewis, J. & Feany, M. B. Tau promotes neurodegeneration through global chromatin relaxation. *Nat Neurosci* **17**, 357-366, doi:10.1038/nn.3639 (2014).
155 You, A., Tong, J. K., Grozinger, C. M. & Schreiber, S. L. CoREST is an integral component of the CoREST- human histone deacetylase complex. *Proceedings of the National Academy of Sciences of the United States of America* **98**, 1454-1458 (2001).
156 Majello, B., Gorini, F., Saccà, C. D. & Amente, S. Expanding the Role of the Histone Lysine-Specific Demethylase LSD1 in Cancer. *Cancers* **11**, 324, doi:10.3390/cancers11030324 (2019).
157 Metzger, E. *et al.* LSD1 demethylates repressive histone marks to promote androgen-receptor-dependent transcription. *Nature* **437**, 436-439 (2005).
158 Nicholson, T. B. & Chen, T. LSD1 demethylates histone and non-histone proteins. *Epigenetics* **4**, 129-132, doi:10.4161/epi.4.3.8443 (2009).
159 Katz, D. J., Edwards, T. M., Reinke, V. & Kelly, W. G. A C. elegans LSD1 demethylase contributes to germline immortality by reprogramming epigenetic memory. *Cell* **137**, 308-320 (2009).
160 Rudolph, T. *et al.* Heterochromatin formation in Drosophila is initiated through active removal of H3K4 methylation by the LSD1 homolog SU(VAR)3-3. *Mol Cell* **26**, 103-115 (2007).
161 Szabad, J., Reuter, G. & Schroder, M. B. The effects of two mutations connected with chromatin functions on female germ-line cells of Drosophila. *Mol Gen Genet* **211**, 56-62 (1988).

162 Wang, J. *et al.* The lysine demethylase LSD1 (KDM1) is required for maintenance of global DNA methylation. *Nature genetics* **41**, 125-129, doi:10.1038/ng.268 (2009).
163 Wasson, J. A. *et al.* Maternally provided LSD1/KDM1A enables the maternal-to-zygotic transition and prevents defects that manifest postnatally. *eLife* **5**, doi:10.7554/eLife.08848 (2016).
164 Ancelin, K. *et al.* Maternal LSD1/KDM1A is an essential regulator of chromatin and transcription landscapes during zygotic genome activation. *Elife* **5**, doi:10.7554/eLife.08851 (2016).
165 Whyte, W. A. *et al.* Enhancer decommissioning by LSD1 during embryonic stem cell differentiation. *Nature* **482**, 221-225, doi:nature10805 [pii]
10.1038/nature10805 (2012).
166 Lyons, D. B. *et al.* An epigenetic trap stabilizes singular olfactory receptor expression. *Cell* **154**, 325-336, doi:10.1016/j.cell.2013.06.039 (2013).
167 Duteil, D. *et al.* LSD1 promotes oxidative metabolism of white adipose tissue. *Nat Commun* **5**, 4093, doi:10.1038/ncomms5093
ncomms5093 [pii] (2014).
168 Fuentes, P., Canovas, J., Berndt, F. A., Noctor, S. C. & Kukuljan, M. CoREST/LSD1 control the development of pyramidal cortical neurons. *Cereb Cortex* **22**, 1431-1441, doi:10.1093/cercor/bhr218 (2012).
169 Zibetti, C. *et al.* Alternative splicing of the histone demethylase LSD1/KDM1 contributes to the modulation of neurite morphogenesis in the mammalian nervous system. *J Neurosci* **30**, 2521-2532, doi:10.1523/JNEUROSCI.5500-09.2010 (2010).
170 Laurent, B. *et al.* A specific LSD1/KDM1A isoform regulates neuronal differentiation through H3K9 demethylation. *Mol Cell* **57**, 957-970, doi:10.1016/j.molcel.2015.01.010 (2015).
171 Wang, J. *et al.* LSD1n is an H4K20 demethylase regulating memory formation via transcriptional elongation control. *Nat Neurosci* **18**, 1256-1264, doi:10.1038/nn.4069 (2015).
172 Dai, C. *et al.* Functional Identification of Neuroprotective Molecules. *PLoS ONE* **5**, e15008, doi:10.1371/journal.pone.0015008 (2010).
173 Christopher, M. A. *et al.* LSD1 protects against hippocampal and cortical neurodegeneration. *Nature Communications* **8**, 805, doi:10.1038/s41467-017-00922-9 (2017).
174 Hayashi, S. & McMahon, A. P. Efficient recombination in diverse tissues by a tamoxifen-inducible form of Cre: a tool for temporally regulated gene activation/inactivation in the mouse. *Dev Biol* **244**, 305-318 (2002).
175 Wegorzewska, I., Bell, S., Cairns, N. J., Miller, T. M. & Baloh, R. H. TDP-43 mutant transgenic mice develop features of ALS and frontotemporal lobar degeneration. *Proc Natl Acad Sci U S A* **106**, 18809-18814, doi:10.1073/pnas.0908767106 (2009).
176 Kim, D. *et al.* TopHat2: accurate alignment of transcriptomes in the presence of insertions, deletions and gene fusions. *Genome Biology* **14**, R36, doi:10.1186/gb-2013-14-4-r36 (2013).

177 Trapnell, C. *et al.* Transcript assembly and quantification by RNA-Seq reveals unannotated transcripts and isoform switching during cell differentiation. *Nature Biotechnology* **28**, 511-515, doi:10.1038/nbt.1621 (2010).
178 Gentleman, R. C. *et al.* Bioconductor: open software development for computational biology and bioinformatics. *Genome Biology* **5**, R80, doi:10.1186/gb-2004-5-10-r80 (2004).
179 Suzuki, R. & Shimodaira, H. Pvclust: an R package for assessing the uncertainty in hierarchical clustering. *Bioinformatics* **22**, 1540-1542, doi:10.1093/bioinformatics/btl117 (2006).
180 Falcon, S. & Gentleman, R. Using GOstats to test gene lists for GO term association. *Bioinformatics* **23**, 257-258, doi:10.1093/bioinformatics/btl567 (2007).
181 Subramanian, A. *et al.* Gene set enrichment analysis: A knowledge-based approach for interpreting genome-wide expression profiles. *Proceedings of the National Academy of Sciences* **102**, 15545-15550, doi:10.1073/pnas.0506580102 (2005).
182 Lawrence, M., Gentleman, R. & Carey, V. rtracklayer: an R package for interfacing with genome browsers. *Bioinformatics* **25**, 1841-1842, doi:10.1093/bioinformatics/btp328 (2009).
183 Scharer, C. D., Barwick, B. G., Youngblood, B. A., Ahmed, R. & Boss, J. M. Global DNA Methylation Remodeling Accompanies CD8 T Cell Effector Function. *The Journal of Immunology* **191**, 3419-3429, doi:10.4049/jimmunol.1301395 (2013).
184 Afgan, E. *et al.* The Galaxy platform for accessible, reproducible and collaborative biomedical analyses: 2016 update. *Nucleic Acids Res* **44**, W3-w10, doi:10.1093/nar/gkw343 (2016).
185 Afgan, E. *et al.* The Galaxy platform for accessible, reproducible and collaborative biomedical analyses: 2018 update. *Nucleic Acids Research* **46**, W537-W544, doi:10.1093/nar/gky379 (2018).
186 Gregory R. Warens, B. B., Lodewijk Bonebakker, Robert Gentleman, Wolfgang Huber Andy Liaw, Thomas Lumley, Martin Maechler, Arni Magnusson, Steffen Moeller, Marc Schwartz, Bill Venables. *gplots: Various R Programming Tools for Plotting Data versiou 3.0.1.1.*, < https://CRAN.R-project.org/package=gplots> (2019).
187 Blighe, K. *EnhancedVolcano: Publication-ready volcano plotswith enhanced colouring and labeling.*, <https://github.com/kevinblighe/EnhancedVolcano> (2019).
188 Wang, J., Duncan, D., Shi, Z. & Zhang, B. WEB-based GEne SeT AnaLysis Toolkit (WebGestalt): update 2013. *Nucleic Acids Res* **41**, W77-83, doi:10.1093/nar/gkt439 (2013).
189 Wang, J., Vasaikar, S., Shi, Z., Greer, M. & Zhang, B. WebGestalt 2017: a more comprehensive, powerful, flexible and interactive gene set enrichment analysis toolkit. *Nucleic Acids Res* **45**, W130-w137, doi:10.1093/nar/gkx356 (2017).
190 Liao, Y., Wang, J., Jaehnig, E. J., Shi, Z. & Zhang, B. WebGestalt 2019: gene set analysis toolkit with revamped UIs and APIs. *Nucleic Acids Res* **47**, W199-w205, doi:10.1093/nar/gkz401 (2019).
191 Zhang, B., Kirov, S. & Snoddy, J. WebGestalt: an integrated system for exploring gene sets in various biological contexts. *Nucleic Acids Res* **33**, W741-748, doi:10.1093/nar/gki475 (2005).

192 Zhang, B. *et al.* Integrated systems approach identifies genetic nodes and networks in late-onset Alzheimer's disease. *Cell* **153**, 707-720, doi:10.1016/j.cell.2013.03.030
S0092-8674(13)00387-5 [pii] (2013).
193 Chen-Plotkin, A. S. *et al.* Variations in the progranulin gene affect global gene expression in frontotemporal lobar degeneration. *Hum Mol Genet* **17**, 1349-1362, doi:10.1093/hmg/ddn023
ddn023 [pii] (2008).
194 Zhang, Y., James, M., Middleton, F. A. & Davis, R. L. Transcriptional analysis of multiple brain regions in Parkinson's disease supports the involvement of specific protein processing, energy metabolism, and signaling pathways, and suggests novel disease mechanisms. *Am J Med Genet B Neuropsychiatr Genet* **137B**, 5-16, doi:10.1002/ajmg.b.30195 (2005).
195 Nam, H. J. *et al.* Phosphorylation of LSD1 by PKCalpha is crucial for circadian rhythmicity and phase resetting. *Mol Cell* **53**, 791-805, doi:10.1016/j.molcel.2014.01.028
S1097-2765(14)00111-7 [pii] (2014).
196 Su, S. T. *et al.* Involvement of histone demethylase LSD1 in Blimp-1-mediated gene repression during plasma cell differentiation. *Mol Cell Biol* **29**, 1421-1431, doi:MCB.01158-08 [pii]
10.1128/MCB.01158-08 (2009).
197 Saleque, S., Kim, J., Rooke, H. M. & Orkin, S. H. Epigenetic regulation of hematopoietic differentiation by Gfi-1 and Gfi-1b is mediated by the cofactors CoREST and LSD1. *Mol Cell* **27**, 562-572, doi:S1097-2765(07)00483-2 [pii]
10.1016/j.molcel.2007.06.039 (2007).
198 Kerenyi, M. A. *et al.* Histone demethylase Lsd1 represses hematopoietic stem and progenitor cell signatures during blood cell maturation. *Elife* **2**, e00633, doi:10.7554/eLife.00633
00633 [pii] (2013).
199 Zhu, D. *et al.* Lysine-specific demethylase 1 regulates differentiation onset and migration of trophoblast stem cells. *Nat Commun* **5**, 3174, doi:10.1038/ncomms4174
ncomms4174 [pii] (2014).
200 Jiang, D., Yang, W., He, Y. & Amasino, R. M. Arabidopsis relatives of the human lysine-specific Demethylase1 repress the expression of FWA and FLOWERING LOCUS C and thus promote the floral transition. *Plant Cell* **19**, 2975-2987, doi:tpc.107.052373 [pii]
10.1105/tpc.107.052373 (2007).
201 Di Stefano, L., Ji, J. Y., Moon, N. S., Herr, A. & Dyson, N. Mutation of Drosophila Lsd1 disrupts H3-K4 methylation, resulting in tissue-specific defects during development. *Curr Biol* **17**, 808-812 (2007).
202 Chong, J. A. *et al.* REST: a mammalian silencer protein that restricts sodium channel gene expression to neurons. *Cell* **80**, 949-957 (1995).
203 Ballas, N. *et al.* Regulation of neuronal traits by a novel transcriptional complex. *Neuron* **31**, 353-365 (2001).
204 Macfarlan, T. S. *et al.* Endogenous retroviruses and neighboring genes are coordinately repressed by LSD1/KDM1A. *Genes & development* **25**, 594-607, doi:10.1101/gad.2008511 (2011).

205 Lambrot, R., Lafleur, C. & Kimmins, S. The histone demethylase KDM1A is essential for the maintenance and differentiation of spermatogonial stem cells and progenitors. *FASEB journal : official publication of the Federation of American Societies for Experimental Biology* **29**, 4402-4416, doi:10.1096/fj.14-267328 (2015).

206 Sangiorgi, E. & Capecchi, M. R. Bmi1 is expressed in vivo in intestinal stem cells. *Nature genetics* **40**, 915-920, doi:10.1038/ng.165 (2008).

207 Yauch, R. L. *et al.* A paracrine requirement for hedgehog signalling in cancer. *Nature* **455**, 406-410, doi:10.1038/nature07275 (2008).

208 Schulz, C. *et al.* A lineage of myeloid cells independent of Myb and hematopoietic stem cells. *Science* **336**, 86-90, doi:10.1126/science.1219179 (2012).

209 Guy, J., Gan, J., Selfridge, J., Cobb, S. & Bird, A. Reversal of neurological defects in a mouse model of Rett syndrome. *Science* **315**, 1143-1147, doi:10.1126/science.1138389 (2007).

210 Oakley, H. *et al.* Intraneuronal beta-amyloid aggregates, neurodegeneration, and neuron loss in transgenic mice with five familial Alzheimer's disease mutations: potential factors in amyloid plaque formation. *J Neurosci* **26**, 10129-10140, doi:10.1523/JNEUROSCI.1202-06.2006 (2006).

211 Takahashi, K. & Yamanaka, S. Induction of pluripotent stem cells from mouse embryonic and adult fibroblast cultures by defined factors. *Cell* **126**, 663-676 (2006).

212 Cameron, B. & Landreth, G. E. Inflammation, microglia, and Alzheimer's disease. *Neurobiol Dis* **37**, 503-509, doi:10.1016/j.nbd.2009.10.006 (2010).

213 Stephan, A. H., Barres, B. A. & Stevens, B. The complement system: an unexpected role in synaptic pruning during development and disease. *Annu Rev Neurosci* **35**, 369-389, doi:10.1146/annurev-neuro-061010-113810 (2012).

214 Selkoe, D. J. Alzheimer's disease is a synaptic failure. *Science* **298**, 789-791, doi:10.1126/science.1074069 (2002).

215 Lin, M. T. & Beal, M. F. Mitochondrial dysfunction and oxidative stress in neurodegenerative diseases. *Nature* **443**, 787-795, doi:10.1038/nature05292 (2006).

216 Busser, J., Geldmacher, D. S. & Herrup, K. Ectopic cell cycle proteins predict the sites of neuronal cell death in Alzheimer's disease brain. *J Neurosci* **18**, 2801-2807 (1998).

217 Rabin, S. J. *et al.* Sporadic ALS has compartment-specific aberrant exon splicing and altered cell-matrix adhesion biology. *Hum Mol Genet* **19**, 313-328, doi:10.1093/hmg/ddp498 (2010).

218 Neumann, M. *et al.* Ubiquitinated TDP-43 in frontotemporal lobar degeneration and amyotrophic lateral sclerosis. *Science* **314**, 130-133, doi:314/5796/130 [pii] 10.1126/science.1134108 (2006).

219 Masters, C. L. *et al.* Neuronal origin of a cerebral amyloid: neurofibrillary tangles of Alzheimer's disease contain the same protein as the amyloid of plaque cores and blood vessels. *Embo J* **4**, 2757-2763 (1985).

220 Glenner, G. G. & Wong, C. W. Alzheimer's disease and Down's syndrome: sharing of a unique cerebrovascular amyloid fibril protein. *Biochem Biophys Res Commun* **122**, 1131-1135, doi:0006-291X(84)91209-9 [pii] (1984).

221 Bai, B. *et al.* U1 small nuclear ribonucleoprotein complex and RNA splicing alterations in Alzheimer's disease. *Proc Natl Acad Sci U S A* **110**, 16562-16567, doi:10.1073/pnas.1310249110
1310249110 [pii] (2013).
222 Wischik, C. M. *et al.* Isolation of a fragment of tau derived from the core of the paired helical filament of Alzheimer disease. *Proc Natl Acad Sci U S A* **85**, 4506-4510, doi:10.1073/pnas.85.12.4506 (1988).
223 Barage, S. H. & Sonawane, K. D. Amyloid cascade hypothesis: Pathogenesis and therapeutic strategies in Alzheimer's disease. *Neuropeptides* **52**, 1-18, doi:10.1016/j.npep.2015.06.008.
224 Karran, E., Mercken, M. & De Strooper, B. The amyloid cascade hypothesis for Alzheimer's disease: an appraisal for the development of therapeutics. *Nat Rev Drug Discov* **10**, 698-712, doi:10.1038/nrd3505 (2011).
225 Gomez-Isla, T. *et al.* Neuronal loss correlates with but exceeds neurofibrillary tangles in Alzheimer's disease. *Ann Neurol* **41**, 17-24, doi:10.1002/ana.410410106 (1997).
226 Bejanin, A. *et al.* Tau pathology and neurodegeneration contribute to cognitive impairment in Alzheimer's disease. *Brain* **140**, 3286-3300, doi:10.1093/brain/awx243 (2017).
227 Hurtado, D. E. *et al.* A{beta} accelerates the spatiotemporal progression of tau pathology and augments tau amyloidosis in an Alzheimer mouse model. *Am J Pathol* **177**, 1977-1988, doi:10.2353/ajpath.2010.100346 (2010).
228 He, Z. *et al.* Amyloid-beta plaques enhance Alzheimer's brain tau-seeded pathologies by facilitating neuritic plaque tau aggregation. *Nat Med* **24**, 29-38, doi:10.1038/nm.4443 (2018).
229 Choi, S. H. *et al.* A three-dimensional human neural cell culture model of Alzheimer/'s disease. *Nature* **515**, 274-278, doi:10.1038/nature13800
http://www.nature.com/nature/journal/v515/n7526/abs/nature13800.html#supplementary-information (2014).
230 Hanger, D. P., Betts, J. C., Loviny, T. L., Blackstock, W. P. & Anderton, B. H. New phosphorylation sites identified in hyperphosphorylated tau (paired helical filament-tau) from Alzheimer's disease brain using nanoelectrospray mass spectrometry. *J Neurochem* **71**, 2465-2476, doi:10.1046/j.1471-4159.1998.71062465.x (1998).
231 Morishima-Kawashima, M. *et al.* Hyperphosphorylation of tau in PHF. *Neurobiol Aging* **16**, 365-371; discussion 371-380 (1995).
232 Castellani, R. J. & Perry, G. Tau Biology, Tauopathy, Traumatic Brain Injury, and Diagnostic Challenges. *J Alzheimers Dis* **67**, 447-467, doi:10.3233/jad-180721 (2019).
233 Masliah, E. *et al.* Altered expression of synaptic proteins occurs early during progression of Alzheimer's disease. *Neurology* **56**, 127-129, doi:10.1212/wnl.56.1.127 (2001).
234 Ingelsson, M. *et al.* Early Abeta accumulation and progressive synaptic loss, gliosis, and tangle formation in AD brain. *Neurology* **62**, 925-931, doi:10.1212/01.wnl.0000115115.98960.37 (2004).
235 Kinney, J. W. *et al.* Inflammation as a central mechanism in Alzheimer's disease. *Alzheimer's & Dementia: Translational Research & Clinical Interventions* **4**, 575-590, doi:https://doi.org/10.1016/j.trci.2018.06.014 (2018).

236 Rubio-Perez, J. M. & Morillas-Ruiz, J. M. A review: inflammatory process in Alzheimer's disease, role of cytokines. *TheScientificWorldJournal* **2012**, 756357-756357, doi:10.1100/2012/756357 (2012).
237 Bellucci, A. *et al.* Induction of Inflammatory Mediators and Microglial Activation in Mice Transgenic for Mutant Human P301S Tau Protein. *The American Journal of Pathology* **165**, 1643-1652, doi:http://dx.doi.org/10.1016/S0002-9440(10)63421-9 (2004).
238 Iba, M. *et al.* Tau pathology spread in PS19 tau transgenic mice following locus coeruleus (LC) injections of synthetic tau fibrils is determined by the LC's afferent and efferent connections. *Acta Neuropathol* **130**, 349-362, doi:10.1007/s00401-015-1458-4 (2015).
239 Foster, C. T. *et al.* Lysine-specific demethylase 1 regulates the embryonic transcriptome and CoREST stability. *Molecular and cellular biology* **30**, 4851-4863, doi:10.1128/MCB.00521-10 (2010).
240 Jin, L. *et al.* Loss of LSD1 (lysine-specific demethylase 1) suppresses growth and alters gene expression of human colon cancer cells in a p53- and DNMT1(DNA methyltransferase 1)-independent manner. *The Biochemical journal* **449**, 459-468, doi:10.1042/BJ20121360 (2013).
241 Giasson, B. I. & Mushynski, W. E. Aberrant stress-induced phosphorylation of perikaryal neurofilaments. *J Biol Chem* **271**, 30404-30409, doi:10.1074/jbc.271.48.30404 (1996).
242 Liu, Y. L. *et al.* Alternation of neurofilaments in immune-mediated injury of spinal cord motor neurons. *Spinal Cord* **47**, 166, doi:10.1038/sc.2008.90 (2008).
243 Moon, L. D. F. Chromatolysis: Do injured axons regenerate poorly when ribonucleases attack rough endoplasmic reticulum, ribosomes and RNA? *Dev Neurobiol* **78**, 1011-1024, doi:10.1002/dneu.22625 (2018).
244 Cragg, B. G. What is the signal for chromatolysis? *Brain Res* **23**, 1-21, doi:10.1016/0006-8993(70)90345-8 (1970).
245 Sil, S., Goswami, A. R., Dutta, G. & Ghosh, T. Effects of naproxen on immune responses in a colchicine-induced rat model of Alzheimer's disease. *Neuroimmunomodulation* **21**, 304-321, doi:10.1159/000357735 (2014).
246 Riancho, J. *et al.* Compensatory Motor Neuron Response to Chromatolysis in the Murine hSOD1(G93A) Model of Amyotrophic Lateral Sclerosis. *Front Cell Neurosci* **8**, 346, doi:10.3389/fncel.2014.00346 (2014).
247 Cataldo, A. M., Hamilton, D. J. & Nixon, R. A. Lysosomal abnormalities in degenerating neurons link neuronal compromise to senile plaque development in Alzheimer disease. *Brain Res* **640**, 68-80, doi:10.1016/0006-8993(94)91858-9 (1994).
248 Eftekharzadeh, B. *et al.* Tau Protein Disrupts Nucleocytoplasmic Transport in Alzheimer's Disease. *Neuron* **99**, 925-940.e927, doi:https://doi.org/10.1016/j.neuron.2018.07.039 (2018).
249 Sheffield, L. G., Miskiewicz, H. B., Tannenbaum, L. B. & Mirra, S. S. Nuclear Pore Complex Proteins in Alzheimer Disease. *Journal of Neuropathology & Experimental Neurology* **65**, 45-54, doi:10.1097/01.jnen.0000195939.40410.08 (2006).
250 Frost, B., Bardai, F. H. & Feany, M. B. Lamin Dysfunction Mediates Neurodegeneration in Tauopathies. *Curr Biol* **26**, 129-136, doi:10.1016/j.cub.2015.11.039 (2016).
251 Skrabana, R., Sevcik, J. & Novak, M. Intrinsically Disordered Proteins in the Neurodegenerative Processes: Formation of Tau Protein Paired Helical Filaments and

Their Analysis. *Cellular and Molecular Neurobiology* **26**, 1083-1095, doi:10.1007/s10571-006-9083-3 (2006).

252 Skrabana, R., Skrabanova, M., Csokova, N., Sevcik, J. & Novak, M. Intrinsically disordered tau protein in Alzheimer's tangles: a coincidence or a rule? *Bratisl Lek Listy* **107**, 354-358 (2006).

253 Zhu, S. *et al.* Hyperphosphorylation of intrinsically disordered tau protein induces an amyloidogenic shift in its conformational ensemble. *PloS one* **10**, e0120416-e0120416, doi:10.1371/journal.pone.0120416 (2015).

254 Bishof, I. *et al.* RNA-binding proteins with basic-acidic dipeptide (BAD) domains self-assemble and aggregate in Alzheimer's disease. *J Biol Chem* **293**, 11047-11066, doi:10.1074/jbc.RA118.001747 (2018).

255 Jin, Y. *et al.* Nuclear import of human histone lysine-specific demethylase LSD1. *J Biochem* **156**, 305-313, doi:10.1093/jb/mvu042 (2014).

256 Shi, Y. J. *et al.* Regulation of LSD1 histone demethylase activity by its associated factors. *Mol Cell* **19**, 857-864, doi:10.1016/j.molcel.2005.08.027 (2005).

257 Shrinivas, K. *et al.* Enhancer Features that Drive Formation of Transcriptional Condensates. *Molecular Cell* **75**, 549-561.e547, doi:https://doi.org/10.1016/j.molcel.2019.07.009 (2019).

258 Ahmed, Z., Mackenzie, I. R., Hutton, M. L. & Dickson, D. W. Progranulin in frontotemporal lobar degeneration and neuroinflammation. *J Neuroinflammation* **4**, 7, doi:10.1186/1742-2094-4-7 (2007).

259 Gjoneska, E. *et al.* Conserved epigenomic signals in mice and humans reveal immune basis of Alzheimer's disease. *Nature* **518**, 365-369, doi:10.1038/nature14252 (2015).

260 Stevens, B. *et al.* The classical complement cascade mediates CNS synapse elimination. *Cell* **131**, 1164-1178, doi:10.1016/j.cell.2007.10.036 (2007).

261 Feng, G. *et al.* Imaging neuronal subsets in transgenic mice expressing multiple spectral variants of GFP. *Neuron* **28**, 41-51, doi:10.1016/s0896-6273(00)00084-2 (2000).

262 Rice, R. A. *et al.* Elimination of Microglia Improves Functional Outcomes Following Extensive Neuronal Loss in the Hippocampus. *J Neurosci* **35**, 9977-9989, doi:10.1523/jneurosci.0336-15.2015 (2015).

263 Au - Mostany, R. & Au - Portera-Cailliau, C. A Craniotomy Surgery Procedure for Chronic Brain Imaging. *JoVE*, e680, doi:doi:10.3791/680 (2008).

264 Goldberg, A. D., Allis, C. D. & Bernstein, E. Epigenetics: a landscape takes shape. *Cell* **128**, 635-638, doi:10.1016/j.cell.2007.02.006 (2007).

265 Campbell, K. H., McWhir, J., Ritchie, W. A. & Wilmut, I. Sheep cloned by nuclear transfer from a cultured cell line. *Nature* **380**, 64-66, doi:10.1038/380064a0 (1996).

266 Gurdon, J. B., Elsdale, T. R. & Fischberg, M. Sexually mature individuals of Xenopus laevis from the transplantation of single somatic nuclei. *Nature* **182**, 64-65, doi:10.1038/182064a0 (1958).

267 Soufi, A., Donahue, G. & Zaret, K. S. Facilitators and impediments of the pluripotency reprogramming factors' initial engagement with the genome. *Cell* **151**, 994-1004, doi:10.1016/j.cell.2012.09.045 (2012).

268 Heintzmann, R. & Huser, T. Super-Resolution Structured Illumination Microscopy. *Chem Rev* **117**, 13890-13908, doi:10.1021/acs.chemrev.7b00218 (2017).

269 Price, J. L. & Morris, J. C. Tangles and plaques in nondemented aging and "preclinical" Alzheimer's disease. *Ann Neurol* **45**, 358-368, doi:10.1002/1531-8249(199903)45:3<358::aid-ana12>3.0.co;2-x (1999).

270 Oddo, S. *et al.* Triple-transgenic model of Alzheimer's disease with plaques and tangles: intracellular Abeta and synaptic dysfunction. *Neuron* **39**, 409-421, doi:10.1016/s0896-6273(03)00434-3 (2003).